Feeder Reconfiguration on Distribution Network Considering Harmonics

Thesis presented for the degree of

Doctor of Philosophy

at the University of Strathclyde

by

ZHENGRUI PENG

Supervisor: Professor K.L.Lo

Power System Research Group

Institute of Energy and Environment

Department of Electronic and Electrical Engineering

University of Strathclyde

2017

Declaration

This thesis is the result of the author's original research. It has been completed by the author and has not been previously submitted for examination which has led to the award of a degree.

Acknowledgements

I would like to express my sincere appreciate to my supervisor, Professor K.L.Lo, Head of the Power System Research Group (PSRG), for his continuous guidance, encouragement, helpful comments, kind advice and capable supervision throughout my PhD study. The completion of this thesis would not have been possible without his constant encouragement and patient guidance.

I also wish to extend my gratitude to my colleagues, Jianfeng Lv and Cheng Ding, for their help and support at various stages of this research work.

Most importantly, I would like to thank my parents, Shaochun Peng, Ling Wang for their love, support and encouragement throughout my PhD study.

Abstract

One of the most important measures that can be employed to enhance the supply reliability and quality of electrical energy in a distribution network is feeder reconfiguration. Many studies have been conducted in this area, but only a minor proportion have considered the concept of system harmonics in feeder reconfiguration. In recent years, an increasing number of invertor/converter-based renewable generators are being connected to the distribution network, and given that these generators are harmonic sources, it is important to consider the impacts of the system harmonics in the feeder reconfiguration.

Load flow analysis is used to determine a suitable network structure for specific purposes in the feeder reconfiguration problem. In this thesis, a new load flow method is proposed based on the backward/forward sweep method. This method can analyse distribution network load flow under both fundamental and harmonic conditions with distributed generators. Following this, a hybrid optimization method is proposed based on the salient features of the ant colony system and particle swarm optimization. This hybrid method has a higher searching accuracy performance for feeder reconfiguration when compared, on test system, with the ant colony system and particle swarm optimization. Finally, a 118 mid-voltage level distribution system is used to investigate the impacts of renewable generators and system harmonics. The test results verify that system harmonics will have a significant influence on feeder reconfiguration and, consequently, cannot be ignored. Furthermore, other factors including the different capacities of renewable generators, fluctuations in load demands over 24 hours, and the variable output of the renewable generators in different seasons are also investigated in the feeder reconfiguration problem.

Contents

List of Figures

List of Tables

Nomenclature

h	It represents harmonic order in the thesis. h = 1, 2, 3 , ….
I	Current
$I_n^{(h)}$	h^{th} harmonic order branch current at branch n
$V_n^{(h)}$	h^{th} harmonic order bus voltage at bus n
P	Active power
$p.u.$	Per unit
pf	Total power factor
Q	Reactive power
R	Resistance
THD_i	Total harmonic current distortion
THD_v	Total harmonic voltage distortion
V	Voltage
MVA	Mega Volt Amperes
MW	Megawatt
MVAr	Mega volt-ampere reactive
MWh	Megawatt Hours
P_{loss}	Network loss
I_{ij}	Branch current on branch ij

Y	Network admittance
random()	Random number between 0 and 1
τ_{ij}	Strength of pheromone trails on feeder ij
η_{ij}	Reciprocal value of the resistance of branch ij
Sigmoid	Sigmoid function
ω	Inertia weight
$Pbest_i$	Local best position of the particle i
$Gbest_i$	Global best position of the particle i
EU	European Union
CPU	Central Processing Unit
GB	Gigabyte
RAM	Random access memory
PV	Photovoltaic
GW	Gigawatt
MW	Megawatt
Ofgem	Office of the Gas and Electricity Markets
ACO	Ant colony system
PSO	Particle swarm optimization

Chapter 1 Introduction

1.1 Introduction

Over the past century, human activities have released large amounts of carbon dioxide and other greenhouse gases into the atmosphere. This has caused an increase of 1.5 °C in Global Surface Mean Temperature in this period, and the 21st century is expected to witness a further increase of 0.5 to 8.6 °C. The majority of greenhouse gases emissions come from burning fossil fuels to produce energy [1]. In order to meet emissions reductions in line with national energy policies, electricity networks are, therefore, as the principle source of greenhouse gases, being targeted for improvements. As a result of the development of technology, renewable energy generation costs are continuously falling. Hence, the target of limiting greenhouse gases emissions can be achieved by replacing fossil fuel plants with wind turbines, photovoltaic generators, and other renewable generators.

As part of the effort to reduce greenhouse gases emissions, an increasing number of renewable generators have been installed in the distribution network. However, the fact cannot be overlooked that common types of renewable generators, including wind turbines and photovoltaic generators, also bring about problems for the power network. Both of these types of generators produce direct current and transform it into alternating currents through the use of a converter or inverter. In the process of transforming the current, the converter/inverter also generates harmonics, and system harmonics can lead to multiple negative effects across distribution networks. Effects of this kind include power loss in equipment and power transmission lines, the reduction of equipment lifespan, the overheating of neutral wires and transmission, and the production of a series of parallel harmonic

resonances, which thereby leads to equipment damage as a consequence of overvoltage or overcurrent [2-4]. Hence, parts of functions for distribution networks need to be improved from the perspective of system harmonics.

Feeder reconfiguration is one automation function in steady state of power system which can enhance the reliability and quality of electrical energy in the distribution network, and it can be achieved at a relatively low cost. It is defined as altering the topological structures of distribution feeders by changing the open/closed states of the sectionalizing and tie switches [5]. Under normal operating conditions, the system operators can adjust the network structure according to actual demand by changing the status of the sectionalizing and tie switches. This is the process of feeder reconfiguration and it will be introduced in this thesis. Then, the load in the network can be balanced; the overload can be eliminated; and the network losses can be reduced. Furthermore, when an electrical fault occurs, the range of the outage can also be reduced by feeder reconfiguration. For example, system operators can transform the important loads from one feeder to anther or an islanding system by using the result of the feeder reconfiguration. Once the fault has been eliminated, the electric energy supply can also be rapidly restored. Thus, feeder reconfiguration is a multi-objective combinatorial optimization problem. One method to solve such problems is to choose a single primary objective and to treat the others as the constraints. The objective of feeder reconfiguration is normally proposed according to the specific requirements, such as loss reduction, load balancing, voltage profile improvement, and service restoration [6]. A significant volume of research has been carried out in each area. In reference [7], loss reduction and optimum operation are used as the objectives. Loss reduction and load balancing are the objectives in reference [8]. Service restoration and load balancing are chosen as the objectives in reference [9]. When feeder reconfiguration is used to reduce the network loss, heavy load can be transferred from one feeder to another. Then, voltage drop will be improved on each bus. Thus,

due to the overload, the load balance rate and the power quality may be improved with a reduction of the network losses, it is important to recognise that the problem of network loss reduction is consistently selected as the primary objective of the feeder reconfiguration problem, such as in references [10-14].

After the renewable generators connect to the distribution network, the system harmonics also inject into the network. Although this is an important method for enhancing the reliability and quality of electrical energy for distribution networks, very few studies have focused on investigating the impacts of system harmonics. Nevertheless, system harmonics cannot be ignored before their impacts are investigated and the test results have verified that these impacts have no effects on feeder reconfiguration. This is especially the case in the context of a situation where an increasing number of invertor/convertor-based generators are being connected to the distribution network. The impact of the system harmonics will be investigated in Chapter 7.

Feeder reconfiguration can be divided into three parts: a) Choose an objective and establish the objective function and constraint conditions for a distribution network; b) Calculate the required information for objective function and constraint conditions by the load flow analysis method in each network, which is established by optimization methods, including bus voltages and branch currents in the distribution network; c) Establish a feasible network structure and determine the optimal structural arrangement by employing the optimization method according to the objective function and constraint conditions. In these three parts, the objective function and constraint conditions will be established first and they will not be changed. All parameters of the devices in the system normally choose its rated value. In order to find accuracy results, average values in a time interval are chosen as the parameters of the devices in this thesis in Chapter 7. In view of the fact that the objective function is variable, investigating the impacts of harmonics

before determining the objective function is inevitably a difficult task. The optimization method will construct a network structure in each iteration, and each network will be analysed by the load flow method; following this, a value of the objective function will be obtained. The process of how optimization method work is shown in Chapter 5. The optimal network is the network for which the objective function value is maximum or minimum. Due to the system harmonics, it is necessary to improve the load flow method so that the value of the required information for the objective function can be calculated correctly. Consequently, the solution for the feeder reconfiguration can also be calculated correctly when system harmonic is considered.

Due to differing R/X ratios between transmission networks and distribution networks and the radial structure of a distribution network, the backward/forward sweep method [15] is a fast and accurate load flow method that can be applied. Furthermore, it is widely used in feeder reconfiguration. However, the backward/forward sweep method cannot analyse a distribution network under harmonic condition; notably, when inverter/convertor-based generators are connected to the distribution network, a harmonic load flow analysis method is required. The main harmonic load flow analysis methods are listed as follows: the Newton-Raphson based harmonic power flow method [16, 17]; the decoupled harmonic power flow method [18-22]; the fast decoupled harmonic power flow method [23-26]; the fuzzy harmonic power flow method [27]; the probabilistic harmonic power flow method [28-31]; and the modular harmonic power flow method [32-34]. Despite the abundance of methods, relatively few of them have the capacity to analyse large-scale distribution networks with sufficient speed.

A fast harmonic power flow method based on the basic backward/forward sweep method has been proposed in recent years [35-37]. Although the accuracy of this method is not as high as the aforementioned primary harmonic analysis methods,

it can obtain acceptable results quickly. However, in the literature on this method, the position of the harmonic sources is a special condition, thereby meaning that this method may not be suitable for all conditions. Furthermore, each load flow method has been proposed specifically in regards to harmonic load flow analysis without considering the special characteristics of feeder reconfiguration. One notable example of this is that certain load flow methods require code buses in the network to help the method calculate the load flow. However, in feeder reconfiguration problem, different network structures will be established in each iteration during the searching process of the optimization method. The load flow methods may need to recode buses before calculating. Even if the recoding process can be automatically accomplished, it will also waste extensive computing time to recode buses. Hence, the author in this thesis proposes a load flow method for feeder reconfiguration which not only can calculate the load flow under harmonic condition, but can also avoid the recoding problem. The introduction of this method is shown in section 4.7.

Nowadays, the artificial intelligence optimization methods are commonly used method in feeder reconfiguration. The ant colony system [38-40] and particle swarm optimization [41, 42] have proven to be two of most common used optimization methods in recent years, and many researchers have devoted their work to the improvement of the optimization methods' searching efficiency. However, each artificial optimization method may have its special deficiency. It is important to note that these defects may stem from the theory itself, thereby meaning that they are difficult to avoid unless the basic theory of the method is modified. For example, due to the pheromone trails of the ants, an ant colony system can quickly identify more effective solutions based on an existing solution, but it cannot quickly find feasible solutions in all possible search areas. Additionally, owing to the lack of limitations regarding initial velocity and direction in particle swarm optimization, it offers high-performance in finding

feasible solutions in all possible search areas while not being sufficiently competent in terms of its detailed searching ability around an existing solution. In this way, it is evident that each method's advantages and disadvantages come from their basic theory. If a newly formulated method could capitalise on both of advantages through an appropriate combination of each, then the searching efficiency would be greatly improved. Hence, the author in this thesis attempts to combine the two methods in an appropriate manner so as to facilitate better searching efficiency.

The impacts of renewable generators in feeder reconfiguration include not only system harmonics but also variable output power. In the actual engineering project, the peak load demand varies over 24 hours and the output power of some renewable generators will change with the weather and the season. However, in the majority of studies, the load demand and the output of the generators are set as unchanged. In fact, the load flow will change dramatically with variations in the peak demand of the loads and the output of the generators in the distribution network. Consequently, the load flow will concurrently change, the result of which is that the solution of the feeder reconfiguration subsequently changes. Hence, the fluctuations in load demands and output of the generators are important factors in the feeder reconfiguration problem, the impacts of which must be investigated.

Overall, the contribution of this project will be to investigate the impacts of renewable generators in feeder configuration following their connection to the distribution network.

1.2 Thesis Objectives

The aim of this thesis is to achieve feeder reconfiguration considering system harmonics on a modern distribution network. The objectives of this thesis include:

a) The development of a fast load flow analysis method for both fundamental and harmonic condition to calculate the network loss in a distribution network with renewable generators. Moreover, the method should be suitable for the feeder reconfiguration problem.

   In order to meet these objectives, the following specific details must be adhered to:

   1) The PQ type distributed generator, which means a distributed generator with known active and reactive out power, can simply be treated as a load. However, the same method cannot be used to offer a PV type distributed generator solution. The issues surrounding PV type distributed generators in distribution networks must be solved.

   2) The optimization method is used to obtain some feasible network structures in the process of the feeder reconfiguration. Then, according to the optimization method, hundreds of network structures may be established by changing the status of the sectionalizing and tie switches. Thus, when the network structure is changed, this method can still be used to analyse the load flow automatically.

b) The development of an accurate optimization method for optimal distribution network configuration, which means the new method can find better final solutions than the commonly used method. Moreover, this method should offer high levels of accuracy when employed in large distribution networks. It is better to propose a hybrid method based on two optimization methods which incorporates their advantages and eliminates their disadvantages.

   In order to meet these objectives, the following specific details must be adhered to:

   1) A brief review of the present efficiency optimization methods for

distribution network feeder reconfiguration.

2) Choose two common used methods. Next, the theory underpinning these methods should be understood, they should be modelled using software and tested.

3) Explore their advantages and disadvantages in detail.

c) Apply the proposed method to a large distribution network to investigate the impacts of system harmonics and distributed generators on the feeder reconfiguration problem. Also, the impacts of the variable load demands and output of the renewable generators in distribution networks over 24 hours on the feeder reconfiguration problem are investigated.

In order to meet these objectives, the following specific details must be adhered to:

1) Different levels of the system harmonic penetration and variable capacity of the distributed generators should be considered in the test system. Then, the different effects which are produced by variable harmonic penetration levels and capacity of the distributed generators are investigated.

2) To obtain more useful and practical data regarding the impact of system harmonics and renewable generators. Different load types and the fluctuation of peak load demands should be considered. The formal status and forecast of the system harmonic penetration and the capacity of the wind and solar generators in the distribution network should be specified. In addition, the variable output of the generators should be considered.

1.3 Main contributions of the Thesis

The factors contributing to the success of this study can be summarized as follows:

a) The computing process is following the system levels instead of flowing the code of buses and branches in the layered backward/forward sweep method in fundamental frequency. The harmonic backward/forward sweep method can analyse a distribution network in harmonic frequency. By combining the characteristics of these two methods, the author proposed a fast harmonic load flow analysis method for distribution networks. This method is developed from the original harmonic backward/forward sweep algorithm. The original harmonic backward/forward sweep algorithm will not divide the system into levels, so the code on buses needs to be recoded when the system structure is changed in the feeder reconfiguration problem. Furthermore, this original method will ignore the harmonic branch current on those tributaries which do not connect with the harmonic source. The layered method is applied to the proposed method. Then, the load flow calculation will follow the sequence of system levels instead of following the sequence of the bus codes. Hence, this method can continue calculating the load flow without recoding bus codes when the network structure is changed in the process of feeder reconfiguration. Moreover, an additional forward current sweep is applied in the proposed method so that all harmonic branch currents are calculated. Hence, the proposed method can analyse the load flow quickly and accurately in the distribution network considering system harmonics and distributed generators.

b) Due to the advantages of the ant colony system and discrete particle swarm optimization can be complementary, a hybrid optimization method based on these two methods is proposed by the author in this thesis. The ant colony

system can quickly search for better solutions based on an existing solution, which means that the local search ability of the ant colony system is satisfactory. However, it does not offer a comprehensive search direction. Discrete particle swarm optimization can quickly find feasible solutions in all possible search areas, meaning that the global search ability of particle swarm optimization is satisfactory. However, it lacks the ability to find better solutions based on existing solutions to an acceptable standard. The hybrid method combines the advantages of these two methods so that the optimization ability of the proposed hybrid method is superior to that offered by either of the two methods on their own. Furthermore, an adaptive function is proposed for enhancing the searching ability of the proposed hybrid method by controlling the probability of performing a local or global search.

This hybrid method is tested in small, middle and large size distribution systems respectively. The test results confirm that the hybrid method offers superior performance to either the ant colony system or discrete particle swarm optimization.

c) The proposed hybrid method based on the ant colony system and discrete particle swarm optimization is applied to a large size distribution system to investigate the impacts of system harmonics and the fluctuations of peak load demands and output of the distributed generators over 24 hours on feeder reconfiguration. The load types include residential, commercial, industrial and public lighting. The distributed generators include wind turbines and photovoltaic generators. The test results show that the optimal network structure for minimum network losses can be changed by considering system harmonics. In addition, network losses may increase if the fluctuations of peak load demands and output of the distributed generators are ignored.

1.4 Thesis Structure

Based on the objectives and the proposed methodology, this thesis can be divided into three main parts and is organized into eight chapters. The contents are summarized below

Chapter 1 provides an introduction to the whole thesis. It covers the rationale underpinning this study, research objectives and factors contributing to the success of this thesis.

The first part of the thesis mainly describes the suitable load flow method for feeder reconfiguration considering system harmonics and distributed generators. This part contains Chapter 2 to Chapter 4.

Chapter 2 provides a brief introduction of the main objectives of feeder reconfiguration. The feeder reconfiguration described in this thesis has network loss reduction as its main objective. To calculate the network losses, the widely used backward/forward sweep algorithm in the distribution network is studied in this chapter. Next, the layered method, which divides the network into levels, is applied to this method to avoid recoding the system code when the network structure is changed by the feeder reconfiguration. Finally, the layered backward/forward sweep algorithm is applied to the 12-bus and the 33-bus distribution system to calculate the fundamental load flow.

Chapter 3 presents an overview of the basic harmonic theory which will be used in this thesis. It briefly introduces the definition of harmonics, the harmonic expressions such as Fourier series, and several important formulations and measures for harmonic calculations and analysis. Wind turbines and photovoltaic generators – being the principal renewable sources, distributed generators and the harmonic sources – are described in this chapter. The harmonic distortion limitation standards are also introduced. Finally, a fast harmonic analysis method

based on the backward/forward sweep algorithm and the method to calculate the power loss in cables considering harmonics are presented.

Chapter 4 provides a method for transforming all types of distributed generators to minus load. Then, the distribution networks with a different number of harmonic sources are analysed, leading to the finding that the harmonic branch currents on the tributaries without harmonic sources will be missed by the existing harmonic backward/forward sweep method. Next, an improved harmonic backward/forward sweep method is proposed so that this method can be used to calculate the harmonic load flow for all kinds of distribution network. In the improved method, an additional branch current forward sweep based on system levels is applied to calculate the branch current which belongs to the tributaries without harmonic sources. Distributed generators are taking into consideration in the test networks, and the positions of harmonic sources are selected at random. Finally, this improved method is applied to a 12-bus system to verify its accuracy.

The second part of the thesis mainly describes the optimization methods for feeder reconfiguration. This part contains Chapter 5 and Chapter 6.

Chapter 5 studies the application of the ant colony system and the discrete particle swarm optimization method for distribution network feeder reconfiguration. As there is a risk of deriving an impractical solution, the graphic theory is applied to two methods to minimise this risk. Due to the system parameters of these two methods being determined by experience, the suitable value of these system parameters is determined by applying these two methods to 33-bus and 69-bus distribution systems and analysing the results.

Chapter 6 proposes a hybrid method based on the ant colony system and the discrete particle swarm optimization. The proposed hybrid method combines the advantages of both ant colony system and discrete particle swarm optimization so that its search performance is superior to that offered by either of the two methods

on their own. Furthermore, an adaptive function is proposed for enhancing its search ability. Finally, the proposed hybrid method is applied to 33-bus, 69-bus and 118-bus distribution systems in three different maximum iterations to verify that the accuracy of the hybrid method is higher than the two other methods.

The third part of the thesis mainly investigates the impacts of system harmonics and renewable generators on the distribution network feeder reconfiguration problem. This part contains Chapter 7.

Chapter 7 applies the proposed hybrid method to investigate the impact of system harmonics and distributed generators on the feeder reconfiguration problem. Three different harmonic penetrations on residential, commercial and public lighting load and two different wind turbine and solar generator capacity levels are considered. Moreover, the impacts of variable peak load demands and output of the renewable generators over 24 hours on feeder reconfiguration are also investigated. The 24-hour periods are separated into three segments in line with the demands created by people's lifestyles. In these tests, solar generators are modelled with two sets of parameters, thus creating a summer model and a winter model.

Chapter 8 summarises the conclusions drawn in this thesis and discusses possible future works.

1.5 Associated Publication

P. Zhengrui and K. L. Lo, "A method for harmonic analysis in distribution system with distributed generator" in Power Engineering Conference (UPEC), 2013 48th International Universities', 2013, pp. 1-5.

P. Zhengrui and K. L. Lo, "A harmonic load flow method based on backward/forward sweep algorithm", under preparation.

P. Zhengrui and K. L. Lo, "A hybrid optimization method based on ant colony system and particle swarm optimization", under preparation.

1.6 References

[1] United States Environmental Protection Agency, "Climate Change: Basic Information," https://www3.epa.gov/climatechange/basics/, last data of access 11.06.2016.

[2] G. K. Singh, "Power system harmonics research: a survey," *European Transactions on Electrical Power,* vol. 19, pp. 151–172, 2009.

[3] W. M. Grady and S. Santoso, "Understanding Power System Hannonics," *Power Engineering Review, IEEE,* vol. 21, pp. 8-11, 2001.

[4] G. Mahesh, R. Ganesan, and S. K. Das, "Effects of power harmonics and its control techniques," in *Electromagnetic Interference and Compatibility '99. Proceedings of the International Conference on*, 1999, pp. 400-405.

[5] S. Civanlar, J. J. Grainger, H. Yin, and S. S. H. Lee, "Distribution feeder reconfiguration for loss reduction," *IEEE Transactions on Power Delivery,* vol. 3, pp. 1217-1223, 1988.

[6] T. Lei, Y. Fang, and M. Jingran, "A survey on distribution system feeder reconfiguration: Objectives and solutions," in *Innovative Smart Grid Technologies - Asia (ISGT Asia), 2014 IEEE*, 2014, pp. 62-67.

[7] F. Hosseinzadeh, B. Alinejad and K. Pakfa, "A new technique in Distribution Network reconfiguration for loss reduction and optimum operation," *Electricity Distribution - Part 1, 2009. CIRED 2009. 20th International Conference and Exhibition on, Prague, Czech Republic,* pp. 1-3, 2009.

[8] S. Thiruvenkadam, A. Nirmalkumar and A. Sakthivel, "MVC architecture based neuro-fuzzy approach for distribution feeder reconfiguration for loss reduction and load balancing," *2008 IEEE/PES Transmission and Distribution Conference and Exposition, Chicago, IL,* pp. 1-7, 2008.

[9] M. M. Adibi, "Distribution Feeder Reconfiguration for Service Restoration and Load Balancing," *in Power System Restoration:Methodologies & Implementation Strategies , 1, Wiley-IEEE Press,* pp. 647-652, 2000.

[10] V. C. Veera Reddy, N. Perumal and Y. Rajasekharareddy, "Loss reduction in distribution networks by network reconfiguration: a two stage solution approach," *Power and Energy Conference, 2004. PECon 2004. Proceedings. National,* pp. 241-246, 2004.

[11] M. A. Ghorbani, S. H. Hosseinian and B. Vahidi, "Application of Ant Colony System algorithm to distribution networks reconfiguration for loss reduction," *Optimization of Electrical and Electronic Equipment, 2008. OPTIM 2008. 11th International Conference on, Brasov,* pp. 269-273, 2008.

[12] M. Moga, F. Molnar-Matei and M. Biriescu, "Application software for minimum loss configuration of the distribution networks," *EUROCON 2009, EUROCON '09. IEEE, St.-Petersburg,* pp. 2083-208, 2009.

[13] Y. H. Song, G. S. Wang, A. T. Johns and P. Y. Wang, "Distribution network reconfiguration for loss reduction using fuzzy controlled evolutionary programming," *in IEE Proceedings - Generation, Transmission and Distribution,* vol. 144, pp. 345-350, 1997.

[14] P. Kritavorn, T. Lantharthong and N. Rugthaicharoencheep, "The combined loss reduction approach to apply in distribution system with distribution generation," *TENCON 2014 - 2014 IEEE Region 10 Conference,*

Bangkok, pp. 1-5, 2014.

[15] P. S. Nagendra Rao and K. S. Prakasa Rao, "A fast load flow method for radial distribution systems," *Proceeding of platinum jublee conferance on systems and signal processing,* pp. 471 -474, 1986.

[16] D. Xia and G. T. Heydt, "Harmonic Power Flow Studies - Part II Implementation and Practical Application," *IEEE Transactions on Power Apparatus and Systems,* vol. PAS-101, pp. 1266-1270, 1982.

[17] E. F. Fauchs and M. A. S. Masoum, *Power Quality in Power Systemsand Electrical Machines*: Elsevier, 2008.

[18] K. L. Lian and T. Noda, "A Time-Domain Harmonic Power-Flow Algorithm for Obtaining Nonsinusoidal Steady-State Solutions," *IEEE Transactions on Power Delivery,* vol. 25, pp. 1888-1898, 2010.

[19] Y. Baghzouz, "Effects of nonlinear loads on optimal capacitor placement in radial feeders," *IEEE Transactions on Power Delivery,* vol. 6, pp. 245-251, 1991.

[20] Z. A. Marinos, J. L. R. Pereira, and S. Carneiro, "Fast harmonic power flow calculation using parallel processing," *IEE Proceedings - Generation, Transmission and Distribution,* vol. 141, pp. 27-32, 1994.

[21] A. Ulinuha, M. A. S. Masoum, and S. M. Islam, "Harmonic power flow calculations for a large power system with multiple nonlinear loads using decoupled approach," in *Power Engineering Conference, 2007. AUPEC 2007. Australasian Universities*, 2007, pp. 1-6.

[22] V. Sharma, R. I. Fleming, and L. Niekamp, "An iterative approach for analysis of harmonic penetration in the power transmission networks," *IEEE Transactions on Power Delivery,* vol. 6, pp. 1698-1706, 1991.

[23] B. Stott, "Decoupled Newton Load Flow," *IEEE Transactions on Power Apparatus and Systems,* vol. PAS-91, pp. 1955-1959, 1972.

[24] B. Stott and O. Alsac, "Fast Decoupled Load Flow," *IEEE Transactions on Power Apparatus and Systems,* vol. PAS-93, pp. 859-869, 1974.

[25] R. D. Zimmerman and C. Hsiao-Dong, "Fast decoupled power flow for unbalanced radial distribution systems," *IEEE Transactions on Power Systems,* vol. 10, pp. 2045-2052, 1995.

[26] J. Arrillaga and B. J. Harker, "Fast-decoupled three-phase load flow," *Electrical Engineers, Proceedings of the Institution of,* vol. 125, pp. 734-740, 1978.

[27] H. Ying-Yi, L. Jun-Shin, and L. Chien-Hsun, "Fuzzy harmonic power flow analyses," in *Power System Technology, 2000. Proceedings. PowerCon 2000. International Conference on*, 2000, pp. 121-125 vol.1.

[28] P. Chen, Z. Chen, and B. Bak-Jensen, "Probabilistic load flow: A review," in *Electric Utility Deregulation and Restructuring and Power Technologies, 2008. DRPT 2008. Third International Conference on*, 2008, pp. 1586-1591.

[29] A. A. Romero, H. C. Zini, G. Ratta, and R. Dib, "Harmonic load-flow approach based on the possibility theory," *IET Generation, Transmission & Distribution,* vol. 5, pp. 393-404, 2011.

[30] P. Caramia, G. Carpinelli, T. Esposito, P. Varilone, I. Mastandrea, and F. Tarsia, "Probabilistic harmonic power flow for assessing waveform distortions in distribution systems with wind embedded generation," in *Power Electronics, Electrical Drives, Automation and Motion, 2006. SPEEDAM 2006. International Symposium on*, 2006, pp. 818-823.

[31] T. Esposito, G. Carpinelli, P. Varilone, and P. Verde, "Probabilistic harmonic power flow for percentile evaluation," in *Electrical and Computer Engineering, 2001. Canadian Conference on*, 2001, pp. 831-838 vol.2.

[32] A. Semlyen and M. Shtash, "Principles of modular harmonic power flow methodology," *IEE Proceedings - Generation, Transmission and Distribution,* vol. 147, pp. 1-6, 2000.

[33] G. N. Bathurst, B. C. Smith, N. R. Watson, and J. Arillaga, "A modular approach to the solution of the three-phase harmonic power-flow," in *Harmonics and Quality of Power Proceedings, 1998. Proceedings. 8th International Conference On*, 1998, pp. 653-659 vol.2.

[34] M. Shlash and A. Semlyen, "Efficiency issues of modular harmonic power flow," *IEE Proceedings - Generation, Transmission and Distribution,* vol. 148, pp. 123-127, 2001.

[35] T. Jen-Hao and C. Chuo-Yean, "A fast harmonic load flow method for industrial distribution systems," in *Power System Technology, 2000. Proceedings. PowerCon 2000. International Conference on*, 2000, pp. 1149-1154 vol.3.

[36] T. Jen-Hao and C. Chuo-Yean, "Fast harmonic analysis method for unbalanced distribution systems," in *Power Engineering Society General Meeting, 2003, IEEE*, 2003, pp. 1-1249 Vol. 2.

[37] J. H. Teng and C. Y. Chang, "Backward/Forward Sweep-Based Harmonic Analysis Method for Distribution Systems," *IEEE Transactions on Power Delivery,* vol. 22, pp. 1665-1672, 2007.

[38] A. Ahuja and A. Pahwa, "Using ant colony optimization for loss minimization in distribution networks," in *Power Symposium, 2005.*

Proceedings of the 37th Annual North American, 2005, pp. 470-474.

[39] C. Chung-Fu, "Reconfiguration and Capacitor Placement for Loss Reduction of Distribution Systems by Ant Colony Search Algorithm," *Power Systems, IEEE Transactions on,* vol. 23, pp. 1747-1755, 2008.

[40] W. Yuan-Kang, L. Ching-Yin, L. Le-Chang, and T. Shao-Hong, "Study of Reconfiguration for the Distribution System With Distributed Generators," *Power Delivery, IEEE Transactions on,* vol. 25, pp. 1678-1685, 2010.

[41] W. Wu-Chang and T. Men-Shen, "Application of Enhanced Integer Coded Particle Swarm Optimization for Distribution System Feeder Reconfiguration," *Power Systems, IEEE Transactions on,* vol. 26, pp. 1591-1599, 2011.

[42] A. R. Malekpour, T. Niknam, A. Pahwa, and A. K. Fard, "Multi-Objective Stochastic Distribution Feeder Reconfiguration in Systems With Wind Power Generators and Fuel Cells Using the Point Estimate Method," *Power Systems, IEEE Transactions on,* vol. 28, pp. 1483-1492, 2013.

Chapter 2 Purposes of Feeder Reconfiguration and Load Flow Analysis in Distribution Network.

2.1 Introduction

Load flow calculation is the basis of power system analysis and feeder reconfiguration problem. Researchers have paid much attention to the area of load flow calculation methods in the transmission network. Although standard methods[4], such as Gauss-Seidel[5] and Newton-Raphson[6, 7], are widely used in transmission network load flow calculation, different characteristics between transmission network and distribution network may limit the applying standard methods to distribution network directly.

The first widely used power flow analysis method is the Gauss-Seidel method. This is a simple and easy understand method. However, its convergence speed is very slow. In an ill-condition system, Gauss-Seidel method cannot even converge. One of the ill-conditioned systems is a radial system with relatively long distribution line. And this method cannot be used in such a distribution network. With the fast convergence speed and good applicability, Newton-Raphson method is a common load flow analysis method used nowadays. But, the calculation for elements in Jacobian Matrix slows down the computing speed and also makes this method complex. So, in the transmission system, decoupled method is developed based on Newton-Raphson for reducing the calculation. Although Newton-Raphson can analyse distribution load flow, it is better to find a new way for distribution network analysis. In the process of developing decoupled method, there is an important assumption which is that the reactance of the power line much larger than resistance. However, in the distribution network, the resistance of the power line is

normally close to or larger than reactance. So that, decoupled method cannot be used in the distribution network. Even though researchers try to add compensating reactance to meet the assumption condition, it is still complex to handle this compensating reactance. Thus, developing a special method which is just for the distribution network should be better.

The first method for the radial network is proposed in reference [8], PQ loads are converted into its equivalent impedance. Driving point network admittance is used to calculate the bus voltage directly. Kersting and Mendive used ladder network theory to analyse the radial network[9]. Sun and her colleagues improved Gauss iterative with Z bus which can easily calculate the load flow[10]. The earliest edition of backward/forward sweep algorithm appeared in reference [11]. By using a special coding method, bus voltages are calculated after several backward/forward sweep iterations. Shirmohamadi et al divided the radial network into levels for increased calculation efficiency. The key point of this reference focuses on the weakly meshed system[12]. The quadratic based method was proposed in references [13, 14]. An estimated value of voltage is required in reference [13]. However, in reference [14], the requirement of such an estimated value is avoided so that the convergence and the efficiency of this method are improved. Different from reference [11], a branch current based on backward/forward sweep algorithm was proposed in reference [15]. In this method, branch current is the assumed constant value in backward sweep process. Backward/forward sweep based method for strong meshed network is presented in reference [16]. In this reference, the loops are converted into two branches with two breaking points. Reference [17] combine Z-bus and backward/forward sweep method together. Z-bus handles the ring-net parts and backward/forward sweep handles the radial parts to increase efficiency. References [18, 19] focus on the problem of PV type buses in the distribution network. These two papers are also backward/forward sweep method based. Reference [20] shows a new approach to

incorporate PV-Buses into sweep-based unbalanced distribution system power flow algorithms. Reference [21] consider the effect of dispersed generators base on the backward/forward sweep technology. A node-branch incidence matrix was presented in references [22-24]. The bus voltages can be calculated by this improved backward/forward sweep algorithm in parallel without using special coding method. So this method is particularly suitable for feeder reconfiguration. Backward/forward sweep algorithm is a widely used load flow method especially for distribution network. According to reference [11], this method takes a simple backward and forward sweep in each iteration to calculate the bus voltages and branch currents. It avoids the complex Jacobian Matrix elements calculation process so that the computation efficiency is highly increased and computer memory requirements also reduced. According to the results in section 2.5, after doing few backward/forward sweep iterations, backward/forward sweep algorithm can get the results which meet the engineering requirements.

This chapter mainly introduces the objectives of feeder reconfiguration and backward/forward sweep algorithm. A brief introduction of the main purposes of the feeder reconfigurations is presented in section 2.2. Section 2.3.1 explains that due to high R/X ratio of distribution line and radial network structure of the distribution network, the commonly used load flow methods cannot achieve a good efficiency in distribution networks. The normal backward/forward sweep algorithm which is proposed for distribution network load analysis is introduced in section 2.3.2. In the normal backward/forward sweep algorithm, the power and voltage calculation sequence on each node is based on the buses code. However, system topology will change after feeder reconfiguration. Thus, the original bus sequence is disrupted and the codes on each bus cannot guide calculation sequence anymore. So, a recoding program needs to be done at every single iteration of feeder reconfiguration before doing the load flow calculation. An improved backward/forward sweep algorithm which solved the recoding problem is

described in section 2.4. Section 2.5 is a case study that illustrates the efficiency and accuracy of the proposed method in section 2.4.

2.2 Common Objective of Feeder Reconfiguration

2.2.1 Active Power Loss Reduction

It is reported that active power loss in UK distribution network is estimated about 5.5%[25]. And the loss in China is estimated around 9%[26]. All the research results show that feeder reconfiguration in distribution network for loss reduction can improve power system economically. So, loss reduction is a primary target of feeder reconfiguration. In this study, only the active power loss on distribution lines is considered. Using a mathematical equation to represent the active power loss on distribution line shows in equation 2-1 [27].

$$P_{loss} = \sum_{i=1}^{N_b} R_i \frac{P_i^2 + Q_i^2}{V_i^2} \tag{2-1}$$

Where P_i and Q_i are the real and reactive power on transmission line flowing out of bus i, N_b is the number of branches, R_i is the branch resistance which ends with bus i. V_i is the voltage at bus i.

Due to the apparent power S equal to $\sqrt{P^2 + Q^2}$ and it also equal to VI^*, equation (2-1) can modify as follows.

$$P_{loss} = \sum_{i=1}^{N_b} I_i^2 r_i \tag{2-2}$$

Where I_i is the injection current on bus i.

2.2.2 Load Balancing

Each load may consist of consuming load, industrial load and domestic load in the distribution network. Daily load curves of these loads are entirely different so that the peak load of each feeder will appear at various time in the day. By feeder reconfiguration, parts of the loads can be transferred from the heavily loaded feeders or the overloaded feeders to the light loaded feeders. This transfer of loads not only eliminates overload and balance the line loading but also improves power quality and reduce power loss to a certain extent.

2.2.3 Voltage Profile Improvement

In distribution network, voltage normally drops along the distribution line connecting the substation to the load. In order to avoid excessive voltage drop and maintain the voltage value in a limited range, feeder reconfiguration can be an alternative method in addition to reactive power compensation and voltage regulator. Especially, feeder reconfiguration will have a significant effect, when the voltage drop is caused by overload or long distribution line.

2.2.4 Service Restoration

In an emergency condition, such as a fault, feeder reconfiguration can isolate the fault by changing the status of switches and transfer parts or all loads at the faulted feeder to the normal working feeders. In the concept of the smart grid, feeder reconfiguration can arrange parts of distributed generators to supply an islanding system for ensuring the power supply to maintain the critical area. Such as, hospital or naval shipboard power system[28]. Thus, feeder reconfiguration plays a major role in power restoration.

2.2.5 Multi-Objectives

In common optimization system operation, the voltage limitation must be taken into account during the feeder reconfiguration for loss reduction. Equipment life is also an important economic factor so that the number of switching can be an objective of feeder reconfiguration. Some papers proposed a weight coefficient for each objective. The final objective function will be the sum of each single objective with their weight coefficients[29].

Due to feeder reconfiguration for loss reduction, it can also improve the voltage profile and balance the load to a certain extent. So, loss reduction is also chosen as the target of feeder reconfiguration in this thesis. It shows in equation (2-1) and (2-2) that bus voltages and branch currents in the system are the basic elements for assessing the objective results. The following part of this chapter will introduce the widely used load flow analysis method in the distribution network and its improvement.

2.3 Methods for Load Flow Analysis in Distribution Network

Load flow calculation is the basis of distribution system analysis. Load flow data is necessary for feeder reconfiguration, fault analysis, reactive power optimization and so on. According to the network topology and operation condition, load flow calculation can evaluate all important elements in the system. Such as, voltage magnitude, voltage angle, power distribution and power loss. In feeder reconfiguration, all of these system elements will be calculated many times. So, a suitable method for feeder reconfiguration is very important.

2.3.1 Models and Characteristics of Distribution Network

Power flow calculation has a long history since 1956 by J.B.Ward [30]. Algorithms for power flow calculation developed from Gauss-Seidel iterative method to the Newton-Raphson method and then to the fast decoupled P-Q method[31]. Researchers have already developed a variety of effective load flow calculation methods. However, all of these methods generally only applied to the transmission network.

Distribution networks normally operate in open-loop and the loop is closed only in switching load or fault situation. The size of distribution line in the distribution network is smaller when compared with a transmission line in the transmission network. It leads to that the R/X ratio of the distribution network is higher. Table 2.1 shows typical electrical parameters of overhead lines and underground cables[32]. R/X ratio is smaller 1 when system voltage is higher than 20kV. If the system voltage is equal or lower than 20kV, R/X ratio is usually larger than 1.

Distribution line normally less than 100km and its system voltage is normally smaller than 60kV[1]. In this kind of distribution line, its length is far small than an electromagnetic wavelength (600km) and the system voltage is low when comparing with the transmission system. The corona phenomenon hardly occurs so that conductance parameters are ignored. Also, because of the low system voltage, capacitor current is small. The electrical admittance parameters caused by the small capacitor current is negligible. Then, the distribution line can be expressed by $R + jX$.

Table 2-1 Typical electrical parameters of overhead lines and underground cables[1]

Type	System Voltage (kV)	Phase conductor Al/Fe,(mm^2)	Resistance Ω/km ($+20^{\circ}C$)	Reactance Ω/km (50Hz)
Overhead line	0.4	25/0	1.06	0.30
Overhead line	0.4	50/0	0.64	0.28
Overhead line	0.4	35/0	0.87	0.1
Underground cable	0.4	120/0	0.25	0.07
Overhead line	11	50/0	0.64	$\cong 0.4^{*}$
Underground cable	11	185/0	0.16	0.08
Overhead line	20	54/0	0.54	$\cong 0.4^{*}$
Underground cable	20	120/0	0.25	0.11
Overhead line	110	242/39	0.12	$\cong 0.4^{*}$

* Value depends om spacing and cross arm construction

Another significant characteristic of the distribution system is that its structure is radial or weak-mesh. This is one of the ill-conditions of the Gauss-Seidel Method. In the case of the radial distribution system, the system Jacobian matrix is usually ill-conditioned because of high R/X ratio in line segments. This causes a lack of diagonal dominance of the system Jacobian[33]. And, R/X ratio near to zero is the premise conditions of the fast decoupled P-Q method [1]. Characteristics of the distribution system hinder the classical algorithms, but, in another hand, radial structure means the connection between each feeder is weak and high R/X ratio simplifies the model of the distribution line. According to these characteristics of the distribution network, a method with simple backward and forward sweep process is described in details in reference [11]. Although it can only use in the distribution network, backward/forward sweep algorithm and its improvement edition are widely applied in the distribution network calculation because its fast calculation speed and good convergence.

The normal assumption of a balanced three phase load on the system is also

assumed in this thesis when preforming load flow calculation. It is defined that power distribution at each load is considered as known and constant.

2.3.2 Backward/Forward Sweep Algorithm[11]

Backward/forward Sweep Algorithm takes a simple backward and forward sweep process base on Ohm's law in each iteration for calculating all node voltages. In the backward sweep, branch currents in the network are calculated according to the assumption that all initial bus voltages are equal to the source voltage and loads power on each bus are known. In the forward sweep that follows, the calculated branch currents are assumed to be constant and used to compute the new buses voltage. These two steps are defined as one iteration. When the difference of node voltages on the same bus between two successive iterations is sufficiently smaller than a tolerance value which is set in advance, the voltage values are considered to be acceptable results.

A simple radial feeder distribution network which is used to elaborate on backward/forward sweep algorithm is shown in Figure 2-1.

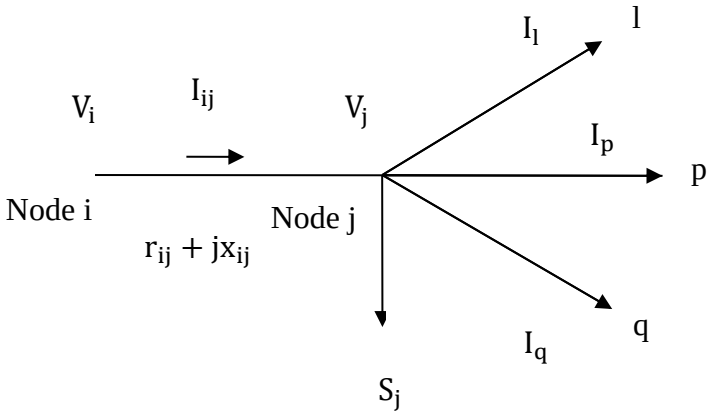

Figure 2-1 Simple radial feeder distribution network

The steps of backward/forward sweep algorithm are as follows:

1. Assigned the initial voltage value to the source bus and assumed that all buses voltage is equal to source bus voltage. Generally, backward/forward method can use rated values as its initial value. So, it can be assigned that $\dot{V}_i = V_N \angle 0^\circ$. Where V_N is rated value of the voltage.

2. In the backward sweep, calculations of current distribution using equation (2-3) from the end node to the source node in each of the lines.

$$\dot{I}_{ij}^{(k)} = \dot{I}_j^{(k)} + \sum_{m \in N_j} \dot{I}_{jm}^{(k)} = \frac{P_j - jQ_j}{\dot{V}_j^{*(k)}} + \sum_{m \in N_j} \dot{I}_{jm}^{(k)} \tag{2-3}$$

Where I_{ij} is the current on branch ij, $\dot{I}_j$ is the load current output from node j. If node j is a sending node, then N_j is the set of the receiving nodes which connects with node j. m is one node belongs to the set of N_j. P_j and Q_j are the active and reactive power of loads of node j. $\dot{V}_j^*$ is the conjugate voltage on node j. And k is the iteration orders.

3. In the forward sweep, calculations of node voltage using equation (2-4) start at the source node to the end node of in each of the lines.

$$\dot{V}_j^{(k)} = \dot{V}_i^{(k)} - \dot{I}_i^{(k)}(r_{ij} + jx_{ij}) \tag{2-4}$$

4. Convergence. This is done by comparing the maximum difference value of voltage magnitude between the last two iterations to be within a tolerance value ε. If $\max|\Delta V_i| < \varepsilon$, then the calculation is terminated. If $\max|\Delta V_i| \geq \varepsilon$, then, repeat the procedure for the next iteration calculation.

$$\max\left\{\left|\dot{V}_i^{(k+1)} - \dot{V}_i^{(k)}\right|\right\} < \varepsilon \tag{2-5}$$

The flow chart of backward/forward sweep algorithm shows in figure 2-2.

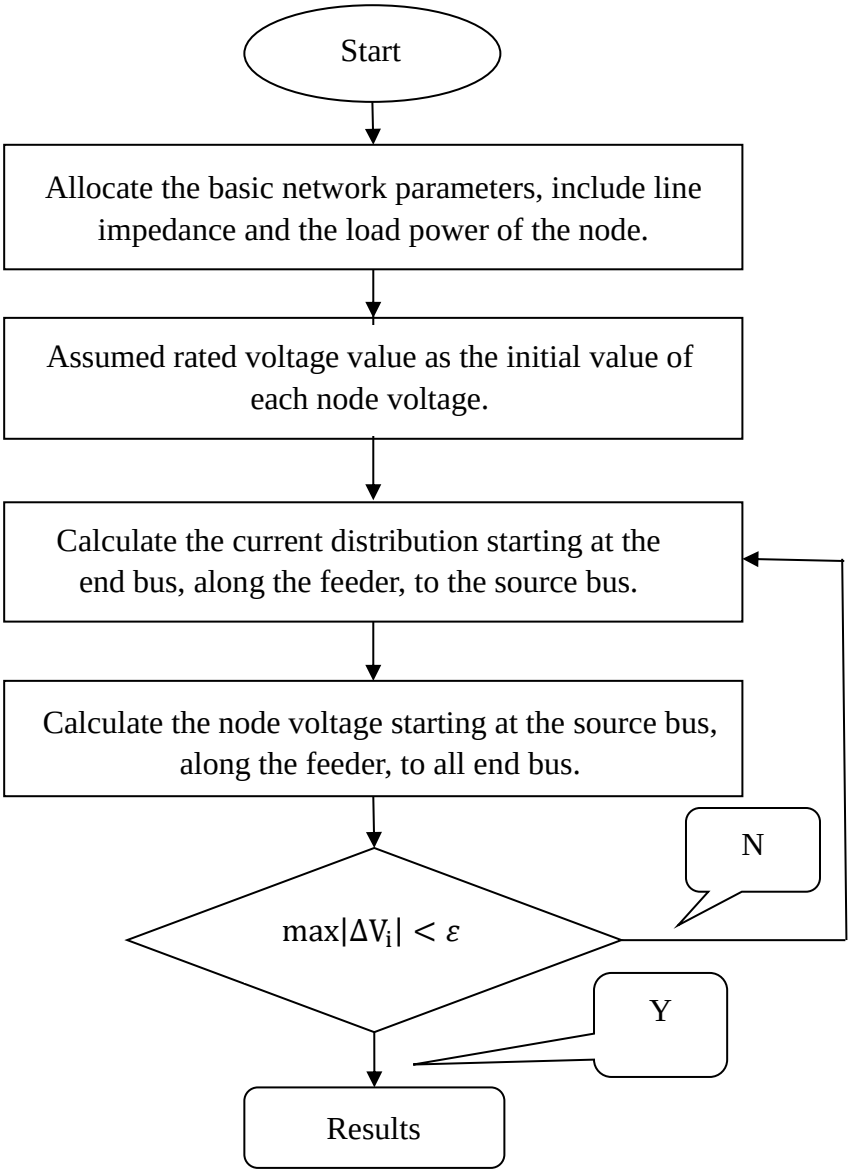

Figure 2-2 Step of backward/forward sweep method

Results of backward/forward sweep algorithm contain not only system nodes voltage but also node voltage angle and system branch currents. Then, system power loss can be calculated by equation 2-1 or 2-2.

2.4 Backward/Forward Sweep Algorithm in Feeder Reconfiguration

In the process of the feeder reconfiguration, the status of tie switches and sectionalizing switches are assumed to be changed. When the status of these switches changed, the topology of the system network is also changed, which means a new distribution network topology has been established. Backward/forward sweep algorithm uses a special coding method for all nodes to calculate the bus voltages in paper [11], which involves recoding network in every single calculation process. Paper [12] proposed a method of layered node system at several levels. To some extent, the method improves the calculation efficiency. However, it has not yet been solving the recoding problem when applying backward/forward sweep algorithm in feeder reconfiguration. In paper [22-24], node-branch incidence matrix, which represents system topology in a matrix, is proposed to avoid recoding process when system structure changes. Furthermore, this matrix will guide the algorithm to calculate branch currents and bus voltages with the same level. It also increases calculation efficiency.

The method in reference [22-24] will be introduced in following. Figure 2-3 shows a 12-bus tree network. The coding method of buses and branches are natural integer coding method which means code starts from 1 and all code is natural number. The maximum code number is equal to the number of the buses or branches. The code on bus or branch is randomly. There is no relationship between code and network structure. Furthermore, the largest node code and branch code must equal to the total number of buses and branches respectively. When the system structure is

transferred into the matrix, the number of the rows and columns in this matrix is continuous positive integer. If the largest node code was larger than the total number of buses, parts of the codes had no corresponding node in the system. But, these node codes still occupy the position in this matrix. These part of codes will waste computer memory.

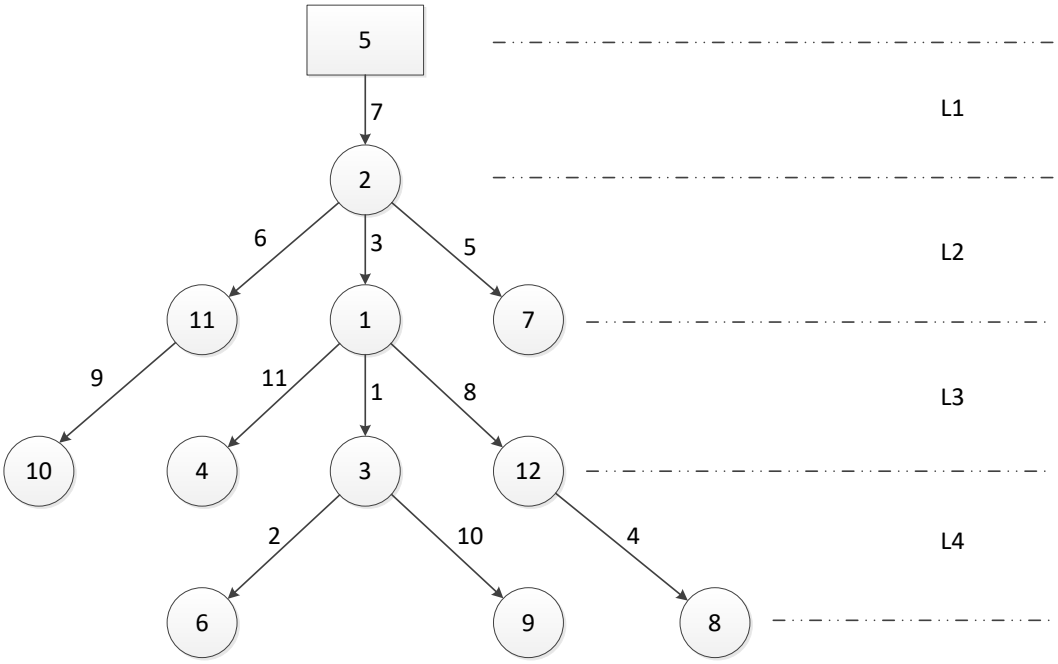

Figure 2-3 12-bus distribution network

Figure 2-3 shows a distribution network branches supported within levels. In this 12-bus network, it can be seen that the branch 6, 5 and 3 belong to the same level. So, the equivalent current and the voltage drop can be calculated simultaneously. Similarly, branch 9, 11, 1 and 8 are also at the same level. Its equivalent current and voltage drop also can be calculated at the same time. Thus, according to Figure 2-3, it can visually be seen that the network is split into four levels. The situation of branches in each layer and starting and ending bus of each branch are also known[34]. Following the sequence of these system levels, branch currents and node voltages can be calculated. The improvement of this method is using the level

number instead of the code number to guide the sequence of the calculation. In this mode, no matter how the structure changes, the system levels always start at level one on the source node and terminate following the sequence of natural number. Current backward calculated from the largest system level to level one and voltage forward calculated from level one to the largest network level. Thus, code on nodes or branches has no relationship with the calculation sequence anymore. So, this improvement solves the problem that backward/forward sweep algorithm need to recode the system after each feeder reconfiguration iterations. How this improved algorithm works is outlined in details in the following section.

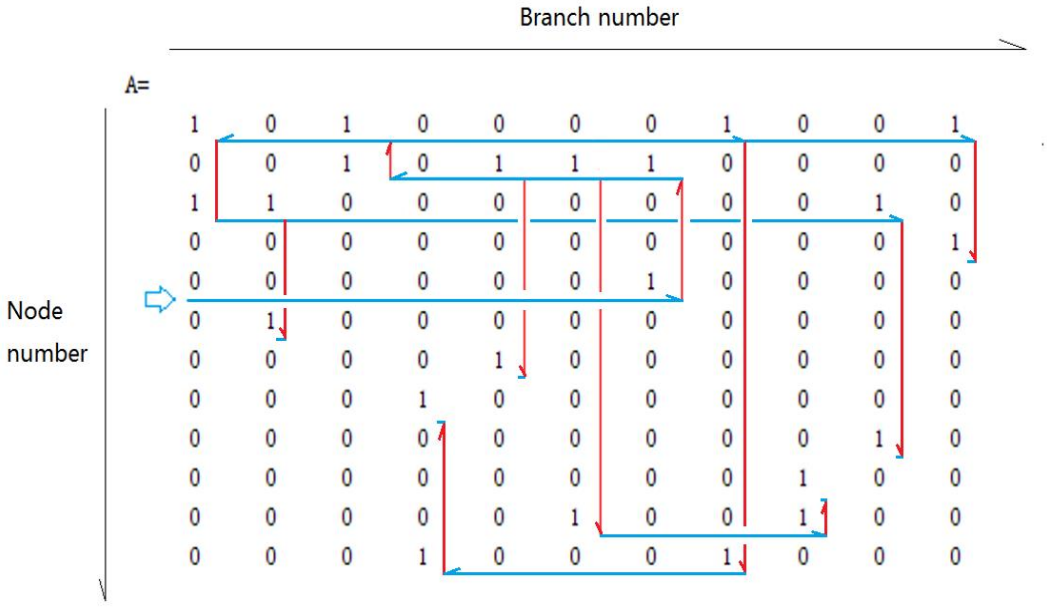

Figure 2-4 Node-branch incidence matrix

Figure 2-4 is the node-branch incidence matrix of the 12-bus distribution system which is shown in Figure 2-3. Due to this method is applied by Matlab software, matrices are used to explain the system structure to the computer. To achieve this method, several matrices should be established for the relationship between nodes, branches and levels. First of all, the node-branch incidence matrix is established.

This matrix is similar to the normal node-branch incidence matrix. However, it is unnecessary to use '-1' to express the direction of the branch current. Because the distribution network will be divided into levels by this method, in order to express the system levels to the computer, node and branch hierarchical matrix must be established. Figure 2-4 with the blue and red line are used to explain how to establish these two matrices. In node-branch incidence matrix, the number of the row is the same as the code number of the node and the number of the column is the same as the code number of the branch. Then, it is defined that the blue and red line represents node and branch respectively in Figure 2-4. It can be seen from top to bottom in Figure 2-3, the system is node 5 and branch 7 are belong to the first system level. Thus, the blue line is drawn start at row 5. When the line arrival at column 7, it will turn red and draws following the column 7. The second level in Figure 2-3 contains node 2 and branch 3, 5 and 6. Thus, when the red line draws at row 2, it needs to turn blue again and draws following the row in matrix. Due to 3 branches are connected to the node 2 in the second level, the blue line will need to turn red three times at column 3, 5 and 6 respectively. Then, do the same steps until all system levels are mentioned. Under these steps, the node and branch hierarchical matrix can be built and the computer will understand the system level according to these two matrices.

Table 2-2 Branch hierarchical matrix

B Matrix	Branches in each level			
System Branch Levels	7			
	3	5	6	
	1	8	9	11
	2	4	10	

Table 2-3 Node hierarchical matrix

N Matrix	Nodes in each level			
System Node Levels	5			
	2			
	1	7	11	
	3	12	10	4
	6	8	9	

Although the levels of the system are defined, the relationship between node and node, branch and branch is also important. Without this relationship, it cannot identify that which branches belong to the same feeder tributary and which node is the sending node or receiving node of branches. Table 2-4 indicates the relationship between nodes. This node level incidence matrix transforms from node-branch incidence matrix. In this matrix, the column still means the code number of branches. However, the elements in the first row of the matrix are the codes of the sending nodes and the elements in the second row of the matrix are the codes of the receiving nodes. Then, all elements in the first row are the code number of sending nodes and the elements in the second row is the code number of receiving nodes.

Table 2-4 Node level incidence matrix

S&E	Location of the column is the branch code										
Sending Node	1	3	2	12	2	2	5	1	11	3	1
Receiving Node	3	6	1	8	7	11	2	12	10	9	4

The relationship between branches represents in branch level incidence matrix which is shown in Table 2-5. In this matrix, the meaning of the row in the matrix is the following branch and the meaning of the column is the upper branch. For instance, the value 1 in the 1st row and the 3rd column means branch 1 follows after branch 3. The value 0 represents that there is not any connection between its corresponding upper and following branch.

Table 2-5 Branch level incidence matrix

Branch level incidence matrix	upper branch										
Following branch	0	0	1	0	0	0	0	0	0	0	0
	1	0	0	0	0	0	0	0	0	0	0
	0	0	0	0	0	0	1	0	0	0	0
	0	0	0	0	0	0	0	1	0	0	0
	0	0	0	0	0	0	1	0	0	0	0
	0	0	0	0	0	0	1	0	0	0	0
	0	0	0	0	0	0	0	0	0	0	0
	0	0	1	0	0	0	0	0	0	0	0
	0	0	0	0	0	1	0	0	0	0	0
	1	0	0	0	0	0	0	0	0	0	0
	0	0	1	0	0	0	0	0	0	0	0

In this improved method, backward sweep starts at the last level of branch hierarchical matrix. Branch currents at this level will be calculated and add to the upper level according to the branch level incidence matrix. The calculation is terminated at the first level of branch hierarchical matrix. When the backward

sweep ends, forward sweep starts at the first level of node hierarchical matrix. The node voltages at the second level will be calculated according to the node level incidence matrix which indicates the sending and receiving nodes. This is one iteration of the improved backward/forward sweep algorithm. The rest part of this algorithm is the same as the normal one.

Depending on the characteristics of the backward/forward sweep algorithm and system structure, each branch current is calculated by summing the current of those branches that follow and the injection current at its receiving node during the backward sweep. Each bus voltage is decided by the frontal bus voltage and the voltage drop of the distribution line in the forward sweep. Such characteristics limit current backward and voltage forward on the different branch cannot be operated simultaneously. Nevertheless, on the other hand, it also shows that there is no backward and forward linkage between the current of branches on the same level if the branches are sorted by layers. Thus, parallel calculation of current or voltage on the same level can be achieved.

The parallel calculation can avoid low efficiency model that only one branch current or bus voltage is computed after searching one receiving node of a branch. The layered network also significantly reduces the search area for receiving node of each branch. After avoiding the recoding process and calculating bus voltages and branch currents parallel. Moreover, in this way, the efficiency of backward/forward sweep algorithm is highly increased in feeder reconfiguration.

2.5 Case Study in 12-Bus System.

The above theory is programmed using Matlab, and the results of the 12 bus distribution network are illustrated in figure 2-1. The system capacity is 15MVA and the rated voltage is 23kV.

Table 2-6 12-bus test results

Layer B/F sweep method			Reference [2]		
Node no.	Voltage magnitude	Phase angle	Node no.	Voltage magnitude	Phase angle
5	1.000000	0.00000	5	1.000000	0.00000
2	0.997180	-0.24706	2	0.997184	-0.26469
11	0.996418	-0.26523	11	0.996423	-0.26486
1	0.994869	-0.43454	1	0.994883	-0.43403
7	0.995562	-0.26493	7	0.995567	-0.26469
10	0.995656	-0.28343	10	0.995561	-0.28306
4	0.994161	-0.45449	4	0.994176	-0.45411
3	0.993976	-0.50736	3	0.993995	-0.50679
12	0.993531	-0.46652	12	0.993545	-0.46599
6	0.993021	-0.53023	6	0.993040	-0.52965
9	0.991875	-0.53063	9	0.991895	-0.53022
8	0.992193	-0.49858	8	0.992208	-0.49804

The first three columns in Table 2-6 show the test results using the above method. The final three columns show the results which are obtained from the same distribution network in reference [2] for comparison purposes. It can easily be seen that both voltage magnitude and phase angle are almost the same within an acceptable tolerance. The proposed method is simple to program and parallel calculation in the same feeder level can be done. Furthermore, it does not need to recode when the network topology is changed.

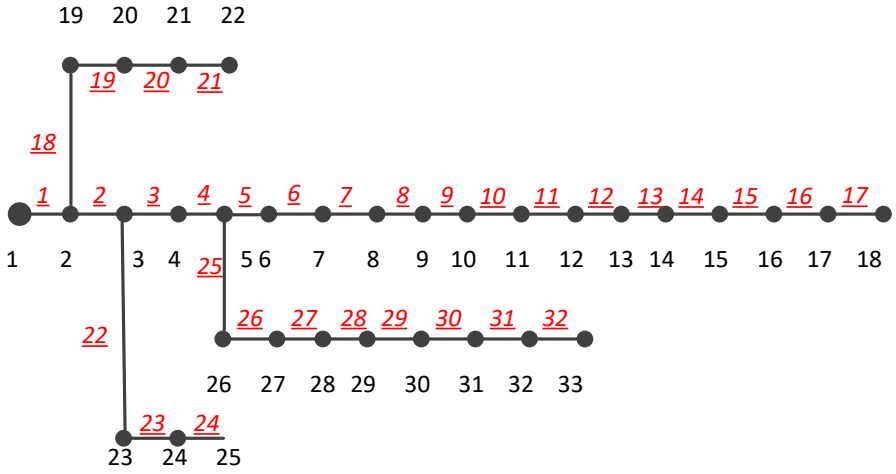

Figure 2-5 IEEE 33-bus syste

Table 2-7 33-Bus test results

Node no.	Voltage magnitude		Node no.	Voltage magnitude	
	Layer B/F sweep	Reference [3]		Layer B/F sweep	Reference [3]
1	1	1	18	0.91402	0.91253
2	0.99768	0.99703	19	0.99715	0.99650
3	0.98359	0.98278	20	0.99357	0.99292
4	0.97612	0.97526	21	0.99287	0.99222
5	0.96873	0.96783	22	0.99223	0.99158
6	0.95034	0.94910	23	0.98001	0.97920
7	0.94686	0.94561	24	0.97334	0.97252
8	0.94202	0.94077	25	0.97002	0.96920
9	0.93575	0.93450	26	0.94841	0.94717
10	0.92994	0.92869	27	0.94585	0.94461
11	0.92908	0.92783	28	0.93442	0.93303
12	0.92759	0.92633	29	0.92621	0.92481
13	0.92148	0.92021	30	0.92265	0.92125
14	0.91921	0.91794	31	0.91850	0.91708
15	0.91780	0.91653	32	0.91758	0.91617
16	0.91643	0.91516	33	0.91730	0.91588
17	0.91441	0.91313			

Table 2-8 Results comparisons of two methods

System	Layer B/F sweep method		Normal B/F sweep method		Computing time reduction in percentages (%)
	Iteration	Time(s)	Iteration	Time(s)	
12-bus	3	0.0268	4	0.0284	5.6
33-bus	3	0.0347	5	0.0496	26.0
69-bus	4	0.0451	5	0.1036	43.5

Another test is performed on the IEEE 33-bus system to verify the method accuracy again. System structure and code are presented in figure 2-5 and Appendix A.1 respectively. The results are shown in Table 2-7. The voltage phase angle cannot be compared because its value is not shown in reference [3]. In Table 2-7, the largest gap between two results is at the bus 33. Its value is 0.00142. This gap is appropriately 0.15% base on the bus voltage which calculated by layered backward/forward sweep algorithm. Thus, the calculation of the voltage magnitude is accurate.

To compare the efficiency and convergence property, the results of power flow calculation in the same convergence precision in 12-bus, IEEE 33-bus and IEEE 69-bus are shown in Table 2-8. The improvements of backward/forward sweep algorithm not only decrease the number of convergence iteration but also reduce the total computing times. In the proposed method, the establishment of matrixes for solving the recoding problem occupies a large part of the computing time. So, the gap of total computing time between two methods in a small system is not noticeable. However, with the increasing size of the distribution system, a considerable computing time can be saved.

2.6 Summary

This chapter presents the main objective of feeder reconfiguration: active power loss, load balancing, voltage profile, service restoration and multi-objective. When feeder reconfiguration is done for active power loss, the results will have an effect on the voltage profile and load balancing. As a primary target of feeder reconfiguration, this thesis mainly discusses how to reduce active power loss.

Characteristics of distribution network are not the same with transmission system including radial network topology, high R/X ratio of distribution line and all system bus voltages can be assumed as the same at beginning of the iteration calculation. To calculate the distribution system bus voltages, backward/forward sweep algorithm which considers the network characteristics of the system is more suitable than those commonly used load flow methods in the transmission system. The method mentioned in this chapter can perform load flow within few iterations by simple branch currents and bus voltages sweep. The calculation sequence from source bus to ending buses is the key of this sweep. However, feeder reconfiguration will change the system structure so as to the sequence of buses are changed. So, codes on buses and branches need to be recoded on every single iteration of reconfiguration.

The Improved backward/forward sweep algorithm represent the network topology by a node-branch incidence matrix. This matrix not only shows the relationship of all branches and buses in the network but also divides the network into several levels. This algorithm can compute the bus voltages and branch currents parallel at the same level so that the computing time is reduced. On the other hand, load flow calculation follows the sequence of network levels instead of the sequence from source bus to end buses. Recoding problem is solved and so that it greatly increases the efficiency of backward/forward sweep algorithm in feeder reconfiguration. The

detailed results of the 12-bus system and IEEE 33-bus system in this chapter support the good accuracy of the backward/forward sweep algorithm and its fast convergence speed is verified by the results in Table 2-8.

2.7 Reference

[1] M. S. S. J.Duncan Glover, Thomas J.Overbye, *Power System Analysis and Design*. USA: Westgroup, 2009.

[2] B. C. Dan Wang, "A New Coding Method for Power Flow Calculation in Distribution Network," *Power System and Its Automatic,* vol. 15, pp. 22-26, 2003.

[3] S. K. Goswami and S. K. Basu, "A new algorithm for the reconfiguration of distribution feeders for loss minimization," *IEEE Transactions on Power Delivery,* vol. 7, pp. 1484-1491, 1992.

[4] J. Zhu, "Power Flow Analysis," in *Optimization of Power System Operation*, ed: Wiley-IEEE Press, 2015, pp. 1-664.

[5] G. M. Gilbert, D. E. Bouchard, and A. Y. Chikhani, "A comparison of load flow analysis using DistFlow, Gauss-Seidel, and optimal load flow algorithms," in *Electrical and Computer Engineering, 1998. IEEE Canadian Conference on*, 1998, pp. 850-853 vol.2.

[6] E. Acha and B. Kazemtabrizi, "A New STATCOM Model for Power Flows Using the Newton–Raphson Method," *Power Systems, IEEE Transactions on,* vol. 28, pp. 2455-2465, 2013.

[7] E. Acha, B. Kazemtabrizi, and L. M. Castro, "A New VSC-HVDC Model for Power Flows Using the Newton-Raphson Method," *Power Systems, IEEE Transactions on,* vol. 28, pp. 2602-2612, 2013.

[8] R. Berg, E. S. Hawkins, and W. W. Pleines, "Mechanized Calculation of Unbalanced Load Flow on Radial Distribution Circuits," *Power Apparatus*

and Systems, IEEE Transactions on, vol. PAS-86, pp. 415-421, 1967.

[9] W. H. Kersting, "A Method to Teach the Design and Operation of a Distribution System," *Power Apparatus and Systems, IEEE Transactions on,* vol. PAS-103, pp. 1945-1952, 1984.

[10] D. I. H. Sun, S. Abe, R. R. Shoults, M. S. Chen, P. Eichenberger, and D. Farris, "Calculation of Energy Losses in a Distribution System," *Power Apparatus and Systems, IEEE Transactions on,* vol. PAS-99, pp. 1347-1356, 1980.

[11] P. S. Nagendra Rao and K. S. Prakasa Rao, "A fast load flow method for radial distribution systems," *Proceeding of platinum jublee conferance on systems and signal processing,* pp. 471 -474, 1986.

[12] D. Shirmohammadi, H. W. Hong, A. Semlyen, and G. X. Luo, "A compensation-based power flow method for weakly meshed distribution and transmission networks," *Power Systems, IEEE Transactions on,* vol. 3, pp. 753-762, 1988.

[13] G. X. Luo and A. Semlyen, "Efficient load flow for large weakly meshed networks," *Power Systems, IEEE Transactions on,* vol. 5, pp. 1309-1316, 1990.

[14] R. J. R. Kumar and P. S. Nagendra Rao, "A new successive displacement type load flow algorithm and its application to radial systems," in *Electrical Energy Systems (ICEES), 2014 IEEE 2nd International Conference on*, 2014, pp. 15-19.

[15] B. Das, "Radial distribution system power flow using interval arithmetic", International Journal of Electrical Power & Energy Systems," *International Journal of Electrical Power & Energy Systems,* vol. 24, pp. 827 -836, 2002.

[16] W.C. Wu and B.M. Zhang, "A three-phase power flow algorithm for distribution system power flow based on loop-analysis method," *International Journal of Electrical Power & Energy Systems,* vol. 30, pp. 8 -15, 2008.

[17] J. He, B.-x. Zhou, Q. Zhang, Y.-c. Zhao, and J.-h. Liu, "An Improved Power Flow Algorithm for Distribution Networks Based on Zbus Algorithm and Forward/Backward Sweep Method," in *Control Engineering and Communication Technology (ICCECT), 2012 International Conference on*, 2012, pp. 1-4.

[18] C. S. Cheng and D. Shirmohammadi, "A three-phase power flow method for real-time distribution system analysis," *Power Systems, IEEE Transactions on,* vol. 10, pp. 671-679, 1995.

[19] Y. Zhu and K. Tomsovic, "Adaptive power flow method for distribution systems with dispersed generation," *Power Delivery, IEEE Transactions on,* vol. 17, pp. 822-827, 2002.

[20] U. Eminoglu and M. H. Hocaoglu, "Three-Phase Controlled-Q Updating Method for Forward/Backward Sweep-Based Distribution Systems Power Flow Algorithms," in *Power Tech, 2007 IEEE Lausanne*, 2007, pp. 380-384.

[21] J.-j. Wang, L. Lu, J.-Y. Liu, and S. Zhong, "Reconfiguration of Distribution Network with Dispersed Generators Based on Improved Forward-Backward Sweep Method," in *Power and Energy Engineering Conference (APPEEC), 2010 Asia-Pacific*, 2010, pp. 1-5.

[22] YAN Wei, LIU Fang, WANG Guan-jie, XU Guo-yu, HUANG Shang-lian, "Layer-by-layer Back/forward Sweep Method for Radial Distribution Load Flow," *[Online].Available: http://en.cnki.com.cn/Article_en/CJFDTOTAL-ZGDC200308015.htm*, last data of access 10.11.2015.

[23] S. S. W. X. R. Huaipu, "Power Flow Calculation for Radial Network Based on Layered Forward and Backward Substitution with Branch Current," *[Online].Available: http://d.wanfangdata.com.cn/periodical/xbdljs201108011*, last data of access 10.11.2015.

[24] W. T. Limei Zhang, Honghao Guan, "The Back/Forward Sweep-based Power Flow Method for Distribution Networks with DGs," *the International Conference on Power Electronics and Intelligent Transportation System,* 2009.

[25] Ofgem, "Electricity Distribution Loss Percentages by Distribution Network Operator (DNO) Area," *[Online].Available: https://www.ofgem.gov.uk/ofgem-publications/43516/distribution-units-and-loss-percentages-summary.pdf*, last data of access 10.11.2015.

[26] P. B. Jian Liu, Wenyu Yang, "Theory and Application in Distribution Network (in Chinese)," *China's Water Conservancy And Hydropower Press,* pp. 36-41, 2007.

[27] W. Yuan-Kang, L. Ching-Yin, L. Le-Chang, and T. Shao-Hong, "Study of Reconfiguration for the Distribution System With Distributed Generators," *Power Delivery, IEEE Transactions on,* vol. 25, pp. 1678-1685, 2010.

[28] K. L. Butler-Purry and N. D. R. Sarma, "Self-healing reconfiguration for restoration of naval shipboard power systems," *Power Systems, IEEE Transactions on,* vol. 19, pp. 754-762, 2004.

[29] A. Swarnkar, N. Gupta, and K. R. Niazi, "Reconfiguration of radial distribution systems with fuzzy multi-objective approach using adaptive particle swarm optimization," in *Power and Energy Society General*

Meeting, 2010 IEEE, 2010, pp. 1-8.

[30] D. L. Johnson and J. B. Ward, "The Solution of Power System Stability Problems by Means or Digital Computers [includes discussion]," *Power Apparatus and Systems, Part III. Transactions of the American Institute of Electrical Engineers,* vol. 75, p. 1, 1956.

[31] Z. W. Yangzhan He, *Power System Analysis*, 3 ed. vol. 2. Wuhan: Huazhong University of Science and Technology Publishing House, 2001.

[32] Erkki Lakervi , E. J. Holmes, *Electricity Distribution Network Design*, 2 ed. London: Peter Peregrinus Ltd, 1995.

[33] M. Abdel-Akher, "Voltage stability analysis of unbalanced distribution systems using backward/forward sweep load-flow analysis method with secant predictor," *Generation, Transmission & Distribution, IET,* vol. 7, pp. 309-317, 2013.

[34] P. Zhengrui and K. L. Lo, "A method for harmonic analysis in distribution system with distributed generator," in *Power Engineering Conference (UPEC), 2013 48th International Universities'*, 2013, pp. 1-5.

Chapter 3 Harmonic Analysis in Feeder Reconfiguration

3.1 Introduction

In the past decades, a major part of the domestic and commercial loads are linear loads. So, researches on feeder reconfiguration problems typically consider the fundamental system condition. Nowadays, power electronic devices are widely installed in the power network, such as control of furnaces and electrical machines [5]. Especially, with the growth of green energy, the number of converters which transform DC to AC for the wind and photovoltaic generators is increased in the distribution system. Although they are used for seeking higher system reliability and efficiency, they produce a large number of power system harmonic. The effects of power system harmonic are the power loss in equipment and power transmission line, reduction of equipment life, overheating of neutral wires and transmission and producing series or parallel harmonic resonant and leading to equipment damage because of over-voltage or over-current[6-8]. Even if the harmonic filter can reduce a large amount of power system harmonic, it may still have a big influence on the feeder reconfiguration problem. In order to solve the distribution system feeder reconfiguration problem in a more realistic power system environment, system harmonics should be considered.

The main purpose of this thesis is solving the feeder reconfiguration problem so that the knowledge of power system harmonic will not be introduced in all aspect in this chapter. Only the parts of system harmonic analysis knowledge which may relate to the distribution network feeder reconfiguration will be mentioned. For example, the backward/forward sweep method has proved to be a high-efficiency load flow method for feeder reconfiguration in the distribution network. Especially,

the layered based backward/forward sweep method can avoid system recoding after each reconfiguration iteration. This method has introduced in section 2.4. The other method may reduce the computing efficiency but then cannot handle the system recoding problem easily. Therefore, the layered method is necessary for solving the distribution network feeder reconfiguration problem. For this reason, the backward/forward sweep based load flow method is the priority choice for solving the feeder reconfiguration considering harmonics. Thus, only backward/forward sweep based fast harmonic analysis method is introduced in details in this chapter.

The definition, the characteristics and the measurement of the harmonics are the basic knowledge for power system harmonic analysis. This information is introduced from section 3.2.1 to section 3.2.4. The harmonic distortion limit standard is provided in section 3.2.5. These standards are the limitation which is constituted to judge the system harmonic content is acceptable or not. Considering harmonics, the system component models will be different from the one on fundamental frequency. So, how to simulate system models under harmonics will be described in section 3.3.1. The models of the harmonic source are important information for harmonic analysis. Part of harmonic sources which appear in recent years are shown in section 3.3.2. In section 3.4, backward/forward based harmonic analysis method for the distribution network is illustrated in details. In section 3.5, the method for calculating the power loss in power cable considering the effect of system harmonics is introduced.

3.2 Basic Knowledge of Harmonic

3.2.1 Definition of Harmonics

The common definition for a harmonic in the power system is “a sinusoidal

component of a periodic wave or quantity having a frequency that is an integral multiple of the fundamental frequency [9]". Normally, the frequency of the power system is 50Hz in large part of the world. However, it is 60Hz in America and Japan [10]. In the power system, the stable voltage and current are expected to be a sine wave. But, the power system always contains kinds of the nonlinear load so that system will produce harmonics. Harmonics in power network include integer harmonic, inter harmonic[11] and sub harmonic[12]. Integer harmonic is sinusoidal periodical waves having frequencies which are integral multiple of the fundamental frequency and can be expressed by equation 3-1[9].

$$f^{(h)}(t) = A^{(h)} * \sin\left(2\pi hft + \alpha^{(h)}\right) \tag{3-1}$$

Where A is the harmonic amplitude. f is the fundamental frequency. h is an integer which shows the harmonic order. And α is the harmonic phase angle.

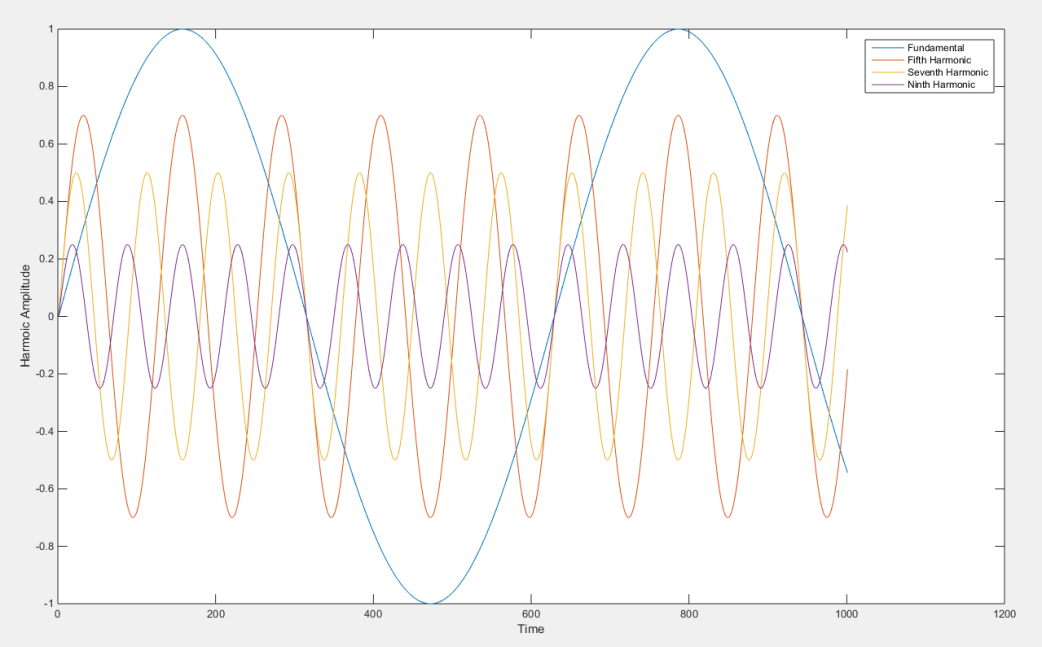

Figure 3-1 First, fifth, seventh and ninth harmonic waveforms

The different inter harmonic waveforms are shown in Figure 3-1.

The inter harmonic and sub harmonic can also be expressed by equation 3-1. But, the value of the h is different. If the h is non-integer and larger than fundamental frequency (e.g. $h = 1.3,1.7,2.5, ...$), the inter harmonic is expressed by equation 3-1. If the h is non-integer and smaller than fundamental frequency(e.g. $0 < h < 1$), the sub harmonic is expressed by equation 3-1. Both of them are the uncommon type of harmonic. Thus, they will not be discussed in this thesis.

3.2.2 Harmonic Expression

Due to the installations of nonlinear devices, the stable system voltage and current wave are non-sinusoidal. The waveform in Figure 3-2 is a typical non-sinusoidal harmonic waveform.

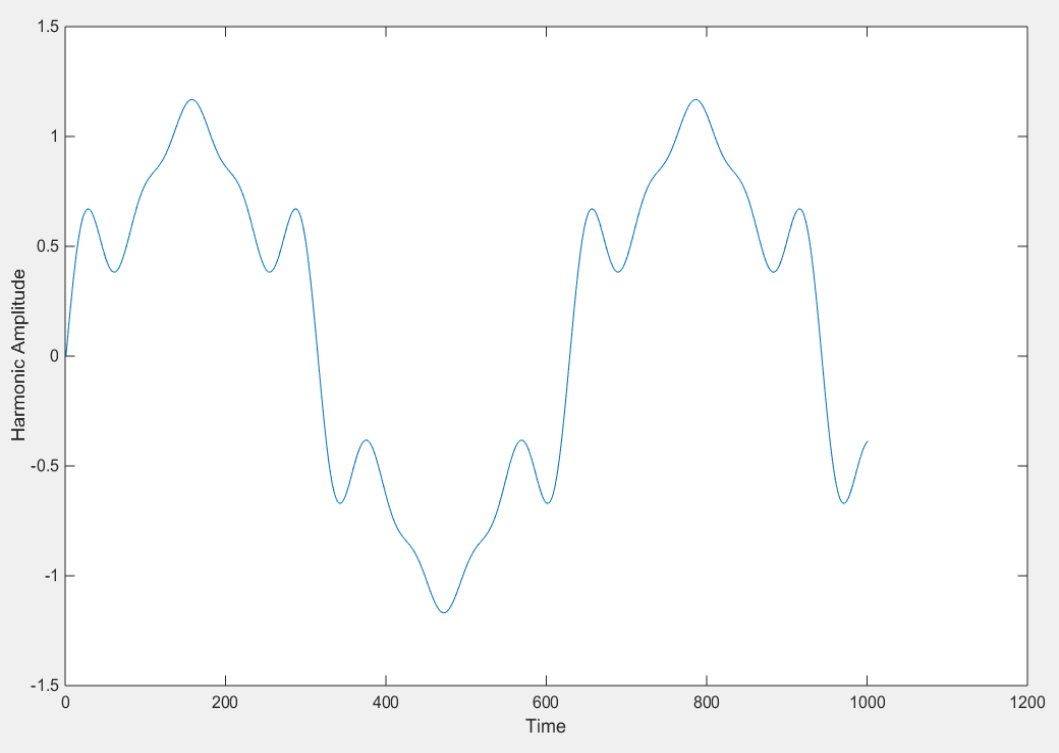

Figure 3-2 A non-sinusoidal periodical voltage waveform

Comparing with the single waveform of integer harmonic in Figure 3-1, the non-sinusoidal harmonic waveform in Figure 3-2 cannot be expressed by a simple sine

equation. To simplify and analyse non-sinusoidal harmonic, Fourier series is involved in reformulating such a non-sinusoid [13-16].

Fourier series is a widely used harmonic analysis method. It decomposes the non-sinusoidal periodical harmonic waveform into a set of sinusoidal harmonic waveforms. Then, it analyses sinusoidal harmonic waveforms in each harmonic order of the power system. After combining all power system harmonic response in each harmonic order, the total harmonic system parameters can be calculated.

Normally, any non-sinusoidal periodical function can be expressed by the Fourier series which is shown in equation 3-2[16].

$$f(t) = A^{(0)} + \sum_{h=1}^{\infty} [A^{(h)} \cos(h\omega_0 t) + B^{(h)} \sin(h\omega_0 t)] \tag{3-2a}$$

$$= A^{(0)} + \sum_{h=1}^{\infty} C^{(h)} \sin\left(h\omega_0 t + \varphi^{(h)}\right) \tag{3-2b}$$

Where $f(t)$ is the periodical function at frequency f_0. Its angular frequency is $\omega_0 = 2\pi f_0$, with period $T = 1/f_0 = 2\pi/\omega_0$. $C^1 \sin(\omega_0 t + \varphi)$ is the fundamental component. And $C^{(h)} \sin(h\omega_0 t + \varphi^h)$ is the h^{th} harmonic component. $C^{(h)}$ is amplitude, frequency is hf_0, phase angle is $\varphi^{(h)}$.

A, B, C and φ^h are the Fourier coefficients which are shown in the following equations.

$$A^{(0)} = \frac{1}{T}\int_0^T f(t)\, dt = \frac{1}{2\pi}\int_0^{2\pi} f(t)\, d(t) \quad (x = \omega_0 t) \tag{3-3}$$

$$A^{(h)} = \frac{2}{T}\int_0^T f(t)\cos(h\omega_0 t)\,dt = \frac{1}{\pi}\int_0^{2\pi} f(t)\cos(hx)\,d(t) \tag{3-4}$$

$$B^{(h)} = \frac{2}{T}\int_0^T f(t)\sin(h\omega_0 t)\,dt = \frac{1}{\pi}\int_0^{2\pi} f(t)\sin(hx)\,d(t) \tag{3-5}$$

$$C^{(h)} = \sqrt{(A^{(h)})^2 + (B^{(h)})^2} \tag{3-6}$$

$$\varphi^{(h)} = \arctan(\frac{A^{(h)}}{B^{(h)}}) \tag{3-7}$$

Figure 3-3 are the decomposed four harmonic waveforms which are analysed by Fourier series.

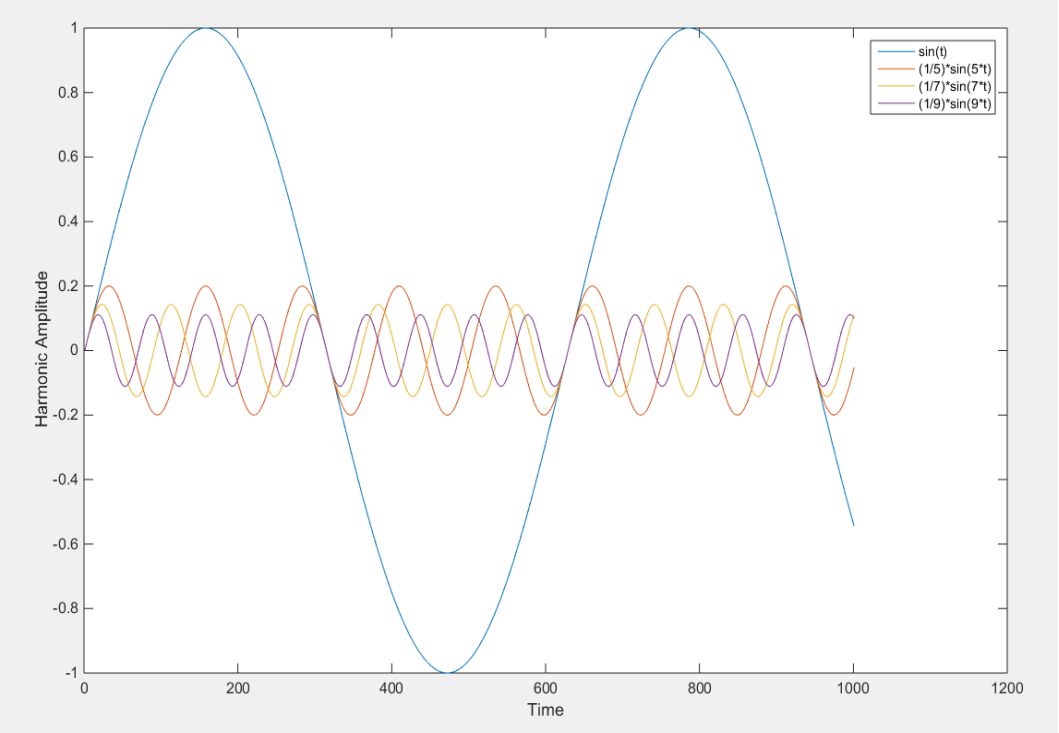

Figure 3-3 The harmonic components of the non-sinusoidal waveform

3.2.3 Power system harmonic characteristics[16].

The characteristics of harmonic in the power system can simplify the harmonic analysis. So, harmonic characteristics are introduced below.

(a) In the balanced three-phase power system, voltage and current waveform have half-wave symmetry. The half-wave symmetry is that system harmonic has no Direct-Current component and the even harmonic components can be offset. So, normally, all even harmonic components in the power system can be ignored.

(b) In a balanced three-phase system, the single-frequency harmonic component can only be single positive sequence, single negative sequence or single zero sequence. This feature can be seen from the Fourier series equation of phase

voltage. Moreover, according to reference [16], the fundamental harmonic, 4^{th}, 7^{th} ….are positive-sequence, the 2^{nd}, 5^{th}, 8^{th}….are negative-sequence and the 3^{rd}, 6^{th}, 9^{th}…..are zero-sequence. In addition, in a balanced 3-phase power system, triple harmonic current components are zero-sequence. Zero-sequence currents could flow in the star winding if there is a neutral connection and corresponding zero-sequence currents circulate in the delta winding. However, no zero-sequence currents can enter or leave the star winding without neutral connection or delta winding [17]. Thus, triple harmonic orders can be ignored in those systems which have the circuit with the delta winding connection or star winding without the neutral connection.

(c) In a balanced power system, the linear network has independent effects on different harmonics. This feature allows us to analyse all the harmonic component respectively. That means we can simulate system equivalent circuit on each harmonic order in the frequency domains and calculate harmonic voltage and current. The overall response can be obtained by the sum of all harmonic components in the time domains.

3.2.4 Harmonic Measures [5, 6, 18-20].

In order to analyse and calculate power system harmonic, the measures and formulations of the harmonic are necessary. Thus, they are introduced in the following section.

3.2.4.1 Harmonic Node Voltage and Branch Current

In power system harmonic analysis, the two harmonic elements of bus voltages and branch currents are the primary targets. By using Fourier series expansion in

general, the mathematical equations of harmonic node voltage and branch current can be expressed as follows:

$$v(t) = \sum_{h=1}^{\infty} V^{(h)} \cos(h\omega_0 t + \theta^{(h)}) \tag{3-8}$$

$$i(t) = \sum_{h=1}^{\infty} I^{(h)} \cos(h\omega_0 t + \varphi^{(h)}) \tag{3-9}$$

In the above equation,

$V^{(h)}$ –maximum value of the h^{th} harmonic node voltage

$I^{(h)}$ –maximum value of the h^{th} harmonic branch current

$\theta^{(h)}$ –value of the h^{th} harmonic node voltage phase angle

$\varphi^{(h)}$ –value of the h^{th} harmonic branch current phase angle

ω_0 – fundamental angular frequency, and $\omega_0 = 2\pi f_0$.

f_0 – fundamental frequency, and $f_0 = 50Hz \; or \; 60Hz$.

3.2.4.2 Root Mean Square (*rms*) Value of Node Voltage and Branch Current

For the Fourier series,

$$\mathrm{F}_{rms}^2 = \frac{1}{T}\int_0^T f^2(t)\, dt - \frac{1}{2}\sum_{h=1} F_h^2 = \sum_{h=1} F_{h\,rms}^2 \tag{3-10}$$

So, the root mean square value of node voltage and branch current can be expressed by equation (3-11) and (3-12) respectively.

$$V_{rms} = \sqrt{\sum_{h=1}^{n=\infty} (v_{rms}^{(h)})^2} = \sqrt{(v_{rms}^{(1)})^2 + (v_{rms}^{(2)})^2 + \cdots + (v_{rms}^{(n)})^2}$$

(3-11)

$$I_{rms} = \sqrt{\sum_{h=1}^{n=\infty} (i_{rms}^{(h)})^2} = \sqrt{(i_{rms}^{(1)})^2 + (i_{rms}^{(2)})^2 + \cdots + (i_{rms}^{(n)})^2}$$

(3-12)

Where $v_{rms}^{(h)}$ and $i_{rms}^{(h)}$ is the h^{th} harmonic *rms* value of node voltage and branch current respectively.

3.2.4.3 Total Harmonic Distortion (THD)

Total harmonic distortion (*THD*) is defined as the summation of all harmonic components of the voltage or current waveform compared against the fundamental component of the voltage or current wave [21]. The value of THD is a percentage comparing the harmonic components to the fundamental component of a non-sinusoidal signal. The mathematical expressions of total harmonic voltage and current distortion are shown below.

Total harmonic voltage distortion:

$$THD_V = \frac{1}{V^{(1)}} \sqrt{\sum_{h=2}^{\infty} (V^{(h)})^2} = \sqrt{(\frac{V_{rms}}{V^{(1)}{}_{rms}})^2 - 1}$$

(3-13)

Total harmonic current distortion:

$$THD_I = \frac{1}{I^{(1)}}\sqrt{\sum_{h=2}^{\infty}(I^{(h)})^2} = \sqrt{(\frac{I_{rms}}{I^{(1)}{}_{rms}})^2 - 1}$$

(3-14)

Where $V^{(1)}$ is the fundamental voltage and $I^{(1)}$ is the fundamental current.

3.2.4.4 Harmonic Active Power and Reactive Power

The instantaneous active power is defined that $p(t) = v(t)i(t)$. So, the mathematical equation of total harmonic active power is:

$$P = \frac{1}{T}\int_0^T p(t)\,dt$$

(3-15 a)

$$= \frac{1}{2}\sum_{h=1}^{n=\infty} V^{(h)}I^{(h)}\cos\left(\theta^{(h)} - \varphi^{(h)}\right)$$

(3-15 b)

$$= \sum_{h=1}^{n=\infty} V^{(h)}{}_{rms}I^{(h)}{}_{rms}\cos\left(\theta^{(h)} - \varphi^{(h)}\right)$$

(3-15 c)

The harmonic reactive power is defined as follow:

$$Q = \frac{1}{2}\sum_{h=1}^{n=\infty} V^{(h)}I^{(h)}\sin\left(\theta^{(h)} - \varphi^{(h)}\right)$$

(3-16 a)

$$= \sum_{h=1}^{n=\infty} V^{(h)}{}_{rms}I^{(h)}{}_{rms}\sin\left(\theta^{(h)} - \varphi^{(h)}\right)$$

(3-16 b)

3.2.4.5 Harmonic Apparent Power

According to the root mean square value of harmonic node voltage and branch current shown in equation 3-11 and 3-12, the harmonic apparent power *S* can be expressed by:

$$\mathrm{S} = V_{rms} I_{rms} \tag{3-17 a}$$

$$= \sqrt{\sum_{h=1}^{\infty} {V^{(h)}}^2{}_{rms} {I^{(h)}}^2{}_{rms}} \tag{3-17 b}$$

$$= V_{1_{rms}} I_{1_{rms}} \sqrt{1 + {THD_V}^2} \sqrt{1 + {THD_I}^2} \tag{3-17 c}$$

$$= S_1 \sqrt{1 + {THD_V}^2} \sqrt{1 + {THD_I}^2} \tag{3-17 d}$$

Where S_1 is the fundamental apparent power.

3.2.4.6 Distortion Power

Power system apparent power S is defined as $S^2 = P^2 + Q^2$. However, if voltage and current are non-sinusoidal waveforms, the apparent power should redefine under harmonic condition. Two vector graphics of apparent power under fundamental and harmonic condition are shown in Figure 3-4 and Figure 3-5 respectively. A parameter D named distortion power is included to redefine the harmonic apparent power. According to Figure 3-5, the new equation for harmonic apparent power can be presented by:

$$S^2 = P^2 + Q^2 + D^2 \tag{3-18}$$

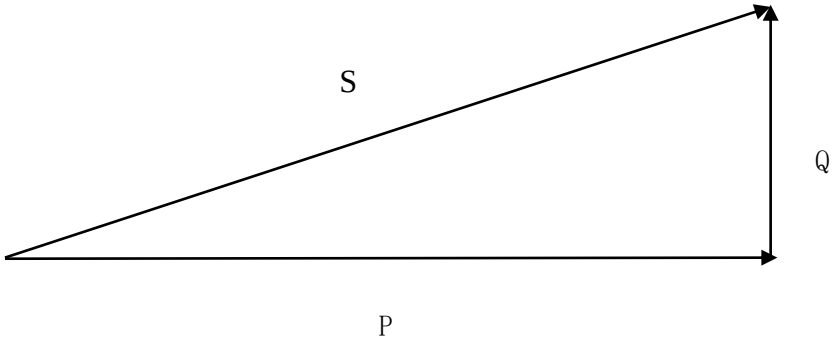

Figure 3-4 Power vector graphic under fundamental condition

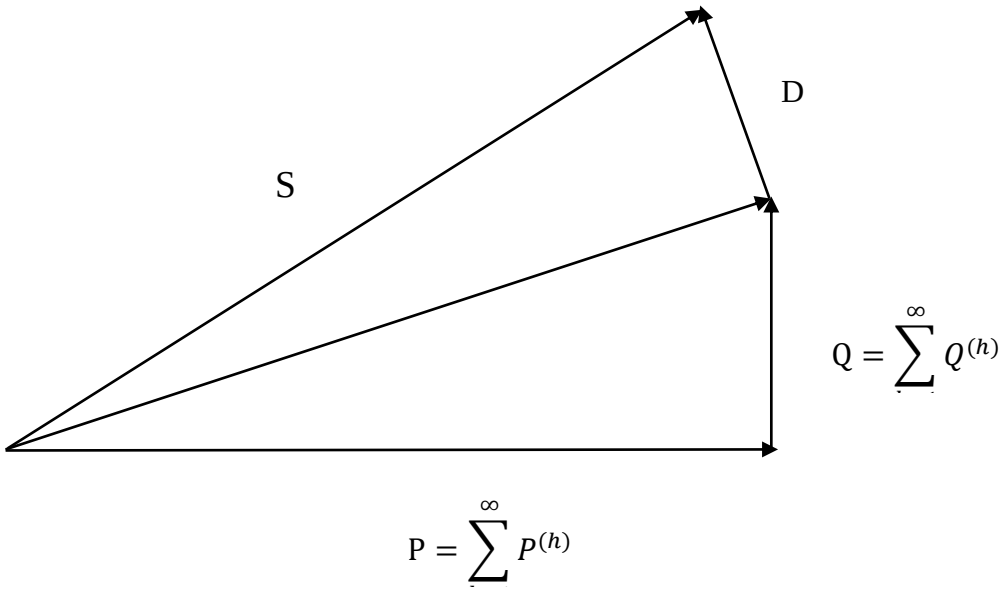

Figure 3-5 Power vector graphic under harmonic condition

Thus, the distortion power D can be calculated by equation 3-19.

$$D^2 = S^2 - P^2 - Q^2$$

$$= \sqrt{S^2 - (\sum_{h=1}^{\infty} P^{(h)})^2 - (\sum_{h=1}^{\infty} Q^{(h)})^2}$$

(3-19)

3.2.4.7 Total Power Factor

Normally, power factor is the value of active power divided by the apparent power. Under the harmonic condition, distortion power D is included in the apparent power. So, the equation of total power factor of a non-sinusoidal waveform is

$$pf = \frac{P}{S} = \frac{P}{\sqrt{P^2 + Q^2 + D^2}} = \frac{P}{S_1\sqrt{1 + THD_V{}^2}\sqrt{1 + THD_I{}^2}}$$

(3-20)

3.2.5 Harmonic Distortion Limit Standards

Power system harmonic cannot be completely avoided. Hence, limitations for power system harmonic are necessary. Harmonic distortion limit standard is a standard to limit the system harmonic to an acceptable limit. After doing the system harmonic analysis, a comparison of system bus harmonic voltage, branch harmonic current and their total harmonic distortion with the harmonic distortion limit standard can help the system operator to check the system and maintain the system harmonic to an acceptable level.

The following part will introduce the harmonic distortion limit standard which is determined by IEEE (Institute of Electrical and Electronics Engineers), IEC (International Electrotechnical Commission) and EN (European Norms). Due to different countries have different harmonic distortion limit standard, the limited values in this section are references and should not be considered binding in all cases. In this thesis, distribution feeder reconfiguration only considers harmonic

voltage and current at the point of common coupling at the low voltage level. Thus, the limitation for others will not be illustrated.

a) IEEE Harmonic Distortion Limit Standard

According to reference [9, 22], IEEE 519 standard provides a limitation for system harmonic bus voltage at the point of common coupling which is shown in Table 3-1.

Table 3-1: IEEE-519 Harmonic voltage limits for public power systems[9, 22]

Voltage at PCC Harmonic	Single harmonic Voltage(%)	THD_v(%)
$V < 69kV$	3.0	5.0
$69 \leq V < 161kV$	1.5	2.5
$V \geq 161kV$	1.0	1.5

b) IEC Harmonic Distortion Limit Standard

IEC gives a detailed limitation for harmonic voltage distortion at the point of common coupling in low voltage level [15, 16]. Table 3-2 is the details about the IEC harmonic distortion limit standard.

Table 3-2: IEC 61000-2-2 Harmonic voltage distortion compatibility levels for public LV power systems[15, 16]

Odd harmonics (Non-multiple of three)		Even harmonics		Odd harmonics (Multiple of three)	
Harmonic order'h'	Harmonic voltage(%)	Harmonic order'h'	Harmonic voltage(%)	Harmonic order'h'	Harmonic voltage(%)
5	6	2	2	3	5
7	5	4	1	9	1.5
11	3.5	6	0.5	15	0.3
13	3	8	0.5	$\geq$ 21	0.2
17	2	10	0.5		
19	1.5	$\geq$ 12	0.2		
23	1.5				
25	1.5				
$\geq$ 29	x				
The total harmonic voltage distortion level is $THD_V \leq 8\%$ x = 0.2+12.5/*h*. For *h* = 29, 31, 35, 37, $V^{(h)}$ = 0:63%,0.6%,0.56%,0.54%.					

c) EN Harmonic Distortion Limit Standard

EN standard is approved by the European Committee for Electro Technical Standardization[9, 22]. And its limitation is illustrated in Table 3-3.

Table 3-3: EN50160 Harmonic voltage distortion compatibility levels for public LV power systems[9, 22]

Odd harmonics (Non-multiple of three)		Even harmonics		Odd harmonics (Multiple of three)	
Harmonic order‘h’	Harmonic voltage(%)	Harmonic order‘h’	Harmonic voltage(%)	Harmonic order‘h’	Harmonic voltage(%)
5	6	2	2	3	5
7	5	4	1	9	1.5
11	3.5	6…24	0.5	15	0.5
13	3			21	0.5
17	2				
19	1.5				
23	1.5				
25	1.5				

The values of system harmonic which order are larger than 25 are too small and it is hard to estimate their resonance. Thus, the limitation for them is not provided in this table.

3.3 Distribution System Component Models Considering Harmonic

Distribution network is composed of distribution line, load, transformer, switch and affiliated facilities. These system component models show different performance between fundamental and harmonic condition. Simulating the system models correctly is important to ensure a relatively accurate analysis results when analysing system harmonic.

For the feeder reconfiguration problem at one voltage level, the system network normally contains power cables, buses and loads. In such a network, harmonic sources also need to be involved. So, network components models which may involve are introduced in this section.

3.3.1 Network component models considering harmonic [16, 23-26]

a) Distribution network component model in this thesis.

Impedance Z which contains resistant R and inductance reactance $X_L = 2\pi fL$ can be expressed by equation $Z = R + jX_L$ in the fundamental condition. But, if the harmonic condition is considered, the equation of such a system component would change to

$$Z(h) = R + jhX_L \tag{3-21}$$

Where h is the harmonic order.

On the other hand, if the system component is capacitance, such a capacitive reactance which is $X_C = 1/2\pi fC$ would change to

$$X_C(h) = X_C/h \tag{3-22}$$

In section 2.3.1, it has introduced that the distribution line can be simply represented by $R + jX$. If the skin effect is ignored, the distribution line could be expressed by equation 3-21 under the harmonic condition in distribution network feeder reconfiguration. (Skin effect is the tendency of an alternating electric current to become distributed within a conductor such that the current density is largest near the surface of the conductor, and decreases with greater depths in the conductor.[27])

In distribution network, the source node of the whole network normally considers as one transformer substation of the transmission network. In this thesis, sources node of the distribution network is assumed as an ideal constant voltage source

without harmonic. So, the model of the main generator is not used in the distribution network feeder reconfiguration problem.

In the distribution network feeder reconfiguration problem, all system buses and branches are at the same voltage level, so there is no transformer in the reconfiguration network.

The load in the distribution network feeder reconfiguration can be divided into two types – linear load and nonlinear load. All load active and reactive power are known elements. The linear load model can be expressed by resistance and reactance (or inductance) and the nonlinear load model can be expressed by an ideal harmonic current source which injects harmonic current into the distribution network. The harmonic source will be introduced in section 3.2.5.

b) Common network component models considering harmonics in the power system

Commonly, the harmonic system models were more complex than mentioned above. The details of these models can be found in the following reference. And skin effect is not ignored on these models.

In references [25, 26, 28], the model of the generator is defined as equation 3-23.

$$Z_{eq}(h) = \sqrt{h}R_f + jhX_f \tag{3-23}$$

Where R_f and X_f is the fundamental resistance and impedance respectively. $Z_{eq}(h)$ is the equivalent internal impedance of the generator at the h^{th} harmonic order.

In the model for transformer, it can be expressed by [26, 28, 29]

$$Z_{eq}(h) = \sqrt{h}R_f + jhX_f$$

(3-24)

Where $Z_{eq}(h)$ is the equivalent internal impedance of the transformer at the h^{th} harmonic order.

After taking account skin effect into the power system, the resistance of the power cable will become bigger with the increasing of the harmonic order. For common specification transmission line, the resistance model of the transmission line can be defined as following equation [30]:

$$\mathrm{R}_{eq}(h) = 0.288R_f + 0.138\sqrt{hR_f}$$

(3-25)

Where $R_{eq}(h)$ is the equivalent resistance of the transmission line at the h^{th} harmonic order.

Thus, the model of the power cable is formulated as:

$$Z(h) = \mathrm{R}_{eq} + jhX_f$$

(3-26)

In reference [16], the load is divided into two types. One is the series load which normally suitable for the single load. The other is the parallel load which commonly represents the concentrated load. And they are defined by the following equations respectively.

$$Z_{series}(h) = R + jhX$$

(3-27)

$$Z_{parallal}(h) = 1/(\frac{1}{R} - jh\frac{1}{X})$$

(3-28)

3.3.2 Harmonic Source

Nonlinear equipment and components are the main harmonic sources in the power system. Reference [6] specifies those nonlinear equipment or components into three types: saturated devices which include transformers, motors and generators; arcing equipment which contains arc furnaces, fluorescent as well as mercury lights; and power electronic equipment which involves inverters, rectifiers, and switched mode power supplies.

The inverter based generator inject more harmonic to power network than the traditional generator. Moreover, electric vehicle is another important renewable energy application in the daily life. Although electric vehicle brings benefit to the environment, its charger injects more harmonic to the power network. As important harmonic sources for the distribution network, two common types of renewable generators and the charger of the electric vehicle is introduced as follows. These generators and the charger of the electric vehicle will also be used as the harmonic source models in this thesis.

a) Wind generator

According to the wind turbine speed control, wind generators can be classified into two types. One is fixed speed wind turbine and the other is variable speed wind turbines. Due to the simple, cheap and reliable performance, the fixed speed wind turbine is commonly used wind generator model in the past. Nowadays, disadvantages overshadow advantages that the wind speed and reactive power consumption are not controllable and the controlling of power quality has limitation so as to the power quality of this type of wind turbine cannot satisfy the modern power system. Variable speed wind turbines overcome these disadvantages

of the fixed speed wind turbine and improve the power quality produced by the wind generators. However, on the other hand, variable speed wind turbines needs more electrical equipment which is the main harmonic source provider. Two types of variable speed wind turbines are shown in the following figure.

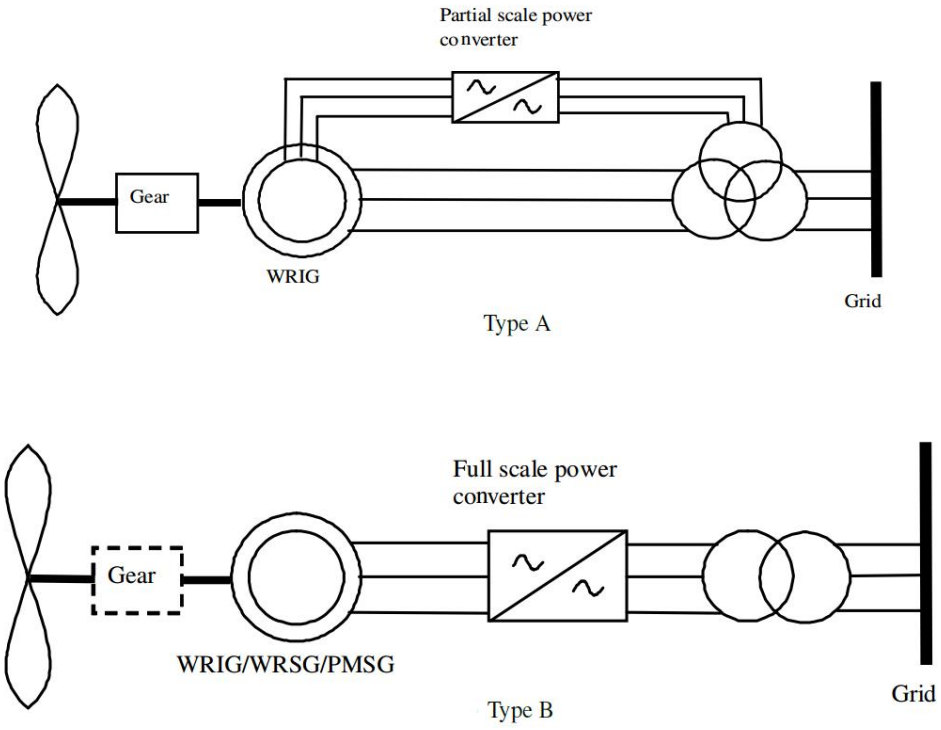

Figure 3-6 Configuration of variable speed wind turbine

Power converter isolates the generators from the grid to some extent in type A generator and completely isolates the generators from the grid in type B generator. According to references [1, 32, 33], harmonics are generated by the grid-side power electrical converters.

Harmonic emissions measurement for the wind turbine has published in many references, such as references [1, 4, 34, 35]. References [1] and [4] publish the harmonic emissions spectra of the wind farm consisted by 72 SWT-2.3-93 wind turbines and the wind farm with a total of 54 permanent magnet synchronous generators (PMSG) respectively. And two harmonic emissions spectra are shown

in Table 3-4 and Table 3-5, and the data of these two tables will be cited as wind turbine harmonic sources in the testing cases of this thesis.

Table 3-4: Harmonic currents generated by the wind farm with 72 SWT-2.3-93 wind turbines [1]

Harmonic Order "h"	$\frac{I^{(h)}}{I^1}$ (%)	Harmonic Order "h"	$\frac{I^{(h)}}{I^1}$ (%)	Harmonic Order "h"	$\frac{I^{(h)}}{I^1}$ (%)
1	100	11	1.46	22	0.33
2	0.34	13	1.58	23	0.37
4	0.20	14	0.48	25	0.24
5	0.44	16	0.37	26	0.20
7	0.47	17	0.76	28	0.13
8	0.40	19	0.42	29	0.27
10	0.55	20	0.32		

Table 3-5: Harmonic currents generated by the wind farm with 54 PMSGs [4]

Harmonic Order "h"	$\frac{I^{(h)}}{I^1}$ (%)	Harmonic Order "h"	$\frac{I^{(h)}}{I^1}$ (%)	Harmonic Order "h"	$\frac{I^{(h)}}{I^1}$ (%)
1	100	11	1.40	21	0.04
2	1.12	12	0.09	22	0.03
3	0.65	13	0.60	23	0.09
4	0.52	14	0.06	24	0.03
5	1.83	15	0.06	25	0.09
6	0.27	16	0.05	26	0.04
7	0.60	17	0.09	27	0.03
8	0.17	18	0.03	28	0.04
9	0.14	19	0.09	29	0.07
10	0.12	20	0.03		

b) Photovoltaic Generator

Photovoltaic energy is an alternative renewable energy for wind turbine. The

photovoltaic generator is relatively small, cheap and simple to install. The installation scale of the rooftop photovoltaic generator increases rapidly in the low voltage distribution network. The block diagram of a typical grid connected 3-phase photovoltaic system is shown in Figure 3-7 [36]. Electrical equipment transforms the direct current power which generator by the photovoltaic array to alternating current power and injects to the grid. In the meantime, these electrical equipment (boost converter and DC/AC converter) also generator harmonics.

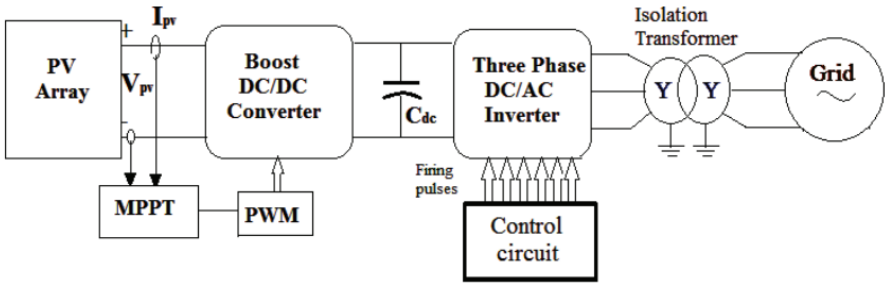

Figure 3-7 Block diagram of grid connected three phase PV system

The author of reference [37] proposes that the harmonic current emission spectra of photovoltaic strongly depends on the type of technology used. But, the photovoltaic generator is only treated as known constant harmonic current source in this thesis. Thus, a reference harmonic current emission spectra is cited and shown in Table 3-6 [3].

Table 3-6: Harmonic currents generated by 2 kW PG inverter [3]

Harmonic Order "h"	$\frac{I^{(h)}}{I^{1}}$ (%)	Harmonic Order "h"	$\frac{I^{(h)}}{I^{1}}$ (%)
1	100	9	0.4
3	1.5	11	0.21
5	0.6	13	0.2
7	0.3		

The harmonic current above 13th order is ignored for its small value.

c) Electric Vehicle Chargers

Vehicle emission is one of the primary air pollution sources. With the increasing level of the environment protection, the electric vehicle has a rapid development in recent years. Because of the electric energy, the emission of the electric vehicle is zero for the environment. But, in the power system environment, the chargers of the electric vehicle will emit harmonics. Due to the electric vehicles are normally charged at residential provides, it becomes an important new harmonic source in the distribution network.

The schematic diagram of the on-broad charger is shown in Figure 3-8 [38]. In this figure, not only the DC to DC inverter, but also the rectifier will emit harmonics. Two filters are used to reduce the harmonics in this system.

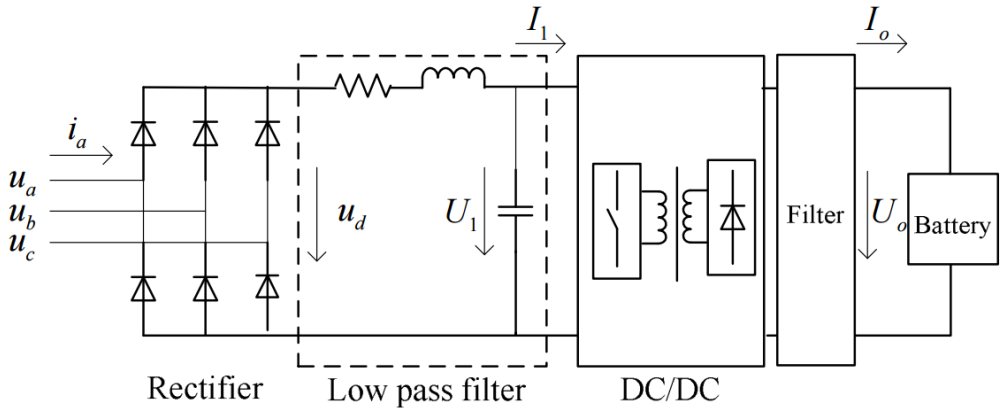

Figure 3-8 The schematic diagram of the on-broad charger

Reference [39] indicates that the installation of electric vehicle charger point commonly has several on-board chargers in charging. The real situation cannot only considers one on-boarder charger. Many factors will have significantly influenced on the harmonic emission of the on-boarder charger. Such as the starting time of the charging and the initial battery state-of-charge. After considering several possible influential factors, reference [2] gives a reliable harmonic

emission of a cluster of on-boarder chargers which is shown in Table 3-7.

Table 3-7: Harmonic currents generated by a cluster of 10 EV battery chargers [2]

Harmonic Order "h"	$\frac{I^{(h)}}{I^{1}}(\%)$	Harmonic Order "h"	$\frac{I^{(h)}}{I^{1}}(\%)$
1	100	9	14.3
3	31.9	11	9.5
5	24.7	13	4.5
7	17.4	15	3.3

The harmonic current above 15th order is ignored for its small value.

The specifications of the EV battery charger studied are designed under following conditions.

a) For leaded acid battery pack of 20 kWh (@ 5-hour rate), which is equivalent to a battery pack of about 160 Ahr @ 5-hour rate.

b) Overall voltage of battery: 120 Vdc.

c) Input voltage: 220 Vac, 50 Hz.

d) Input current at the initial charging: about 36 A.

e) Charging time about 6 hours.

3.4 Harmonic Load Flow Method for Feeder Reconfiguration

Harmonic load flow evaluation method is the base of harmonic analysis. Researchers have already proposed many harmonic load flow evaluation methods in the past decades. For example: Newton-Raphson based harmonic power flow

method [5, 40], decoupled harmonic power flow method [24, 41-44], fast decoupled harmonic power flow method [45-48], fuzzy harmonic power flow method [49], probabilistic harmonic power flow method [50-53], and modular harmonic power flow method [54-56]. Similar to the load flow evaluation method in fundamental, a large part of these harmonic load flow evaluation methods is proposed base on the transmission network. A special harmonic load flow evaluation method for the distribution network is necessary.

In Chapter 2, the backward/forward sweep algorithm is suggested as one of the best load flow evaluation methods for feeder reconfiguration problem. It is because that not only the backward/forward sweep algorithm is a special load flow evaluation method for the distribution network but also its improved version can avoid the recode problem in the feeder reconfiguration problem. If system node and branch codes must recode at every iteration when the network structure change, it may have a large negative effect on the efficiency of the load flow method when it is applied to the feeder reconfiguration problem. Thus, a special harmonic load flow evaluation method for feeder reconfiguration should be proposed which is based on the layered backward/forward sweep method.

T. Jen-Hao and C. Chuo-Yean proposed a fast harmonic power flow method [57-59] based on the basic backward/forward sweep method. Backward/forward sweep method is a powerful method in the distribution network. Base on the network structure of the distribution network, equivalent injection current and backward/forward sweep method, it can evaluate the bus voltages, branch currents with less computing time by simple backward/forward sweep.

The equivalent current injections are widely used for the application of the distribution network. Reference [60] gives the details that the harmonic injection currents are calculated by equation 3-29.

$$I_i^{(1,k)} = \left(\frac{P_i^{sp} + jQ_i^{sp}}{V_i^{(1,k)}} \right)^*$$

(3-29)

Where $V_i^{(1,k)}$ represents the voltage of linear bus i at the k[th] iteration. P_i^{sp} and Q_i^{sp} is the specified active and reactive powers at bus i respectively. The symbol '*' represents the conjugate value.

In the fundamental load flow calculation, the bus voltage V_i^1 will be updated after each forward sweep. It causes that the injection current I_i^1 will be modified after each backward sweep iteration. A relatively accurate value will be calculated when the tolerance fulfils the requirement. In reference [57, 60], it is said that the harmonic injection current does not need to be updated at each end of iterations. Because they are already obtained based on the harmonic analysis. But, there are normally no value of the P_i^{sp} and the Q_i^{sp} (the specified active and reactive powers at bus i) in the given data of the distribution network. Thus, measurement of the harmonic injection current which proposed in reference needs to modify in these test systems.

In section 3.3.2, the harmonic emission spectra of wind turbine generator, photovoltaic generator and electric vehicle are provided by the harmonic analysis of the equipment. It means that the harmonic injection current at each harmonic order of bus i can be calculated according to the harmonic emission spectra when the fundamental injection current and the harmonic emission spectra at bus i are known. Then the total harmonic injection current can be explained by equation 3-30:

$$I_i = \sqrt{(I_i^1)^2 + (I_i^2)^2 + (I_i^3)^2 + \cdots + (I_i^n)^2}$$

(3-30)

Where I is root mean square value of the harmonic injection current at bus i and n is the maximum required harmonic order at bus i.

So, if the special data for harmonic equivalent current injections was not provided, the first step of backward/forward sweep based harmonic load flow method is to solve the fundamental load flow and calculate the value of the harmonic injection currents at each harmonic order according to the harmonic emission spectra of nonlinear loads.

Backward/forward sweep method is prepared for calculating the harmonic injection current and bus voltage at a single harmonic order. The total response of system harmonic branch currents and harmonic bus voltages are calculated by summing of the fundamental component and all harmonic components in the time domain or calculate the root mean square value by using equation 3-11 and equation 3-12.

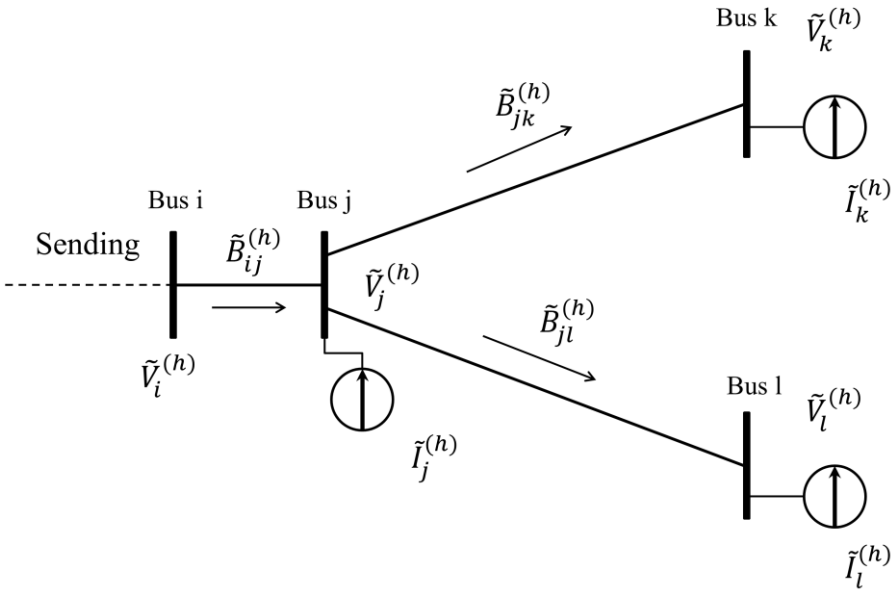

Figure 3-9 Parts of a distribution system

Figure 3-9 is a graph of parts of a distribution system which is used to illustrate the

backward/forward sweep method in harmonic load flow analysis. In this figure, $\tilde{I}_j^{(h)}$, $\tilde{I}_k^{(h)}$ and $\tilde{I}_l^{(h)}$ is harmonic injection currents at bus j, k and l respectively. After analyzing the fundamental load flow, the fundamental injection currents at these buses are calculated. The value of harmonic injection current components of these buses can be easily calculated according to the harmonic emission spectra of its corresponding harmonic source. $\tilde{V}_i^{(h)}$, $\tilde{V}_j^{(h)}$, $\tilde{V}_k^{(h)}$ and $\tilde{V}_l^{(h)}$ is the bus voltages at bus i, j, k and l respectively. $\tilde{B}_{ij}^{(h)}$, $\tilde{B}_{jk}^{(h)}$ and $\tilde{B}_{jl}^{(h)}$ are branch currents on the distribution lines. All of these elements are the value at the h^{th} harmonic order. According to Kirchhoff's Law, the relationship between branch currents and harmonic injection currents in backward sweep process can be described by equations 3-31[57]:

$$\begin{cases} \tilde{B}_{jk}^{(h)} = -\tilde{I}_k^{(h)} \\ \tilde{B}_{jl}^{(h)} = -\tilde{I}_l^{(h)} \\ \tilde{B}_{ij}^{(h)} = \tilde{B}_{jk}^{(h)} + \tilde{B}_{jl}^{(h)} - \tilde{I}_j^{(h)} \end{cases} \tag{3-31}$$

Where h is equal to 2, 3, 4 $\cdots$ h_{max}.

And its general equation of harmonic injection current in backward sweep can be represented by equation 3-32 [57]as long as the bus j is the receiving bus of the branches.

$$\tilde{B}_{ij}^{(h)} = -\tilde{I}_j^{(h)} + \sum_{n=j}^{n} \tilde{B}_{jn}^{(h)} \tag{3-32}$$

Where n in equation 3-32 is the number of buses which is connected to bus j.

Similar to the harmonic injection currents backward sweep, the relationship between harmonic bus voltages and branch currents can be represented by equation

3-33 [57] in the forward sweep process.

$$\begin{cases} \tilde{V}_j^{(h)} = \tilde{V}_i^{(h)} - \tilde{B}_{ij}^{(h)} \cdot \tilde{Z}_{ij}^{(h)} \\ \tilde{V}_k^{(h)} = \tilde{V}_j^{(h)} - \tilde{B}_{jk}^{(h)} \cdot \tilde{Z}_{jk}^{(h)} \\ \tilde{V}_l^{(h)} = \tilde{V}_j^{(h)} - \tilde{B}_{jl}^{(h)} \cdot \tilde{Z}_{jl}^{(h)} \end{cases} \tag{3-33}$$

Where $\tilde{Z}_{ij}^{(h)}$, $\tilde{Z}_{jk}^{(h)}$ and $\tilde{Z}_{jl}^{(h)}$ are the equivalent branch impedance of the 'h' harmonic order.

And its general equation of harmonic bus voltage in forward sweep can be expressed as [57]:

$$\tilde{V}_j^{(h)} = \tilde{V}_i^{(h)} - \tilde{Z}_{ij}^{(h)} \cdot \tilde{B}_{ij}^{(h)} \tag{3-34}$$

The harmonic bus voltages and branch currents at each harmonic order can be obtained by the above steps. Then, the harmonic branch current on each branch and harmonic bus voltage on each bus can be obtained by equation 3-35.

$$\begin{cases} I_{branch(ij)} = \sqrt{(\tilde{B}_{ij}^{(1)})^2 + (B_{ij}^{(2)})^2 + (B_{ij}^{(3)})^2 + \cdots + (B_{ij}^{(n)})^2} \\ V_{bus(i)} = \sqrt{(\tilde{V}_i^{(1)})^2 + (\tilde{V}_i^{(2)})^2 + (\tilde{V}_i^{(3)})^2 + \cdots + (\tilde{V}_i^{(n)})^2} \end{cases} \tag{3-35}$$

The basic theory of the backward/forward sweep method is the same as its fundamental version. The key difference was the equation for calculating the equivalent injection current if the special active and reactive power which shows in equation 3-29 are not given.

In fundamental, the equation for calculation equivalent injection current is [60]:

$$I_i^n = \left(\frac{P_i + jQ_i}{V_i^n}\right)^*$$

(3-36)

Where n is the number of iterations.

In equation 3-36, the bus voltage V_i^n is assumed to be the same value as the reference voltage at the first iteration. Thus, the value of system branch currents and bus voltages needs to be updated at each iteration for reducing the tolerance. However, under the harmonic condition, injection currents are calculated according to the fundamental injection currents and harmonic emission spectra of the equipment. Both of them are known and constant system parameters. Hence, update for branch currents and bus voltages is absent and the iteration process in the harmonic backward/forward sweep method is unnecessary.

The flow chart of the harmonic backward/forward sweep method can be illustrated as follow:

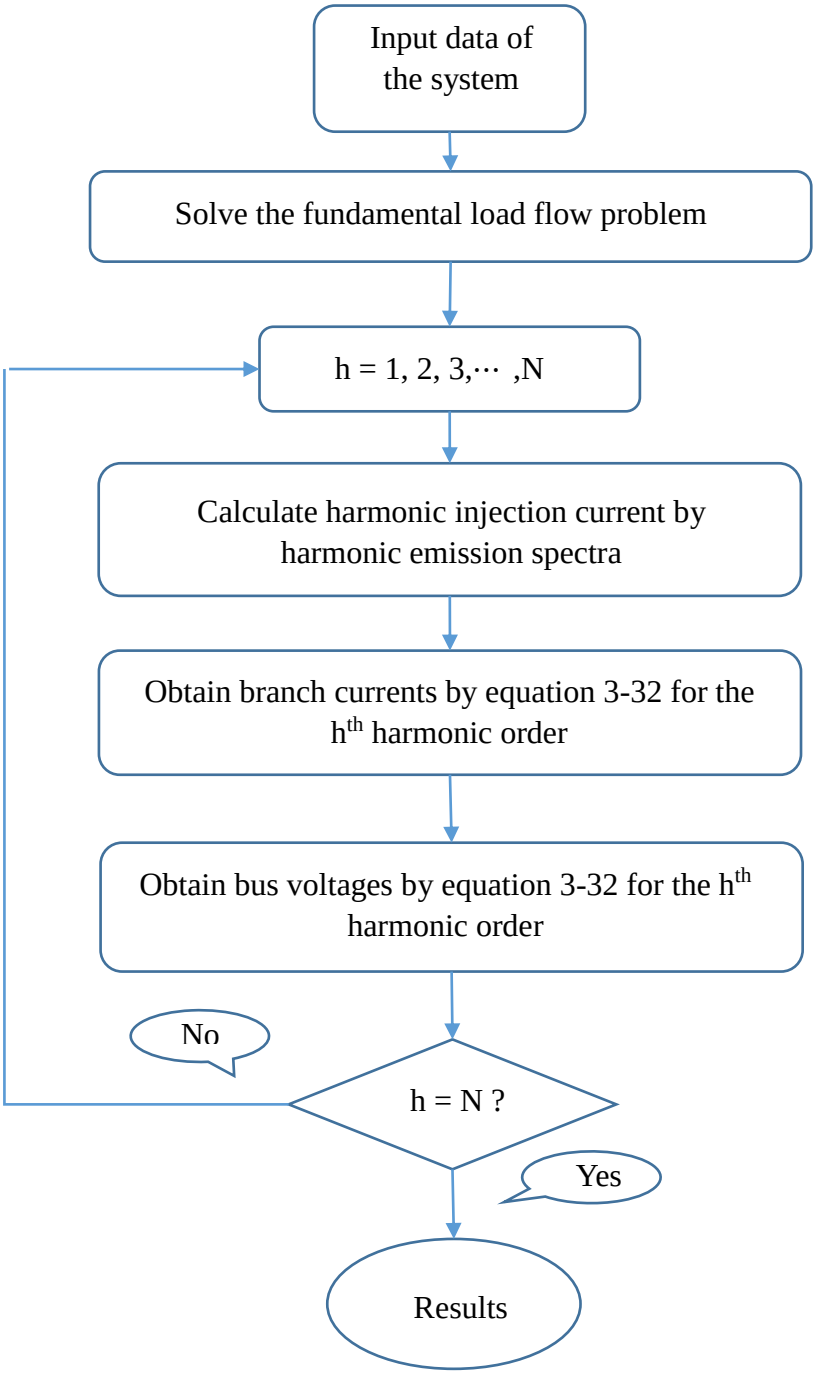

Figure 3-10 The flow chart of harmonic backward/forward sweep method.

3.5 Power Loss in Cables Considering Harmonics.

Normally the power cable will be transformed to π equivalent diagram and analyse the power loss. However, the power cable is simulated as a simple impedance in distribution network in this thesis. Its reason has been introduced in section 2.3.1. Thus, the measurement of power loss calculation will be different.

a) Cable loss in normal condition[60].

The π equivalent diagram of a power cable is shown in Figure 3-11.

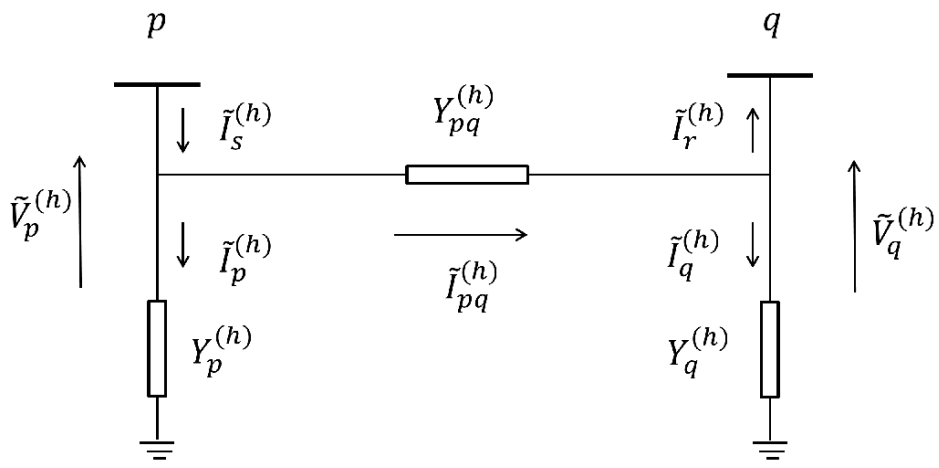

Figure 3-11 π equivalent diagram of power cable

According to the law of conservation of energy, the active power loss on power cable can be defined as:

$$P_{loss}^{(h)} = P_s^{(h)} - P_r^{(h)} \tag{3-37}$$

Where $P_{loss}^{(h)}$ is the active power loss on power cable pq at the h^{th} harmonic order. $P_s^{(h)}$ and $P_r^{(h)}$ is the active power at the sending end and receiving end at the h harmonic order respectively.

The active power of sending end and receiving end at the h harmonic order can be calculated by the following equation:

$$S_s^{(h)} = \tilde{V}_p^{(h)}(\tilde{I}_s^{(h)})^* = P_s^{(h)} + jQ_s^{(h)} \tag{3-38}$$

$$S_r^{(h)} = \tilde{V}_q^{(h)}(\tilde{I}_r^{(h)})^* = P_r^{(h)} + jQ_r^{(h)} \tag{3-39}$$

Where $S_s^{(h)}$ and $S_r^{(h)}$ is the apparent power of sending end and receiving end at the h^{th} harmonic order respectively. $Q_s^{(h)}$ and $Q_r^{(h)}$ denotes the reactive power of sending end and receiving end at the h^{th} harmonic order respectively.

In this model of the transmission line, the bus voltage and cable impedance are known elements. From equation 3-38 and equation 3-39, it can find that if $\tilde{I}_s^{(h)}$ and $\tilde{I}_r^{(h)}$ are calculated, $P_s^{(h)}$ and $P_r^{(h)}$ would be obtained easily. In Figure 3-11, the relationship between bus voltage, current and admittance can be shown as follows:

$$\begin{aligned} \tilde{I}_p^{(h)} &= \tilde{V}_p^{(h)}\tilde{Y}_p^{(h)} = \left|V_p\right|^{(h)}\angle\theta_p^{(h)}Y_p^{(h)} \\ &= \left|V_p\right|^{(h)}(cos\theta_p^{(h)} + jsin\theta_p^{(h)})Y_p^{(h)} \end{aligned} \tag{3-40}$$

$$\begin{aligned} \tilde{I}_q^{(h)} &= \tilde{V}_q^{(h)}\tilde{Y}_q^{(h)} = \left|V_q\right|^{(h)}\angle\theta_q^{(h)}Y_q^{(h)} \\ &= \left|V_q\right|^{(h)}(cos\theta_q^{(h)} + jsin\theta_q^{(h)})Y_q^{(h)} \end{aligned} \tag{3-41}$$

and

$$\tilde{I}_{pq}^{(h)} = (\tilde{V}_{p}^{(h)} - \tilde{V}_{q}^{(h)})\tilde{Y}_{pq}^{(h)}$$

(3-42)

Then, according to the Kirchhoff's current law, the current at sending end and receiving end can be expressed by:

$$\tilde{I}_{s}^{(h)} = \tilde{I}_{p}^{(h)} + \tilde{I}_{pq}^{(h)}$$

(3-43)

$$\tilde{I}_{r}^{(h)} = \tilde{I}_{pq}^{(h)} - \tilde{I}_{q}^{(h)}$$

(3-44)

After the value of $\tilde{I}_{s}^{(h)}$ and $\tilde{I}_{r}^{(h)}$ calculated and ignoring skin effect, the active power loss at power cable can be obtained according to equation 3-37, equation 3-38 and equation 3-39.

b) Cable loss in feeder reconfiguration problem for network loss reduction.

Similar to the loss in the common situation, the skin effect of the harmonic is also ignored in this model. For the reason that short cable length and low system voltage which explain in section 2.3.1, the power cable in the distribution system normally expressed by $R + jX$. Figure 3-12 is the diagram of the power cable in the distribution system. The phase to ground impedance is ignored so that the power loss on cable can be defined as:

$$P_{loss}^{(h)} = (\tilde{I}_{pq}^{(h)})^{2} R_{pq}$$

(3-45)

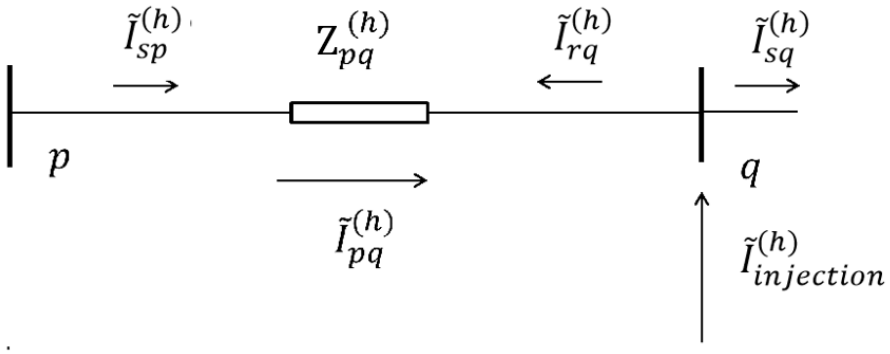

Figure 3-12 equivalent diagram of power cable in feeder reconfiguration

In feeder reconfiguration problem, the known elements have introduced in section 3.4 and they are the cable impedance $Z_{pq}^{(h)}$, sending harmonic current $\tilde{I}_{sq}^{(h)}$ and injection harmonic current $\tilde{I}_{injection}^{(h)}$ at bus q. Thus, the active power loss on cable pq at h^{th} harmonic order can be expressed by:

$$P_{loss}^{(h)} = (\tilde{I}_{sq}^{(h)} - \tilde{I}_{injection}^{(h)})^2 R_{pq} \tag{3-46}$$

3.6 Summary

With the application of the electrical technology based equipment, the harmonic analysis in the power system is more and more important for the accuracy of system load flow analysis. Renewable generators and electric vehicles may be large-scale applied in the future in the distribution network. Thus, the basic knowledge about harmonic analysis has been introduced in this chapter so that the program which proposed in this thesis can solve the feeder reconfiguration problem considering harmonic.

The difference of the backward/forward sweep method in fundamental and harmonic is the calculation of equivalent injection current at each bus. The basic

theory of this method is the same no matter it is applied to analyse the fundamental or harmonic load flow. Thus, the layered method can also be used in system harmonic analysis to avoid the recode problem. Then a fast harmonic analysis method especially for the distribution network feeder reconfiguration problem is ready.

Harmonic sources involve not only loads but also generators. A distribution network with the PV type distribution generators cannot be analysed directly by the layered backward/forward sweep algorithm. However, the wind and solar generator which are important for future energy supplement are PV type distribution generators. These two type of generator may also be parts of the main harmonic sources in the distribution network in future. To improve the harmonic backward/forward sweep method, the method for solving the PV type distribution generators in load flow analysis are introduced in next chapter.

3.7 Reference

[1] K. K. Munji and R. Bhimasingu, "Mitigation of harmonics in grid integrated wind farms," in *Power and Energy Systems (ICPS), 2011 International Conference on*, 2011, pp. 1-5.

[2] Fok, Chun-cheong, "Electric vehicle battery chargers: harmonics, modeling and charging strategies," *Master's thesis, The Hong Kong Polytechnic University,* 2001.

[3] A. Celebi and M. Colak, "The effects of harmonics produced by grid connected photovoltaic systems on electrical networks," *http://www.emo.org.tr/ekler/0172ea66506f59c_ek.pdf*, last date of access, 25.02.2016.

[4] H. P. G. Mendonc¸a, and S. Silva,, "Wind farm and system modelling evaluation in harmonic propagation studies," *International Conference on Renewable Energies and Power Quality (ICREPQ12),* 2012.

[5] E. Fuchs and M. Masoum,, *Power Quality in Power Systemsand Electrical Machines*: Elsevier, 2008.

[6] G. K. Singh, "Power system harmonics research: a survey," *European Transactions on Electrical Power,* vol. 19, pp. 151–172, 2009.

[7] W. M. Grady and S. Santoso, "Understanding Power System Hannonics," *Power Engineering Review, IEEE,* vol. 21, pp. 8-11, 2001.

[8] G. Mahesh, R. Ganesan, and S. K. Das, "Effects of power harmonics and its control techniques," in *Electromagnetic Interference and Compatibility '99. Proceedings of the International Conference on*, 1999, pp. 400-405.

[9] "IEEE Recommended Practice and Requirements for Harmonic Control in Electric Power Systems," *IEEE Std 519-2014 (Revision of IEEE Std 519-1992),* pp. 1-29, 2014.

[10] Wikipedia, "Utility frequency," *https://en.wikipedia.org/wiki/Utility_frequency*, last date of access, 27.02.2016.

[11] M. H. J. Bollen, Y. Liangzhong, S. K. Ronnberg, and M. Wahlberg, "Harmonic and interharmonic distortion due to a windpark," in *Power and Energy Society General Meeting, 2010 IEEE*, 2010, pp. 1-6.

[12] Z. Leonowicz, "Analysis of sub-harmonics in power systems," in *Environment and Electrical Engineering (EEEIC), 2010 9th International Conference on*, 2010, pp. 125-127.

[13] L. Hsiung Cheng, "Inter-Harmonic Identification Using Group-Harmonic Weighting Approach Based on the FFT," *Power Electronics, IEEE Transactions on,* vol. 23, pp. 1309-1319, 2008.

[14] B. Rehman, M. Ahmad, and J. Hussain, "Analysis of power system harmonics using singular value decomposition, least square estimation and FFT," in *Energy Systems and Policies (ICESP), 2014 International Conference on*, 2014, pp. 1-5.

[15] E. Fuchs and M. Masoum, *Power quality in power systems and electrical machines*: Academic Press, 2008.

[16] G. J. Wakileh, *Power systems Harmonics: Fundamentals, Analysis and Filter Design*: China machine press, 2003.

[17] M. S. S. J.Duncan Glover, Thomas J.Overbye, *Power System Analysis and Design*. USA: Westgroup, 2009.

[18] M. M. S. Chattopadhyay, and S. Sengupta, *Electric power quality*: Springer, 2011.

[19] R. G. Ellis, "Power system harmonics: a reference guide to causes, effects and corrective measures," *Allen-Bradley, Tech. Rep.*http://literature.rockwellautomation.com/idc/groups/literature/documents/wp/mvb-wp011-en-p.pdf, last date of access, 27.03.2016.

[20] J. Lundquist, "On harmonic distortion in power systems," *Ph.D. dissertation, Chalmers University of Technology , http://webfiles.portal.chalmers.se/et/Lic/LundquistJohanLic.pdf*, 2001.

[21] A. P. Technologies, "Total Harmonic Distortion and Effects in Electrical Power Systems," *http://www.aptsources.com/resources/pdf/Total%20Harmonic%20Distortion.pdf*, last date of access, 15.03.2016.

[22] C. K. Duffey and R. P. Stratford, "Update of harmonic standard IEEE-519: IEEE Recommended Practices and Requirements for Harmonic Control in Electric Power Systems," in *Petroleum and Chemical Industry Conference, 1988, Record of Conference Papers., Industrial Applications Society 35th Annual*, 1988, pp. 249-255.

[23] K. M. Goh, "Harmonic analysis for electrical power systems," *Master's thesis , University of Strathclyde,* pp. 64-88, December 1984.

[24] A. Ulinuha, M. A. S. Masoum, and S. M. Islam, "Harmonic power flow calculations for a large power system with multiple nonlinear loads using decoupled approach," in *Power Engineering Conference, 2007. AUPEC 2007. Australasian Universities*, 2007, pp. 1-6.

[25] "Modeling and simulation of the propagation of harmonics in electric

power networks. I. Concepts, models, and simulation techniques," *IEEE Transactions on Power Delivery,* vol. 11, pp. 452-465, 1996.

[26] S. Ranade and W. Xu, "An Overview of Harmonics Modeling and Simulation," http://calvin.edu/~pribeiro/IEEE/ieee_cd/chapters/pdffiles/c1pdf.pdf, last date of access, 26.03.2016.

[27] Wikipedia, "Skin effect," https://en.wikipedia.org/wiki/Skin_effect, last data of access 12.07.2016.

[28] S. A. Papathanassiou and M. P. Papadopoulos, "Harmonic analysis in a power system with wind generation," *IEEE Transactions on Power Delivery,* vol. 21, pp. 2006-2016, 2006.

[29] G. Li, C. Xu, G. Liu, and C. Zhao, "Calculation of three-phase harmonic power flow in power systems with traction loads," in *Power System Technology, 1998. Proceedings. POWERCON '98. 1998 International Conference on*, 1998, pp. 1565-1570 vol.2.

[30] X. C. L. Gengyin, L. Guanqi, and Z. Chengyong, "Calculation of threephase harmonic power flow in power systems with traction loads," *in Power System Technology, 1998. Proceedings. POWERCON'98. 1998 International Conference on,* vol. 2, pp. 1565–1570, 1998.

[31] D. L. Tennenhouse, J. M. Smith, W. D. Sincoskie, D. J. Wetherall, and G. J. Minden, "A survey of active network research," *IEEE Communications Magazine,* vol. 35, pp. 80-86, 1997.

[32] H. Abniki, S. Nateghi, R. Ghandehari, and M. N. Razavi, "Harmonic analyzing of wind farm based on harmonic modeling of power system components," in *Environment and Electrical Engineering (EEEIC), 2012*

11th International Conference on, 2012, pp. 667-672.

[33] S. Tentzerakis, N. Paraskevopoulou, S. Papathanassiou, and P. Papadopoulos, "Measurement of wind farm harmonic emissions," in *Power Electronics Specialists Conference, 2008. PESC 2008. IEEE*, 2008, pp. 1769-1775.

[34] F. Medeiros, D. C. Brasil, C. A. G. Marques, C. A. Duque, and P. F. Ribeiro, "Considerations on the aggregation of harmonics produced by large wind farms," in *Harmonics and Quality of Power (ICHQP), 2012 IEEE 15th International Conference on*, 2012, pp. 364-369.

[35] H. Novanda, P. Regulski, V. Stanojevic, and V. Terzija, "Assessment of Frequency and Harmonic Distortions During Wind Farm Rejection Test," *IEEE Transactions on Sustainable Energy,* vol. 4, pp. 698-705, 2013.

[36] A. Chidurala, T. K. Saha, N. Mithulananthan, and R. C. Bansal, "Harmonic emissions in grid connected PV systems: A case study on a large scale rooftop PV site," in *PES General Meeting | Conference & Exposition, 2014 IEEE*, 2014, pp. 1-5.

[37] J. Schlabbach, "Harmonic current emission of photovoltaic installations under system conditions," in *Electricity Market, 2008. EEM 2008. 5th International Conference on European*, 2008, pp. 1-5.

[38] X. Yan, R. En, and Y. Li, "Research on Power Supply Mode for Electric Vehicle Charging Devices in Residential Community," in *Vehicle Power and Propulsion Conference (VPPC), 2013 IEEE*, 2013, pp. 1-4.

[39] P. T. Staats, W. M. Grady, A. Arapostathis, and R. S. Thallam, "A statistical method for predicting the net harmonic currents generated by a concentration of electric vehicle battery chargers," *IEEE Transactions on*

Power Delivery, vol. 12, pp. 1258-1266, 1997.

[40] D. Xia and G. T. Heydt, "Harmonic Power Flow Studies Part I - Formulation and Solution," *IEEE Transactions on Power Apparatus and Systems,* vol. PAS-101, pp. 1257-1265, 1982.

[41] K. L. Lian and T. Noda, "A Time-Domain Harmonic Power-Flow Algorithm for Obtaining Nonsinusoidal Steady-State Solutions," *IEEE Transactions on Power Delivery,* vol. 25, pp. 1888-1898, 2010.

[42] Y. Baghzouz, "Effects of nonlinear loads on optimal capacitor placement in radial feeders," *IEEE Transactions on Power Delivery,* vol. 6, pp. 245-251, 1991.

[43] Z. A. Marinos, J. L. R. Pereira, and S. Carneiro, "Fast harmonic power flow calculation using parallel processing," *IEE Proceedings - Generation, Transmission and Distribution,* vol. 141, pp. 27-32, 1994.

[44] V. Sharma, R. I. Fleming, and L. Niekamp, "An iterative approach for analysis of harmonic penetration in the power transmission networks," *IEEE Transactions on Power Delivery,* vol. 6, pp. 1698-1706, 1991.

[45] B. Stott, "Decoupled Newton Load Flow," *IEEE Transactions on Power Apparatus and Systems,* vol. PAS-91, pp. 1955-1959, 1972.

[46] B. Stott and O. Alsac, "Fast Decoupled Load Flow," *IEEE Transactions on Power Apparatus and Systems,* vol. PAS-93, pp. 859-869, 1974.

[47] R. D. Zimmerman and C. Hsiao-Dong, "Fast decoupled power flow for unbalanced radial distribution systems," *IEEE Transactions on Power Systems,* vol. 10, pp. 2045-2052, 1995.

[48] J. Arrillaga and B. J. Harker, "Fast-decoupled three-phase load flow," *Electrical Engineers, Proceedings of the Institution of,* vol. 125, pp. 734-

740, 1978.

[49] H. Ying-Yi, L. Jun-Shin, and L. Chien-Hsun, "Fuzzy harmonic power flow analyses," in *Power System Technology, 2000. Proceedings. PowerCon 2000. International Conference on*, 2000, pp. 121-125 vol.1.

[50] P. Chen, Z. Chen, and B. Bak-Jensen, "Probabilistic load flow: A review," in *Electric Utility Deregulation and Restructuring and Power Technologies, 2008. DRPT 2008. Third International Conference on*, 2008, pp. 1586-1591.

[51] A. A. Romero, H. C. Zini, G. Ratta, and R. Dib, "Harmonic load-flow approach based on the possibility theory," *IET Generation, Transmission & Distribution,* vol. 5, pp. 393-404, 2011.

[52] P. Caramia, G. Carpinelli, T. Esposito, P. Varilone, I. Mastandrea, and F. Tarsia, "Probabilistic harmonic power flow for assessing waveform distortions in distribution systems with wind embedded generation," in *Power Electronics, Electrical Drives, Automation and Motion, 2006. SPEEDAM 2006. International Symposium on*, 2006, pp. 818-823.

[53] T. Esposito, G. Carpinelli, P. Varilone, and P. Verde, "Probabilistic harmonic power flow for percentile evaluation," in *Electrical and Computer Engineering, 2001. Canadian Conference on*, 2001, pp. 831-838 vol.2.

[54] A. Semlyen and M. Shtash, "Principles of modular harmonic power flow methodology," *IEE Proceedings - Generation, Transmission and Distribution,* vol. 147, pp. 1-6, 2000.

[55] G. N. Bathurst, B. C. Smith, N. R. Watson, and J. Arillaga, "A modular approach to the solution of the three-phase harmonic power-flow," in *Harmonics and Quality of Power Proceedings, 1998. Proceedings. 8th*

International Conference On, 1998, pp. 653-659 vol.2.

[56] M. Shlash and A. Semlyen, "Efficiency issues of modular harmonic power flow," *IEE Proceedings - Generation, Transmission and Distribution,* vol. 148, pp. 123-127, 2001.

[57] T. Jen-Hao and C. Chuo-Yean, "A fast harmonic load flow method for industrial distribution systems," in *Power System Technology, 2000. Proceedings. PowerCon 2000. International Conference on*, 2000, pp. 1149-1154 vol.3.

[58] T. Jen-Hao and C. Chuo-Yean, "Fast harmonic analysis method for unbalanced distribution systems," in *Power Engineering Society General Meeting, 2003, IEEE*, 2003, pp. 1-1249 Vol. 2.

[59] J. H. Teng and C. Y. Chang, "Backward/Forward Sweep-Based Harmonic Analysis Method for Distribution Systems," *IEEE Transactions on Power Delivery,* vol. 22, pp. 1665-1672, 2007.

[60] J. Lv, "A New Method for Harmonic Penetration Study in Power Networks with Renewable Generation," *PhD thesis at the University of Strathclyde,* 2014.

[61] J. Desmet, G. Vanalme, R. Belmans, and D. V. Dommelen, "Simulation of losses in LV cables due to nonlinear loads," in *Power Electronics Specialists Conference, 2008. PESC 2008. IEEE*, 2008, pp. 785-790.

Chapter 4 Impact of Harmonic Sources on Distribution Network Load Flow Analysis

4.1 Introduction

New harmonic sources that have appeared in recent years, have been introduced in Chapter 3. Among them, the wind turbine and the photovoltaic are not only harmonic sources, but are also the electricity generators. Large scale wind or photovoltaic generators can provide electrical energy as the main power source in the transmission network. However, they can also generate electrical energy as distributed generators.

Because of the need for more flexible electrical systems, energy saving and environmental protection, distributed generation has become an important part of electricity generation and its significance will continue to increase. Distributed generator is the application of small power generation technologies, which are normally installed within consumers' premises and are connected at the distribution level. Proper installation of the distribution network in the power systems can produce many benefits, such as reducing power loss and on-peak operating costs, improving voltage profiles, as well as deferring or eliminating for system upgrades [2-4]. However, with the emergence of DG units, distribution level has had a profound impact on grid security, operation and planning [5, 6]. Thus, the impact and analysis method of the distributed generators on load flow analysis cannot be ignored when solving the distribution network feeder reconfiguration problem.

More and more distributed generators are utilised as renewable generators, such as wind turbines and photovoltaic generators. The converter based generator is not only a distributed generator but also a harmonic source. After considering the power system harmonics, issues about converter based distributed generators in

harmonic conditions are discussed in this chapter.

Firstly, the impact of distributed generators on distribution networks is introduced in Section 4.2. Section 4.3 discusses the simulation of all types of distributed generators in harmonic load flow analysis, as well as the four bus types; all distributed generators are normally classified into three bus types. Following on, how they can be simulated is illustrated in Section 4.4. The PV type of distributed generators is a special one. Thus, a sensitive matrix-based method for solving these PV type distributed generators is introduced in Section 4.5. In order to verify the accuracy of the harmonic backward/forward sweep method, a 12-bus system is used to test in two scenarios in Section 4.6. After comparing the results with results obtained by using other harmonic analysis method, a deficiency of the harmonic backward/forward sweep method was discovered in scenario two. An improved version to avoid this deficiency is proposed in Section 4.7. Finally, two case studies are analysed in Section 4.8. One case demonstrates the accuracy of the proposed method for harmonic load analysis in the distribution network. The other case investigates the impact of the distributed generators.

4.2 Impact of the Distributed Generators on the Distribution Network

With the rapid development of distributed generators, it has become clear that distributed generators have significant advantages in modern power systems. Its main advantages can be highlighted in the following four points: [1]

The first point to note is that, whereas traditional large power stations can take years to complete the installation, distributed generators can begin to provide electrical energy within a few weeks. This rapid installation characteristic of

distributed generators can be extremely useful when there is a sudden rise in energy demand. Distributed generators can be utilised when fast power restoration is required, for example, in the wake of any natural disasters.

Secondly, due to their capacity, distributed power stations can be expanded or reduced according to the demand. This scalability is superior than with traditional large power stations. The costs of installation, operation and maintenance of the distributed power stations are lower than the traditional large power stations. An expended distributed power station can be built easily in regions where there is a high demand for critical power infrastructure.

Thirdly, the installation of traditional large power stations needs large amounts of investment. However, the demand for the energy in some remote areas cannot be sustained to the same level as that generated by traditional large power stations. Due to their relatively small size and low investment of distributed power stations, the power energy demand of any remote areas can be satisfied with an appropriate distributed power station.

Finally, distributed power stations can be located close to demand areas. They can facilitate the controls, operations and maintenance of the distributed power station. The advantage is that specific needs of any remote area can be satisfied, whilst enabling system operators to monitor and customise distributed power solutions.

However, every coin has two sides. Distributed generators provide many benefits, but they also bring many challenges. All of these challenges come from the power system and can be divided into four aspects:

I. Challenge of power system bus voltage [7, 8]*:*

Distributed generators are mostly connected to the distribution network. After distributed generators connected to the distribution network, the framework of distribution network transforms from a radial network to a multi-power source

network. The loads which close to the distributed generators may not supply by the transmission network anymore. The direction and quantity of the load flow in the distribution network could change substantially. This may be followed by a change in the stable system bus voltages. The original voltage regulator strategy may not satisfy the requirements of the system voltage, after connecting the distributed generators to the distribution network. Thus, an assessment of the impact of distributed generators on the distribution network is necessary. Load flow analysis is the primary method for a quantitative analysis of this impact, although a majority of the distribution network power flow method ignores this impact. Large tolerance cannot be avoided when any distribution network with distributed generators is analysed using these methods.

In the steady state, a compensation algorithm based on the sensitivity matrix, which takes into account the impact of the distributed generators, is mentioned in Reference [7, 8]. This compensation algorithm can also be used in the backward/forward sweep technology, and so it will be introduced in Section 4.5. This thesis will also use this algorithm in order to analyse the distribution network with distributed generators.

II. Challenge on power quality[9]*:*

Almost all renewable electrical power generators are based on power electronics technology. The amount of non-linear load is significantly increased by the application of the power electronic converters. The converter is the main harmonic source in the power system. Therefore, the adverse impact of the power system harmonic is brought to the distribution network for the distributed generator, such as harmonic voltage, current distortion and harmonic resonance.

III. Challenge on power system protection [10, 11]*:*

At one time, the topology of the distribution network was radial. The main purpose of this topology is the simplicity of operations and the economy of the over-current protection. When a distributed generator is connected to a distribution network, its radial network nature will become a multi-source network. The direction of the power flow is no longer only from the substation to the loads. Then, the distribution of the branch currents is also changed. Due to the changing on branch currents, the device of power protection may not operate correctly. Therefore, distributed generators have a large impact on the original power protection method.

IV. Challenge on electricity market [12]*:*

If the owners of the distributed generators are the consumers in the conventional electrical market, these owners would have three choices within the electricity market:

- buy electrical energy from the grid,
- generate their own electrical energy to the level of self-sufficiency,
- sell the surplus electrical energy to the market.

The regulations of the electricity market would be greatly transformed if consumers selling electrical energy to the market is accepted.

4.3 The Bus Type in the Distribution Network

If the power station setup is divided into the traditional large power station and the distributed power station, many kinds of generators could be installed at the distributed level. To simplify the simulation during the load flow calculation, different types of distributed generators and loads are categorised into different types of buses. In the same type of bus, the difference in distributed generator and

loads is that the generator generates power energy, however the load absorbs power energy. Therefore, the simulation of all kinds of distributed generators and loads can be transformed to the simulation of the bus type. Similar to the transmission network, the buses are categorised into four types:

1. slack bus or swing bus,
2. PQ bus or linear bus,
3. PV bus or voltage control bus,
4. PS bus or nonlinear bus.

A brief introduction of the bus types are shown as follows: [7, 13, 14]:

a) Slack bus

Normally, there is only one balance node in one power system. Before beginning the load flow analysis, the total power consumption including loss of the system is unknown. Thus, the active and reactive power on at least one node cannot be fully specified in the system. Additionally, one node with zero voltage phase angle and known node voltage must exist within the system. The voltage phase angle of this node will be the reference point for all the other nodes in the system. Normally, this can simplify the calculation process where these two types of combinations are set on one bus. This bus is called the slack bus or swing bus. Because the active and reactive is unknown, the slack bus is chosen as one directly connected to a main power plant or substation. In this thesis, only one bus with known voltage magnitude in the distribution network is the source node (main substation). Therefore, the voltage phase angle on the source bus is assumed to be zero.

b) PQ bus

Both the active and reactive power are specified on this bus type. The bus voltage magnitude and phase angle of this bus type are unknown in the power flow

calculation. Linear loads or the generator with known active and reactive power belong to this bus type.

c) PV bus

For this bus type, the active power and voltage magnitude are the given parameters. Therefore, the reactive power and voltage phase angle on this bus are the unknown variables. Because the bus voltage magnitude is specified, the adjustable range of the reactive power must be large. Thus, this bus type is normally a generator bus. In the distribution network, the bus that normally connects to the distributed generator is a typical PV bus.

d) PS bus

There is no PS bus in the classification for the fundamental power system. The PS bus is defined according to the power system harmonic. Due to the active and apparent power of harmonic source is known, the bus that is connected to the nonlinear loads can be classified as the PS bus. Normally, depending on the characteristic of the nonlinear loads, this bus type can transform to PQ bus or PV bus. When nonlinear loads with the known active and reactive power connect to the bus, these loads are converted to PQ bus with the fundamental load flow calculation, such as an electric vehicle battery charger. If convertor-based generators are connected to the bus, these generators will be treated as PV bus in fundamental load flow calculations. Examples of these are wind turbine generators and photovoltaic arrays. In the harmonic load flow calculation, the PS bus is regarded as the harmonic source.

4.4 Analysis Methods for Different Types of Distributed Generators

In Section 4.3, all generators are considered to be one of the four types of system

bus. This classification allows the analysis method of the various types of distributed generators be allocated as one of the four types of the system bus. It greatly simplifies the process of distribution system simulation.

As mentioned previously in this thesis, both the fundamental and harmonic load flow analysis is determined by the backward/forward sweep-based algorithm. Because the given power distribution in the distribution network is the fundamental values, back-forward sweep method can only calculate the power flow of the distribution network without PV type of distributed generators. But if the generator is converter-based, the reactive power output of this generator could not be determined in advance. In order to analyse the distribution network by using backward/forward sweep technology, the unknown element of the PV type generator must be obtained. Thus, the analysis method of four types of system bus types will be illustrated as follows.

4.4.1 PQ type of generator

In a typical distribution network, a large number of the buses are PQ type. Because the active and reactive power are known, these loads can be simulated simply. In the simulation of the distribution network, nodes with known active and reactive power are simulated as PQ type load. Comparing with the PQ type loads, the only difference between PQ type distributed generators is that the direction of power flow is opposite. Thus, the PQ type distributed generator can be assumed as the minus PQ type load. It can be mathematically expressed as the following:

$$\begin{cases} P_{node} = -P_g \\ Q_{node} = -Q_g \end{cases} \tag{4-1}$$

where P_{node} and Q_{node} are active and reactive power on one node of the distribution network. P_g and Q_g are active and reactive power of PQ type

distributed generator.

4.4.2 PV type of generator

In PV type of distributed generators, the active power P_g and voltage magnitude V_g are known elements. However, the reactive power Q is unknown. The PQ type bus connected to a distributed generator can be simply treated as load. Following this rule, if the PV type bus connected to a distributed generator is also treated as the minus load, its mathematical expression can be [8]:

$$\begin{cases} P_{node} = -P_g \\ |V_{node}| = |V_g| \end{cases} \tag{4-2}$$

With the backward/forward sweep method, the required known system parameters are the active power (P) and reactive power (Q) of the bus. Consequently, this equation cannot be used directly.

According to the theoretical analysis and practice, reference [15] indicates that:

a) The value of a reactive power on any system node will relate to the node voltage magnitude.
b) If the active power of a distributed generator is unchanged, the output voltage of this distributed generator would grow with the increase of its reactive power.

Thus, the reactive power of the distributed generator can be modified, based on the node voltage deviation. It can be expressed as:

$$Q_g^t = Q_g^{t-1} + \Delta Q_g = Q_g^{t-1} + f\left(\Delta V_g^t\right) \tag{4-3}$$

where t is the number of iteration, $f(\Delta V_g^t)$ is the expression of ΔQ_g.

Generators normally have limitations on their output of reactive power. If the calculated reactive power was over or below its limiting value, the output value of the generator should be fixed at its maximum or minimum value. Thus, the equation 4-3 can be modified as [8]:

$$Q_g^t = \begin{cases} -(Q_g^{t-1} + \Delta Q_g) & -Q_g^{max} \le -(Q_g^{t-1} + \Delta Q_g) \le -Q_g^{min} \\ -Q_g^{max} & Q_g^{t-1} + \Delta Q \le -Q_g^{max} \\ -Q_g^{min} & Q_g^{t-1} + \Delta Q \ge -Q_g^{min} \end{cases} \tag{4-4}$$

where Q_g^{max} and Q_g^{min} are the upper and lower limitations of the PV type generator respectively.

4.4.3 PS type of generator

There are two categories of PS type generators; one with known active and reactive power that converts to PQ type generation in fundamental load flow analysis; the other with known active power and voltage magnitude that is converted to PV type generator, in fundamental load flow analysis. In the harmonic load flow analysis, both of them are regarded as the harmonic source. Their simulation and analysis methods are already introduced in Chapter 3.

4.5 Sensitive Matrix-based Method for Compensative Reactive Power on the PV Type Distributed Generator

All kinds of generators are classified and their simulation method is provided in Section 4.4. The issue of reactive power compensation of PV type generators has

still not been resolved however. It is only known that there is a relationship between the reactive power compensation of PV type generator and its voltage magnitude. In references[7, 8, 16], a sensitive matrix-based method for solving this problem is provided.

Assuming that there are several PV type generators in a distribution network and the injection current on its connection bus is positive. Then, the relationship between injection current increment vector ΔI and bus voltage increment vector ΔV can express by the following equation[8]

$$Z\Delta\bar{I} = \Delta\bar{V} \tag{4-5}$$

where Z is the node impedance matrix $\Delta\bar{I}$ and $\Delta\bar{V}$ is the injection current and bus voltage increment vector respectively.

Normally in the distribution network, the per unit value of the voltage magnitude on each bus is approximately equal to 1, and the voltage phase angle is small. Thus, the per unit value of rated bus voltage can be approximately as $1\angle 0^{\circ}$. Then, the equation 4-5 can be modified as:

$$V_R * Z\Delta\bar{I} = V_R * \Delta\bar{V} \tag{4-6a}$$

$$Z * \bar{V}_R\Delta\bar{I} = 1 * \Delta\bar{V} \tag{4-6b}$$

$$Z * \Delta\bar{S}^* = \Delta\bar{V} \tag{4-6c}$$

$$\begin{bmatrix} X & R \\ -R & X \end{bmatrix} \begin{bmatrix} \Delta\bar{Q} \\ \Delta\bar{P} \end{bmatrix} = \begin{bmatrix} \Delta|V| \\ \Delta\delta \end{bmatrix}$$

(4-6d)

where V_R is the rated bus voltage in per unit, $\Delta\bar{S}$, $\Delta\bar{P}$, $\Delta\bar{Q}$ is the incremental matrix of apparent, active and reactive power respectively. $\Delta|V|$ and $\Delta\bar{\delta}$ is the incremental matrix of voltage magnitude and the voltage phase angle respectively. * is the symbol of the conjugate.

Ignoring the relationship of voltage phase angle $\Delta\delta$, equation 4-6d shows that：

$$X\Delta\bar{Q} + R\Delta\bar{P} = \Delta|V|$$

(4-7)

Because the active power of PV type generator is constant, the value of the active power increment ΔP is equal to 0. Thus, equation (4-7) can be updated as:

$$\Delta\bar{Q} = X^{-1} * \Delta|V|$$

(4-8)

where X is the reactance matrix which is constituted by the imaginary part of the Z matrix. It is defined as the node reactance matrix of the PV type distributed generator.

It is clear from equation 4-8 that the reactive power compensation ΔQ of the PV type distributed generator, not only has relations between the magnitude of the bus voltage and its deviation $\Delta|V|$ of itself, but also relates to the magnitude of the bus voltage and voltage deviation of all other PV type distributed generators in the distribution network. Therefore, the reactive power compensation ΔQ of a PV type distributed generator mainly depends on bus voltage deviation $\Delta|V|$ of each distributed generator, as well as the node reactance matrix, X.

$$\begin{bmatrix} \Delta Q_1 \\ \Delta Q_2 \\ \vdots \\ \Delta Q_c \end{bmatrix} = \begin{bmatrix} X_{11} & X_{12} & \cdots & X_{1c} \\ X_{21} & X_{11} & \cdots & X_{2c} \\ \vdots & \vdots & \ddots & \vdots \\ X_{c1} & X_{11} & \cdots & X_{cc} \end{bmatrix}^{-1} * \begin{bmatrix} \Delta|V|_1 \\ \Delta|V|_2 \\ \vdots \\ \Delta|V|_c \end{bmatrix}$$

(4-9)

where c is the total number of distributed generators in the distribution network.

The equation 4-9 is the expansion of equation 4-8. In this equation, reactive compensation ΔQ is the required value. If matrixes of $\Delta|V|$ and X are known, the matrix of ΔQ can be determined. Then, the reactive power Q_g in equation 4-4 will be obtained, so that the PV type distributed generators can be converted to PQ type distributed generator.

Bus voltage deviation $\Delta|V|$ can be calculated from equation 4-10. The node reactance matrix can be obtained using the method shown in reference [8].

$$\Delta|V|_i = \Delta|V|_i^k - \Delta|V|_i^{k+1}$$

(4-10)

where i is the code of the bus and k is the number of iteration in the process of the backward/forward sweep algorithm.

It is assumed that there are n PV type distributed generators in the network. Then, the node reactance matrix should be a matrix with $n \times n$ elements, which is illustrated in equation 4-9. The diagonal element x_{ii} is the self-reactance of the PV type distributed generator on bus i. Its value is equal to the sum of the branch reactance from resource bus to bus i. The non-diagonal element x_{ij} is the mutual reactance of these PV type distributed generators and its value is equal to the sum of the reactance of the common branches, between the source node and all PV type generators. An example showing the method schematic is illustrated in Figure 4-1.

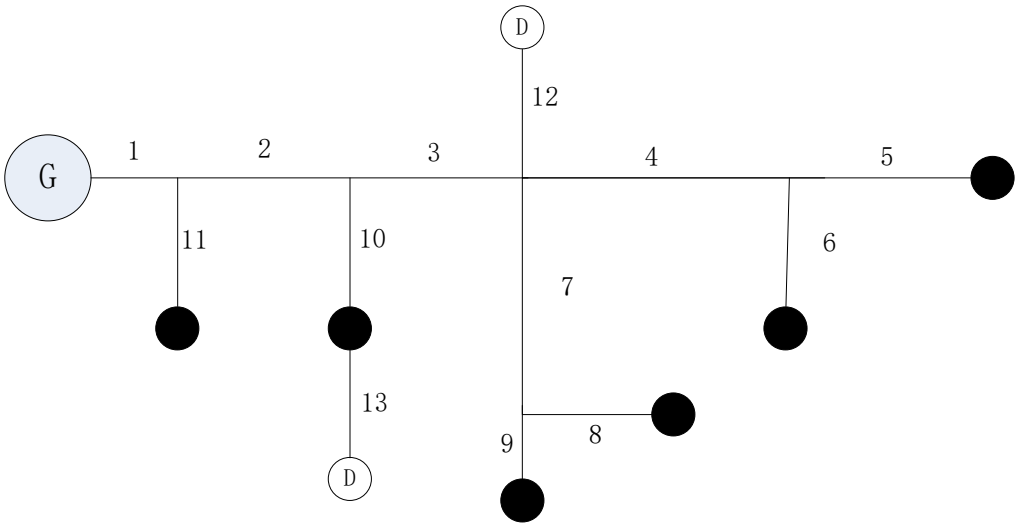

Figure 4-1 A simple distributed network with two distributed generators

In Figure 4-1, G is the source bus. D is the bus with distributed generators. The rest are general buses. The numbers are the code of the branches. Two PV type distributed generators are installed at the end of the branch 12 and 13 respectively. Therefore, the size of the node reactance matrix is 2×2 with mathematical expression shown in equation 4-11.

$$X = \begin{bmatrix} x_{11} & x_{12} \\ x_{21} & x_{22} \end{bmatrix} \tag{4-11}$$

In equation 4-11, the equation for obtaining the self-reactance x_{11} and x_{22} and the mutual reactance x_{12} and $x_{21}$are shown as follows:

$$\begin{cases} x_{11} = x_1 + x_2 + x_3 + x_{12} \\ x_{22} = x_1 + x_2 + x_{10} + x_{13} \\ x_{12} = x_{21} = x_1 + x_2 \end{cases} \tag{4-12}$$

where $x_1, x_2, x_3, x_{10}, x_{12}$ and x_{13} is reactance of branches 1,2,3,10,12 and 13 respectively.

The reactive power compensation of a PV type distributed generator is calculated after obtaining the node reactance matrix. According to equation 4-4, the value of the reactive power of the PV type bus can be determined easily. Thus, the PV type distributed generators can transform to PQ type by using this reactive power. The backward/forward sweep algorithm can then analyse the distribution network with distributed generators in fundamental frequency. In harmonic analyses, the equivalent harmonic injection currents of all kinds of harmonic sources are determined by harmonic current spectrum. After solving all issues on distribution generators and harmonics, the special harmonic load flow analysis for the distribution network reconfiguration with distributed generator can be determined.

4.6 Case Study for the Original Harmonic Forward/Backward Sweep Method

Case studies for harmonic backward/forward sweep method are divided into two parts. In order to investigate the accuracy of this method, a 12-bus system without any distributed generator, which is similar to the network in reference [17] is tested first. The harmonic backward/forward sweep method is proposed in reference [17]. Following on, the case studies investigating the impact of a distributed generator in a 12-bus system will be tested in Section 4.8.

One of the assumptions for the feeder reconfiguration problem is that the distribution system is a three-phase balanced system. Thus, all the test systems in this thesis are three-phase balanced distribution systems. In Section 3.2.3, it is explained that all even harmonic components in the power system can be ignored, as well as the triple harmonic orders in the three-balanced system, which has the circuit with delta winding connection or star winding, without the neutral

connection. Accordingly, with these harmonic characteristics, the even and triple times system harmonic orders can be set to ignore in all case studies in this thesis. If needed, an analysis of the even and triple times system harmonic orders could be done by simply adding the even and triple times harmonic spectra into the system input data.

4.6.1 Scenario one

a) Test system

In order to illustrate the harmonic backward/forward sweep method, the test system is the 12-bus system. The system data of the 12-bus is shown in Appendix A.4. It is assumed that the main power source for this 12-bus system is an ideal voltage source. The voltage magnitude is 1 per unit. The phase angle is 0. The code for the main source is number 5. All loads in this scenario are set to be nonlinear load, which is the same as in reference [17]. Nonlinear load model is the electrical vehicle charger clusters and its harmonic emission spectra, as shown in Table 3-7. The network structure is shown in Figure 4-2.

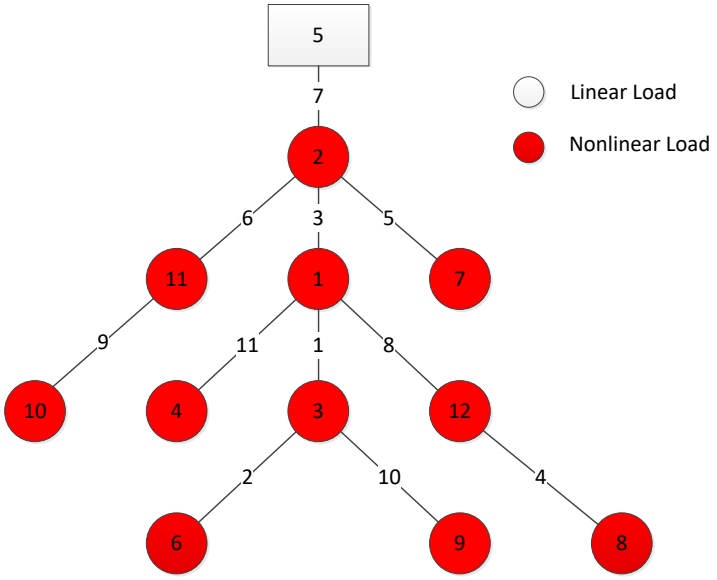

Figure 4-2 12-buses system with all nonlinear loads

b) Results of Scenario One

The fundamental distribution load flow analysed by the backward/forward sweep algorithm, is introduced in Chapter 2. By using the results of fundamental load flow analysis and the harmonic backward/forward sweep method, which is introduced in Chapter 3, the scenario results of bus voltages magnitude are shown in Table 4-1 in per unit.

Table 4-1 The fundamental and the higher harmonic bus voltage magnitudes in per unit in a 12-bus power system with all nonlinear loads

Bus No.	1^{st}	5^{th}	7^{th}	11^{th}	13^{th}
5	1	0	0	0	0
2	0.9972	0.0197	0.0194	0.0166	0.0093
11	0.9964	0.0210	0.0207	0.0177	0.0099
1	0.9949	0.0311	0.0307	0.0263	0.0147
7	0.9956	0.0207	0.0204	0.0175	0.0098
10	0.9957	0.0217	0.0214	0.0183	0.0103
4	0.9942	0.0318	0.0314	0.0269	0.0151
3	0.9940	0.0348	0.0343	0.0294	0.0165
12	0.9935	0.0335	0.0330	0.0283	0.0158
6	0.9930	0.0356	0.0351	0.0301	0.0169
9	0.9919	0.0361	0.0356	0.0305	0.0171
8	0.9922	0.0347	0.0342	0.0293	0.0164

The curves in Figure 4-3 and Figure 4-4 show the fundamental voltage magnitude, as well as the harmonic voltage magnitude components in per unit respectively. The curve in Figure 4-3 is the fundamental bus voltage magnitude in per unit. Its harmonic components are shown in Figure 4-4, which is a three-dimensional diagram. The harmonic order increases from inside to outside. From this three-dimensional diagram, the harmonic voltages on the 5^{th}, 7^{th} and 11^{th} harmonic order are much larger than the 13^{th} harmonic order. This implies that the higher harmonic order components have less influence on the harmonic voltage distortion.

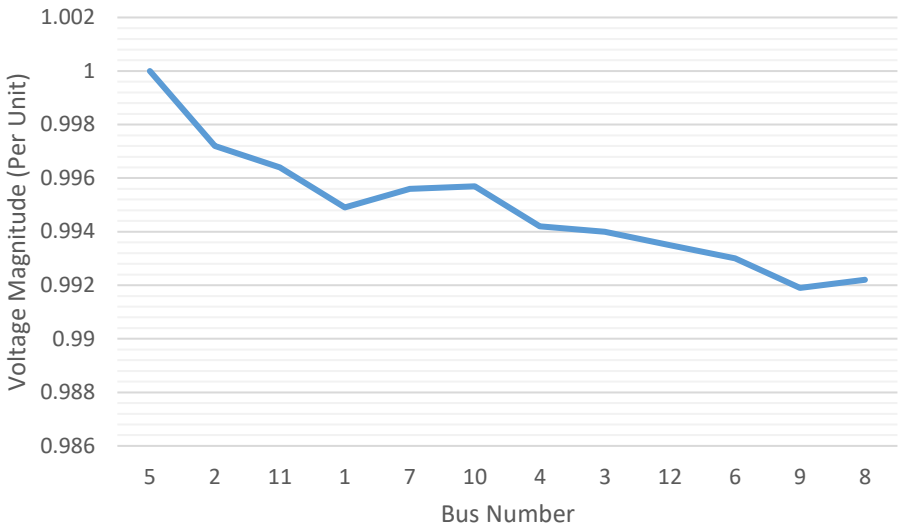

Figure 4-3 The fundamental bus voltage magnitude

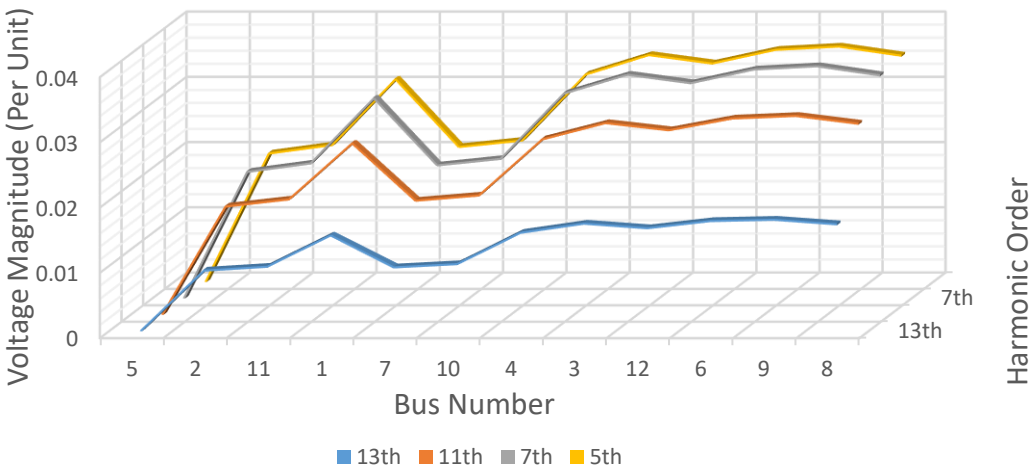

Figure 4-4 The harmonic bus voltage magnitude of scenario one

Figure 4-5 shows a histogram for the total harmonic voltage distortion. The histogram displays the rate of change between the total harmonic voltage and the fundamental voltage. The highest total harmonic voltage distortion in this distribution system is at bus 9 and its value is 6.2089%.

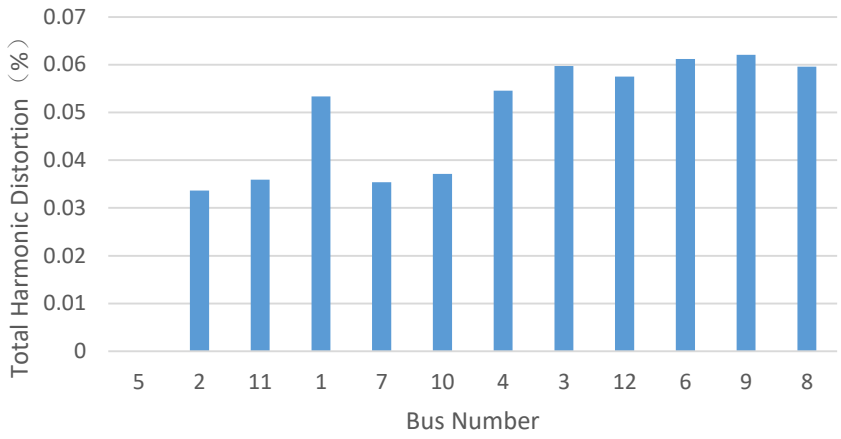

Figure 4-5 The total harmonic voltage distortion on buses of scenario one

According to the IEEE 519 standard limitation, the harmonic voltage distortion of a single harmonic order cannot be larger than 3% and the total harmonic voltage distortion should be below 5%. From Figure 4-5, it can be seen that over half of the total harmonic voltage distortion is over 5% limitation. In Table 4-1, the largest single harmonic voltage component is the 5^{th} harmonic order on bus 9. Its' harmonic voltage magnitude is 0.0361, as seen in Table 4-1 with red ink. The percentage of highest harmonic voltage distortion on the signal harmonic order in this scenario is 0.0361/0.9930*100 = 3.64%. This shows that this system cannot allow electrical vehicles with the use of scale charges at the same time.

The system active power loss is 14.074kW according to the fundamental load flow analysis. If all buses have the electrical vehicle charger clusters, the system active power loss would increase to 22.600kW. This result shows that system harmonics can increase the system loss during the electric energy transmission. The large scale of the nonlinear loads without the harmonic filter will highly increase the system active power loss. In this scenario, the active power loss increased by 60.58% with electrical vehicle charger clusters.

c) Comparison and discussion on scenario one

Equation 4-13 is a widely used conventional method for the analysis of the harmonic load flow. The accuracy of this conventional method is approved by many searchers, such as in reference [8]. However, the admittance matrix Y in the distribution network is a singular matrix. Therefore, Y^{-1} in the distribution network cannot be calculated. Although Y^{-1} is equal to the impedance matrix Z, it is still difficult to ascertain the value of the impedance matrix Z. This conventional method also cannot solving the recode problem, when trying to resolve the feeder reconfiguration problem. To investigate the accuracy of the harmonic backward/forward sweep method, the 12-buses test system is analysed using the conventional harmonic method which is mentioned above.

$$I^{(h)} = V^{(h)}Y^{(h)} \tag{4-13}$$

Figure 4-6 shows the results of the comparison of total harmonic voltage distortion on each bus. The results obtained from the harmonic backward/forward sweep method are shown with the blue bar. The results calculated by the conventional method are shown with the orange bar. All values of the total harmonic voltage distortion on each bus, which are calculated by two different methods, are almost the same. The maximum gap between the value of blue bars and orange bars are approximately 0.2% on bus 3. Its means that the biggest tolerance of these two methods is about 3%. Although tolerance exists between these two methods, such a difference is within acceptable limits. Thus, the accepted accuracy of the harmonic backward/forward sweep method is proved by scenario one.

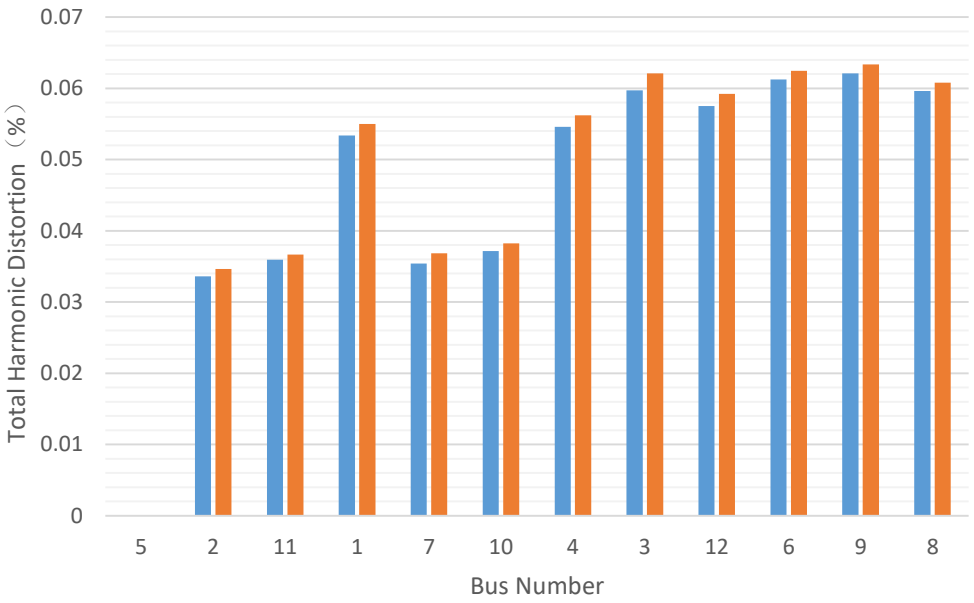

Figure 4-6 The results of the comparison of total harmonic voltage distortion on buses in scenario one

4.6.2 Scenario two

a) Test system

Virtually all settings in scenario two are the same as scenario one, with one exception: the settings of the nonlinear loads. In this scenario, only the loads on bus 6, 8 and 9 are set to be nonlinear loads. The rest of the loads in the system are linear. The network structure is shown in Figure 4-7.

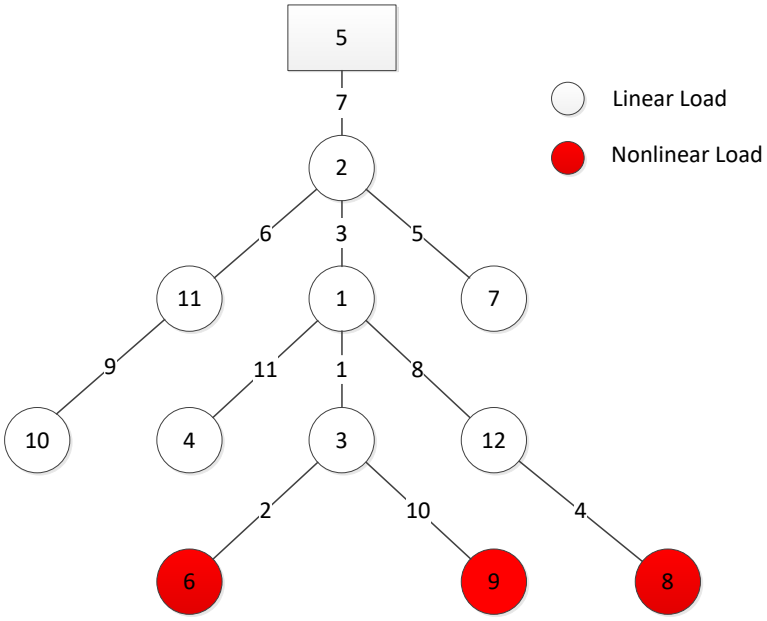

Figure 4-7 12-buses system with 3 nonlinear loads

b) Results of scenario two

The results of the fundamental load flow analysis are the same as in scenario one. This is expected since the test system for both scenarios are the same. One main difference with scenario one, is that only 3 of the loads are set to the electrical vehicle charger cluster, in accordance with the harmonic backward/forward sweep method. The results of the system harmonic voltage components on each bus are shown in Table 4-2.

Table 4-2 The fundamental and the higher harmonic bus voltage magnitudes, in per unit in a 12-bus power system with 3 nonlinear loads

Bus No.	1^{st}	5^{th}	7^{th}	11^{th}	13^{th}
5	1	0	0	0	0
2	0.9972	0.0028	0.0027	0.0024	0.0013
11	0.9964	0.0028	0.0027	0.0024	0.0013
1	0.9949	0.0056	0.0055	0.0047	0.0026
7	0.9956	0.0028	0.0027	0.0024	0.0013
10	0.9957	0.0028	0.0027	0.0024	0.0013
4	0.9942	0.0063	0.0062	0.0053	0.0030
3	0.9940	0.0063	0.0062	0.0053	0.0030
12	0.9935	0.0068	0.0067	0.0057	0.0032
6	0.9930	0.0071	0.0070	0.0060	0.0034
9	0.9919	0.0063	0.0062	0.0053	0.0030
8	0.9922	0.0068	0.0067	0.0057	0.0032

Again similar to the scenario one, most parts of the conclusions are the same. The general shape of the harmonic voltage magnitude curve is the same in Figure 4-8. There were only three nonlinear loads in the system in scenario two. As a result, the maximum value of the harmonic voltage magnitude in single harmonic order is smaller than in scenario one. The largest single harmonic voltage magnitude component is the 5^{th} harmonic voltage at bus 6, which is marked in red.

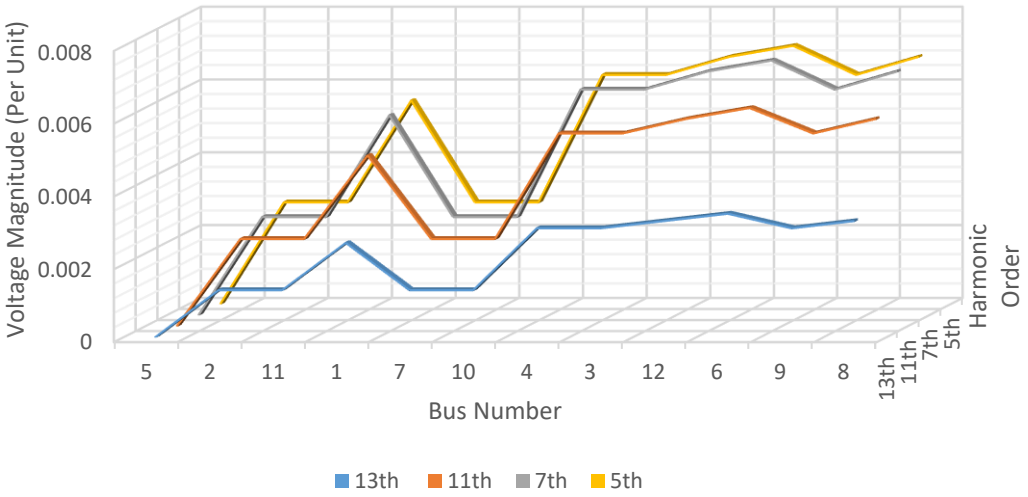

Figure 4-8 The harmonic bus voltage magnitude of scenario two

The total harmonic voltage distortion in scenario two is shown in the bar chart in Figure 4-9. The highest total harmonic voltage distortion in this scenario is 1.2272% on bus 6. From this figure, the total harmonic voltage distortion on each bus is less than 5%. The largest single harmonic voltage value is 0.0071 per unit on bus 6. Therefore, the percentage of highest harmonic voltage distortion on the signal harmonic order in scenario two is 0.0071/0.9930*100 = 0.72%. Comparing with the results of the IEEE limitation standard, this system can allow more electrical vehicle clusters to be connected and charged at the same time.

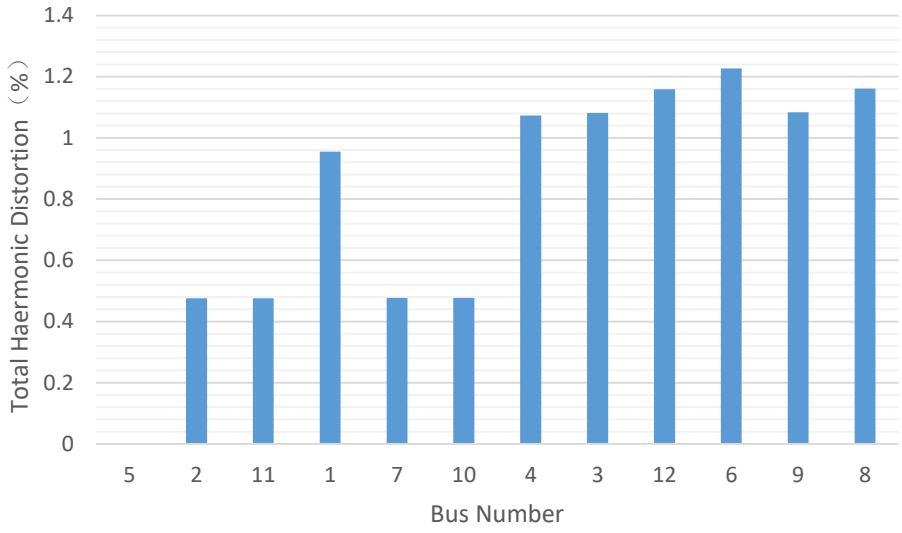

Figure 4-9 The total harmonic voltage distortion on the buses

The system's active power loss is 14.468kW, according to the harmonic backward/forward sweep method. If buses 6, 8 and 9 were not the electrical vehicle chargers, the system's active power loss would be 14.074kW. In this scenario, the active power loss is increased by 2.8% due to the connection of the three electrical vehicle charger clusters.

c) Comparison and discussion of scenario two

In order to further confirm the accuracy of the harmonic backward/forward sweep method, scenario two is tested. The results of the comparison of total harmonic voltage distortion on each bus in scenario two is provided in Figure 4-10. The results from the fast harmonic method is shown by the blue bar. The results calculated by the conventional method ($I = VY$) are shown with the orange bar. Clearly, almost all of the total harmonic voltage distortions have a large tolerance, expect bus 8. With the bus 7 in particular, the tolerance between the two methods is over 95%. Such tolerance is not in the allowable range. Consequently, there must have been some deficiency in the harmonic backward/forward sweep method.

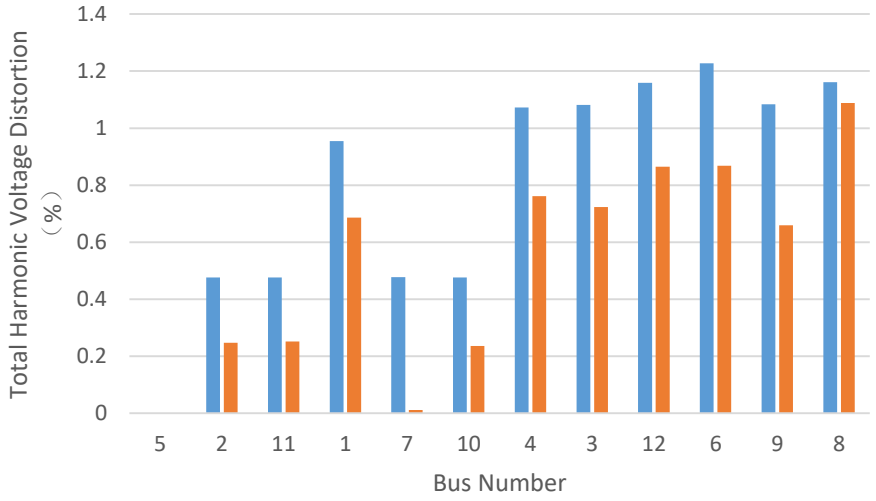

Figure 4-10 The results comparison of total harmonic voltage distortion on buses

In order to discover the deficiency in the harmonic backward/forward sweep method, as well as to improve this method, the results of the harmonic branch currents should be analysed. Table 4-3 shows the details of the harmonic injection currents on each branch in the system.

Table 4-3 The fundamental and the higher harmonic branch current magnitudes in per unit in a 12-bus power system with 3 nonlinear loads

Branch Number	1^{st}	5^{th}	7^{th}	11^{th}	13^{th}
7	0.2679	0.0299	0.0211	0.0115	0.0054
6	0.0254	0	0	0	0
3	0.2057	0.0299	0.0211	0.0115	0.0054
5	0.0368	0	0	0	0
9	0.0254	0	0	0	0
11	0.0445	0.011	0.0077	0.0042	0.002
1	0.0797	0.0079	0.0055	0.003	0.0014
8	0.0446	0.011	0.0078	0.0042	0.002
2	0.0318	0.0079	0.0055	0.003	0.0014
10	0.0478	0	0	0	0
4	0.0446	0	0	0	0

Table 4-3 shows that all the harmonic branch current of branches 6, 5, 9, 10 and 4 are zero. This cannot be correct. Kirchhoff's current law states that at any node (junction) in an electrical circuit, the sum of currents flowing into that node is equal to the sum of the currents flowing out of that node or equivalently. Since all the branches are connected to the test system, each branch should have its own fundamental and harmonic currents.

In the test system of reference [17], all buses are assumed to have nonlinear loads. Under such a supposition, each branch has its backward harmonic injection current. However, not all branches can have injection harmonic current under all conditions, according to the harmonic backward/forward sweep method, such as the test system in scenario two. The harmonic load flow diagram shown in Figure 4-11 illustrates the details of the harmonic load flow, when not all loads have the nonlinear load.

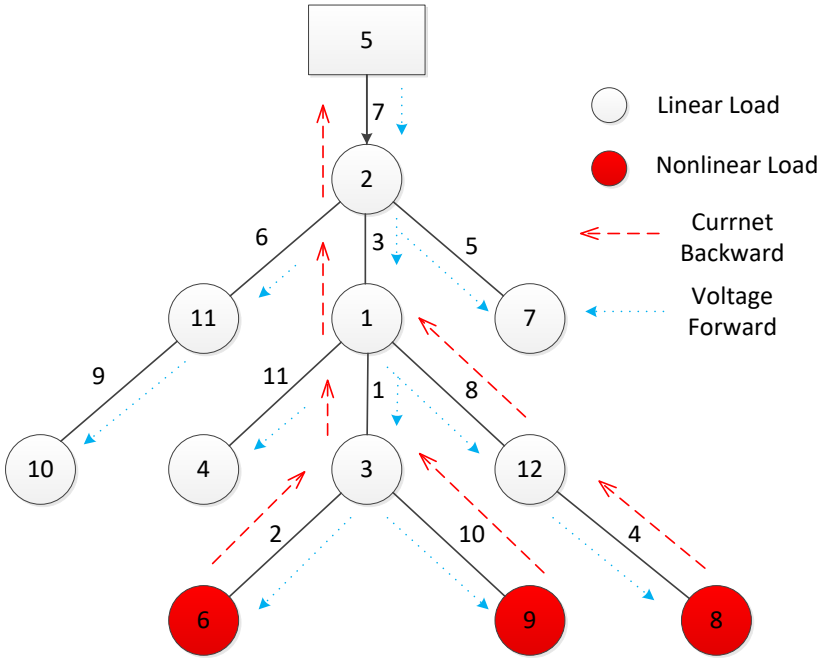

Figure 4-11 System current flow diagram using harmonic backward/forward sweep method

In Figure 4-11, according to the theory of harmonic backward/forward sweep

method, which is proposed by reference [17-19], the branch current flow in the current backward sweep is represented by the red dash line. The branch current flow in the voltage forward sweep is expressed by the blue dotted line. Comparing the blue dotted line with the red dash line, it is determined that the calculation of the branch harmonic current component is incorrect in the backward current sweep. For example, the backward current flow at node 1 is $I_3^{(h)} = I_1^{(h)} + I_8^{(h)}$. However, Kirchhoff's current law indicates that the current flow at node 1 should be $I_3^{(h)} + I_{11}^{(h)} = I_1^{(h)} + I_8^{(h)}$.

The current flows on the tributaries that are without nonlinear load are ignored in the harmonic backward/forward sweep method. This is why the results of the total harmonic voltage distortion have a large tolerance with the results which are calculated by the conventional method. An improvement is needed in the harmonic backward/forward sweep method in order to obtain a more accurate result by using the harmonic backward/forward sweep method.

4.7 Improvement of the Harmonic Backward/Forward Sweep Method

In Section 4.6, after comparing the results of the harmonic backward/forward sweep method with the conventional method, the reason why there is a tolerance in the result of total harmonic voltage distortion has been discovered. The test system results show that parts of the system harmonic injection currents are equal to zero. When comparing the differences between the two scenarios, it is clear that the primary reason why the harmonic backward/forward sweep method has a

different accuracy is the different location of the harmonic sources.

Reference [20] is the follow-up paper by the same author for the harmonic backward/forward sweep method for an unbalanced three-phase distribution system. Figure 4-12 shows the test system in this reference. In Figure 4-12, nodes, which are located at bus 3 and bus 6, are the ending nodes of one tributary. They do not connect to harmonic sources. Their upper buses are bus 2 and bus 4 respectively. According to the discussion about scenario two in Section 4.6, the node voltages in the same tributary, without connecting to the harmonic source, will be the same on each harmonic order. Table 4-4 shows the test results of this system, which is taken from the reference. The results of the node voltages on these two tributaries are shown in red and blue respectively. The value is the same in each harmonic order in the same tributary. It can thus be concluded that the harmonic backward/forward sweep method has a deficiency, which is caused by the location of harmonic sources.

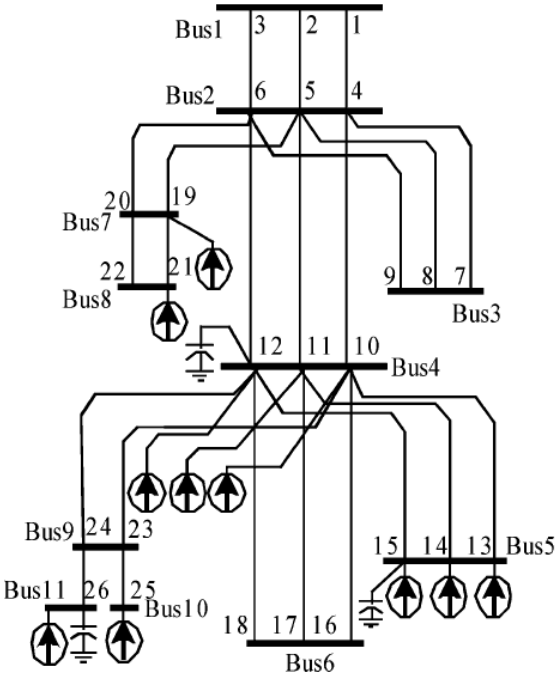

Figure 4-12 Eleven-bus unbalanced three-phase feeder

Table 4-4 Test results of 11-bus system [20]

Node Number	Nodes Voltage (p. u.)											THD
	Fund	3th	4th	5th	6th	7th	8th	9th	11th	13th	15th	(%)
1	1	0	0	0	0	0	0	0	0	0	0	0
2	1	0	0	0	0	0	0	0	0	0	0	0
3	1	0	0	0	0	0	0	0	0	0	0	0
4	0.977	0.008	0.002	0.005	0.018	0.006	0.0006	0.0026	0.0017	0.0012	0.001	2.2734
5	0.98	0.002	0.004	0.002	0.009	0.005	0.0007	0.0022	0.0013	0.0008	0.0006	1.2892
6	0.984	0.011	0.005	0.012	0.045	0.01	0.0005	0.002	0.0008	0.0004	0.0003	5.0479
7	0.976	0.008	0.002	0.005	0.018	0.006	0.0006	0.0026	0.0017	0.0012	0.001	2.2749
8	0.98	0.002	0.004	0.002	0.009	0.005	0.0007	0.0022	0.0013	0.0008	0.0006	1.2889
9	0.984	0.011	0.005	0.012	0.045	0.01	0.0005	0.002	0.0008	0.0004	0.0003	5.0483
10	0.956	0.018	0.006	0.011	0.038	0.012	0.0012	0.0053	0.0036	0.0026	0.0022	4.8952
11	0.979	0.001	0.011	0.005	0.022	0.01	0.0012	0.0038	0.0023	0.0014	0.001	2.7142
12	0.967	0.025	0.006	0.026	0.091	0.02	0.001	0.0039	0.0015	0.0007	0.0005	10.4536
13	0.951	0.019	0.005	0.011	0.038	0.012	0.0012	0.0055	0.0038	0.0028	0.0024	5.0166
14	0.979	0.001	0.011	0.005	0.022	0.01	0.0012	0.0038	0.0023	0.0014	0.001	2.7165
15	0.964	0.026	0.006	0.026	0.093	0.02	0.001	0.0039	0.0014	0.0007	0.0004	10.6913
16	0.956	0.018	0.005	0.011	0.038	0.012	0.0012	0.0053	0.0036	0.0026	0.0022	4.8952
17	0.979	0.001	0.011	0.005	0.022	0.01	0.0012	0.0038	0.0023	0.0014	0.001	2.7142
18	0.967	0.025	0.005	0.026	0.091	0.02	0.001	0.0039	0.0015	0.0007	0.0005	10.4536
19	0.97	0.004	0.005	0.002	0.008	0.005	0.0008	0.0026	0.0016	0.001	0.0007	1.3336
20	0.987	0.011	0.005	0.012	0.044	0.01	0.0005	0.0021	0.0009	0.0005	0.0004	4.9784
21	0.965	0.005	0.005	0.002	0.007	0.006	0.0008	0.0028	0.0018	0.0012	0.0009	1.417
22	0.988	0.011	0.005	0.012	0.044	0.01	0.0005	0.0022	0.001	0.0006	0.0004	4.9513
23	0.953	0.018	0.006	0.012	0.041	0.012	0.0013	0.0055	0.0037	0.0027	0.0022	5.1957
24	0.963	0.027	0.012	0.028	0.098	0.021	0.0011	0.0042	0.0015	0.0007	0.0004	11.3405
25	0.95	0.018	0.006	0.012	0.041	0.013	0.0013	0.0055	0.0038	0.0027	0.0023	5.2248
26	0.962	0.028	0.012	0.029	0.103	0.022	0.0012	0.0044	0.0016	0.0007	0.0005	11.8895

To eliminate this deficiency, an improvement is suggested on the harmonic backward/forward sweep method.

According to Figure 4-13 (A), the deficiency appears at the injection current backward sweep. The harmonic branch currents of the tributaries, without harmonic source, are ignored by the harmonic backward/forward method. If these harmonic currents are calculated and participate in the voltage forward sweep calculation, the deficiency would be overcome.

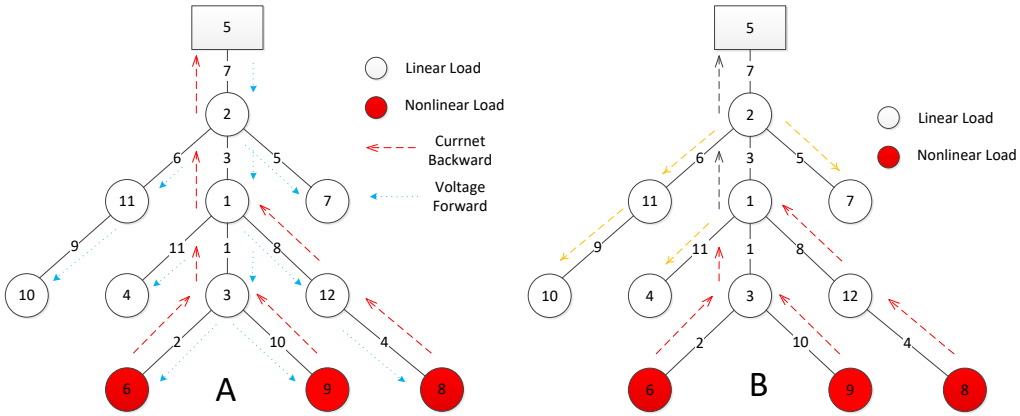

Figure 4-13 System current flow diagram during fast harmonic method

Following this rule, the flow diagram of the injection current backward sweep should be the same with Figure 4-13 (B). In this figure, the red dash line is the complete injection harmonic current, which is generated by the harmonic sources. The ignored harmonic branch current is represented by the yellow dash line. Its direction is from the source bus to the ending bus of each tributary that does not connect to harmonic sources. For easy to distinguish different branch currents, this kind of harmonic branch currents is defined as ‘forward harmonic branch current’ in this thesis. The true backward harmonic branch current flow to the source bus is represented by the black dash line. Tributaries without harmonic sources will not produce a harmonic injection current. However, it cannot ignore the existence of the harmonic current on these tributaries. Kirchhoff's Current Law states that the

sum value of current, represented by the red line in Figure 4-13 (B), should equal to the summation value of the yellow and black lines. Thus, the basic theory for improving the harmonic backward/forward method is that the forward harmonic branch current on those tributaries, which have no connection with the harmonic source, must be calculated in the current backward sweep.

In general, location conditions of the harmonic source in the tributaries can be divided into three types. The first is all ending buses connect to harmonic source in the tributary. The yellow area in Figure 4-14 illustrates this status. The second condition is that part of the ending buses connect to harmonic source in the tributary. The buses in the green triangle in Figure 4-14 illustrate this situation. The third condition is that the tributary is without any harmonic source, which is the grey part in Figure 4-14. These three cases need to be solved respectively.

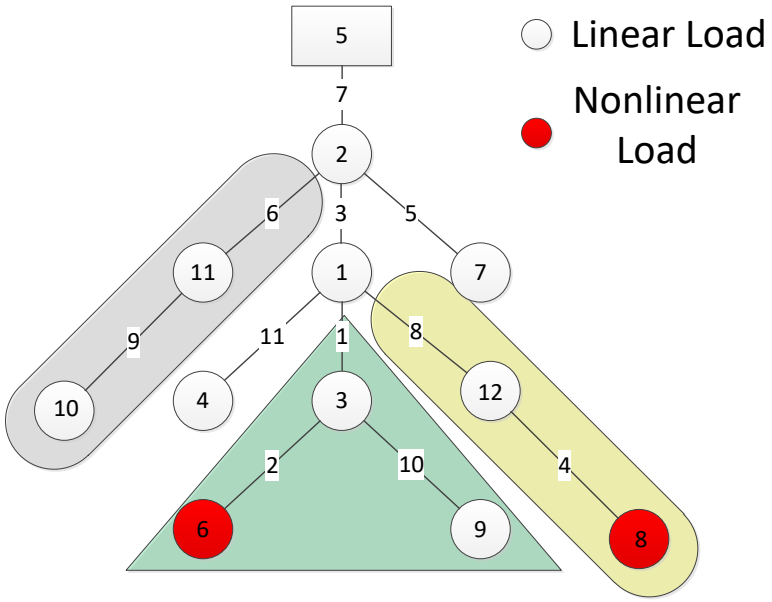

Figure 4-14 12-bus system with harmonic sources

a) Yellow type tributary

In the yellow area, due to all the ending buses that connect to harmonic sources, all branches in this tributary have their harmonic branch currents. This is the same

with the case in the reference [17] and scenario one in Section 4.6. The original method already proves its accuracy. Thus, the analysis method for this type is unchanged.

b) Green type tributary

In the situation as indicated in the green triangle appears, the forward harmonic branch current needs to be calculated. In Figure 4-14, the system is split into three parts by the bus 3, with the harmonic source (bus 6) and an ending bus without harmonic source (bus 9), as well as the rest of the whole distributed network. If higher accuracy is required, the equivalent branch impedance of the rest of the whole distributed network needs to be calculated. Kirchhoff's Current Law states that the harmonic current on branch 1, 2 and 10 can then be obtained. Nonetheless, the calculation of the equivalent branch impedance of the rest of the whole distributed network is not simple. If many green type tributaries exist in the distribution network, the calculation for equivalent branch impedance needs to be done several times. In the distribution network feeder reconfiguration, iterations for reconfiguration may need to be done perhaps hundreds of times. If the computing time for the equivalent branch impedance is too long, the cost would be too much for even one iteration. As a result, the whole efficiency of the feeder reconfiguration would be severely reduced. Thus, according to the engineering experience, the equivalent branch impedance is taken instead of the impedance of the branch which connects to the split bus. In the green triangle of Figure 4-14, this branch is branch 1, which connects to the split bus 3. Therefore, the real forward current I_1 can be calculated easily, as well as the ignored harmonic current I_{10}.

c) Grey type tributary

The grey type tributary is the tributary that is without any harmonic source. Because the harmonic sources do not exist in the grey tributary, the harmonic current on this tributary is equal to zero in the current backward sweep. According

to the method for green type in part b), the harmonic current backward sweep can only obtain the harmonic current on the branches which connect directly to the split bus. Branches which are far from the split bus will be ignored, under the above rule. The grey part in Figure 4-14 represents these branches. Harmonic branch currents on the grey tributary are the forward harmonic branch current, which comes from the others tributary in the same network. Therefore, in the backward sweep, the grey tributary will be recorded first. When the injection current backward sweep is finished, the branch in the grey type area, which connects to the split bus, will obtain its harmonic branch current. Then, a current forward sweep is added to calculate these recorded branches in the grey tributary, before the voltage backward sweep. The rules for calculating these branch currents is the same as with part a) and part b).

The layered backward/forward sweep algorithm will divide the network into several levels. It is defined that the first level, level 1, is consider as the lowest level. And the greater the numerical value is, the higher the level is. The sequence of classification for the three types tributaries above also follows these network levels. This means that the classification will only happen at the highest level first. When the classification and the parallel injection current calculation at the highest level are done, the green and yellow type need to convert to an equivalent harmonic source and the three type tributaries need to be classified again at the upper level. This conversion is clearly illustrated in Figure 4-15. Figure 4-15 (B) shows that the yellow part does not exist and a new green triangle appears. The above classification for the three type tributaries and calculations for the forward harmonic branch current need to be done at each network level.

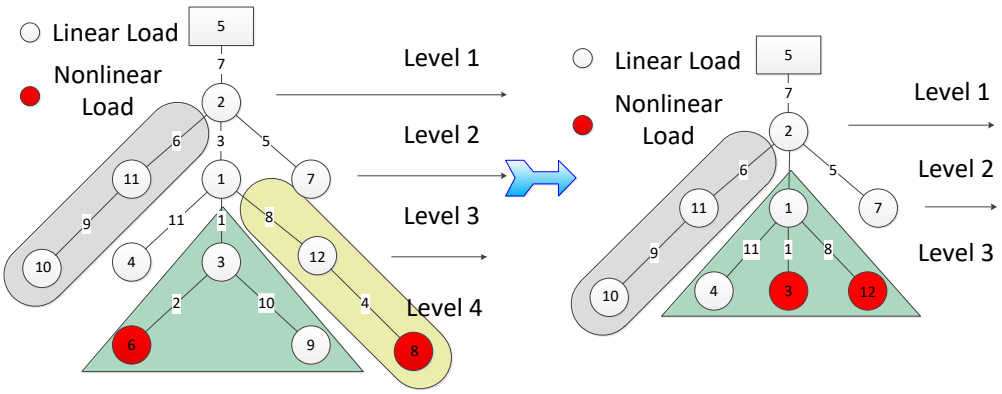

A B

Figure 4-15 conversion processes of equivalent harmonic sources

The calculations for the branch current on the grey type tributary is not the same. When the branch backward sweep is finished, the branch currents on those branches, which are connected to the split buses, are obtained. Then, the branch currents on the grey type tributary can be calculated following the sequence of the system levels. The difference is that this sequence begins from level 1 to the highest level, and the conversion for the equivalent harmonic source is unnecessary.

When all branch harmonic currents have been calculated, the rest of the process is the same as with the harmonic backward/forward sweep method. Then, the calculation for harmonic branch currents and harmonic bus voltages on one harmonic order is finished.

The steps for the improved harmonic backward/forward sweep method are introduced as follows. Compare with the commonly used harmonic backward/forward sweep method, step 3, step 4, step 5 and step 8 are new steps for the proposed method. Due to these additional steps, the ignored harmonic branch current can be calculated.

- Step 1- analyse the fundamental load flow base on the backward/forward sweep algorithm.

- Step 2 - begin calculations from the smallest harmonic order, which has not yet been calculated.
- Step 3 - find all harmonic sources and classify them into three types of tributary, within the highest network level.
- Step 4 - record the branches which belong to the grey type.
- Step 5 - start harmonic branch current calculations at the highest network level.
- Step 6 - convert green and yellow type to the equivalent harmonic source and remove the level temporarily.
- Step 7 - go back to Step 3 until the first level is calculated.
- Step 8 – calculate the harmonic currents for the recorded branch in the current forward sweep, from the first network level to the highest level.
- Step 9 - calculate the harmonic bus voltages in the voltage forward sweep.
- Step 10 - go back to step 2 until the required largest harmonic order has been calculated.
- Step 11 - calculate the required information, dependent on the results at each harmonic order.

The flow chart of the improved harmonic backward/forward sweep method is shown in Figure 4-16.

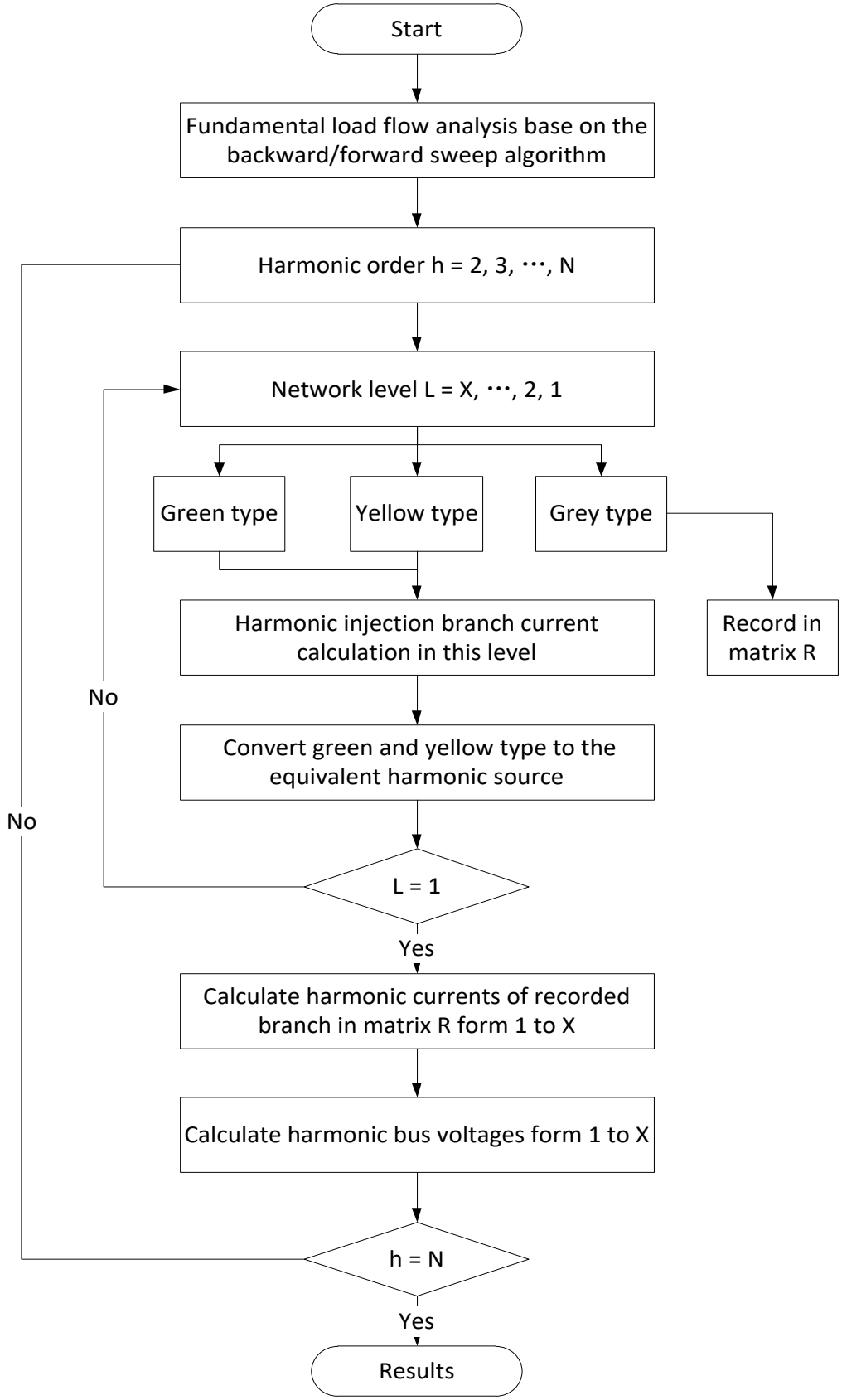

Figure 4-16 Flow chart of improved fast harmonic evaluation method

4.8 Case Study and Discussion for the Improved Harmonic Backward/Forward Sweep Method

After the improved harmonic backward/forward sweep method is introduced, the same system used in the scenario in Section 4.6 is used in scenario one, in order to compare the accuracy of the improved method. Two different types of the distributed generators are connected to the system in scenario two to investigate the impact of the distributed generator. The model for distributed generators and nonlinear loads are assumed as wind generator, photovoltaic array and electrical vehicle chargers, which are introduced in Section 3.3.2. The method used for modelling the distributed generators in the distribution network is the same as with the reference [8].

4.8.1 Scenario one

a) Details of the distribution network

Figure 4-7 illustrates the diagram of the test system. In order to make an accurate comparison between the original and the improved harmonic backward/forward sweep method, it is ensured here that this test system is completely identical to the test system in scenario two in Section 4.6.

b) Results and discussion

In order to compare the differences in results between the original method and the improved method, details of the fundamental and higher harmonic bus voltage magnitudes in per unit are provided in Table 4-5. The largest single harmonic voltage magnitude component is the 5^{th} harmonic voltage at bus 9, which is highlighted in the red colour. Although both largest single harmonic voltage magnitude appeared at the 5^{th} harmonic order, this largest harmonic voltage is on bus 6, when the original method is used and on the bus 9 when the improved

method is used.

Table 4-5 The fundamental and the higher harmonic bus voltage magnitudes in per unit in a 12-bus power system, with 3 nonlinear loads by improved fast harmonic evaluation method

Bus No.	1^{st}	5^{th}	7^{th}	11^{th}	13^{th}
5	1	0	0	0	0
2	0.9972	0.0005	0.0005	0.0004	0.0002
11	0.9964	0.0010	0.0010	0.0008	0.0005
1	0.9949	0.0018	0.0018	0.0015	0.0009
7	0.9956	0.0010	0.0010	0.0008	0.0005
10	0.9957	0.0015	0.0015	0.0012	0.0007
4	0.9942	0.0032	0.0031	0.0027	0.0015
3	0.9940	0.0040	0.0040	0.0034	0.0019
12	0.9935	0.0031	0.0031	0.0026	0.0015
6	0.9930	0.0053	0.0052	0.0045	0.0025
9	0.9919	0.0054	0.0053	0.0045	0.0025
8	0.9922	0.0044	0.0043	0.0037	0.0021

Figure 4-17 shows the general shape of the harmonic voltage magnitude curves in each harmonic order. The same can be seen with the general shape in Figure 4-9 using the original method. These curves are also shown in a three-dimensional diagram. The curve of the bus voltage magnitudes in Figure 4-8 shows a significant fluctuation on bus 1. In contrast, the curve in Figure 4-17 is smoother. Due to the fact that branch 11 cannot obtain the harmonic current from bus 1, all harmonic voltage increments caused by the harmonic currents have an effect on bus 1. Consequently, the value of bus voltage magnitude on bus 1 is much larger than its value in Figure 4-17.

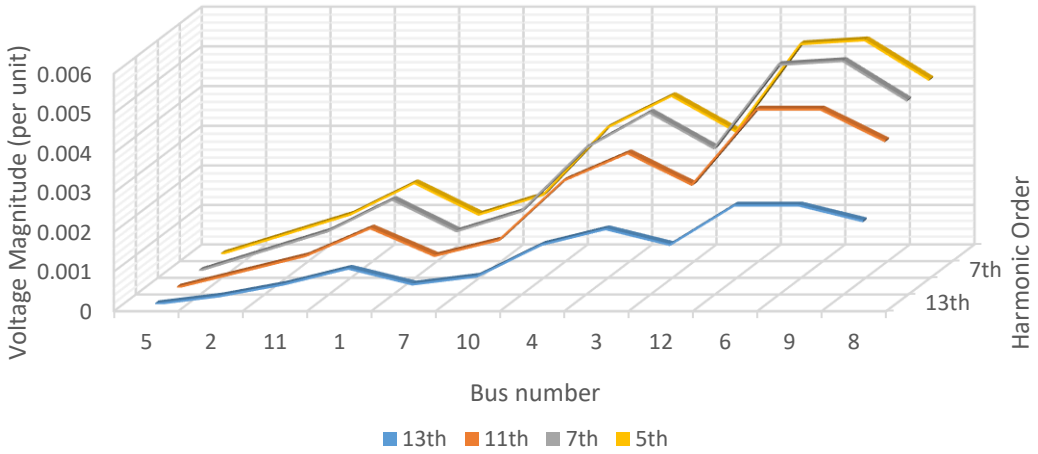

Figure 4-17 The harmonic bus voltage magnitude of scenario one with the proposed method

Figure 4-18 shows the results of the total harmonic voltage distortion obtained by three different methods. In this figure:

- blue bar represents results of the original method,
- orange bar represents results of the improved method,
- grey bar represents results of the conventional method.

The results of the original harmonic backward/forward sweep method have large tolerance with other methods. The results of the improved method are almost the same as the results obtained by the conventional method ($I = VY$). The largest tolerance between the improved method and the conventional method is on bus 4.

From the theory of the improved method, it can be discovered that the tolerance is caused by using the impedance of one branch, instead of the impedance of the equivalent network, in order to analyse the forward harmonic branch current which is defined in Section 4.7. In Figure 4-7, the impedance of branch 3 may be smaller than the equivalent network of branch 3, branch 5, branch 6, branch 7 and branch

9. Thus, when the impedance on branch 11 is constant and in the equivalent network, it is on branch 3, the equivalent impedance becomes smaller, so that the forward harmonic branch current will increase on branch 3. The larger harmonic current on branch 3 will bring about the increment on all branch currents of the equivalent network. Thus, the total harmonic voltage distortion obtained by the improved method will be a little larger than the results of the conventional method, except on bus 4. In addition, the largest tolerance between the improved method and the conventional method is smaller than 10%. This tolerance is acceptable.

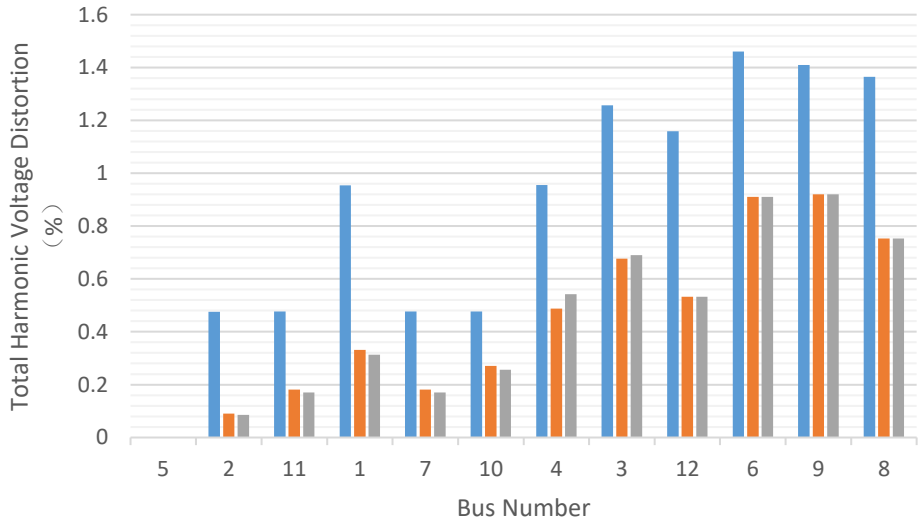

Figure 4-18 The results comparison of total harmonic voltage distortion by different methods

The highest total harmonic voltage distortion by the improved method is 0.92% on bus 9. This value, which was calculated by the original fast harmonic evaluation method, is 1.46%. The result of the original method is 58.7% higher on bus 9. According to the IEEE limitation standard, the 5% limitation for total harmonic voltage distortion will reduce to 3.15% by using original harmonic backward/forward sweep method. The highest harmonic voltage distortion on the signal harmonic order in this scenario is 0.0054/0.9919*100 = 0.54%. The result

obtained by the original method is also 59.3% higher. Therefore, to fulfil the requirements of the total harmonic voltage distortion limitation, more equipment cost on the harmonic filter needed to be installed by using the original method in some cases.

The total active power loss calculated by the improved method is 14.767kW. Comparing the system loss obtained by the original method in Section 4.6, the difference is 0.85% larger. This tolerance is small when compared with the tolerance in the total harmonic voltage distortion limitation. However, this could still lead to an inaccurate final solution to the distribution feeder reconfiguration problem.

4.8.2 Scenario two

a) Details of the distribution network

The system structure for scenario two is illustrated in Figure 4-19. This scenario is composed of one wind turbine, one photovoltaic array and the same distribution system which is used in scenario one. Almost all parts of the network in Figure 4-19 match the network in Figure 4-7, with the exception of the bus 3 and the bus 4. A 500kW 72 SWT 2.3-93 wind turbine connects to bus 3 and its harmonic emission spectra is shown in Table 3-4. A photovoltaic array composed of one hundred, 2kW photovoltaic generators, is connected to bus 4 and its harmonic emission spectra is given in Table 3-7. These two distributed generators are directly connected to the buses, and the impedance of the distribution line between bus and distributed generator is ignored. The rated voltage of both distributed generators is the same, with the system reference voltage.

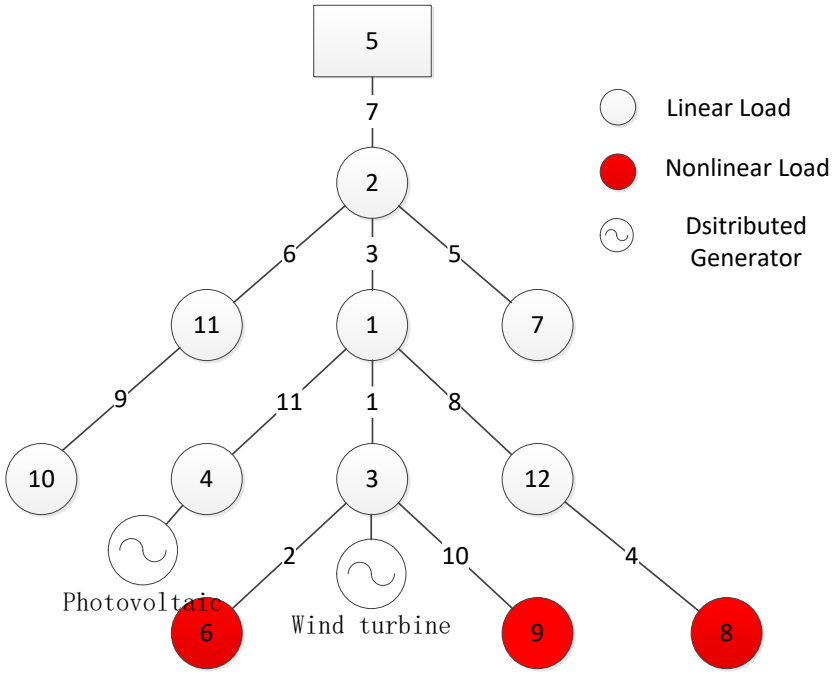

Figure 4-19 System in scenario two

b) Results and discussion

There are two distributed generators that connect to the network. To make a comparison, the fundamental result which calculated without considering system harmonics will be shown in details in this part. The blue curve in Figure 4-20 is the result of the test system only, which is considered fundamental component without harmonic. The results which are considered both fundamental and harmonic are expressed as the orange curve. The maximum harmonic voltage component is 0.0081 per unit at the 5^{th} harmonic order on bus 9, and its fundamental value is 0.9979. The largest gap between the fundamental and harmonic bus voltage magnitude in per unit at the same bus is about 1%. Thus, the two curves in Figure 4-20 are almost superimposed on each other. In this scenario, it can be seen that the impact of harmonic sources on bus voltage is very small. Furthermore, under the effect of the system harmonic, the real bus voltage of PV bus 4 and bus 3 is a little higher than its rated voltage.

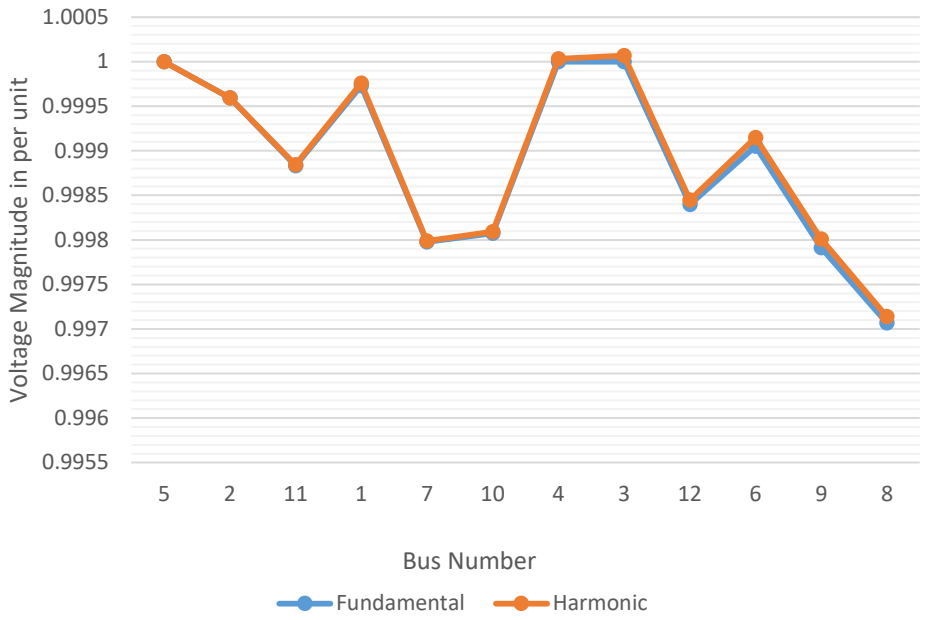

Figure 4-20 Bus voltage magnitudes comparison between fundamental and harmonic

Both curves in Figure 4-21 consider harmonic. The orange curve is the value when the distributed generators are connected to the system; the yellow one is the results of the same system without any distribution generators. The PV type distributed generators are connected to bus 3 and bus 4 respectively. Therefore, the bus voltage magnitude in the orange curve is approximately equal to 1. All the bus voltage magnitudes are increased after the distributed generators are connected to the test system, which can be seen when comparing the orange curve with the yellow one. The system maximum voltage drop reduces from 0.81% to 0.29%. The reduction of voltage drop is 64.2%. The positive impact of the distributed generators on system bus voltage drop can be proved by these results.

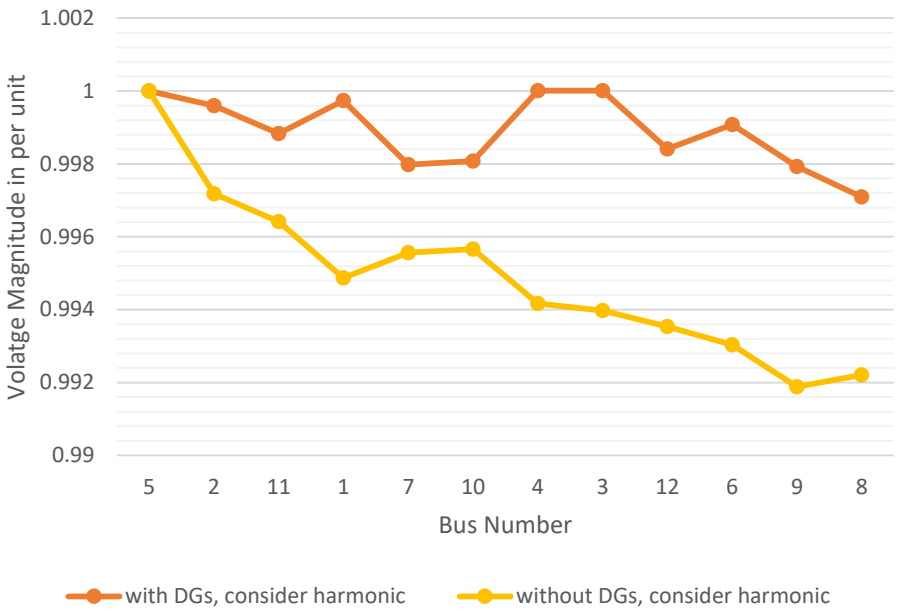

Figure 4-21 Impact of the distributed generators on bus voltage magnitudes

The comparison of the impact of the distributed generators on total harmonic voltage distortion is illustrated in Figure 4-22. Although distributed generators have a significant impact on reducing the drop in system voltage, the PV type distributed generators can increase the system harmonic level. The maximum increment of the total harmonic voltage distortion is 151.78% on bus 2, bus 11 and bus 7 respectively in this scenario. Thus, a harmonic load flow analysis is necessary when the new distributed generators are connected to a high harmonic penetration distribution network.

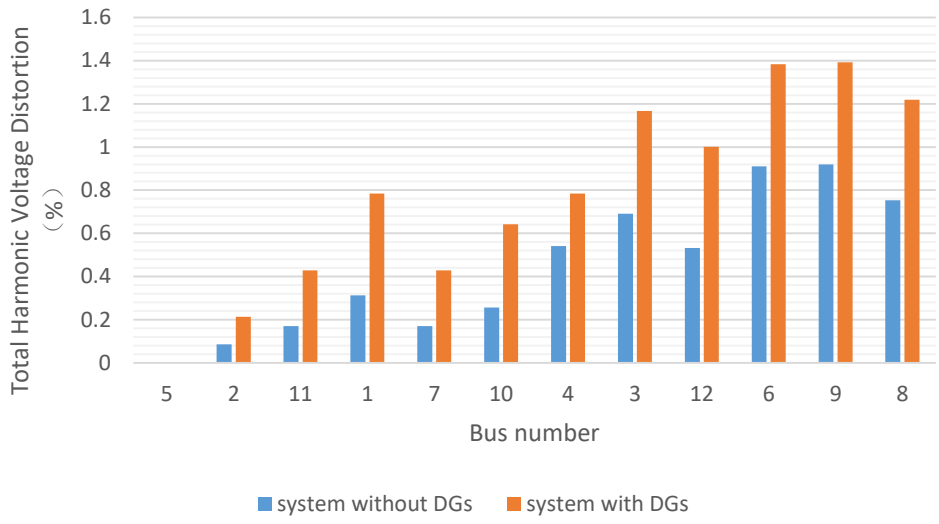

Figure 4-22 Impact of the distributed generators on total harmonic voltage distortion

The network power loss of the test system is 10.757kW, when system harmonics is considered. If the distributed generators are removed from the test system, the new system power loss increased to 14.379kW. The reduction in system power loss is 33.67%, by installing the distributed generator in this scenario. According to the results of the voltage drop and the power loss reduction, distributed generators connected to the distribution network may have a great positive impact on power quality and network loss reduction.

4.9 Summary

PV type generators can be analysed by using backward/forward sweep algorithm, which is introduced in this chapter. This method can analyse the harmonic load flow in any distribution network with distributed generators.

With the simulation of the harmonic backward/forward sweep method for the distribution network, it is found that this method can successfully analyse the system well, when all loads are nonlinear loads. However, if only parts of the system loads are nonlinear load, the tolerance of the harmonic backward/forward sweep method is not acceptable. Therefore, an improvement for calculating the correct harmonic branch currents, that are based on the harmonic backward/forward sweep method is necessary before applying this method to resolve all possible situations within the distribution network.

After analysing the results in detail, the shortcomings of the original harmonic backward/forward sweep method will enlarge the real system harmonic level. By using this method, the permissible level of harmonic limitation is actually smaller than the standard value. There is a higher cost involved, for more equipment, in order to suppress system harmonics. Also, the original harmonic backward/forward sweep method will cause inconsistencies in the network loss. Although these inconsistencies may be small in value, less than a percent, they may still lead to larger monetary losses when it comes to power system management on an industrial scale. Furthermore, these small tolerances will bring an inaccurate optimal solution in the distribution feeder reconfiguration problem. This study has shown that these discrepancies can be avoided using the improved version of analysis.

To overcome the shortcomings of the original harmonic backward/forward sweep method, the location conditions of the harmonic source in the tributaries are

divided into three types by the proposed method in this chapter. Then, parts of the ignored forward harmonic branch currents can be calculated according to these harmonic source types. The rest of ignored harmonic branch currents are obtained by an additional current forward sweep. For these improvements, the proposed method can analyse distribution network with harmonic sources at any position accurately.

Distributed generators performance significantly well on reducing the voltage drop and system power loss in any power distribution network. However, the PV type distributed generator will also increase the system harmonic penetration. Thus, a harmonic load flow analysis is vitally necessary before connecting these distributed generators to a distribution network.

4.10 Reference

[1] B. OWENS, "The Rise of Distributed Power," *https://www.ge.com/sites/default/files/2014%2002%20Rise%20of%20Distributed%20Power.pdf*, last date of access, 31.03.2016.

[2] A. Losi and M. Russo, "Dispersed generation modeling for object-oriented distribution load flow," *IEEE Transactions on Power Delivery,* vol. 20, pp. 1532-1540, 2005.

[3] Y. Zhu and K. Tomsovic, "Adaptive power flow method for distribution systems with dispersed generation," *IEEE Transactions on Power Delivery,* vol. 17, pp. 822-827, 2002.

[4] C. J. J. Huang, R. Xu, "A Review on Distributed Energy Resources and MicroGrid," *Renewable and Sustainable Energy Reviews,* vol. 12, p. 2472~2483, 2008.

[5] W. Caisheng and M. H. Nehrir, "Analytical approaches for optimal placement of distributed generation sources in power systems," *IEEE Transactions on Power Systems,* vol. 19, pp. 2068-2076, 2004.

[6] S. Z. Z. Wang, S. Zhou , R. Huang, L. Wang, "Impacts of Distributed Generation on Distribution System Voltage Profile," *Automation of Electric Power Systems,* vol. 28, p. 56~60, 2004.

[7] X. b. Tang and G. q. Tang, "Power Flow for Distribution Network with

Distributed Generation," in *2010 Asia-Pacific Power and Energy Engineering Conference*, 2010, pp. 1-4.

[8] J. Zhang, Q. Yao, R. Sun, H. Qin, and X. Dong, "The harmonic load flow calculation of distribution network with distributed power," in *Advanced Power System Automation and Protection (APAP), 2011 International Conference on*, 2011, pp. 2088-2092.

[9] I. Wasiak, M. C. Thoma, C. E. T. Foote, R. Mienski, R. Pawelek, P. Gburczyk*, et al.*, "A Power-Quality Management Algorithm for Low-Voltage Grids With Distributed Resources," *IEEE Transactions on Power Delivery,* vol. 23, pp. 1055-1062, 2008.

[10] Marek Mägi, K. Peterson, and E. Pettai, "Analysis of protection and control functions of low voltage part of substation for smart grid applications," in *Electric Power Quality and Supply Reliability Conference (PQ), 2012*, 2012, pp. 1-8.

[11] Y. Sharon, A. Montenegro, A. Gardner, and M. G. Ennis, "New directional protection for distribution networks," in *2015 IEEE Power & Energy Society General Meeting*, 2015, pp. 1-5.

[12] C. Y. Tee and J. B. Cardell, "Market Integration of Distributed Resources Through Coordinated Frequency and Price Droop," *IEEE Transactions on Smart Grid,* vol. 5, pp. 1556-1565, 2014.

[13] E. F. Fauchs and M. A. S. Masoum, *Power Quality in Power Systemsand Electrical Machines*: Elsevier, 2008.

[14] J. Lv, "A New Method for Harmonic Penetration Study in Power Networks with Renewable Generation," *PhD thesis at the University of Strathclyde,* 2014.

[15] W. T. Limei Zhang, Honghao Guan, "The Back/Forward Sweep-based Power Flow Method for Distribution Networks with DGs," presented at the International Conference on Power Electronics and Intelligent Transportation System, 2009.

[16] C. Haiyan, C. Jinfu, S. Dongyuan, and D. Xianzhong, "Power flow study and voltage stability analysis for distribution systems with distributed generation," in *2006 IEEE Power Engineering Society General Meeting*, 2006, p. 8 pp.

[17] T. Jen-Hao and C. Chuo-Yean, "A fast harmonic load flow method for industrial distribution systems," in *Power System Technology, 2000. Proceedings. PowerCon 2000. International Conference on*, 2000, pp. 1149-1154 vol.3.

[18] T. Jen-Hao and C. Chuo-Yean, "Fast harmonic analysis method for unbalanced distribution systems," in *Power Engineering Society General Meeting, 2003, IEEE*, 2003, pp. 1-1249 Vol. 2.

[19] J. H. Teng and C. Y. Chang, "Backward/Forward Sweep-Based Harmonic Analysis Method for Distribution Systems," *IEEE Transactions on Power Delivery,* vol. 22, pp. 1665-1672, 2007.

[20] T. Jen-Hao and C. Chuo-Yean, "Backward/Forward Sweep-Based Harmonic Analysis Method for Distribution Systems," *Power Delivery, IEEE Transactions on,* vol. 22, pp. 1665-1672, 2007.

Chapter 5 Feeder Reconfiguration Based on Ant Colony System and Discrete Particle Swarm Optimization

5.1 Introduction

Feeder reconfiguration is a common method to improve network reliability and to reduce the network power loss. An optimization method is used to decide on how to operate the switches in the distribution network. A suitable optimization method can calculate a better solution of the objective in a less computing time. Furthermore, the suitable optimization method for feeder reconfiguration may make programming easier. However, the optimization program may not convergence by using an unsuitable optimization method.

As a typical optimization problem, most optimization methods are tested in the travelling salesman problem [1]. Ant colony optimization and particles swarm optimization show their good performance in this test problem so that they are used in the thesis to solve the feeder reconfiguration problem. In this chapter, the theory of these two methods for feeder reconfiguration will be introduced in details. Ant colony system and discrete particle swarm optimization is the improved version of the ant colony optimization and particle swarm optimization respectively. These two methods are also introduced for their good performance in the feeder reconfiguration problem.

Two IEEE standard distribution systems (33-bus and 69-bus) are used in the test system in this chapter. For the objective of minimizing network power loss, the searching performance of ant colony system and particles swarm optimization is tested in these two systems. A comparison of these two methods is also made.

In ant colony system, the value of the pheromone trail parameter and the heuristic information parameter is set according to the experience. After doing tests on the travelling salesman problem, the Reference [1] get a conclusion on these two parameters and make a suggestion. However, a suitable value of the pheromone trail parameter and the heuristic information parameter may change in a different optimization problem. In order to obtain better performance of ant colony system, two parameters are tested in this chapter for searching suitable values. For the same reason, the value of the acceleration constants in particle swarm optimization is also needed to test.

Firstly, the review of main optimization technology for feeder reconfiguration is introduced in section 5.2. The system constraints described in section 5.3 are from the topology part of the power system. Section 5.4 introduces the ant colony system and its theory for feeder reconfiguration. The particle swarm optimization and its distinct improvement for feeder reconfiguration are shown in section 5.5. In section 5.6, the search performance of both ant colony system and particle swarm optimization is discussed. Comparisons for tested results and the results in reference are made to verify the correctness of the simulation in this thesis. Finally, simulations for deciding the system parameters of both methods are executed.

5.2 Review of Main Optimization Technology for Feeder Reconfiguration

The concept of feeder reconfiguration was first proposed by Merlin et al[3] in 1975. A blend of optimization techniques and heuristics were used to determine the best structure of the distribution network for reducing the active power loss. Comparing

with installing the capacitor bank in the distribution network to reduce the active power loss, feeder reconfiguration can maximize usage of the existing resource to reduce the active power loss with the minimum cost. Mathematically, feeder reconfiguration is a complex, combinatorial optimization problem. Many types of research have been done in recent 30 years for making the method for feeder reconfiguration accurately and efficiently. Feeder reconfiguration is done in references [4-7] based on heuristic search techniques. However, as distribution system becomes larger and larger, heuristic search techniques become too involved and inefficiency. With the development of computer technology, more and more approaches are based on artificial intelligence. Genetic algorithm is also used for solving feeder reconfiguration problem firstly. References [8, 9] introduce how genetic methodology works on feeder reconfiguration. Recently, the optimization algorithm based on animals' behaviour had proposed. With the same purpose of optimizing, these swarm optimization algorithms are applied to the feeder reconfiguration problem and have got some achievements. Such as, particle swarm optimization and ant colony system. References [10, 11] introduce the basic theory of particle swarm optimization used in feeder reconfiguration. References [12-14] solve the feeder reconfiguration problem with ant colony system.

The objective of a heuristic method is to produce a solution in a reasonable time frame that is good enough for solving the problem at hand. A reasonable time means that the maximum required computing time for a feeder reconfiguration problem. This solution may not be the best of all the actual solutions to this problem, or it may simply approximate the exact solution. But it is still valuable because finding it does not require a prohibitively long time [15]. However, computing time is normally not a critical target for the feeder reconfiguration problem. Most of the feeder reconfiguration problem is not the real time problem so that it has enough time to obtain the solution. The optimal solution for minimizing the network loss or other objectives are the primary purpose of the

feeder reconfiguration. Thus, the artificial intelligent based optimization method is a best choice to solve the feeder reconfiguration problem. According to reference [2], ant colony system and particle swarm optimization have better performance in all artificial intelligent optimization method. Therefore, both of them are analysed in this chapter. The attempt of improving these two methods is also provided in this thesis.

Ant colony optimization (ACO) is a metaheuristic approach in which a colony of artificial ants cooperates to find good solution to difficult discrete optimization problem[1]. The first successful ant colony optimization model is called ant system which was developed by Dorigo, Maniezza and Colorni in 1991[16]. Then, more success improved models show better performance in references [17-23]. Due to ant colony optimization shows good performance in the optimization field, researchers try to solve the feed reconfiguration problem using this algorithm. References [12, 24-26] demonstrate the theory on how to use ant system for resolving the feeder reconfiguration problem. Searching efficiency between different optimization methods is compared in Reference [27] and the results seem to indicate that ant system has better performance. A modification on the choice of the probability of the ants was made in Reference [28] to increase the searching efficiency. References [29-31] show that according to the special system structure of the distribution network, the ant colony system can be improved by the use of graph theory. The feeder reconfiguration problem in a distribution network with distribution generators is illustrated in reference [32]. And reference [33] expand the ant colony system to solve the multi-region objective in distribution network reconfiguration. References [34-38] find that ant colony system can combine with other optimization methods to overcome its defect and increasing the searching efficiency.

As a mimicking swarm intelligent optimization algorithm, particle swarm

optimization (PSO) was proposed by Kennedy and Eberhart in 1995[39, 40]. This is another common used optimization method for feeder reconfiguration in recent years. The original particle swarm optimization is used to solve the discontinuous function optimization problems. So, it cannot use to address the reconfiguration of feeder problem as it is a discrete function optimization problem. References [41-43] modified the original particle swarm optimization in discrete function optimization area. After that, the feeder reconfiguration problem is also solved by discrete particle swarm optimization [44-48]. In the process of solving feeder reconfiguration by discrete particle swarm optimization, the system structure in parts of the solutions which are not radial can significantly affect the search efficiency. Reference [49] indicates the use of tear circuit theory can overcome the difficulty. In graph theory, a minimum spanning tree can be created with special rules by tearing all circuits in the graph. After all circuits are broken, the graph must be a tree structure. Then, each system structure of the solution established by tear circuit theory is radial so that all infeasible solutions are avoided. For increasing the efficiency of finding the global best solution, Reference [50] added a new mechanism for updating the local best solution. A new function for accelerating constants has applied in reference [51] to increase the searching efficiency. Reference [52] using particle swarm to solve the problem that combines capacitor placement and minimizes the active power loss. Reference [53] finds the best size and location for distributed generators to minimize the active power loss by particle swarm optimization. In Reference [54], a comparison between selective particle swarm optimization and binary particle swarm optimization has been made. References [55, 56] combine particle swarm optimization with other optimization methods to improve the searching efficiency.

5.3 System Constraints in Feeder Reconfiguration

Optimization methods are commonly applied and tested in Traveling Salesmen Problem[1]. In this problem, the position and the distance between each city are known. The objective is to determine the shortest total travel distance. The only one constraint is that each city can be visited only once. Although feeder reconfiguration is also an optimization problem, it is more complicated than the Traveling Salesmen Problem as there are more constraints in feeder reconfiguration.

5.3.1 Network Topology Constraints

The distribution network is an open circle network. It contains two types of switches: tie switch (normally open) and sectionalizing switch (normally closed). They are designed for both protection and configuration management in the system[57]. By changing the status of these switches, the structure of the distribution network will be changed for balancing the load and reducing the power losses to improve the power supply capability and power quality. Open circle network means that there is no loop in the system. Even if the system may operate in the weak-mesh condition in the special period, such a circuit will be converted into two branches with two breaking points[58]. Radial topology is the most important feature of the distribution network. Widely used load flow analysis methods in the distribution system (backward/forward sweep algorithm) are proposed based on this feature. So, one important constraint condition is the system network is a radial network topology.

Feeder reconfiguration achieves by changing the status of tie switches and sectionalizing switches in the distribution system. Unlike the Traveling Salesmen

Problem, the connection between buses in the system is fixed, which means new connections between buses in the system are forbidden. So, when every tie switch and sectionalizing switch in the system are closed, the system structure is constant. Furthermore, electric power usually must supply every single consumer in the distribution network. So, islanding model is not allowed.

5.3.2 Power System Parameter Constraints

The system voltage is divided into several levels in the power system. Each level has its acceptable maximum and minimum voltage value. It has a voltage range limitation on any bus in the power system. Equation 5-1 expresses the bus voltage constraint.

$$V_{i,min} \leq V_i \leq V_{i,max} \tag{5-1}$$

Where, $V_{i,min}$ and $V_{i,max}$ is the allowed minimum and maximum bus voltage value on bus i respectively.

Due to the materials and marketing factor, there is a maximum current limitation on each power line. So, equation 5-2 shows the line current constraint.

$$I_i \leq I_{i,max} \tag{5-2}$$

Where, $I_{i,max}$ is the allowed maximum line current value of branch i

5.4 Ant Colony Optimization

Typically, artificial intelligence algorithms are applied to solve the travelling

salesman problem [16]. It is hard to choose a single method as the best one. Each method has its advantages and disadvantages. However, in the feeder reconfiguration problem, the following feeders on every single bus are usually connected to no more than three. This special structure will significantly reduce the choice when ants make their decision. So that, ant colony optimization may have a better performance in feeder reconfiguration when comparing with other artificial intelligence algorithms. This part introduces how ant colony system is working on feeder reconfiguration problems in details.

5.4.1 Basic Theory of Ant Colony Optimization

Ant colony optimization (ACO) [1]is an artificial intelligence optimize algorithm. It is proposed by Marco Dorigo in his Ph.D. thesis in 1992. It comes from the behaviours that ants find the food. Ant colony optimization is a method which simulates the process of finding food by ant. When ants go to locate the food, they will release some signals along the path. This signal is called pheromone. The following ants prefer to choose the way with the strongest signal. So, the strength of the signal will decide which way will be selected by most of the ants. This signal is called pheromone. The process of ant foraging is shown in Figure 5-1.

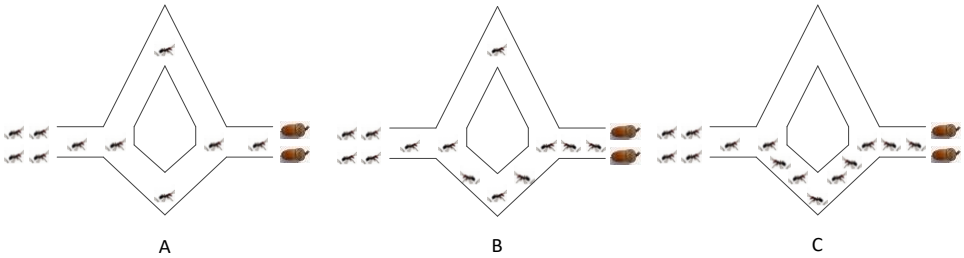

Figure 5-1 Process of ant foraging

In the beginning, ants choose its way randomly. It is assumed that the total quantity of pheromone released by each ant is the same; there is no pheromone on two paths at the beginning; ants must choose the same way back and do not release

pheromone when they return. Ants who choose the shorter path will come back faster so that the aggregation of the pheromone trails on the short path will be faster. With more and more ants pass two different paths, the strength of pheromone trails on the shorter path will further strengthen than the longer path. When ants are making their decision between shorter and longer path again, the strong pheromone trails on the shorter path will impact on the choice of ants. Due to aggregation speed of the pheromone on the short path is faster, all the ants will finally choose the shorter path. This is the basic theory of ant colony optimization.

5.4.2 Versions of Ant Colony Optimization

Ant system is the first successful version of the ant colony optimization and this method can be divided into two parts. The first part is using a probability equation to decide which point should be chosen in each construction step. After every single point has been determined, a possible solution will be found. In the second part, the existing pheromone trails in the system evaporates with a set rate and new pheromone will be released on the footprints which belong to the ant in the first part. Then, the following ants do the same process until ants are requested to stop. Normally, if path A was chosen by ants and the total length of all the chosen paths which contain path A was small, the pheromone trails on this path would get stronger and stronger so as to more and more ants would choose this path in the following iteration process. The shortest path between nest and food source will be chosen in such a mechanism. With the growth of the system size, the performance of ant system may suffer. So, many researchers focus on how to improve the ant system.

The first improved version of ant system is the elitist strategy for ant system (EAS)[17]. In this version, only the pheromone trails in the latest global best solution which is found by previous ants can be reinforced. Comparing with the ant system, the mechanism that only feedback to the latest global best solution can

find the same final solution in the same system with fewer iterations.

Rank-based ant system (ASrank) [18] is similar to the elitist strategy for ant system. Both of them reinforce the pheromone trails on the latest global best solution. Furthermore, ASrank model ranks the solutions by the total length of the structure built by ants. The quantity of pheromone which deposits by an ant is decided according to the rank of the solution. If the total length of the solutions is the same, the solutions can be ranked randomly.

Best-worst ant system (BWAS) is not only focused on the latest global best solution but also pay attention to the current worst solution [19]. The current worst solution will be penalized to reduce the probability of being chosen by ant while the latest global best solution reinforces the probability of being chosen on each iteration. When the latest global best solution cannot improve anymore, a significant improvement of BWAS is the reinitialize mechanism for the system parameters. Furthermore, a new pheromone trails update rule is applied to the pheromone trails update. To do so, each row of the pheromone matrix is changed with a probability by adding or subtracting the same amount of pheromone to the selected trail(a value which depends on the current iteration) [20].

Max-min ant system (MMAS) reinforce the pheromone trails on the latest global best solution [21, 22]. In this version, only the iteration-best ant can be allowed to release pheromone. Unfortunately, this strategy will make all ants focus on the iteration-best solution. Although the convergence speed to find the candidate of the best solution increases, it may miss out other candidates with better performance. To avoid such omission, MMAS limits the possible range of the pheromone trail value within a certain range. So that the MMAS can find more possible solutions in the beginning. MMAS also reinitialize the pheromone trails and other parameters when no better solutions can be found after some iterations.

In order to find a better solution to a complex optimization problem, the main

improvements of ant system are focus on the strength of pheromone trails. However, ant colony system(ACS)[23] applies a new mechanism. The reinitialize mechanism for the system parameters is the same with a mutation for finding more solutions, but there is no difference between re-do the searching process again. In the ant colony system, pseudorandom proportional action provides alternative update rule for the ants when ants make their choice rather than only decide by an equation. More options mean more probable solutions so that better solutions may be found. Furthermore, the pheromone trails on each path would evaporate immediately after passing by the ant. Such steps will reduce the probability that ants make the same choice. Ant colony system also considers the useful improvement in previous models. The pheromone updating will only apply on the iteration-best ant. As a typical representative of ant system theory, ant colony system is chosen to solve the feeder reconfiguration problem in this thesis and introduced in details in the following section.

5.4.3 Feeder Reconfiguration Based on Ant Colony System

In feeder reconfiguration, random radial structures which satisfy the constraints will be built at the beginning. Random radial structures can be treated as the routes of the ants. Moreover, the active power loss for each built structures is treated as the total length of the route. To find more possible solutions, the ants must have more choices. Due to the strength of pheromone trails impact on the choice of ants, the initial strength of pheromone trails is set to the same value to prevent a biased searching at beginning. Artificial ants will release their pheromone on the branches which they chose. After the first group of ants built their structure, the strength of pheromone trails in the system becomes different. The system power loss of each structure cannot be the same, so the strength of pheromone trails will also differ on each branch in the system. With the evaporation of the pheromone trails, more and more pheromone concentrate on those branches which built structures with small

system power loss. When one structure has an overwhelming strength of pheromone trails, it will be the final choice for most ants.

Processes that finding a final solution of feeder reconfiguration is introduced in following parts. Before starting the method, system parameters which appear in the following section a), b) and c) must be set in advance.

a) Build a radial structure

In the distribution system, each branch is connected with two buses. One bus sends power energy and the other receives power energy. It is defined that the sending end is the bus which sends power energy and the receiving end is the bus which receives power energy. The reference bus in the distribution system is normally defined as the main power plant in the distribution system or the connecting point between the transmission system and distribution system.

Electric power sends from the reference bus to each bus in the system through branches. In the distribution system, the direction of the power energy is unidirectional and the structure of the network is radial. If a bus receives power energy from two different branches, this means there are two different connecting paths from one bus to the other buses. In another word, there is a loop between two buses. But, the mesh structure is normally not acceptable in the distribution system. And, in order to avoid islanding condition, each bus must be connected to the distribution system. So, it can be seen that, apart from the reference bus, each bus can become the receiving bus only once. This is an important rule to build a radial network. A feasible solution for feeder reconfiguration is that it must satisfies the topology constraints. Which means when a sending end is decided, the available receiving buses are also decided. Following the above rules, satisfactory radial structure network can be built.

Due to the structure and power lines are constructed in advance. So, the possible

connections between buses in a distribution system are fixed. The IEEE 33-bus system shows in Figure 5-2 is used as an example to illustrate the process of building a radial network. In this figure, the dotted line expresses all possible connection between buses.

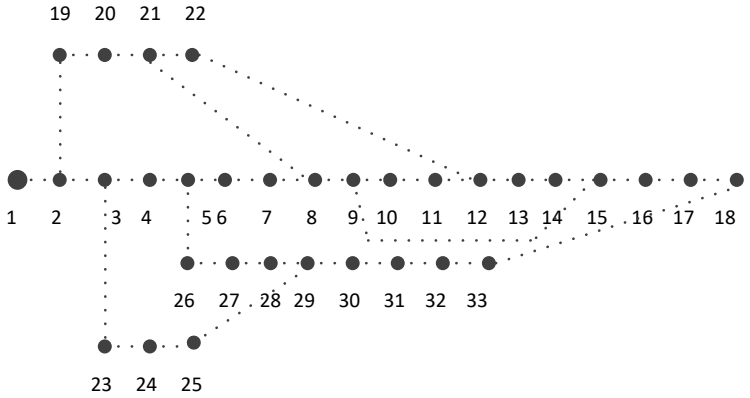

Figure 5-2 All possible connecting between buses in IEEE 33-bus system

In this network, node 1 is the reference bus. The building process by ants starts at the reference bus. When the reference bus is the sending end, it is easy to find from Figure 5-2 that the available receiving end can only be the node 2. Because there is only one bus connects with bus 1 in the system and it is bus 2. When node 2 is the sending end, the available receiving end has two choices---node 3 and node 19. But, if it is assumed that an ant has already built part of the system such as the structure show in Figure 5-3, the available sending end could be nodes 21, 4 and 24 and the receiving end could be nodes 7, 22, 5 and 25 respectively. Where the solid lines represent branches already built by the ant and the dotted lines represent the remaining available connections. Which sending end and its corresponding receiving end should be chosen is the key point of building a radial structure. The sending end and receiving end are two ends of the branches so that by choosing a branch instead of choosing the sending end and the receiving end can simplify the building process. Then, the available connections at this time are branches 21-8,

21-22, 4-5 and 24-25.

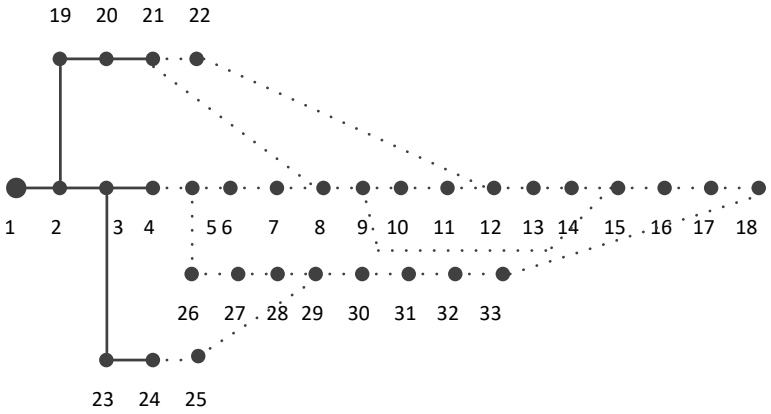

Figure 5-3 Part built 33-bus system

The optimization problem is a complex choice problem. So, ant colony system is used to decide which branches should be chosen. In the real ant world, the strength of pheromone trails is the decisive factor of which path should be chosen. However, in the artificial ant world of ant colony system, some other factors can also influence the decision of ant. Equation 5-3 shows the decision mechanism[23].

$$p_{ij}^{k} = \begin{cases} \arg_{l \in N_i^k} \max\{\tau_{ij}[\eta_{ij}]^{\beta}\} & if q \le q_0 \\ \dfrac{[\tau_{ij}]^{\alpha}[\eta_{ij}]^{\beta}}{\sum_{l \in N_i^k}[\tau_{ij}]^{\alpha}[\eta_{ij}]^{\beta}} & else \end{cases} \tag{5-3}$$

Where p_{ij}^{k} is the probability of ant k chooses branch ij. τ_{ij} is the strength of pheromone trails on feeder ij. η_{ij} means the reciprocal value of the resistance of branch ij. α and β are two system parameters which determine the relative influence of the pheromone trail and the heuristic information. N_i^k is the feasible connections when ant k is at sending end i. which means the set of distribution lines connect to the bus i which ant k has not chosen yet(the probability of choosing a transmission line outside N_i^k is zero). q is a random value between 0

and 1. And q_0 is a value between 0 and 1 and is set in advance. Arg_max means to choose the maximum value.

In the ant system, the decision mechanism only contains the lower part of equation 5-3. Depending on such a mechanism, all ants will focus on the branches with strong pheromone trails. Branches which have little pheromone trails may be ignored by ants with a great chance at the beginning of the search. However, part of these branches may be the key to build a better system structure. In order to increase the chosen probability of the branches with little pheromone trails, the upper part of equation 5-3 are added by using a different choosing mechanism in the ant colony system. The equation $q \leq q_0$ represents the probability of performing this different choosing mechanism. For example, it is assumed the value of the q_0 is 0.3. Then, If the value of the random number $q \leq 0.3$, the upper part of equation (5-3) is performed and the branch with the maximum value of $\tau_{ij}[\eta_{ij}]^{\beta}$ will be chosen. Otherwise, if $q > 0.3$, the lower part of the equation (5-3) is performed and the chosen probability of all available branches will be calculated. Then, the roulette wheel mechanism would be applied to choose one branch from those available branches base on their chosen probability.

It is assumed that the chosen probability of branches 21-8, 21-22, 4-5 and 24-25 is 4.42%, 28.11%, 42.17% and 25.30% respectively. And $q > q_0$. A circle as illustrated in Figure 5-4 is treated as a roulette wheel and the value at 12 o'clock position is set to be zero. The circumference of the circle is 1. There are four available lines so that the circle is divided into 4 pieces. And the area of each part of the circle is equal to the probability of each line. If a random value between 0 and 1 is 0.64, its position will locate at part line 4-5 or if the random value is 0.8, its position will locate at part line 24-25. The part which is located by the random value will be the choice of the artificial ant. This is the roulette wheel mechanism in the ant colony system.

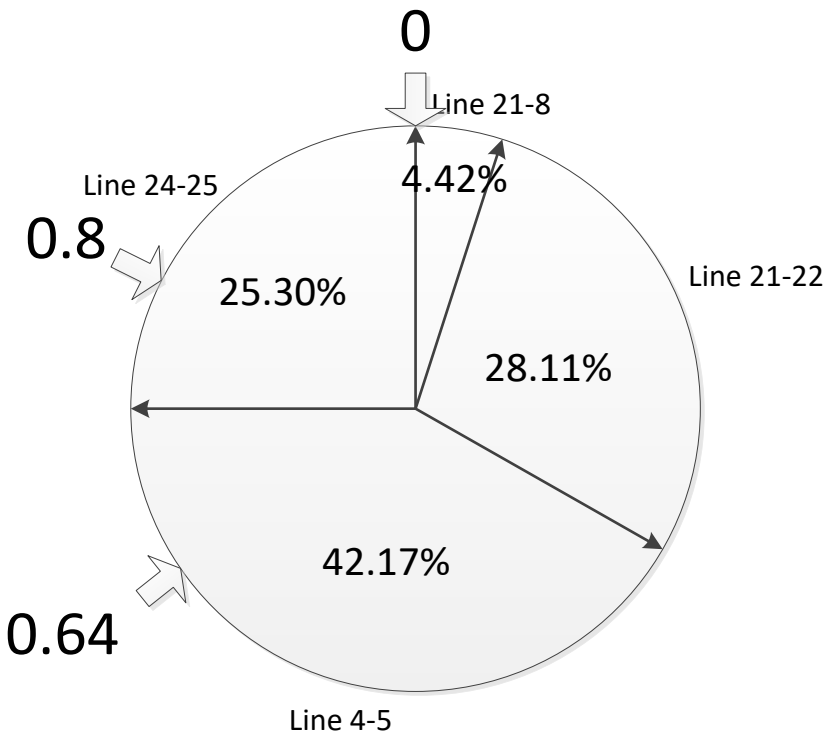

Figure 5-4 roulette wheel selection

After finishing the calculation of equation 5-3, the chosen branches can be decided. If branch 21-8 is chosen, the available feeders for the next step are branch 21-22, 8-7, 8-9, 4-5 and 24-25. Once a node is chosen as the receiving end, the ant will mark it. In Figure 5-5, all ends of the dotted lines have become the receiving end of the other chosen distribution line. So, the ant colony system will prevent these receiving ends from creating a new connection. Until all nodes marked as the receiving end apart from the reference node, the random radial network will be built and the structure may be built as shown in Figure 5-5.

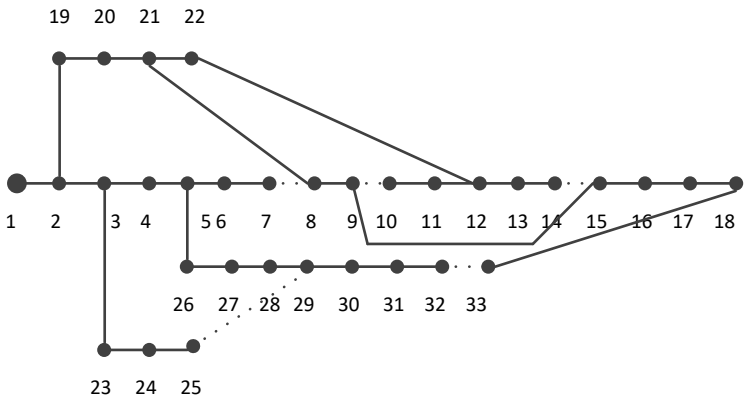

Figure 5-5 Feasible network structure of the 33-bus system

b) Update the pheromone trails

In real ants' world, ants will release pheromone to help the following ants to choose the shorter path. Similar to the real ants, artificial ants also release pheromone. Different from the ant system, the rules of pheromone trails update in the ant colony system will be divided into two part. One is the global pheromone update; the other is local pheromone update.

In the process of global pheromone update, both pheromone releasing and pheromone evaporation will only apply to the current best route in the ant colony system. This is to reduce the calculation complexity in pheromone update and emphasize the influence of iteration best solution. Equation 5-4 shows the rules to update the global pheromone in ant colony system[23]. New pheromone trails on each branch will be calculated according to this equation. This new pheromone trails distribution will be used as the initial τ_{ij} in equation 5-3 when a new ant colony do they search.

$$\tau_{ij}^{k+1} = (1-\rho)\tau_{ij}^{k} + \rho\Delta\tau_{ij}^{bs} \quad \forall(\mathrm{i},\mathrm{j}) \in T^{bs} \tag{5-4}$$

Where $0 < \rho < 1$ is the pheromone evaporation rate for global pheromone update. $\Delta\tau_{ij}^{bs}$ is equal to $1/C^{bs}$. C^{bs} and T^{bs} are the current smallest total network power loss and the current best network structure find by ant in the search process. Then $\forall(\mathrm{i,j}) \in T^{bs}$ means all pheromone can only update on those distribution lines which belong to the latest global best solution in the search process.

Local pheromone trails update is a new mechanism in the ant colony system. To prevent that ants concentrate too rapidly on a certain solution, the local update rule is created. The local pheromone update will apply on every single ant. And the rule of local pheromone update expresses in equation 5-5[23]. New pheromone trails on each branch will be calculated according to this equation. This new pheromone trails distribution will be used as the initial τ_{ij} in equation 5-3 when the next ant colony in the same colony do they search.

$$\tau_{ij}^{k+1} = (1-\xi)\tau_{ij}^{k} + \xi\tau_0 \tag{5-5}$$

Where $0 < \xi < 1$ is pheromone evaporation rate for local pheromone update. According to reference [1], ξ is normally set to 0.1 and τ_0 is set to be the same as the initial value for the pheromone trails. The value of τ_0 is equal to $1/\mathrm{n}C^{nn}$. n is the total number of nodes. If the system structure is built following the rules that ants must choose the power line with the smallest resistance as its next choice, C^{nn} is then the total system power loss of such a system.

At the beginning of the ant colony search, τ_{ij} is equal to τ_0 which means all feasible power lines have an equal chance to be chosen by the first ants. When the first ant creates its own structure. The strength of pheromone trails on each feeder becomes different. According to the equation 5-5, pheromone start to evaporate after the ant release the new pheromones on the chosen power line. The value of pheromone trails on the chosen distribution line will reduce so that the probability

of choosing the same distribution line by the following ants is also reduced. Thus, ants have more chance to choose all distribution lines in the system and so that more feasible solutions may be built.

c) The final solution of ant colony algorithm in feeder reconfiguration

In the artificial intelligent world, the population size of the ants is one artificial ant group in each iteration. When the first iteration finishes which contains above part (a) and (b), the best solution in this iteration is recorded as the latest global best solution. The pheromone trails distribution in all feasible connections is inherited by ants in the next iteration as the initial value of the system pheromone trails. Thus, the searching experience of the previous ants will guide the following ants to find a better solution. Normally, there are two scenarios of defining the final solution. In common iteration method, the terminated condition of the iterations is an acceptable difference in tolerance between two connecting iteration results. In feeder reconfiguration, when the system structure is built, the system power loss is a fixed value. So, the first scenario of the final solution can be defined that when the current minimum system power loss does not change in a given number of iteration, it can be considered that the solution is the best solution in this optimization process. However, due to the pseudorandom proportional mechanism and the big system size, it is hard to decide this given number. A smaller network power loss may be found after selecting the final solution by using the normal criterions. So, a maximum number of iteration is set as the termination condition. This is the second scenario for deciding the final solution. The pseudorandom proportional mechanism is applied in this thesis so that the second scenario is chosen as the criteria for the final solution. The final solution in feeder reconfiguration contains the system structure, the bus voltage, branch current and the active power loss of the distribution system.

The flow chart of ant colony system in feeder reconfiguration shows in Figure 5-

6.

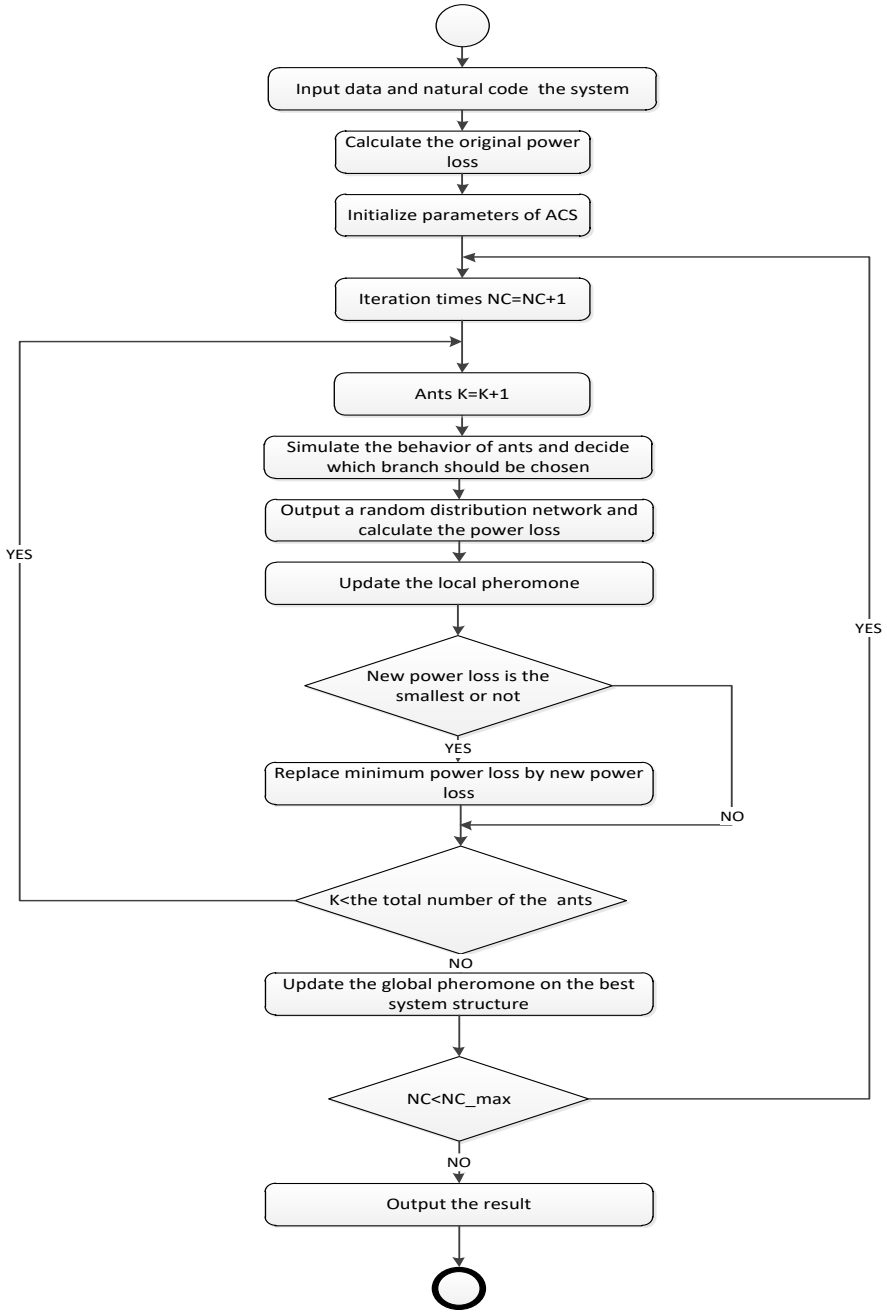

Figure 5-6 Flow chart of ACS in feeder reconfiguration

5.5 Particle Swarm Optimization

Similar to ant system, particle swarm optimization is also simulating the behaviour of a swarm of birds searching for food. In a flock of birds, they track the paths of its neighbors. But, the whole group of birds seems to move around a center point. Particle swarm optimization is proposed base on the research of birds foraging. It is assumed that there is only one food source in the area. The best way to find the food source is that searching nearby locations of bird which is considered as the nearest position to the food source. The bird will finally find the food by updating its position and velocity. Due to the characteristic of simple logic and easy programming, particle swarm optimization is also a common used artificial intelligent optimization method. However, particle swarm optimization is used to solve the in continuous function optimization problems. Before applying this method to solve the feeder reconfiguration problem, modifications and improvements are necessary. The theory of particle swarm optimization and its application in feeder reconfiguration is introduced in the following section.

5.5.1 Basic Theory of Particle Swarm Optimization[39,40]

In particle swarm optimization, there is no nest for birds and no path needs to be chosen. Artificial birds are called particles. Instead of the nest, the position of all particles locates randomly in the searching area and the particles have an initial speed. The food for particles is usually the possible maximum or minimum value of the objective function. The searching direction of particles is controlled by two values. One is the best searching experience of individual particles in each searching iteration (the local best position). And the other is the best solution

searching by any particles until now (the global best position). Figure 5-7 shows the searching diagram of one particle.

In Figure 5-7. The position of the particle locates at x_i, local best position, global best position, and possible food position is shown with blue dot respectively. The arrowed blue line expresses the initial particle velocity. The update of new position and velocity is according to equation (5-6) and (5-7) [39,40].

$$v_i^{k+1} = \omega * v_i^k + c_1 * random() * \left(Pbest_i - x_i^k\right) + c_2 * random() * \left(Gbest_i - x_i^k\right) \tag{5-6}$$

$$x_i^{k+1} = x_i^k + v_i^{k+1} \tag{5-7}$$

Where k means the k[th] iteration. i is the particle code. ω is the inertia weight, c_1 and c_2 is the acceleration constants of local best position and global best position respectively. Random() is a random value between zero and one. x_i is the position of the particle i. v_i is the speed of particle i.

According to equation (5-6), in the update of the particle position and velocity, the local best and the global best position are the main reference which helps particles concentrate around the food position. Two random values in equation (5-6) are the random mechanism for enlarging the searching area and trying to find a better result. The new velocity contains part of the old velocity which is determined by inertia weight and influence factor of local and global best position. Then, the new position can be calculation by equation (5-7). The new velocity is the red arrowed line in Figure 5-7. The gray arrowed dotted line expressed update process of the new velocity and position.

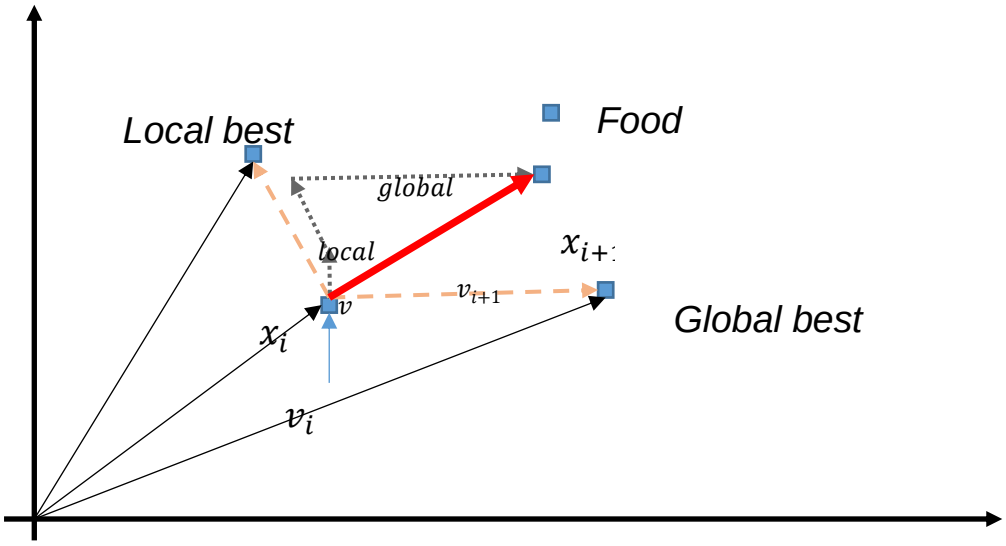

Figure 5-7 Searching diagram of particle swarm optimization

Each particle has its fitness value which is evaluated by the fitness function. The fitness function normally is the objection function of the optimization. Such as the shortest journey in travelling salesman problem or the minimum system power loss in feeder reconfiguration. In Figure 5-7, the fitness value is the distance between particle position and food position. The fitness value is the evaluation criteria for the local best and global best position.

The searching process will end when the solution is found or the termination condition is satisfied. With the same reasoning of ant colony system, searching process of particle swarm optimization normally stops when the termination condition satisfied.

5.5.2 Feeder Reconfiguration Based on Discrete Particle Swarm Optimization

Feeder reconfiguration is achieved by changing the status of tie switch and sectionalizing switch. Normally open and normally closed are the only two statuses

of the switches. So, it is suitable that using binary code zero and one to express the status of the switches which are shown in Figure 5-8. It is normally assumed that one expresses normally close switch and zero expresses normally open switch in the power system and the same assumption applies in this thesis. Then, the problem transfers from building a radial structure for the distribution system to decide the status value of all switches in the distribution system.

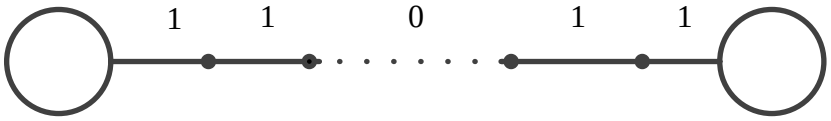

Figure 5-8 Simple distribution network

For applying the real engineer problems, the discrete particle swarm optimization is proposed in 1997[43]. In the discrete particle swarm optimization, the positions of each particle only contain zero and one. But, there is no limitation on the particle velocity. The position of the particles is decided by the value of particle velocity in the sigmoid function.

$$\mathrm{S}(v) = \mathrm{sigmoid(v)} = \frac{1}{1 + e^{-v}} \tag{5-8}$$

From the equation (5-8), the sigmoid value of larger velocity is closer to one which means the bigger velocity means the position may have more opportunity to be one. Relatively, the smaller velocity means the position is more likely to be zero. Then, equation (5-7) provided in section 5.5.1 modified for the discrete problem as shown below.

$$\begin{cases} x_{id} = 1 & if\ random() < S(v) \\ x_{id} = 0 & else \end{cases} \tag{5-9}$$

To avoid saturation of sigmoid function, the maximum and minimum velocity are limited between $[-v_{max}, v_{max}]$. In this thesis, the sigmoid function is modified as equation (5-10).

$$S(v) = \begin{cases} 0.98 & v > 4 \\ \dfrac{1}{1+e^{-v}} & -4 < v < 4 \\ 0.2 & v < -4 \end{cases} \tag{5-10}$$

The main improvements of the particle swarm optimization are described above. This is the theory of the discrete particle swarm optimization. If all status of switches were decided by this theory, it could not satisfy the topology condition limitation. For example, in IEEE 33-bus system, the total number of tie switches must equal to five. But, new tie switches in results which calculated by the discrete particle swarm optimization may not equal to five. So, final modified equations for feeder reconfiguration are shown in (5-11), (5-12) and (5-13)[44]. By such an improvement, the number of new tie switches will satisfy the requirement.

$$v_i^{k+1} = \omega * v_i^k + c_1 * random() * \left(Pbest_i - x_i^k\right) + c_2 * random() * \left(Gbest_i - x_i^k\right) \tag{5-11}$$

$$r_i = S(v_i) - random() \tag{5-12}$$

$$\begin{cases} x_{id} = 1 & if\ r_i < the\ qth\ smallest\ value\ of\ all\ r_i \\ x_{id} = 0 & else \end{cases} \tag{5-13}$$

Where q is equal to the number of the tie switches in the distribution system.

First of all, the sigmoid function will give a value to each switch based on the particle velocity. Then, the branches will be ranked based on these values. The

equation 5-13 means that the switches which have the smallest values need to open. The value of random() in equation 5-12 is between 0 and 1. This random() function is used to disturb the rank of the switches so that the network structure will be built with accident. It may give a new framework of the network. Similar to the original particle swarm optimization, the velocity update will be applied by equation 5-11 after the status of switches are changed.

The final result will be calculated when the termination condition is satisfied.

Above theory is the basic application of particle swarm optimization in feeder reconfiguration. But, there is another issue to be considered. Different from the ant colony system, discrete particle swarm optimization cannot ensure that all the built structure is radial. It can only ensure there are a number of tie switches in the distribution. Normally, a program to filter the radial structure is added in the particle swarm optimization. If the candidate structure is not radial, particle swarm optimization will rebuild a new structure until a radial structure is obtained.

With increasing of system size, it is more and more difficult to build a radial system structure. The number of infeasible structures increases quickly. Computing time of discrete particle swarm optimization then grows exponentially. For increasing the efficiency of discrete particle swarm optimization and avoid redundant calculation, the primary target is to ensure that every single network structure is radial.

In the following section, the tear circuit method for minimal spanning tree in graph theory is combined with discrete particle swarm optimization to ensure that 100% of built structures are radial.

5.5.3 Tear Circuit Method for Feeder Reconfiguration

Because of the random variable elements in the initialization and updating process of discrete particle swarm optimization, a large number of infeasible solutions will

be produced. An infeasible solution is one with mesh or islanding situation. Such a system cannot satisfy the distributed system topology constraint. So, normally, if such an infeasible system network is built, this solution is abandoned and a new solution is required in this iteration by the same particle. With the increasing system size, larger and larger part of the calculation time is spent on building a radial system. Thus, the tear circuit method applies to discrete particle swarm optimization to avoid building infeasible network. The IEEE 33-bus system in Figure 5-9 is used here to explain the tear circuit method in feeder reconfiguration.

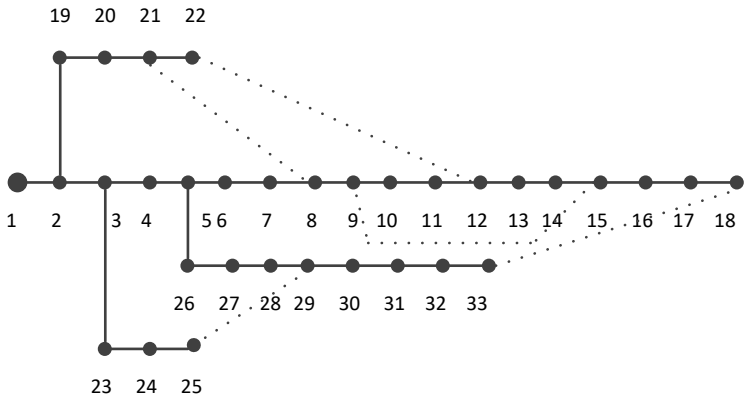

Figure 5-9 original IEEE 33-bus system

In Figure 5-9, the solid line expresses the sectionalizing switch and the dotted line expresses the tie switch. Any tie switch close in this system will create a mesh. If all tie switches closed in the 33-bus system, five meshes would be created which shows in Figure 5-10. A radial structure can be created by opening switches in its corresponding meshes. This is the basic theory of the tear circuit method in feeder reconfiguration.

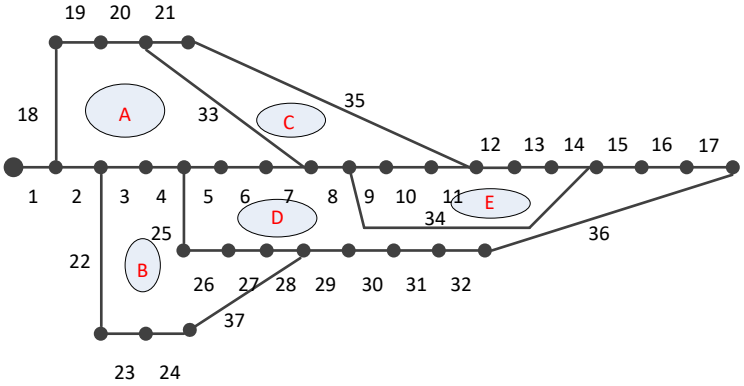

Figure 5-10 All switches closed in 33-bus system

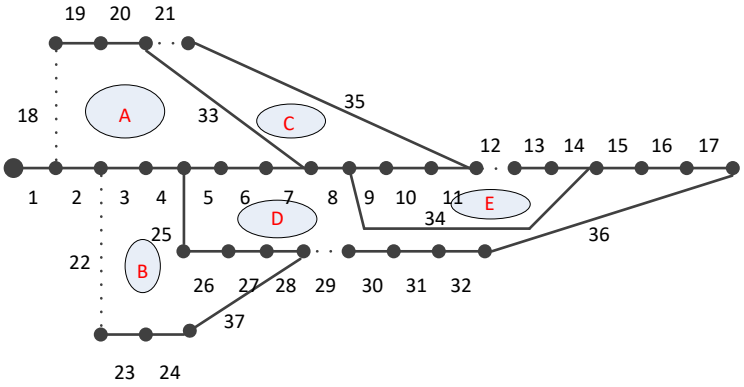

Figure 5-11 Radial 33-bus system

For example, switches 12, 18, 21, 22 and 29 in Figure 5-12 are chosen to be opened by discrete particle swarm optimization. Then, new 33-bus distribution system is illustrated in Figure 5-11 and its network structure is radial. However, a special circumstance needs to be mentioned. Parts of the tributaries in the network belong to two different circuits at the same time. Such as, the tributary which contains switch 3 and switch 4 belong to not only mesh A but also mesh B. If two opened switches are both chosen from one common tributary, islanding bus will be created in the new system. For instance, switch 3 is chosen to open for mesh A and switch 4 is chosen to open for mesh B. The new distribution system structure will contain

an islanding bus (bus 4) which is illustrated in Figure 5-12 within the red circuit. This situation cannot satisfy the structure constraint of the distribution network.

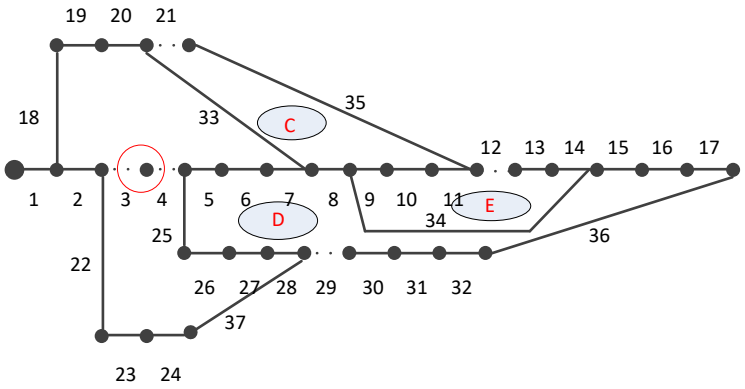

Figure 5-12 Infeasible solution for the 33-bus system

In order to avoid the appearance of the islanding bus in the process of tearing circuit, when a switch in common tributary is opened, all switches belong to this tributary are prohibited from opening again. Thus, before opening the next switch, remove the common tributary which contains the opened switch in the network and re-trace the circuits in the network. Repeat this process until the number of the opened switch satisfies the requirement. It is assumed that the switches which are determined to be opened by the discrete particle swarm are the following the sequence as 3, 25, 33, 9 and 36. The process of tearing five circuits in the 33-bus system is illustrated in Figure 5-13 (a-d). Its final network structure is shown in 5-11 (e) and this network is radial. By following the rules of the above process, the new network built by discrete particle swarm optimization must be radial.

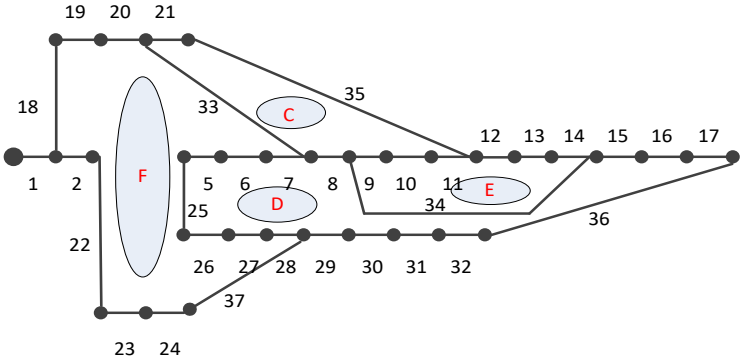

Figure 5-13 The remaining system structure in the process of tear circuit method (a)

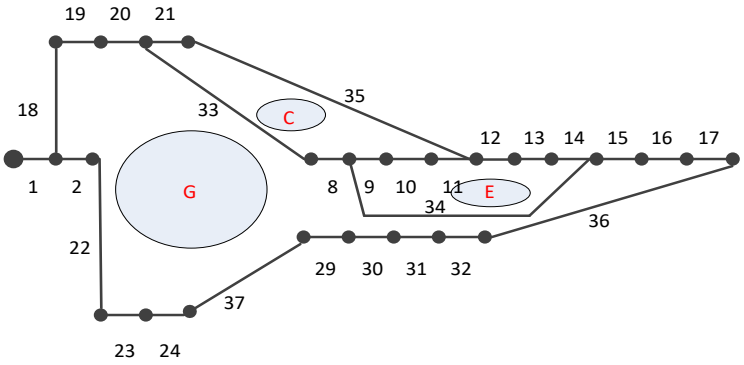

Figure 5-13 The remaining system structure in the process of tear circuit method (b)

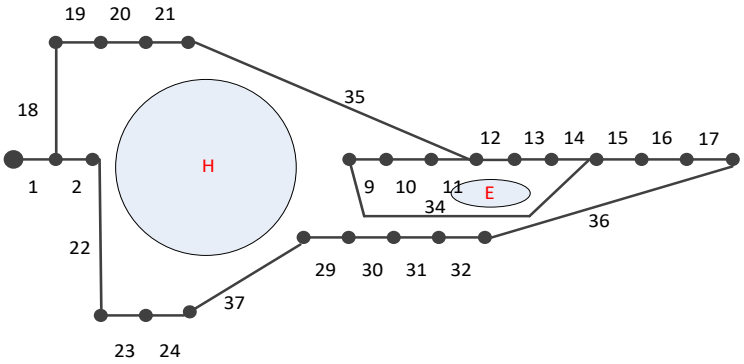

Figure 5-13 The remaining system structure in the process of tear circuit method (c)

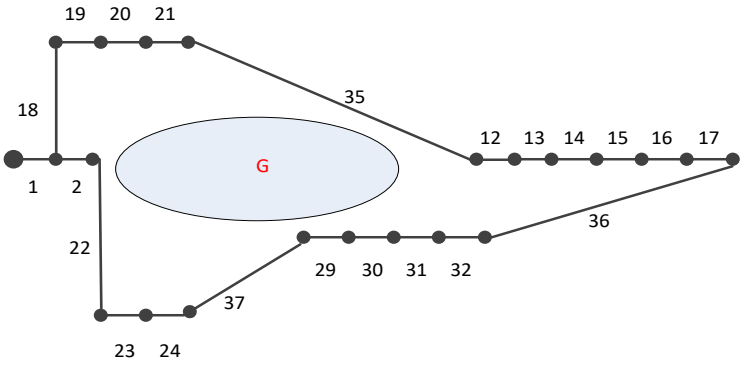

Figure 5-13 The remaining system structure in the process of tear circuit method (d)

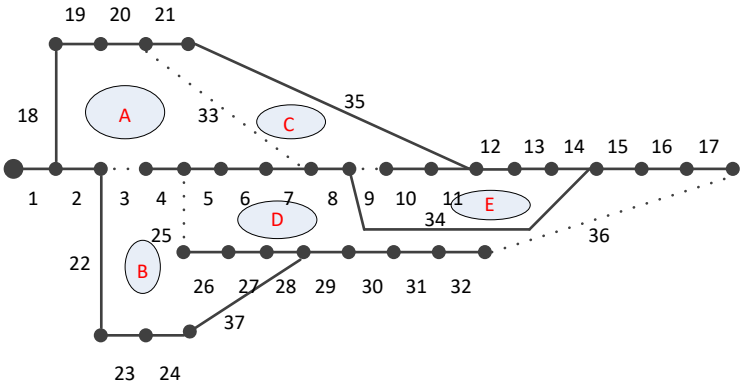

Figure 5-13 The remaining system structure in the process of tear circuit method (e)

Steps of discrete particle swarm optimization in feeder reconfiguration are divided into two parts. Firstly is built a radial structure and then secondly is the update of the particle velocity and the fitness value. The complete steps of tear circuit method in particle swarm optimization for feeder reconfiguration are described below.

1) Initialize the original location and velocity of particles. The initial location is the original test system structure. But the initial velocity is a random value between [-4, 4]. Calculate the original system active power loss.

2) Determine all meshes in the system and put them in a mesh set.

3) Calculating r_i on every switch by equation 5-12 and rank them.

4) Record the switch with the smallest r_i and check the belonging mesh.

5) Open one switch in each mesh according to the tear circuit method and the rank of the r_i

6) Go back to step 4) until the mesh set is empty.

7) Update the velocity of the particle by equation 5-11 bases on the built network structure.

8) Compare the active power loss with the current minimum value and replace it if the new active power loss is smaller.

9) Go back to step 3) if the pre-set condition is not satisfied.

10) Terminate calculation and output the results when the per-set condition is satisfied.

5.6 Case Study of Feeder Reconfiguration

The above two common used artificial intelligence optimization algorithms are programmed using Matlab. The tested systems are IEEE 33-bus distribution system [59]and IEEE 69-bus distribution system[60]. The coding of the nodes and branches of this distribution system is shown in Figure 5-14 and Figure 5-15 respectively. The number in black is node code and the number in red is the branch code.

There are five tie switches represented by the dotted line and 32 sectionalizing switches represented by the solid line in the 33-bus system which is shown in Figure 5-14. Total fundamental demand to be supplied is 5084.26 kW and 2547.32 kVAr. The voltage of the only power source at node 1 is 12.66 kV. System data for this system are given in Appendix A.1.

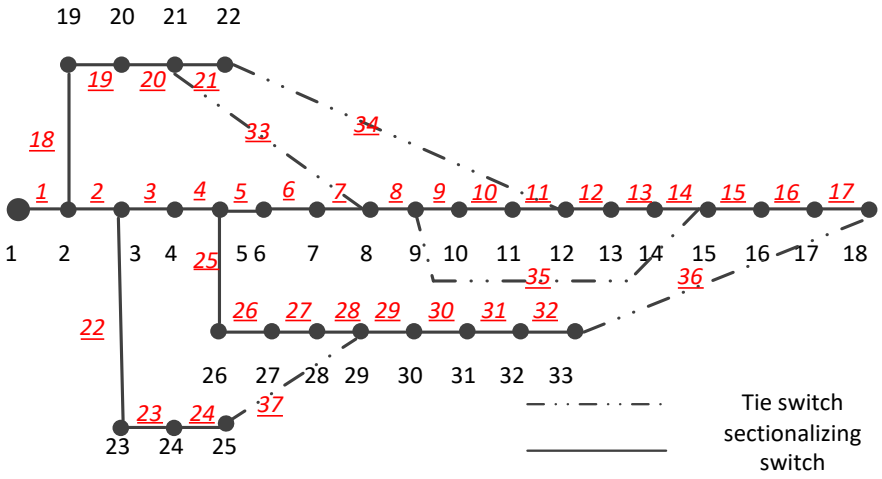

Figure 5-14 Coding situation in IEEE 33-bus system

The five tie switches in dotted line and the 68 sectionalizing switches in solid line of the 69-bus system are shown in Figure 5-15. The total fundamental demand to be supplied is 3802.19 kW and 2694.6 kVAr. The voltage of the only power source at node 1 is 12.66 kV. The system data for this system are given in Appendix A.2.

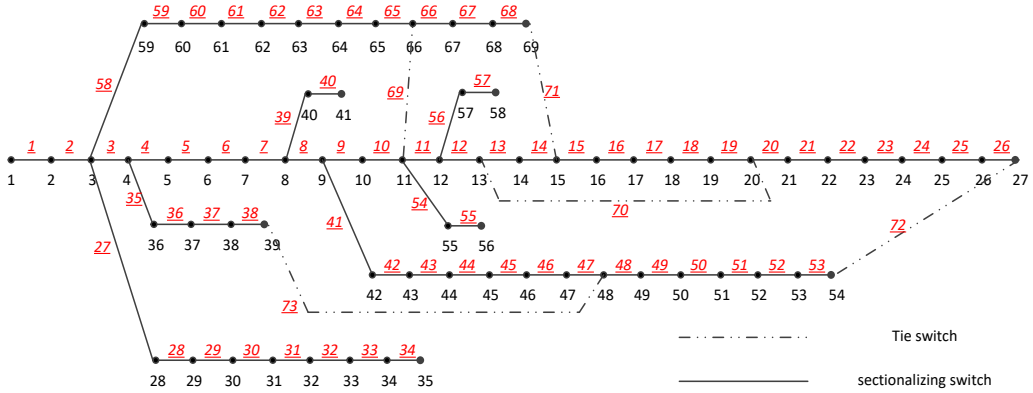

Figure 5-15 Coding situation in IEEE 69-bus system

5.6.1 Feeder Reconfiguration for Loss Reduction by Using Ant Colony System

Both the 33-bus and the 69-bus system are tested. The settings of system parameters are as follows: the population of ant is 10; pseudorandom proportional rate q_0 is equal to 0.3; global pheromone evaporation rate ρ is set to be 0.3; local pheromone evaporation rate ξ is set to be 0.1; maximum number of iteration is set to be 100; influence coefficient α and β are suggested set to be 1 and 2~5 respectively in reference [1], but this suggestion is for the traveling salesman problem. So, the values of these two influence coefficients are obtained by experiment.

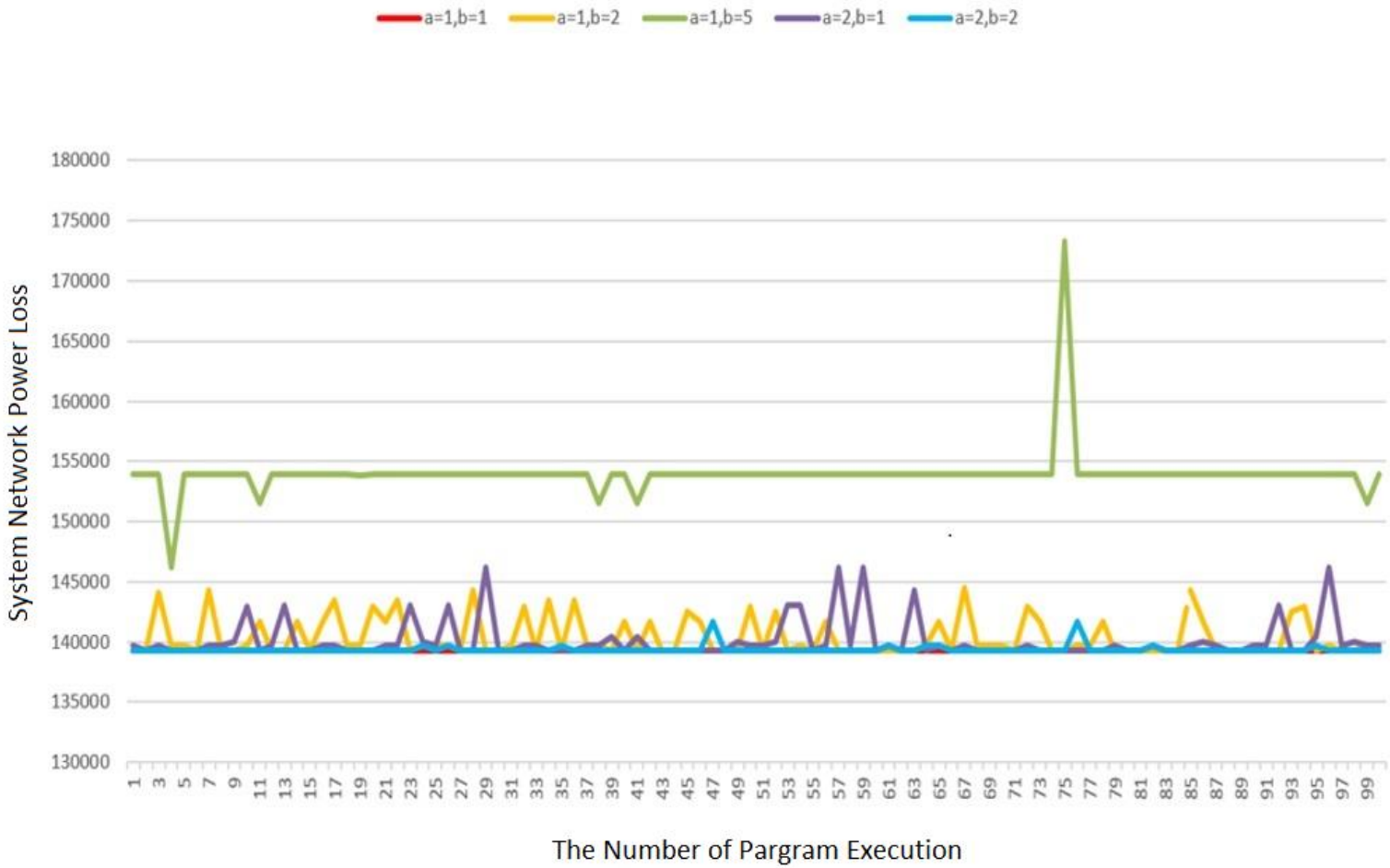

Figure 5-16 Feeder reconfiguration results in different α and β

The results obtained using different influence coefficients by repeating 100 times ant colony system are shown in Figure 5-16. All the results are the best solution when both α and β are equal to 1 which is represented by the red curve. This red curve is a straight line with value of the minimum system power loss in Figure 5-16. Other results curve cannot always find the best solution in 100 times repeating. When $\alpha = 1$ and $\beta = 5$, ant colony system cannot even find the best solution. Thus, both α and β should set to 1 when using the ant colony system for feeder reconfiguration problem. This indicates that the setting of the influence coefficient α and β has an important effect on searching efficiency.

The best solution of each iteration is the minimum network loss in one iteration which is not the same as the latest global best solution. The latest global best solution is the latest minimum network loss find by all ants. The change rate of the best solution of each iteration can show the search performance to some extent. If this rate is small, it reveals that the optimization method focuses their attention on the local best solution and ignores other possible solutions. If this rate is big, although the solutions find by optimization method are not the best right now, the new attempt provides more possibility to find a better solution.

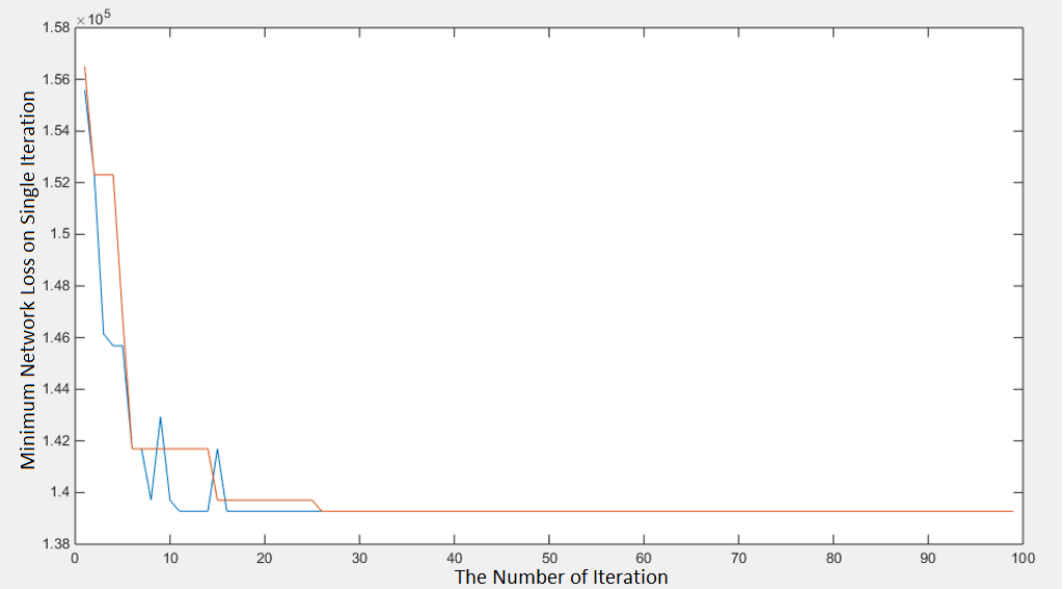

Figure 5-17 Minimum network loss of each iteration by using ant colony algorithm in 33-bus system with 100 maximum iteration

Due to the random and pseudorandom proportional mechanism of the optimization method, curves of the minimum network loss in each iteration is always different. It cannot show all curves in one figure. Thus, two curves are randomly selected from all kinds of curves to represent the characteristic of the minimum network loss in each iteration by using ant colony system and they are shown in Figure 5-17. In this figure, the vertical axis means the network loss and the horizontal axis shows the iteration number. The orange curve shows that the best solution of each iteration is the same with the latest global best solution. The searching mechanism cannot find a new system structure even if the result is worse. It indicates that the pheromone trails on the latest global best solution are too strong to let ant find a new route. This may cause all ant trapped at a local solution. The system power loss continued to reduce until the final solution has been found at the 26th iteration. Comparing with the orange curve, the blue curve has some disturbance around the 10th iteration. It shows that searching mechanism tries to find other different structure. Although this structure is worse than the latest global best solution, the

new attempt contains different framework which was not found before. So, ant colony obtains the final solution at the 11th iteration which is faster than the orange curve. Both curves keep stable after the 26th iteration which means this result should be the possible best solution for the 33-bus system.

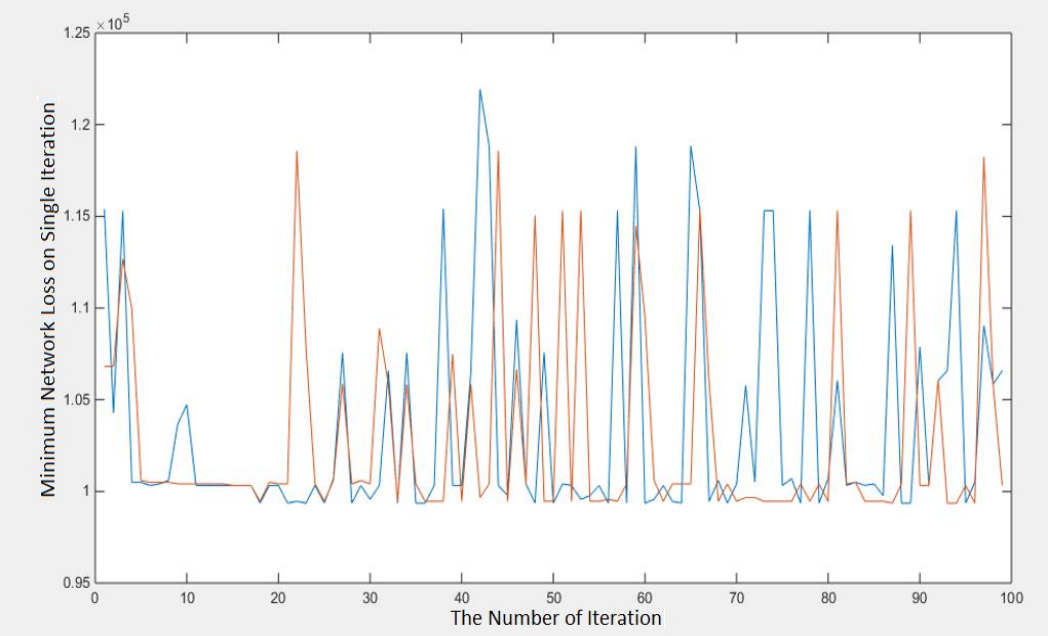

Figure 5-18 Minimum network loss of each iteration by using ant colony algorithm in 69-bus system with 100 maximum iteration

The best solution of each iteration in the 69-bus system is shown in Figure 5-18. These two curves are also two randomly selected results of the same system with the same system parameters. Due to the gap between two smallest solution is $0.001 * 10^5$, it is difficult to determine which curve find the final solution first by looking at Figure 5-18. In the data of the test results, the minimum network loss had been found by the blue curve at the 20th iteration and the orange curve found it in the 89th iteration. In this test, due to the number of iteration is big enough, even though ants trapped at a local solution, the pseudorandom proportional mechanism has enough chance to choose different searching mechanism and finds a new framework for ants. In Figure 5-18, Ants which represented by the blue

curve find the latest global best solution without trapped, so blue curve reach the known global best solution at 20th iteration. Ants which represent by orange curve seem to trap at a local solution. Then, the pseudorandom proportional mechanism cost additional iterations to help the ant escape the trap. Finally, both curves are found the latest minimum network loss.

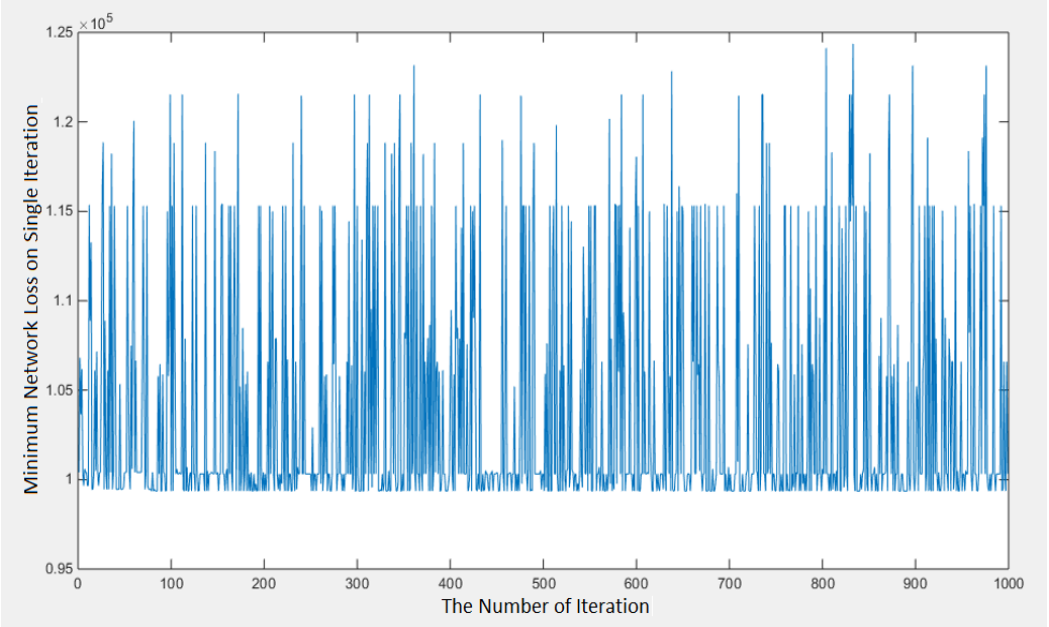

Figure 5-19 Minimum network loss of each iteration by using ant colony algorithm in 69-bus system with 1000 maximum iteration

The 69 bus system is tested again, but this time, the maximum number of iteration is increased to 1000. From the curve in Figure 5-19, it shows that the minimum power loss of each iteration is unstable until the end. This shows that the orange curve in Figure 5-17 is a special case. Alternatively, due to the small number of the possible solutions, the stable curve of the minimum power loss of each iteration can only appear in the small system.

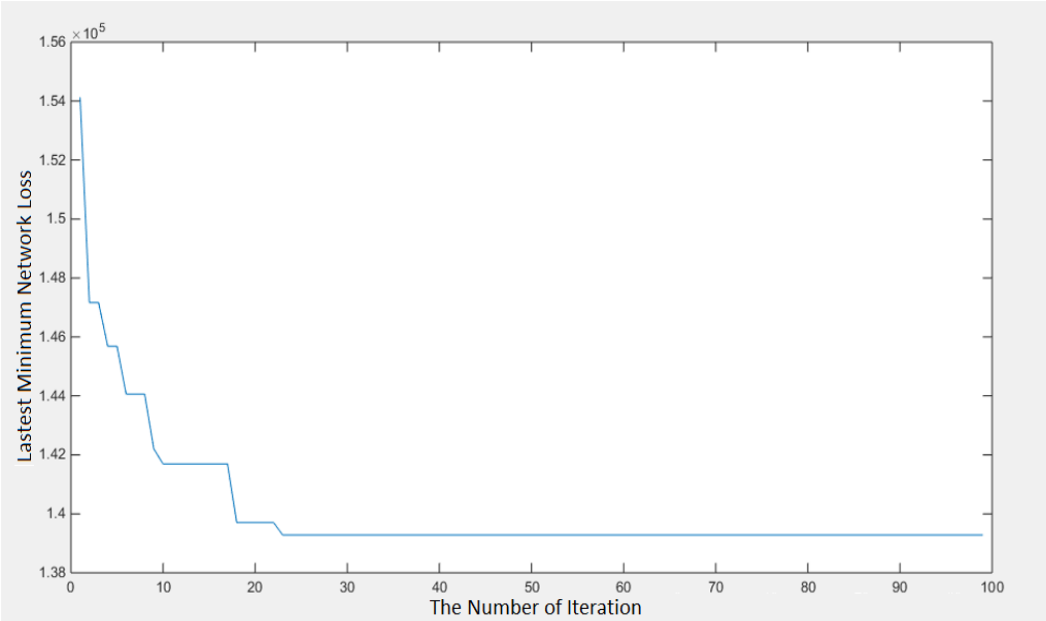

Figure 5-20 Convergence characteristic of ant colony algorithm in 33-bus system

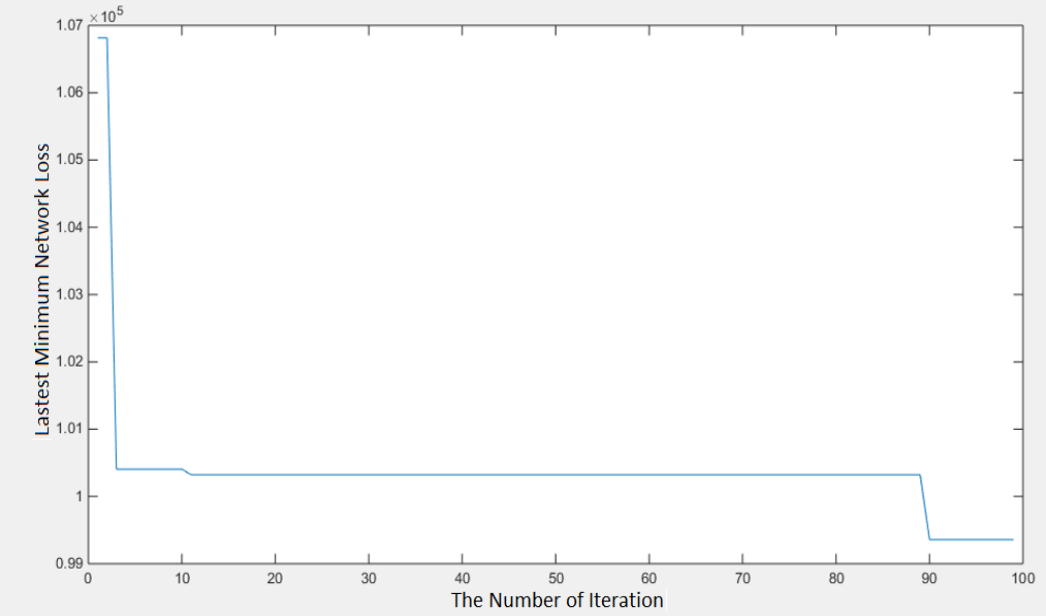

Figure 5-21 Convergence characteristic of ant colony algorithm in 69-bus system

Figure 5-20 and Figure 5-21 shows the convergence characteristic of the ant colony algorithm in above two test system. The curve in Figure 5-20 shows a fast reduction in the current minimum value. It illustrates a good convergence of the ant colony system in the 33-bus system. However, the curve in Figure 5-21 remains

at pseudo minimum value for about 80 iterations. Because of such a characteristic, the final solution found may not be the global best solution. Also due to this characteristic, artificial intelligence based optimization algorithm normally set a maximum iteration as the terminated condition instead of setting the stable time of the latest global best solution in several iterations. Comparing Figure 5-20 with Figure 5-21, 100 as the maximum iteration is sufficient for the 33-bus system. But the maximum iteration should be larger to the 69-bus and the larger systems.

5.6.2 Feeder Reconfiguration for Loss Reduction by Using Discrete Particle Swarm Optimization

Discrete particle swarm optimization for feeder reconfiguration is tested in both IEEE 33-bus and 69-bus system. The settings of system parameters are as follows: the population of particles is 10; influence coefficient of particle speed ω is 0.8; the maximum number of iteration is set to be 100; both the acceleration constants c_1 and c_2 are suggested equal to 2 in references [48, 61]. But the value of these two parameters is set to 0.5 and 1.5 in its improved particle swarm optimization in reference [62]. So, it is necessary to test the best value of the two acceleration constants. The test results of different value of acceleration constants c_1 and c_2 are shown in Figure 5-22.

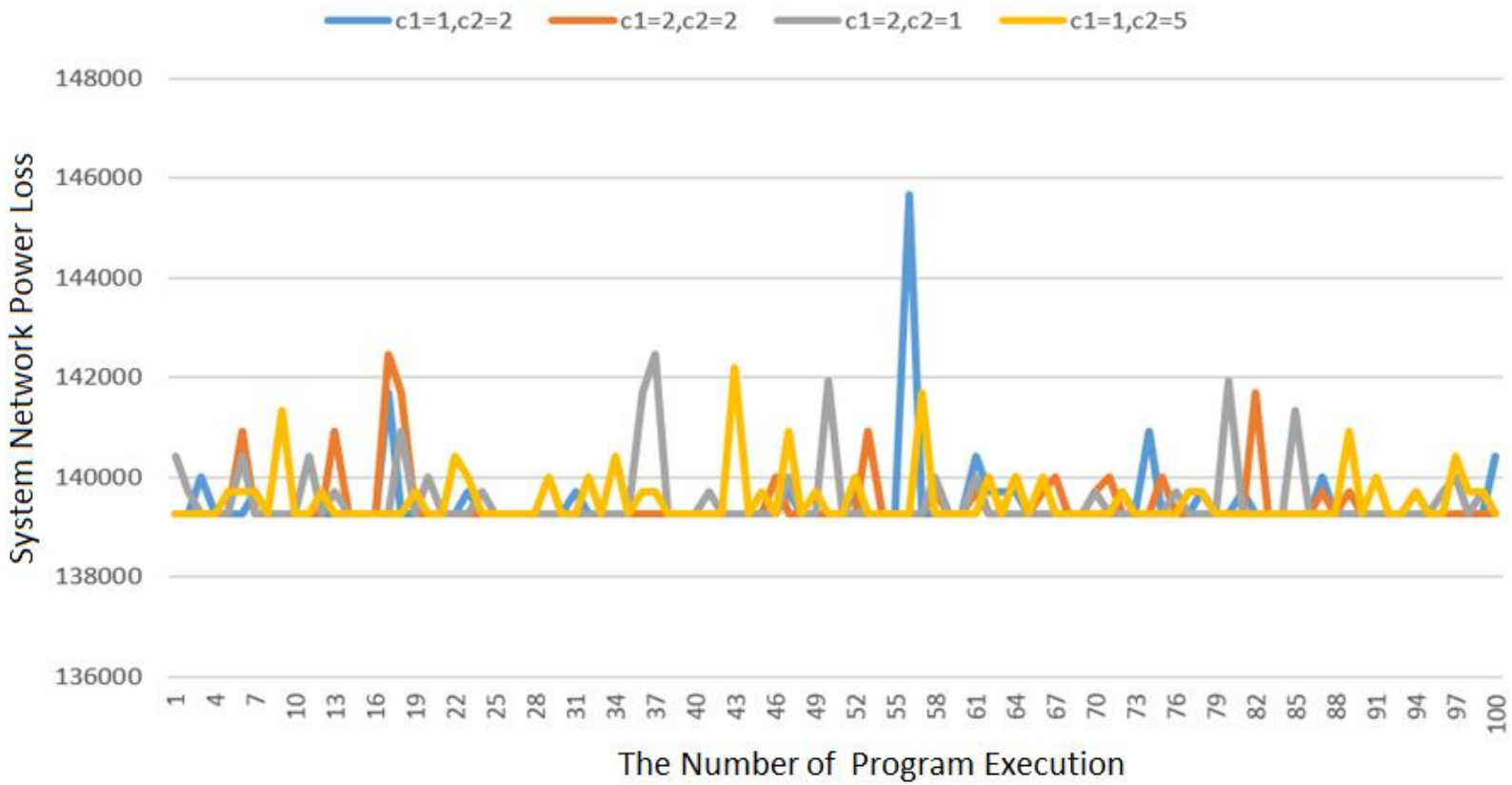

Figure 5-22 Feeder reconfiguration results in different c_1 and c_2

The curves are results of repeating 100 times discrete particle swarm optimization in each setting of acceleration constants. It is not easy to determine out which one has better performance from the curves. This shows that small difference settings on the value of two acceleration constants will not have a big effect on the final result. In this case study, the average value of minimum system power loss is smallest when $c_1 = 1$ and $c_2 = 5$. Thus, the value of acceleration constants for local best position c_1 and global best position c_2 is 1 and 5 respectively and is tested in this thesis for particle swarm optimization with tear circuit method.

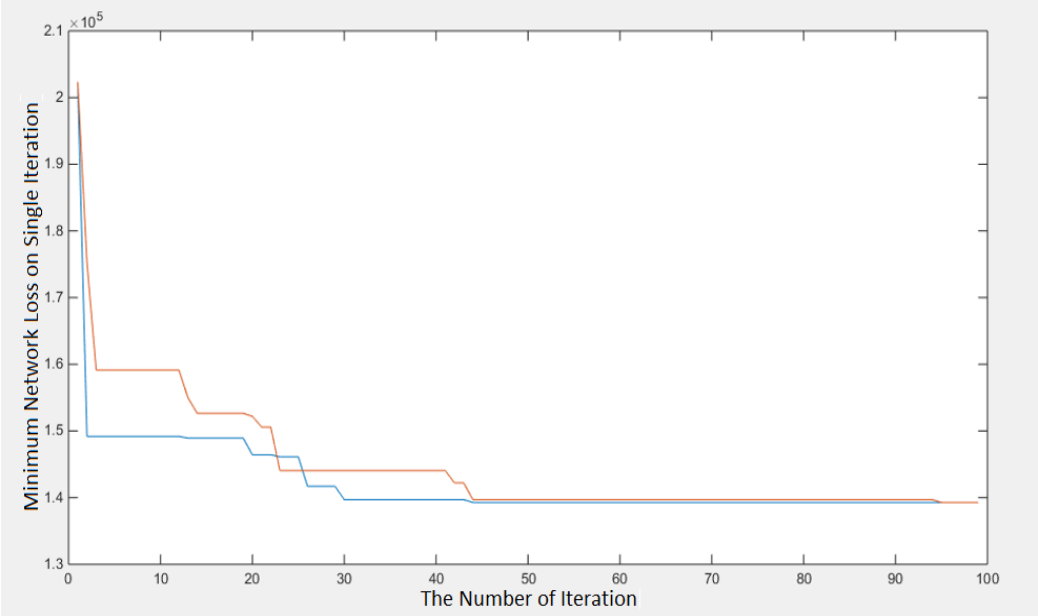

Figure 5-23 Minimum network loss of each iteration by using discrete particle swarm optimization in 33-bus system with 100 maximum iteration

Search performance is tested again in the discrete particle swarm optimization for feeder reconfiguration in the 33-bus system. With the same setting of system parameters, two curves are chosen from two random test and shown in Figure 5-23. Blue curve finds the final solution at the 44th iteration and the red curve finds the final solution at the 95th iteration. In this figure, the minimum network loss of both curves in each iteration is continuing to reduce. Due to the unique particle velocity, each particle has its own solution. The usefulness of the local and global

best position of the particles is to update the particle velocity. All solutions found by each particle may be entirely different. The 33-bus system and its possible number of the solution are both small. Thus, two curves in Figure 5-23 may be considered as the results of one particle and this particle can always find the latest global best solution.

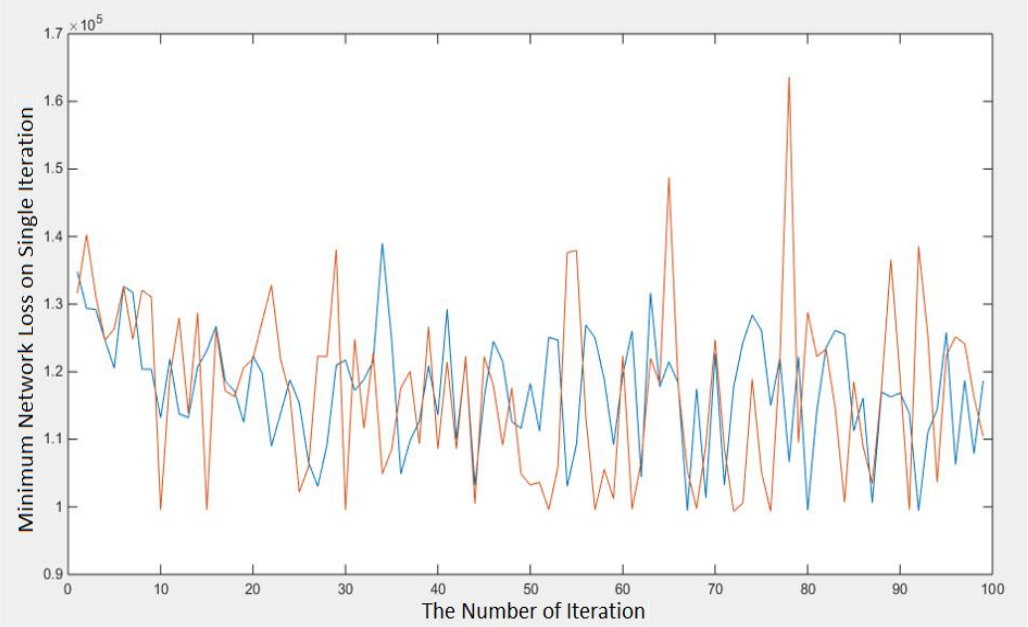

Figure 5-24 Minimum network loss of each iteration by using discrete particle swarm optimization in 69-bus system with 100 maximum iteration

For the 69-bus system, the possible number of solutions of this system is much more than the 33-bus system. One particle cannot always find the current global best solution again. Thus, the curves in Figure 5-24 cannot keep reducing. The minimum network loss of each iteration may be the same in some iterations in Figure 5-18 while they are totally different in Figure 5-24. The orange curve finds the known best solution at the 72nd iteration. The blue curve cannot find the known best solution. Such a result represents that, for the discrete particle swarm optimization, when particles find a better solution than the latest global best solution, more search should be done base on this latest global solution rather than

just treat it as a reference and continues the search in their own way. Thus, the inertia weight ω can be reduced with the iterations.

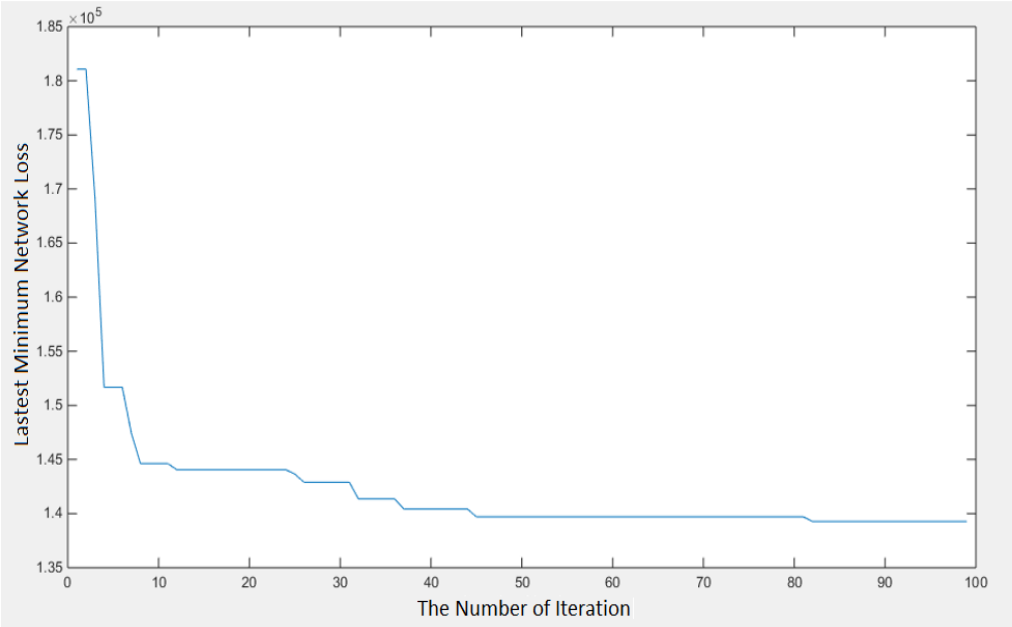

Figure 5-25 Convergence characteristics of the discrete particle swarm optimization in 33-bus system

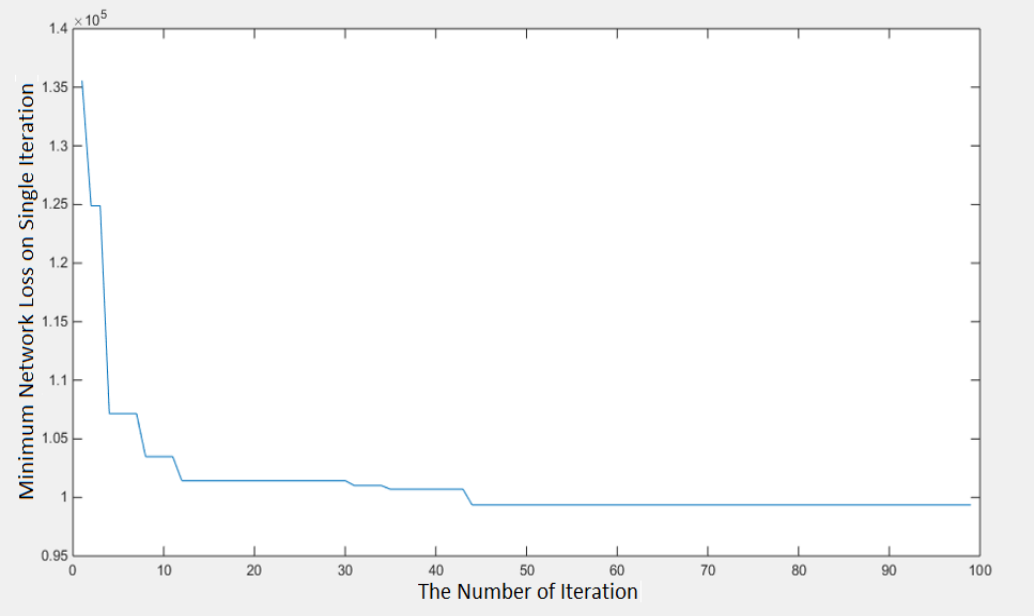

Figure 5-26 Convergence characteristics of the discrete particle swarm optimization in 69-bus system

The convergence characteristic of the discrete particle swarm optimization in the

33-bus system and the 69-bus system is shown in Figure 5-25 and Figure 5-26 respectively. The minimum system power loss in Figure 5-26 is not the known global best solution for this system. The curve in above figures is one randomly selected result of all tests using the discrete particle swarm optimization. These two figures show that the local search ability of the discrete particle swarm optimization is weak.

5.6.3 Comparison and Discussion.

In order to compare the two optimization methods for more details, results are put together in this section. The system setting of both methods is provided in Table 5-1. The same population and maximum iteration number provide a relatively fair test environment.

Table 5-1 Setting of the system parameters

System parameters	α	β	ρ	ξ	Q	P_0
Ant colony system	1	1	0.3	0.1	1	0.3
System parameters	C_{Local}	C_{Global}	ω			
Particle swarm	1	5	0.8			

The results statistics of repeating 100 times on the ant colony system and the discrete particle swarm optimization in feeder reconfiguration are shown in Table 5-2. The population of the ant is set to 10 which is suggested by reference[1]. The population of the particle is set to 20 which is normally approximately equal to the total search points. Maximum iteration of both methods is 50. Both methods find a same best system structure. The worst result of the latest global best solution determines by the ant colony system is better in both two different systems. All results of two systems using both methods are shown as curves in Figure 5-27 and Figure 5-28 respectively. It can be seen that the result curve amplitude of ant colony

system is much smaller than the discrete particle swarm optimization. Thus, the average system power loss of discrete particle swarm optimization is larger than the value obtained by the ant colony system. This shows that in feeder reconfiguration problem, ant colony system has a better searching performance. In the statistics of computing time, ant colony system complete the reconfiguration in both the 33-bus system and the 69-bus system with less computing time. It can consider that the ant colony system may have better performance in the feeder reconfiguration problem. Due to the maximum number of iteration of both methods are not the same, the computing time may be impacted by the personal program skill and the variable frequency skill of CPU, more tests need to be done in a fair situation to compare which method is better.

Table 5-2 Comparisons of ACS and DPSO for IEEE distribution system

Method	System	System Power Loss(kW)			Computing Time (unit)
		Best	Worst	Average	
Ant Colony	33-bus	139.28	139.70	139.29	0.22
	69-bus	99.36	100.32	99.77	0.54
Particle Swarm	33-bus	139.28	145.68	139.47	0.28
	69-bus	99.36	105.78	100.37	0.58
New Tie Switches in Global Best Solution	33-bus	7,9,14,32,37			
	69-bus	14,45,50,69,70			

Results obtained by 100 repeat of execution. The population of ant and particles are 10 and 20 respectively. Both maximum number of iteration are 50.

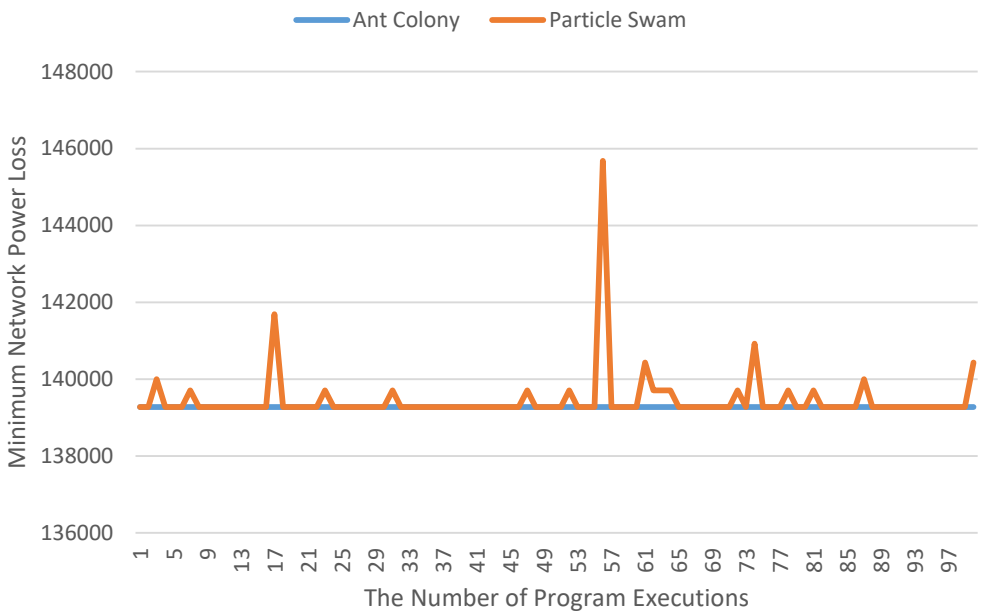

Figure 5-27 Comparison of ACS and PSO in 100 repeat executions in the 33-bus system

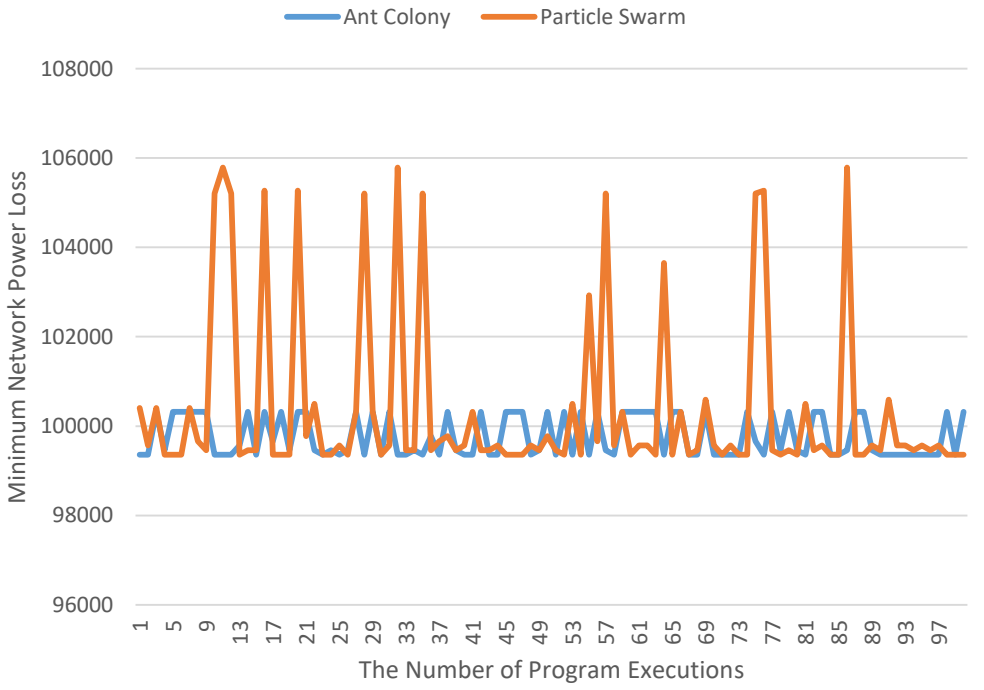

Figure 5-28 Comparison of ACS and PSO in 100 repeat executions in the 69-bus system

Table 5-3 is the comparisons of the results of three artificial intelligence based optimization algorithm which shows in reference [2]. Comparing with the results in Table 5-2, the new tie switches for the best solution is the same. Due to the use of different load flow analysis method, there is tolerance in the minimum system power loss between test results and reference. The computing time depends on the computer performance and personal programming skill. Thus, there is no comparability on the computing time between two tables. The computing time of the particle swarm in the 69-bus system is longer than ant colony system in Table 5-3 which is not the same obtained in Table 5-2. It may be caused by the application of tear circuit method which is used in this thesis.

Table 5-3 Comparisons of the results for IEEE distribution system[2]

Method	System	System Power Loss(kW)			Computing Time (s/per iteration)
		Best	Worst	Average	
Genetic Algorithm	33-bus	139.55	140.24	140.24	0.30
	69-bus	99.58	100.64	100.30	3.30
Adaptation Ant Colony	33-bus	139.55	140.24	140.13	0.21
	69-bus	99.58	100.64	100.29	3.12
Adaptation Particle Swarm	33-bus	139.55	140.24	140.04	0.49
	69-bus	99.58	100.64	100.38	5.34
New Tie Switches in Global Best Solution	33-bus	7,9,14,32,37			
	69-bus	14,45,50,69,70			

Even though the minimum system power losses after feeder reconfiguration in the 33-bus and the 69-bus system are not the same, the new tie switches are the same in references [2, 63, 64]. So, the possible global best solutions of feeder reconfiguration for this two system can be determined.

The initial system power loss in the 33-bus and the 69-bus system is 3.98% and 6.00% respectively. After doing feeder reconfiguration, the new system power loss is 2.74% and 2.64% respectively. The reduction rate of system power loss is 31.16% and 56.05% respectively. Lots of system power loss can be reduced only by changing the status of switches. This shows that feeder reconfiguration analysis for loss reduction is necessary.

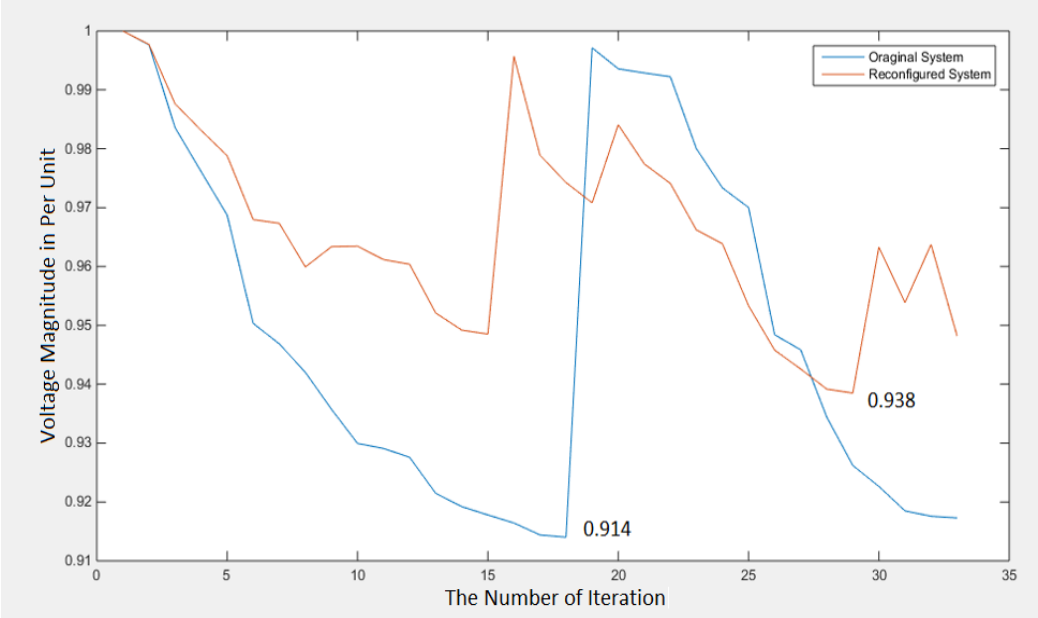

Figure 5-29 Bus voltage magnitude of IEEE 33-bus system

The minimize system voltage drop is an important objective of feeder reconfiguration and power quality enhancement[65]. The system voltage magnitude curves of the original system and the reconfigured system are shown in Figure 5-29. The buses voltage magnitude is shown in per unit. The orange curve represents the voltage profile in reconfigured system and its minimum voltage magnitude is 0.938 per unit. The blue curve is the voltage profile of the original system and its minimum voltage magnitude is 0.914 per unit. It can be seen in Figure 5-29 that the reconfigured bus voltage distribution curve is smoother than

the original one. Feeder reconfiguration can improve electric power quality.

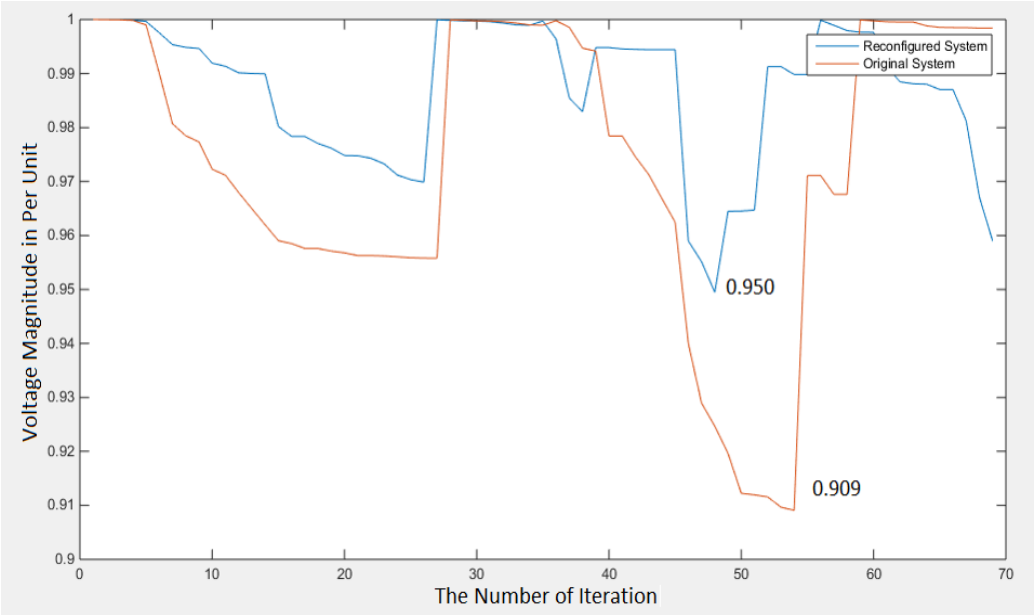

Figure 5-30 Bus voltage magnitude of IEEE 69-bus system

Feeder reconfiguration for loss reduction also reduces the voltage drop in the IEEE 69-bus system. In Figure 5-30, the minimum bus voltage increased from 0.909 per unit to 0.950 per unit. Both the above tests show that although the objective of this test is the system power loss, the power quality is also improved by increasing the minimum system bus voltage. If the objective function mainly considers only the voltage drop, the power quality will be further improved.

5.7 Summary

As the most widely used optimization algorithm in recent years, ant colony system and particle swarm optimization are tested in this chapter. Even though the tear circuit method is applied in the discrete particle swarm optimization to avoid building the infeasible system structure, ant colony system still has better performance to solve the feeder reconfiguration problem. But, one curve of minimum power loss in the single iteration of ant colony system in 33-bus is

continued to reduce without any disturbances. This may indicate that ant colony system has some deficiency in searching new area or structure. The curves of convergence characteristic for both methods show that optimization methods may be trapped at a local solutions long time. Because the pseudorandom proportional mechanism in ant colony system and the weak local search ability of particle swarm optimization finding a new route to the global best solution. Thus, the termination condition for the optimization method commonly depends on the maximum number of iteration.

The settings of the system parameters for both methods are discussed in this chapter. Although references [1] and [48] of these two methods make some suggestions, the results in this chapter show a different case. The initial suggest settings are based on the travelling salesman problem. New settings of system parameters are necessary for feeder reconfiguration problem. The ant colony system cannot even calculate the best solution when the settings system parameter is not suitable. Thus, the system parameters of ant colony system and particle swarm optimization need to be optimal and are different for various types of problem to test and reset in the different problem.

The latest global best results of feeder reconfiguration for system power loss reduction provide by both optimization methods is the same. After reconfiguration, the system power loss has a significant reduction. Furthermore, the maximum voltage drop in the test systems is also significantly improved.

5.8 Reference

[1] Marco Dorigo, Thomas Stu¨tzle, *Ant Colony Optimization*. Cambridge, 2004.

[2] A. Swarnkar, N. Gupta, and K. R. Niazi, "Distribution network reconfiguration using population-based AI techniques: A comparative analysis," in *Power and Energy Society General Meeting, 2012 IEEE*, 2012, pp. 1-6.

[3] B. H. Marlin.A, "Search for a Minimal-loss Operating Spanning Tree Configuration In Urban Power Distribution System," *Proc of 5th Power System Comp Con, cambridge,UK,* p. 2~6, 1975.

[4] S. K. Goswami and S. K. Basu, "A new algorithm for the reconfiguration of distribution feeders for loss minimization," *Power Delivery, IEEE Transactions on,* vol. 7, pp. 1484-1491, 1992.

[5] F. V. Gomes, S. Carneiro, Jr., J. L. R. Pereira, M. P. Vinagre, P. A. N. Garcia, and L. R. Araujo, "A new heuristic reconfiguration algorithm for large distribution systems," in *Power Engineering Society General Meeting, 2006. IEEE*, 2006, p. 1 pp.

[6] E. R. Ramos, A. G. Exposito, J. R. Santos, and F. L. Iborra, "Path-based distribution network modeling: application to reconfiguration for loss reduction," *Power Systems, IEEE Transactions on,* vol. 20, pp. 556-564, 2005.

[7] H. P. Schmidt, N. Ida, N. Kagan, and J. C. Guaraldo, "Fast Reconfiguration of Distribution Systems Considering Loss Minimization," *Power Systems, IEEE Transactions on,* vol. 20, pp. 1311-1319, 2005.

[8] C. Joon-Ho and K. Jae-Chul, "Network reconfiguration at the power distribution system with dispersed generations for loss reduction," in *Power Engineering Society Winter Meeting, 2000. IEEE*, 2000, pp. 2365-2367 vol.4.

[9] N. Kagan and C. C. B. de Oliveira, "Fuzzy decision model for the reconfiguration of distribution networks using genetic algorithms," 1999.

[10] W. Wu-Chang and T. Men-Shen, "Application of Enhanced Integer Coded Particle Swarm Optimization for Distribution System Feeder Reconfiguration," *Power Systems, IEEE Transactions on,* vol. 26, pp. 1591-1599, 2011.

[11] A. R. Malekpour, T. Niknam, A. Pahwa, and A. K. Fard, "Multi-Objective Stochastic Distribution Feeder Reconfiguration in Systems With Wind Power Generators and Fuel Cells Using the Point Estimate Method," *Power Systems, IEEE Transactions on,* vol. 28, pp. 1485-1492, 2013.

[12] A. Ahuja and A. Pahwa, "Using ant colony optimization for loss minimization in distribution networks," in *Power Symposium, 2005. Proceedings of the 37th Annual North American*, 2005, pp. 470-474.

[13] C. Chung-Fu, "Reconfiguration and Capacitor Placement for Loss Reduction of Distribution Systems by Ant Colony Search Algorithm," *Power Systems, IEEE Transactions on,* vol. 23, pp. 1747-1755, 2008.

[14] W. Yuan-Kang, L. Ching-Yin, L. Le-Chang, and T. Shao-Hong, "Study of Reconfiguration for the Distribution System With Distributed Generators," *Power Delivery, IEEE Transactions on,* vol. 25, pp. 1678-1685, 2010.

[15] "Heuristic (computer science),"

https://en.wikipedia.org/wiki/Heuristic_(computer_science), last data of access 05.05.2016.

[16] M. Dorigo, V. Maniezzo, and A. Colorni, "Ant system: optimization by a colony of cooperating agents," *Systems, Man, and Cybernetics, Part B: Cybernetics, IEEE Transactions on,* vol. 26, pp. 29-41, 1996.

[17] L. M. Gambardella and M. Dorigo, "Solving symmetric and asymmetric TSPs by ant colonies," in *Evolutionary Computation, 1996., Proceedings of IEEE International Conference on*, 1996, pp. 622-627.

[18] B. Bullnheimer, R. F. Hartl, and C. Strauss., "A New Rank Based Version of the Ant System - A Computational Study," *Central European Journal for Operations research and Economics,* vol. 7(1), p. 25;38, 1999.

[19] I. F. d. V. Oscar Cordon, Francisco Herrera, Llanos Moreno "A new ACO model integrating evolutionary computation concept: the best-worst ant system," 2000.

[20] I. F. n. d. V. O. CordÃ³n GarcÃa, F. Herrera, "Analysis of the best-worst ant system and its variants on the TSP," *Mathware & Soft Computing,* vol. 9, 2002.

[21] H. H. H. Thomas Stützle, "MAX-MIN Ant System," *Future Generation Computer System,,* vol. 16(8), pp. 889-914, 2000.

[22] T. Stutzle, "Local Search Algorithms for Combinatorial Problems: analysis, Improvements, and New Applications," *DISKI,* vol. 220, 1999.

[23] M. Dorigo and L. M. Gambardella, "Ant colony system: a cooperative learning approach to the traveling salesman problem," *Evolutionary Computation, IEEE Transactions on,* vol. 1, pp. 55-66, 1997.

[24] F. S. Pereira, K. Vittori, and G. R. M. da Costa, "Distribution System

Reconfiguration for Loss Reduction Based on Ant Colony Behavior," in *Transmission & Distribution Conference and Exposition: Latin America, 2006. TDC '06. IEEE/PES*, 2006, pp. 1-5.

[25] F. S. Pereira, K. Vittori, and G. R. M. da Costa, "Ant colony based method for reconfiguration of power distribution system to reduce losses," in *Transmission and Distribution Conference and Exposition: Latin America, 2008 IEEE/PES*, 2008, pp. 1-5.

[26] L. E. da Silva, G. Lambert-Torres, H. G. Martins, M. P. Coutinho, L. E. B. da Silva, and J. C. Neto, "An application of ACO in system reconfiguration," in *Transmission and Distribution Conference and Exposition, 2010 IEEE PES*, 2010, pp. 1-6.

[27] E. Carpaneto and G. Chicco, "Ant-colony search-based minimum losses reconfiguration of distribution systems," in *Electrotechnical Conference, 2004. MELECON 2004. Proceedings of the 12th IEEE Mediterranean*, 2004, pp. 971-974 Vol.3.

[28] H. Wang, L. Zhao, W. Wang, F.-f. Zhou, X. Ji, and H. Zhang, "Distribution network reconstruction based on improved ant colony algorithm of directional pheromones," in *Control and Decision Conference (CCDC), 2015 27th Chinese*, 2015, pp. 1245-1247.

[29] A. Swarnkar, N. Gupta, and K. R. Niazi, "Efficient reconfiguration of distribution systems using ant colony optimization adapted by graph theory," in *Power and Energy Society General Meeting, 2011 IEEE*, 2011, pp. 1-8.

[30] S. Yuanbo, Z. Chengxue, and H. Zhijian, "A reconfiguration method for regional distribution networks with graph-based ant system," in *Mechatronic Sciences, Electric Engineering and Computer (MEC),*

Proceedings 2013 International Conference on, 2013, pp. 3705-3708.

[31] Z. Hao, M. Shuang, and X. Gang, "Network Reconfiguration of Distribution System with Distributed Generation Using State Graph," in *Power and Energy Engineering Conference (APPEEC), 2012 Asia-Pacific*, 2012, pp. 1-4.

[32] G. Wang, L. Liu, and Z. Tieyan, "An improved ant colony search algorithm for reconfiguration of distribution network with distributed generations," in *Innovative Smart Grid Technologies - Asia (ISGT Asia), 2012 IEEE*, 2012, pp. 1-4.

[33] L. Yunfeng, S. Yuanbo, L. Xiaobo, Z. Chengxue, L. Jun, and H. Zhijian, "Multi-Region Distribution System Reconfiguration Based on an Improved Ant Colony Algorithm," in *Power and Energy Engineering Conference (APPEEC), 2012 Asia-Pacific*, 2012, pp. 1-5.

[34] A. Ahuja, S. Das, and A. Pahwa, "An AIS-ACO Hybrid Approach for Multi-Objective Distribution System Reconfiguration," *Power Systems, IEEE Transactions on,* vol. 22, pp. 1101-1111, 2007.

[35] M. S. Tsai and C. C. Chu, "Applications of hybrid EP-ACO for power distribution system loss minimization under load variations," in *Intelligent System Application to Power Systems (ISAP), 2011 16th International Conference on*, 2011, pp. 1-7.

[36] T. Q. D. Khoa and P. T. T. Binh, "A Hybrid Ant Colony Search Based Reconfiguration of Distribution Network for Loss Reduction," in *Transmission & Distribution Conference and Exposition: Latin America, 2006. TDC '06. IEEE/PES*, 2006, pp. 1-7.

[37] A. Y. Abdelaziz, R. A. Osama, S. M. Elkhodary, and E. F. El-Saadany,

"Reconfiguration of distribution systems with distributed generators using Ant Colony Optimization and Harmony Search algorithms," in *Power and Energy Society General Meeting, 2012 IEEE*, 2012, pp. 1-8.

[38] R. A. Osama, A. Y. Abdelaziz, and S. M. Elkhodary, "Ant Colony Optimization and Harmony Search algorithms for distribution networks reconfiguration," in *Informatics and Systems (INFOS), 2012 8th International Conference on*, 2012, pp. BIO-81-BIO-88.

[39] J. Kennedy and R. Eberhart, "Particle swarm optimization," in *Neural Networks, 1995. Proceedings., IEEE International Conference on*, 1995, pp. 1942-1948 vol.4.

[40] S. Yuhui and R. Eberhart, "A modified particle swarm optimizer," in *Evolutionary Computation Proceedings, 1998. IEEE World Congress on Computational Intelligence., The 1998 IEEE International Conference on*, 1998, pp. 69-73.

[41] X. H. Shi , X. L. Xing , Q. X. Wang , L. H. Zhang , X. W. Yang , C. G. Zhou and Y. C. Liang "A discrete PSO method for generalized TSP problem," *Proc. 3rd Int. Conf. Machine Learning and Cybernetics,* vol. 3, pp. 2378 -2383, 2004.

[42] Z. Y.-d. C. Yue , L. Jing and T. Hui, "An integer-coded chaotic particle swarm optimization for traveling salesman problem," *Proc. Progress in Robotics FIRA RoboWorld Congr.,* pp. 372 -379, 2009.

[43] J. Kennedy and R. C. Eberhart, "A discrete binary version of the particle swarm algorithm," in *Systems, Man, and Cybernetics, 1997. Computational Cybernetics and Simulation., 1997 IEEE International Conference on*, 1997, pp. 4104-4108 vol.5.

[44] R. F. Chang and C. N. Lu, "Feeder reconfiguration for load factor improvement," in *Power Engineering Society Winter Meeting, 2002. IEEE*, 2002, pp. 980-984 vol.2.

[45] S. Sivanagaraju, J. V. Rao and P. S. Raju, "Discrete particle swarm optimization to network reconfiguration for loss reduction and load balancing," *Elect. Power Compon. Syst.,* vol. 36, pp. 513 -524, 2008.

[46] W.-C. Wu and M.-S. Tsai, "Feeder reconfiguration using binary coding particle swarm optimization," *Int. J. Control, Autom. Syst.,* vol. 6, pp. 488 -494, 2008.

[47] Y. Shih-An and L. Chan-Nan, "Distribution Feeder Scheduling Considering Variable Load Profile and Outage Costs," *Power Systems, IEEE Transactions on,* vol. 24, pp. 652-660, 2009.

[48] W. M. Dahalan and H. Mokhlis, "Network reconfiguration for loss reduction with distributed generations using PSO," in *Power and Energy (PECon), 2012 IEEE International Conference on*, 2012, pp. 825-828.

[49] S. S. Huaibo Ren, Xiaowei Wang, "Research Base on Improved Binary Particle Swarm Optimization for Feeder Reconfiguration (in Chinese)," *Power Grid and Clean Energy,* vol. 8, pp. 40-43, 2011.

[50] T. Niknam, A. Kavousifard, and J. Aghaei, "Scenario-based multiobjective distribution feeder reconfiguration considering wind power using adaptive modified particle swarm optimization," *Renewable Power Generation, IET,* vol. 6, pp. 236-247, 2012.

[51] F. Batrinu, E. Carpaneto, and G. Chicco, "A novel Particle Swarm method for distribution system optimal reconfiguration," in *Power Tech, 2005 IEEE Russia*, 2005, pp. 1-6.

[52] T. M. Khalil, A. V. Gorpinich, and G. M. Elbanna, "Combination of capacitor placement and reconfiguration for loss reduction in distribution systems using selective PSO," in *Electricity Distribution (CIRED 2013), 22nd International Conference and Exhibition on*, 2013, pp. 1-4.

[53] M. N. M. Nasir, N. M. Shahrin, Z. H. Bohari, M. F. Sulaima, and M. Y. Hassan, "A Distribution Network Reconfiguration based on PSO: Considering DGs sizing and allocation evaluation for voltage profile improvement," in *Research and Development (SCOReD), 2014 IEEE Student Conference on*, 2014, pp. 1-6.

[54] A. Tandon and D. Saxena, "A comparative analysis of SPSO and BPSO for power loss minimization in distribution system using network reconfiguration," in *Computational Intelligence on Power, Energy and Controls with their impact on Humanity (CIPECH), 2014 Innovative Applications of*, 2014, pp. 226-232.

[55] T. Kaboodi, J. Olamaei, H. Siahkali, and R. Bita, "Optimal distribution network reconfiguration using fuzzy interaction and MPSO algorithm," in *Smart Grid Conference (SGC), 2014*, 2014, pp. 1-5.

[56] T. Niknam, "A NEW HYBRID ALGORITHM FOR MULTI-OBJECTIVE DISTRIBUTION FEEDER RECONFIGURATION," *Cybernetics and Systems: An International Journal,* vol. 40, pp. 508-527, 2009.

[57] R. Srinivasa Rao, S.V.L. Narasimham, M. Ramalingaraju, "Optimization of Distribution Network Configuration for Loss Reduction Using Artificial Bee Colony Algorithm," *World Academy of Science, Engineering and Technology,* vol. 45, pp. 708-714, 2008.

[58] W.C. Wu and B.M. Zhang, "A three-phase power flow algorithm for distribution system power flow based on loop-analysis method,"

International Journal of Electrical Power & Energy Systems, vol. 30, pp. 8 -15, 2008.

[59] M. E. Baran and F. F. Wu, "Network reconfiguration in distribution systems for loss reduction and load balancing," *Power Delivery, IEEE Transactions on,* vol. 4, pp. 1401-1407, 1989.

[60] J. S. Savier and D. Das, "Impact of Network Reconfiguration on Loss Allocation of Radial Distribution Systems," *Power Delivery, IEEE Transactions on,* vol. 22, pp. 2475-2480, 2007.

[61] L. Yan and G. Xueping, "Reconfiguration of network skeleton based on discrete particle-swarm optimization for black-start restoration," in *Power Engineering Society General Meeting, 2006. IEEE*, 2006, p. 7 pp.

[62] T. Sawa, "Radial network reconfiguration method in distribution system using mutation Particle Swarm Optimization," in *PowerTech, 2009 IEEE Bucharest*, 2009, pp. 1-6.

[63] J.A. Martín, A.J. Gil, "A new heuristic approach for distribution systems loss reduction," *Electr. Power Syst. Res.,* vol. 78, pp. 1953–1958, 2008.

[64] B. Enacheanu, B. Raison, R. Caire, O. Devaux, W. Bienia, and N. HadjSaid, "Radial Network Reconfiguration Using Genetic Algorithm Based on the Matroid Theory," *IEEE Transactions on Power Systems,* vol. 23, pp. 186-195, 2008.

[65] C. Sankaran, *Power Quality*. Boca Raton London New York Washington, D.C: CRC Press LLC, 2002.

Chapter 6 A Hybrid Based Ant Colony System and Discrete Particle Swarm Optimization

6.1 Introduction

Ant colony optimization and particle swarm optimization have been proposed for many years. Many attempts have tried to improve their performance. For the ant colony optimization, most of the improvement focus on the update rules of the pheromone trails. The improvement of the discrete particle swarm optimization also focused on the update rules of particle velocity. Actually, improvement on different parts of the update equation in both ant colony optimization and particle swarm optimization are relatively independent. Different improvements on different parts of the update equation can be applied at the same time. For example, in reference [1], the new mechanism of ant colony system is a pseudorandom proportional rule to generate more solutions. The hypercube framework of ant system limits a scaling of the objective function values and the pheromone values to the interval (0, 1) so that the pheromone on some path will not be too strong. These two improvements are combined in reference [2]. This kind of combination is more general in the particle swarm optimization, such as in references [3] and [4]. In order to improve the search efficiency from a different angle, an adaptive function is proposed in this chapter for changing the pseudorandom proportional level in the ant colony system and the search area and the random mechanism level in the discrete particle swarm optimization at different search stages.

The same with other artificial intelligent based optimization methods, both of ant colony optimization and particle swarm optimization have its particular advantages and disadvantages. It is difficult to avoid their disadvantages only by modifying

the rules. However, the disadvantages may be overcome by combining two or more artificial intelligent based algorithm together, such as in references [5-9]. In the power system field, not many researches have been done for hybrid method based on the ant system and the particle swarm optimization. So, parts of the experience in other fields are introduced here. References [10-13] divide the hybrid methods into two stages. The first stage is the particle swarm optimization which is used for providing the initial pheromone trails of the ant colony optimization. The second stage is searching the final solution by ant colony system. In this chapter, a hybrid optimization method based on the ant colony system and the tear circuit based discrete particle swarm optimization has been proposed to overcome their disadvantages. Different from the typical hybrid strategy, the search performance of the individual not only relies on the pheromone trails but also consider the initial particle velocity, the local best position and the global best position. Base on the pheromone trails, individuals can search better solutions around an existing solution fast which mean that perfect local search ability is obtained. For the particle velocity, individuals can quickly find feasible solutions in all possible search areas. It is shown that the global search ability of the hybrid method is also excellent.

The method for reducing search scale for the distribution network and the adaptive function is introduced in section 6.2. Case studies and discussions for verifying the search efficiency improvement by the adaptive function are shown in section 6.3. In section 6.4, the general hybrid strategies based on the Pros and Cons of the ant colony system and the particle swarm optimization are introduced. A novel hybrid method is also illustrated in this section. Comparisons and discussions for the novel hybrid method are shown in section 6.5.

6.2 Search Efficiency Improvement for Ant Colony System and Particle Swarm Optimization

6.2.1 Search Size Reduction in Distribution System

Distribution network consists of tie switches and sectionalizing switches. The purpose of the distribution network feeder reconfiguration is finding the best system structure for loss reduction or other objectives by changing the status of each switch in the network. However, the changing on these switches is not arbitrary. To avoid islanding the buses in the distribution network, each bus in the network must have a connection with the system source bus. According to this limitation, some system constraints are proposed for the distribution network feeder reconfiguration. On the other hand, parts of the sectionalizing switches in distribution network must keep close status or the island bus will appear. The IEEE 33-bus distribution system and IEEE 69-bus distribution system is illustrated for such a situation in Figure 6-1 and Figure 6-2 respectively.

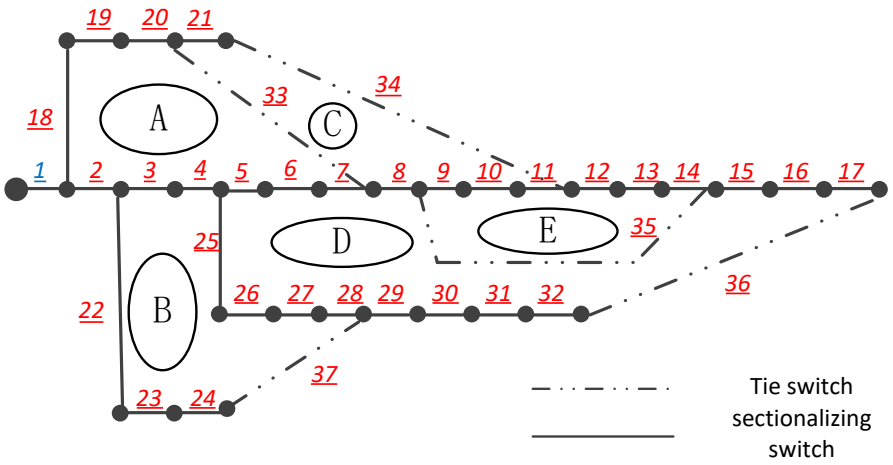

Figure 6-1 The constant close switches IEEE 33-buses system

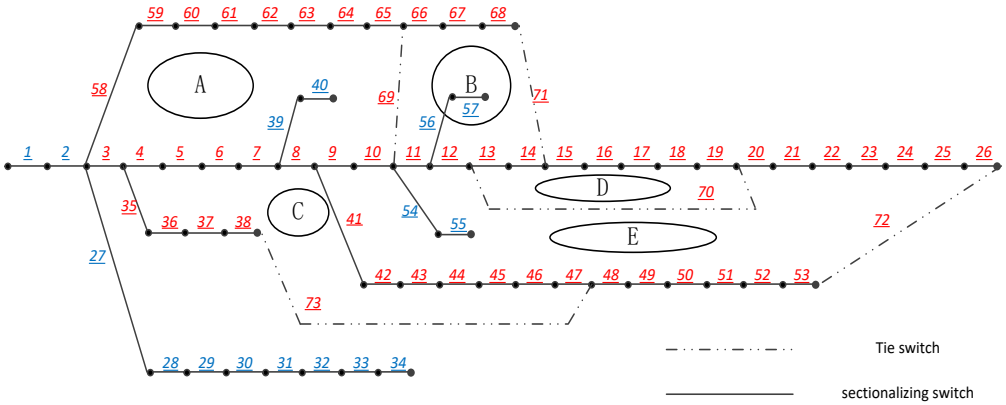

Figure 6-2 The constant close switches in IEEE 69-buses system

These two distribution systems are the standard test systems for distribution network feeder reconfiguration in many papers. So, the characteristics of these two system structures can represent most parts of the distribution network. According to the tear circuit method for particle swarm optimization in section 5.5.3, the network in Figure 6-1 can be divided into five circuits. By changing the status of the switches in these five circuits, the tear circuit method can avoid the infeasible solutions which may find by the discrete particle swarm optimization, so that the efficiency of the discrete particle swarm optimization can be significantly increased. The 69-bus system can also be divided into five circuits according to the tear circuit method, such as shown in Figure 6-2. But, the switches in blue do not belong to any system circuits. Without considering the status of these switches in blue ink, the latest global best solution of the tear circuit based particle swarm optimization in the case studies of Chapter 5 is the same with the ant colony system. The same latest global best solution calculated by two different methods means that the switches in blue in the 69-bus distribution system are meaningless for feeder reconfiguration. From the perspective of the power system analysis, sectionalizing switches in blue is constant closed or islanding system will appear.

For ant colony system and some of other optimization methods for distribution network feeder reconfiguration, the status of each switch in the network will be

decided in the search process. The status decision for constant closed switches is also made in each search iteration. The calculation for these switches is unnecessary. Thus, before doing the feeder reconfiguration, delete the constant closed switches in the search process according to the tear circuit method can reduce the search scale for all optimization method.

For different distribution system, the reduced system size may different. There are 16 constant close switches in IEEE-69 buses system. It is approximately 23% of the whole system size. However, only one constant closed switch exists in the IEEE 33-bus system. Normally, the size of the distribution system is bigger, the number of constant closed switches is larger and more computing time will be saved. Overall, avoiding the calculation on the constant closed switch before doing the optimization calculation will always improve the search efficiency.

6.2.2 Adaptive Function for Optimization Method

Particle swarm optimization is a method which simulates the process of finding food by birds. Particles are the artificial birds. The local best position is the latest best position find by one particle and the global best position is the latest best position find by all particles. In order to locate the position of the food, particle swarm optimization defines a rule to indicate where the particles should go. In the original discrete particle swarm optimization, the update rule of the initial particle velocity is shown in equation 6-1 which has been introduced in Chapter 5.

$$v_i^{k+1} = \omega * v_i^k + c_1 * \text{random}() * \left(\text{Pbest}_i - x_i^k\right) + c_2 * \text{random}() * \left(\text{Gbest}_i - x_i^k\right) \tag{6-1}$$

According to the equation 6-1, the speed update rules can be decided into two parts. One is self-speed part which is $\omega * v_i^k$. v_i^k is the current direction and speed of the particle i at k^{th} iteration. ω limits the impact of the v_i^k on particle i at $k+1$ time. The other is particles position part which includes

c_1*random()*$\left(Pbest_i\text{-}x_i^k\right)$ and c_2*random()*$\left(Gbest_i\text{-}x_i^k\right)$. $Pbest_i\text{-}x_i^k$ is the distance between particle i and local best position at k^{th} iteration. Similarly, $Gbest_i\text{-}x_i^k$ is the distance between particle i and global best position at k^{th} iteration. The initial speed and the direction of all particles are random. If only depended on its self-speed, particles may arrive at any position. The current global and local best position find by other particles give suggestions to particle i that how to find a better position. If all particles only considered the impact of the current global and local best position, they may rapidly gather at a local best position and miss out the better position. Thus, although particles may find a worse position, a big value of the ω to provides more chance for search some area is better.

In order to find a nearer position to the food, particles should allow searching more area at the beginning. Thus, each particle should search mainly rely on themselves rather than the group information. After some search process, most of the area may be searched substantially. A more careful search around the latest global best position will find a better position. According to above theory, comparing with the constant value of ω, a changing ω can provide better performance to the particle swarm optimization.

In reference [3], the inertia weight ω has a new definition which is represented as equation 6-2.

$$\omega_{current} = \omega_{max}\text{-}\left(\frac{\omega_{max}\text{-}\omega_{min}}{iteration_{max}}\right)*iteration_{current} \tag{6-2}$$

Assumed that ω belong to (0.1, 0.8) and the maximum number of iterations is 100, the curve of equation 6-2 is shown in Figure 6-3.

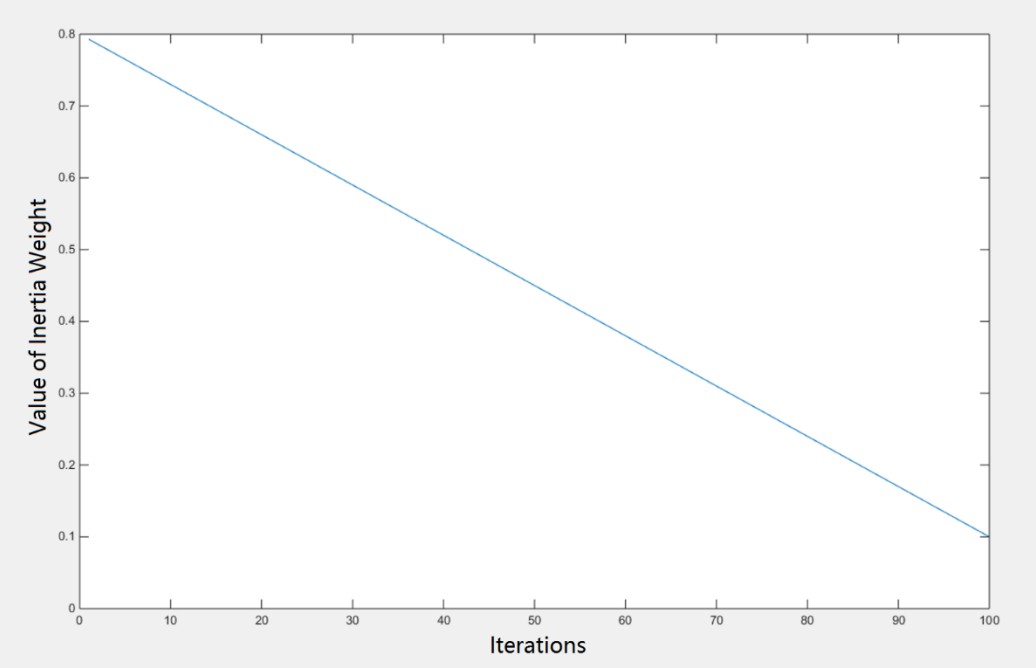

Figure 6-3 The curve of inertia weight.

The curve is a straight line in Figure 6-3. The value of ω is reducing with the increment of iterations linearly. As the inertia weight, this curve means that the search range which is decided by the current particle velocity will decrease linearly when the iteration increases. Such a curve substantially satisfies the requirement that the search range should be enlarged at the beginning and the local search should be enhanced at the end. However, if the search range could stay large at first half stage of the search process and rapidly decreases to a small value at the second half stage, the search performance should be better. To achieve this, a new equation for adjusting the changing rate of inertia weight ω is proposed in equation 6-3.

$$\omega_{current} = a*e^{-20*\left(\frac{iteration_{current}}{iteration_{max}}\right)^{10}} + \omega_{min} \quad (6\text{-}3)$$

Where $a = \omega_{min}\text{-}\omega_{min}$. ω_{max} and ω_{min} is the maximum and minimum value of the inertia weight ω respectively. e is the important mathematical constant that is the base of the natural logarithm. It is approximately equal to 2.71828.

The maximum and minimum value of ω is also set to 0.8 and 0.1 respectively. Then, the curve of the inertia weight ω is illustrated in Figure 6-4.

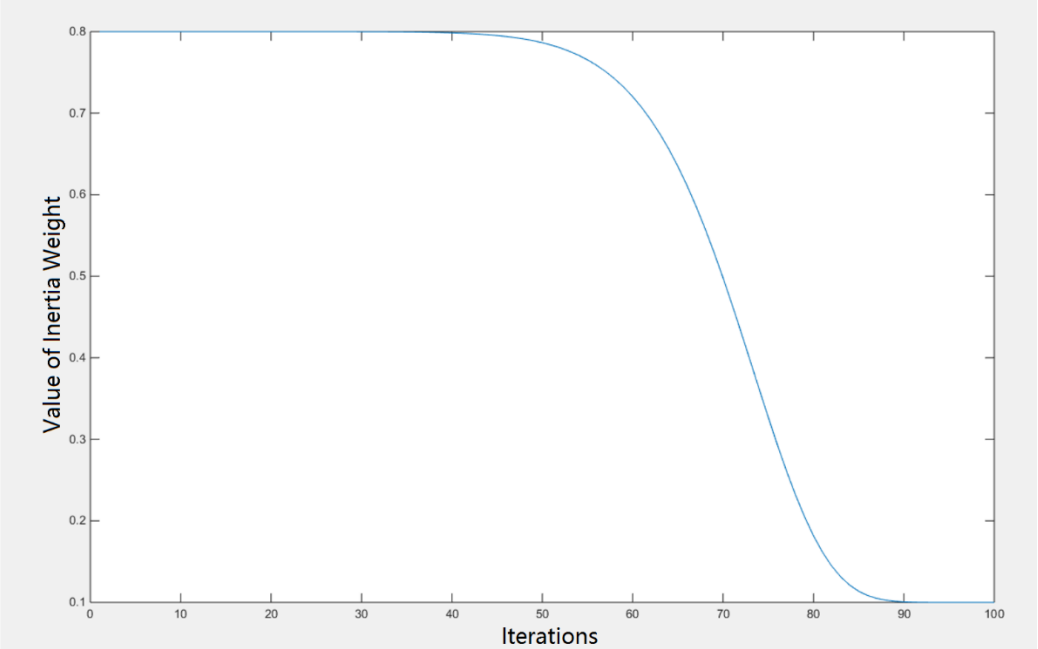

Figure 6-4 New curve of inertia weight

In Figure 6-4, 100 iterations can be seen as the 100% of the iteration process. The drop point of the curve is at around the 40% of the total iteration process. It means that the value of inertia weight ω stay on its maximum level so that the particles will keep their maximum search range at almost all first half stage. Then, the curve drops from the maximum value to the minimum value within 50% of the total search process. It satisfies the requirement of reducing the search range rapidly in the second half stage. At last 10% search process, the particle will enhance search behaviours around the current best position. The maximum value of inertia weight ω is generally set to 0.8. However, it can be larger if it is necessary. Similarly, the

minimum value of the inertia weight ω is generally set to 0.1, but it cannot smaller than zero.

The update rules for the location of particles in discrete particle swarm optimization are given in equation 6-4 and equation 6-5. In this equation, the -random() is the random mechanism of the discrete particle swarm optimization. This mechanism will forcibly change the existing sequence of the r_i, when the discrete particle swarm optimization trapped at a local solution. In the experiment, the discrete particle swarm optimization always trapped without this part.

$$r_i = S(v_i)\text{-random}() \tag{6-4}$$

$$\begin{cases} x_{id} = 1 & \text{if } r_i < \text{the qth smallest value of all } r_i \\ x_{id} = 0 & \text{else} \end{cases} \tag{6-5}$$

Where S() is the sigmoid function, random () is a random value between zero and one.

In Figure 6-4, both values of the sigmoid function and the random value are between zero and one. The value of the r_i is not only decided by particle velocity v_i. According to the equation 6-5, the new tie switches are decided by the q^{th} smallest value of all r_i. If all the value of random () was almost equal to zero, the changing on the sequence of the r_i will be small or there is no changes in this sequence. Then, the construction of network structure is based on the position of the particles in the current iteration. If the value of some random () for each particle is approximately equal to one and others are not, the location of the particles in the sequence of the r_i will have a big change. Then, the construction of network structure will be built in different sequence.

Due to the maximum value of the sigmoid function is equal to 1, the same value of the maximum random() will take a large disturbance in the sequence of r_i. At

the second stage of the search process, a large disturbance in the sequence of r_i will weaken the local search ability of the discrete particle swarm optimization. Thus, the equation 6-3 can be used to limit the disturbance on the sequence of the r_i which is caused by the 'random()' element. Equation 6-3 will provide more probability to build a solution randomly at the first stage of the search process and limit or prevent such a random building when the search process is almost completed. Thus, the new update rules of the discrete particle swarm which proposed in this section is shown below.

$$v_i^{k+1} = \left(a*e^{-20*\left(\frac{\text{iteration}_{\text{current}}}{\text{iteration}_{\max}}\right)^{10}} + \omega_{\min}\right)*v_i^k$$

$$+c_1*\text{random}()*\left(\text{Pbest}_i\text{-}x_i^k\right) + c_2*\text{random}()*\left(\text{Gbest}_i\text{-}x_i^k\right)$$

(6-6a)

$$r_i = S(v_i)\text{-}\left(b*e^{-20*\left(\frac{\text{iteration}_{\text{current}}}{\text{iteration}_{\max}}\right)^{10}} + M_{\min}\right)*\text{random}()$$

(6-6b)

$$\begin{cases} x_{id} = 1 & \text{if } r_i < \text{the qth smallest value of all } r_i \\ x_{id} = 0 & \text{else} \end{cases}$$

(6-6c)

Where $b = M_{\max}\text{-}M_{\min}$. $M_{\max}$ and $M_{\min}$ is the maximum and minimum value of the allowed random() respectively.

By adding equation 6-3 in 6-6a, the impact of self-velocity on particles can then large in the first half stage and small in the second half stage. So that the search direction of the particle search is enlarged at the beginning and reduced at the end. 6-6b means that the disturbance at the switch rank will be reduced with the increasing of the number of iterations.

Due to equation 6-3 can adjust the search range and random level according to the

requirement of the discrete particle swarm optimization, it is named as the adaptive function. After applying the adaptive function to the discrete particle swarm optimization, the search efficiency will be improved. The results and comparisons will be shown in section 6.2.3.

This adaptive function can also work on the ant colony system. The main optimization rules of the ant colony system are illustrated in equation 6-7.

$$p_{ij}^{k} = \begin{cases} \arg_{l \in N_i^k} \max\{\tau_{ij}[\eta_{ij}]^{\beta}\} & \text{if } q \leq q_0 \\ \dfrac{[\tau_{ij}]^{\alpha}[\eta_{ij}]^{\beta}}{\sum_{l \in N_i^k}[\tau_{ij}]^{\alpha}[\eta_{ij}]^{\beta}} & \text{else} \end{cases} \tag{6-7}$$

The value of the p_{ij}^{k} depends on different equations for different value of q. According to equation 6-7, if $q \leq q_0$, the value of the p_{ij}^{k} will equal to the value of the upper equation or the lower equation. q is a random value which is between zero and one. The value of q_0 is set in advance which is also between zero and one. The reference [1] suggests that the q_0 should be equal to 0.1. Then, equation 6-7 means that there is a 10% chance to decide the value of the p_{ij}^{k} by the upper equation. The remaining 90% chance will use the lower equation of the equation 6-7. In another word, main update rule of the ant colony system is the lower equation. The upper equation is a different update rule chosen by pseudorandom proportional for finding a new framework to prevent that ants are trapped at a local solution. Thus, similar to the discrete particle swarm optimization, the adaptive function can also be applied to this pseudorandom proportional of the ant colony system. Then, the equation 6-7 can be modified as in the following:

$$p_{ij}^{k} = \begin{cases} \arg_{l \in N_i^k} \max\{\tau_{ij}[\eta_{ij}]^{\beta}\} & \text{if } A^{*}e^{-20^{*}\left(\frac{\text{iteration}_{\text{current}}}{\text{iteration}_{\max}}\right)^{10}} + q_{\min} \le q_0 \\ \dfrac{[\tau_{ij}]^{\alpha}[\eta_{ij}]^{\beta}}{\sum_{l \in N_i^k}[\tau_{ij}]^{\alpha}[\eta_{ij}]^{\beta}} & \text{else} \end{cases} \quad (6\text{-}8)$$

Where $q_{\min}$ and $q_{\max}$ is the minimum and maximum value of the allowed q_0 respectively. $A = q_{\max}\text{-}q_{\min}$.

6.3 Case Studies and Discussion for the Adaptive Function in Particle Swarm Optimization and Ant Colony System

In order to find out the improvement of the search efficiency by the adaptive function in the particles swarm optimization and the ant colony system. Distribution network feeder reconfiguration has been executed 100 times for both optimization methods in two different test networks. Large maximum number of iteration and population size may cause that all solutions obtained with or without adaptive function are the same. Then, the difference in search efficiency improved by the adaptive function cannot be identified. Thus, maximum number of iteration and the population of both methods for each distribution system are adjusted to an appropriate value. Other parameters are provided in Table 6-1.

Table 6-1 Setting of the methods parameters

System parameters	α	β	ρ	ξ	Q	$P_{0_{max}}$	$P_{0_{min}}$
Ant colony system	1	1	0.3	0.1	1	0.3	0.1
System parameters	C_{Local}	C_{Global}	ω_{max}	ω_{min}			
Particle swarm	1	5	0.8	0.2			

6.3.1 Scenario One: IEEE 33-Bus System

The distribution network for this scenario is illustrated in Figure 6-5. The population of both ant and particle is set to 20. Maximum number of iteration of both optimization method is limited to 20.

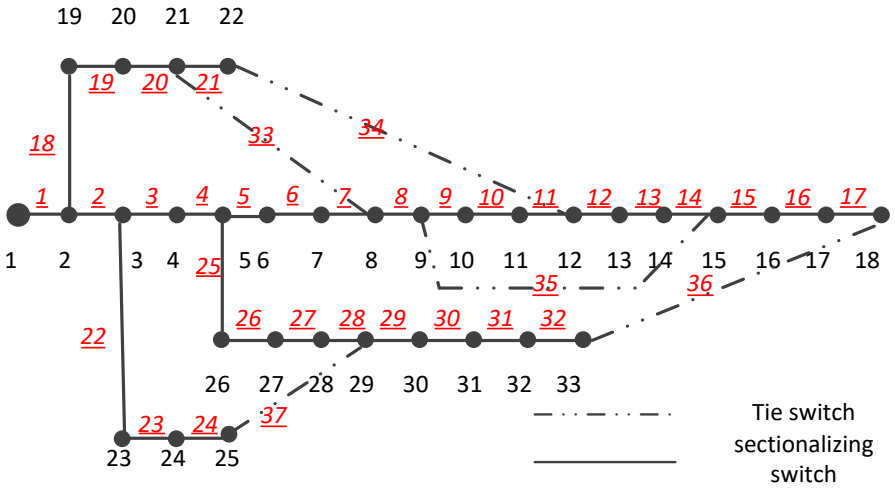

Figure 6-5 Adaptive function test in IEEE 33-bus system

The results of this scenario are presented in Table 6-2. Both ant colony system and particle swarm optimization can find the equivalent smallest system power loss no matter with or without the adaptive function. Due to both methods may find the same latest global best solution, the average value of network power loss indicates

the search performance. The average value of the network power loss obtained by the improved ant colony system is the smallest. The average value calculated by the original ant colony system is a little larger. Although the difference between them is very small, the adaptive function still increased the probability of finding the known minimum network power loss by 10 percentages. Furthermore, the worst system loss find by the improved ant colony system is also small. Such a result verifies the positive impact of the adaptive function in the ant colony system.

The adaptive function also brings positive impact on the particle swarm optimization. The value of both average and worst network power loss obtained by the improved particle swarm optimization method is much smaller than the result calculated by the original one. The probability of finding the known minimum network power loss is increased 36 percentages.

Table 6-2 Comparisons of adaptive function for ACS and DPSO

In IEEE 33-bus distribution system

Method	33-bus System	Network Power Loss(kW)			Probability of finding the known minimum loss
		Best	Worst	Average	
Ant Colony	Without Adaptive Function	139.28	142.90	139.60	84%
	With Adaptive Function	139.28	140.00	139.31	94%
Discrete Particle Swarm	Without Adaptive Function	139.28	147.64	141.56	20%
	With Adaptive Function	139.28	144.63	140.35	56%

Results obtained by 100 repeat of execution. The population and the maximum number of iteration of the ant and the particle is 20 respectively.

6.3.2 Scenario Two: IEEE 69-Bus System

The IEEE 69-bus distribution network for scenario two is illustrated in Figure 6-6. The population of both the ant and the particle is set 20 again. Maximum number of iteration of both optimization method is limited to 40.

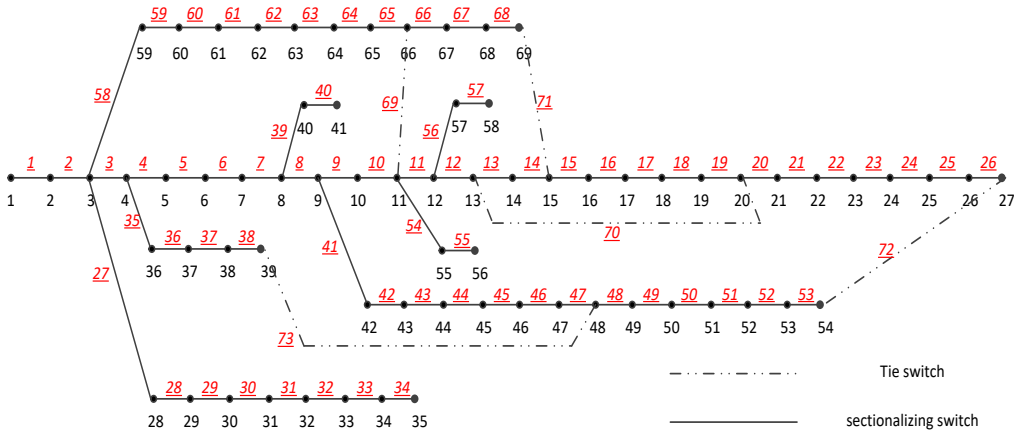

Figure 6-6 Adaptive function test in IEEE 69-bus system

Similar to the test results in IEEE 33-bus system, all methods can find the same smallest system power loss. The methods with the adaptive function have a better performance on searching the best structure of distribution network for minimizing system power loss. However, the difference can also be found when comparing Table 6-3 with Table 6-2.

First of all, the worst network power loss obtained by both ant colony system is the same. The probability of finding the known minimum loss of the improved ant colony system is 4 percentages higher than the original one. This 4 percentages gap on the probability of finding the known minimum loss in the 69-bus system is still verified that the application of the adaptive function can provide better performance. The same situation appears in the discrete particle swarm optimization. This gap increases from 36 percentages in the 33-bus system to 50 percentages in the 69–bus system. Such a result shows that the positive impact of

the adaptive function in particle swarm optimization grows with the size of the test system. Furthermore, the highest probability of finding the known minimum loss is improved in the ant colony system in the 33-bus system. However, it also improved the discrete particle swarm optimization in the 69-bus system. The method with the smallest probability of finding the known minimum loss is not changed. Apart from the test system, the only one change between two scenarios is the maximum number of iteration. Although it is not possible to show a conclusion that the discrete particle swarm optimization has a better performance after improving by the adaptive function. It is reason able to believe that the adaptive function can significantly improve search efficiency of the discrete particle swarm optimization.

Table 6-3 Comparisons of adaptive function for ACS and DPSO in 69-bus distribution system

Method	69-bus System	Network Power Loss(kW)			Probability of finding the known minimum loss
		Best	Worst	Average	
Ant Colony	Without Adaptive Function	99.36	100.32	99.87	38%
	With Adaptive Function	99.36	100.32	99.82	42%
Discrete Particle Swarm	Without Adaptive Function	99.36	106.39	101.92	10%
	With Adaptive Function	99.36	105.20	99.86	60%

Results obtained by 100 repeat of execution. The population of both ant and particles is 20. The maximum number of iterations of both ant and particles are 40.

From the comparison results of these two scenarios, the impact of the adaptive function in the ant colony system and the discrete particle swarm optimization is

positive.

6.3.3 Discussions

Comparing the results of the particle swarm optimization parts in Table 6-2 with results in Table 6-3, the search efficiency of the discrete particle swarm optimization has a significant improvement. The probability of finding the minimum loss is increased 180% and 500% in the 33-bus system and the 69-bus system respectively, however, this increment in ant colony system is 7.8% and 41% respectively. According to the details of the adaptive function application in both methods, the adaptive function only works on the pseudorandom proportional level in the ant colony system. However it applies to both initial particle speed and random mechanism part in the discrete particle swarm.

In order to find out the which part is the main improvement to the search performance, test for the discrete particle swarm optimization which only applies the adaptive function to the initial particle speed has been done in both the 33-bus and 69-bus distribution network and the comparison of the results are shown in Table 6-4.

Table 6-4 Comparisons of adaptive function for DPSO in IEEE 33-bus and IEEE 69-bus distribution system

	Discrete Particle Swarm Optimization	Network Power Loss(kW)			Probability of finding the known minimum loss
		Best	Worst	Average	
33-bus System	Without Adaptive Function	139.28	147.64	141.56	20%
	Adaptive Function Only on Velocity	139.28	146.21	141.56	20%
	Adaptive Function on both parts	139.28	144.63	140.35	56%
69-bus System	Without Adaptive Function	99.36	106.39	101.92	10%
	Adaptive Function Only on Velocity	99.36	107.69	101.69	12%
	Adaptive Function on both parts	99.36	105.20	99.86	60%

Results obtained by 100 repeat of execution. The population of particles is 20. The maximum number of iterations are 40.

In the results of Table 6-4, the impact of the adaptive function only be applied to the particle velocity in the 33-bus system is small. In the 69-bus system, 2 percentages increment on the probability of finding the known minimum loss indicates that the impact of the adaptive function in the particle velocity may perform better in a bigger system. Thus, the improvement of the search performance is mainly contributed by applying the adaptive function to the random mechanism of the discrete particle swarm optimization.

It is worth noting that, after applying the adaptive function, the search performance of the discrete particle swarm optimization is closed to the ant colony system in

the 33-bus system and much better in the 69-bus system. However, without the adaptive function, the performance of ant colony system is always much better than the particle swarm optimization method in both systems.

The curves in Figure 6-7 and Figure 6-8 is the typical convergence characteristic of the ant colony system and the discrete particle swarm optimization with the adaptive function in the 33-bus system respectively. The minimum network power loss in each stage is included in Figure 6-7 and Figure 6-8. In the Table 6-2, ant colony system with the adaptive function has 94% probability to find the minimum network loss. So, the termination point of the curve in Figure 6-7 is the known minimum network loss. On the other hand, this probability is 56% for discrete particle swarm optimization with the adaptive function. Thus, the curve which cannot find the minimum value is chosen in Figure 6-8.

The curve of the convergence characteristic can also show the latest global best solution in every single iteration. Due to update rules of the global best solution are the same in these two optimization methods, the comparison of the curves between these two figures can represent the search range between ants and particles.

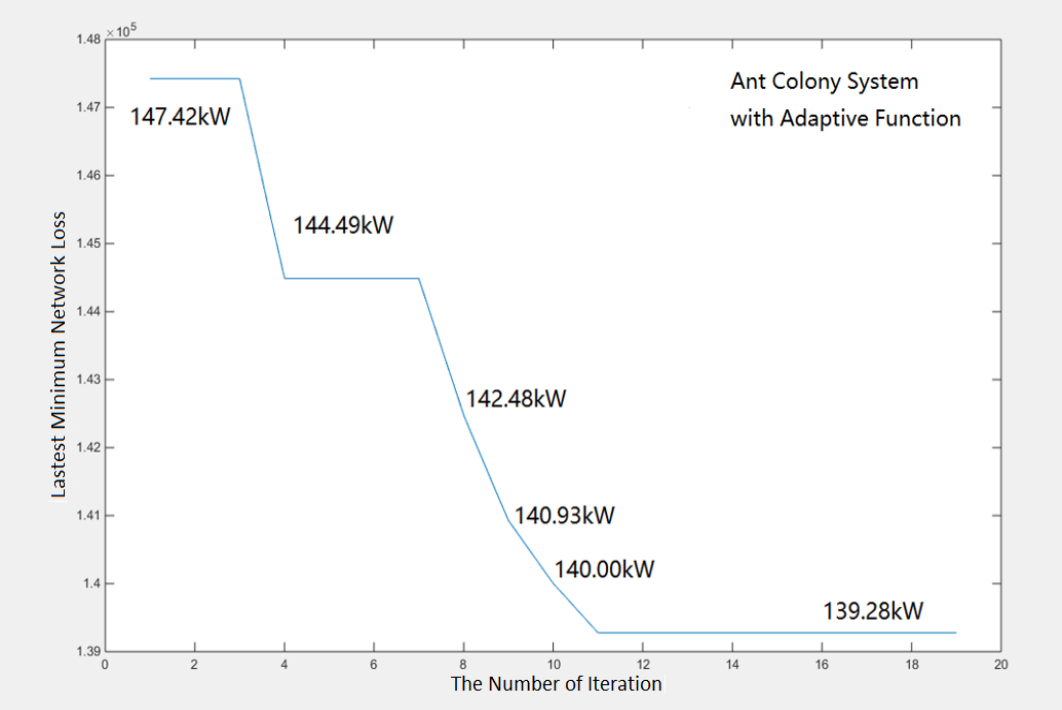

Figure 6-7 Convergence characteristic of ant colony system with the adaptive function in the 33-buses system

In Figure 6-7, ants trapped at the point of 147.42 for 3 iterations. Then, ants trapped at the point of 144.49 for 4 iterations again. After that, the final solution is obtained by ants. The 33-bus system is a small system. Thus, although ants are trapped twice, they can still escape and find the known minimum network loss. The total number of iteration is 20, so the pseudorandom proportional selection may not play much of a role. This curve shows that once the ants escaped from the trap, they can find the latest global best. Thus, strong local search ability is verified.

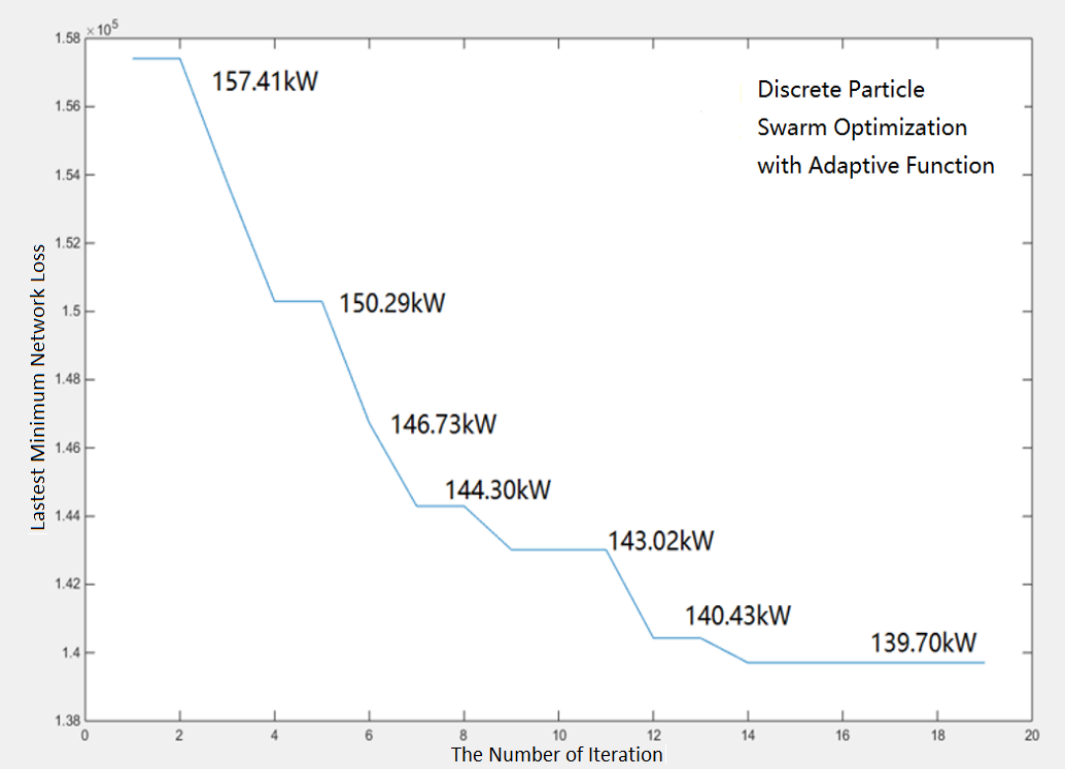

Figure 6-8 Convergence characteristic of discrete particle swarm optimization with adaptive function in 33-buses system

In Figure 6-8, particles seem never been trapped in the process of search. However, they cannot find the same the latest global best solution with the ants at the end of the iterations with 44% probability. This curve shows that particles can always find a different framework to obtain a local solution. Thus, the global search ability is strong. After obtained the local position, it hard to find the known latest global best. So, the local search ability is weak when comparing with the ant colony system.

The curves in Figure 6-9 and Figure 6-10 are also the typical convergence characteristic of the ant colony system and the discrete particle swarm optimization with the adaptive function in the 69-bus system respectively. The curve to illustrate ant colony system cannot find the known minimum loss for the 42% probability of finding the known minimum network loss. With the 60% probability of finding the known minimum loss, the curve reached the known minimum value is chosen in

Figure 6-9 for the discrete particle swarm optimization.

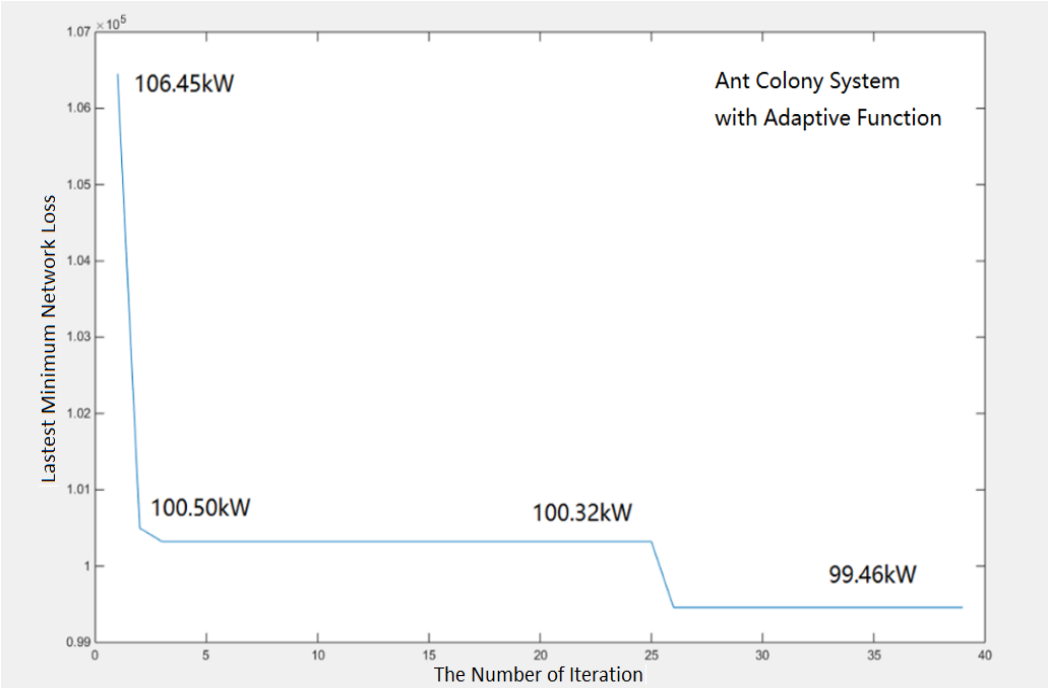

Figure 6-9 Convergence characteristic of ant colony system with the adaptive function in the 69-buses system

Comparing the first value in both Figure 6-9 and Figure 6-10, ants find a very good solution at the beginning. However, this may not be the right route to the known minimum value. Ants are trapped at 100.32 kW for more than half of the search process and trapped at 99.46 kW until the end. This curve shows that once the ant is trapped, they are difficult to escape. Obviously, the pseudorandom proportional cannot provide enough chance to apply the different choosing mechanism for the ants in this curve. It is worth noting that the different choosing mechanism gives ants a hand to escape from the trap in other 42% of the test. Thus, 40 iterations may not be enough for the pseudorandom proportional to select the different choosing mechanism in the ant colony system.

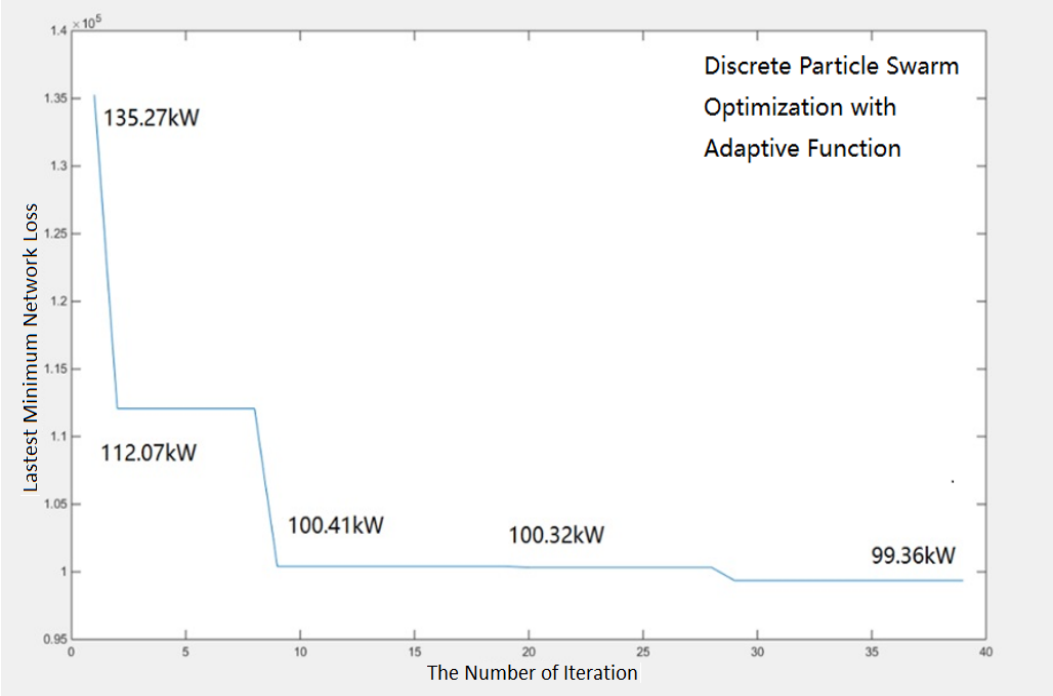

Figure 6-10 Convergence characteristic of discrete particle swarm optimization with the adaptive function in the 69-buses system

Different from the ants, particles are searching based on their own at the beginning of the search. Thus, the value in first 20% search process is poor. But, more areas are searched by particles so that they have more probability to find the known minimum network loss instead of being trapped at a point. Without a strong local search ability, 40% particles cannot find the known minimum network loss of the 69-bus system.

6.4 Modular Hybrid Optimization Algorithm Base on Ant Colony System and Particle Swarm Optimization (MAPO)

Each artificial optimization method may have its special defects. These defects may be caused by the theory so that it is hard to be avoided unless modifying the method itself. Thus, researchers try to combine several optimization together to overcome such defects. The advantages and disadvantages of the ant colony system and the particle swarm optimization are introduced in the section to follow. And a hybrid optimization which contains the advantages of both ant colony system and particle swarm optimization is proposed for further enhancing the search performance in the distribution network feeder reconfiguration.

6.4.1 Pros and Cons of Ant Colony Optimization and Particle Swarm Optimization

A. Pros and Cons of the ant colony optimization

a) Advantages of the ant colony optimization.

According to reference [15], the first advantage of the ant colony optimization is inherent parallelism. When ants search the food base on the ant system, all ants in one group can start to find the food at the same time. It means that artificial ants in one group can do the search process at the same time. This advantage can make full use of the performance of the multicore computer. It can shorten the total computing time.

The second is the positive feedback of the ant colony optimization. The positive feedback mechanism provides a good search performance to ants around a local

solution. If the way from the nest to the food was composed of several separate paths, ants must choose one path with high pheromone trails to continue its search when they come to a junction. Even if some ants had its special choice, the configuration of the new route from the nest to the food would always contain most of the paths which have high pheromone trail. All ants mainly choose their route according to the strength of the pheromone trail. This characteristic provides the strong search ability to find a shorter route around current shortest one.

The third is ant colony optimization have a good robustness. It means that ant colony optimization can easily apply to a new type of optimization problem by a simple modification. For example, the first optimization solved by ant colony optimization is the traveling salesman problem. When ant colony optimization is applied to the distribution network feeder reconfiguration, modification is unnecessary.

b) Disadvantages of the ant colony optimization.

According to results in this thesis and reference [15], the disadvantages of the ant colony optimization are shown as following:

Firstly, parameters setting of the ant colony optimization has a large impact on the search performance. The results in section 5.6 illustrate this impact. Normally, the setting of the system parameters is based on the experience. The unsuitable settings will cause a rapid decrease in the search efficiency.

Secondly, computing time for convergence is uncertain. It is hard to decide when to stop the search process. The ending condition of the basic ant system is that all ants have chosen the same path. But, it is unrealistic in normal engineer project.

Thirdly, initial pheromone trails are deficient. The pheromone trail is released by the ant, however, at the beginning of the search, ants do not release any pheromone signal. The search behaviour of the ants is based on the pheromone trails. So, due

to a lack of initial pheromone trails, the search performance of the ant colony optimization is low in the initial stage.

Fourthly, the global search performance is weak. All search performances of the ants mainly based on the update of the pheromone trails. Ant is always trapped at a local solution.

c) The characteristics of the ant colony system in the distribution network reconfiguration.

Distribution network reconfiguration is not the same as the travelling salesman problem. Normally, there is no existing travel route for the salesman. However, the initial network structure for the distribution network has been built. This existing network structure can always provide the initial pheromone trails for the ant.

Ant colony system adds a new choosing mechanism when ants make their decision at a junction. Thus, the pheromone trail is not the sole criterion which influences the decision of the ants. Ants may choose the shortest path from all possible paths which in front of them instead of the path with the strongest pheromone. Such a choosing mechanism can help all ants choose the new route out of existing pheromone trail framework. Thus, the search ability for the global best solution has been improved.

B. Pros and Cons of the particle swarm optimization

a) Advantages of the particle swarm optimization[16].

The advantage of particle swarm optimization is not much. However, these advantages are outstanding. One is the simple concept of the particle swarm optimization. There are only two equations exists in the whole particle swarm optimization theory and the theory can be understood in a short period so that

learning and programming are also easy. The other is fast computing speed on searching a relatively good solution. The relatively good solution is a solution which closes to the possible global best solution. The position and velocity of the particles are random at the beginning of the search process so that particles may theoretically search everywhere in the possible area. No existing framework limits the action of the particles. Thus, global search ability of the particle swarm optimization is perfect. Particle swarm optimization can find feasible solutions very fast. However, these feasible solutions are not the best.

b) Disadvantages of the particle swarm optimization.

In order to solve the feeder reconfiguration problem, some changes are made on the basic theory of the particle swarm optimization. Such modifications may also be necessary for applying particle swarm optimization to other optimization problem.

Discrete particle swarm optimization does not have a good local search ability. So, particle swarm optimization may have trouble to find better solutions after several iterations in the complex optimization problem.

c) The characteristics of the tear circuit based discrete particle swarm optimization in the distribution network feeder reconfiguration.

In the distribution network feeder reconfiguration, the new tie switches are decided by the position of each particle so that the distribution system constraints are not considered. Then, many solutions which are found by the discrete particle swarm optimization cannot build a radial network. In order to avoid the infeasible solution, tear circuit method is combined with the discrete particle swarm optimization. According to the structure characteristic of the distribution network, only one switch is allowed to be opened in each circuit. Then, all solutions obtained by the tear circuit based version can build a distribution network.

The adaptive function which introduced in section 6.2 provides a changed level of the random mechanism for the discrete particle swarm optimization. According to the results in section 6.3, search performance is significantly increased by applying the adaptive function.

C. Summary of Pros and Cons

Although the ant colony system and the tear circuit based discrete particle swarm optimization improve some disadvantages of their own, the important disadvantages still exist. Such as, the local search ability of the discrete particle swarm optimization is still weak and the global search performance of the ant colony system is also not strong. The source of such weak points comes from the basic theory when the optimization method is first proposed. Thus, it is not easy to improve these weak points on their own. If the local search performance of the ant colony system and the global search performance of the tear circuit based discrete particle swarm optimization is combined, the hybrid optimization method may consist of all advantages of both methods and avoid their disadvantages.

6.4.2 General Hybrid Strategy for Ant Colony System and Particle Swarm Optimization

The general strategy for a hybrid method based on the ant colony optimization can be divided into 3 points.

a) Due to the shortage of the initial pheromone trails, the first route can be obtained by other optimization methods. Then, the initial pheromone trails can be built according to this first solution.

b) Apply other optimizations method in each iteration of the ant colony optimization. The route obtained by ant colony optimization at each iteration is treated as the initial solution of other optimization methods. The better

solution may be calculated by other optimization methods base on the different theory. At least, in this way, the final solution will be better.

c) System parameters α and β in ant colony optimization are mainly decided by experience. The unsuitable value of α and β will weaken the search performance significantly. Thus, the optimal value of α and β can be calculated by other optimization methods.

The strategy for a hybrid method based on particle swarm optimization is similar with the ant colony optimization. The acceleration constants c_1 and c_2 also have large impact on search performance. Their value can be determined by other optimization methods. Other optimization methods can also apply to each iteration of the particle swarm optimization for enhancing its local search ability.

Due to the characteristic of the distribution network, initial pheromone trail exists. The system parameters can be determined after a few tests. According to the results in Chapter 5, subtle differences in the system parameter do not have a big impact on searching performance. From experience, it is shown the strategy that one optimization method is used in the iteration of another optimization method cannot have a better performance. It is hard to decide the termination condition for the embedded method. It is assumed that the number of iterations of the main and the embedded optimization method is n_M and n_E respectively and the computing time for the single iteration of the main and the embedded are T_M and T_E. The total computing time for this hybrid method is $n_M \times T_M + n_M \times n_E \times T_E$. If the number of iterations for embed method was large, the better final results were established at very long computing time. If the number of iterations for embedding method is small, the final results will not improve. Thus, a novel hybrid methodology based on the ant colony system and the discrete particle swarm optimization is necessary.

6.4.3 Modular Hybrid Optimization Method Based on Ant Colony System and Particle Swarm Optimization

In the ant colony system, the choice of the ants is mainly according to the pheromone trails. Update for local pheromone trail is executed on the path immediately after a single ant passed. After this update, the value of pheromone trails on the chosen path will reduce so that the probability of choosing the same path by the following ants is reduced. Update for global pheromone trail is executed only on the latest global best solution. This latest global best solution will indicate the search action of the following ants so that the following ants can find a better solution based on the latest global best solution. Thus, the update of the latest global best solution is the only key information for finding a better solution.

In the same problem, the latest global best solution of the ant colony is equivalent to the latest global best position of the particle swarm. But, the difference is that two more key information for finding a better position in the particle swarm optimization are necessary. They are particle velocity and local best position. The local best position is the current best position of one single particle. Actually, in the ant colony system, each ant also has its local best solution, but this information is not used in the theory of the ant colony system. The particle velocity is the unique information in particle swarm optimization. Its initial value is random and the following value is calculated by the local and the global best position.

According to the above analysis, the key information for finding a better solution in the particle swarm optimization is coexisted in the ant colony system. This is the basis of the hybrid method. In this novel method, each ant is required to have the memory for recording the local best solution which has found. The latest global best solution found by all ants is also recorded. When the first ant colony finishes their search, the latest local best solution of a single ant is recorded as the latest

local best position of a single particle. Due to this reason, the population of the ant colony and the particle swarm must be equal. The latest global best solution of all ants is recorded as the latest global best position of all particles. At this time, the local and global best position have been calculated by ants. The initial particle velocity is random and can be set at the beginning of the search. Thus, all necessary data for the particle swarm optimization are obtained. Then, the particle swarm optimization can be executed. Due to the strength of the particles is global search, equation 6-9 is added as a function of selection probability to reduce the number of executions of the discrete particle swarm optimization in the second half stage. Such a rule can provide more time to ants for the local search when the search process is nearing completion.

$$\mathrm{rand}[0,1] < P_{PSO} \quad (P_{PSO} \in [0,1]) \tag{6-9}$$

Where $\mathrm{rand}[0,1]$ is the random number between zero and one. P_{PSO} is a constant number between zero and one.

The effect of the adaptive function has been introduced in section 6.2.2. The probability of executing the particle swarm optimization in this hybrid method also satisfies the trend of the adaptive function curve. Thus, the adaptive function can also be used for improving searching performance in the hybrid method. Then, the new definition of the selection probability is shown in equation 6-10.

$$\mathrm{rand}[0,1] < a_P * e^{-20*\left(\frac{\mathrm{iteration}_{current}}{\mathrm{iteration}_{max}}\right)^{10}} + P_{Selection_{min}} \quad (P_{PSO} \in [0,1]) \tag{6-10}$$

Where $a_P = P_{Selection_{max}} - P_{Selection_{min}}$. $P_{Selection_{max}}$ and $P_{Selection_{min}}$ is the maximum and minimum value of the selection probability P respectively.

When the execution of the particle swarm optimization is completed, the latest

global best solution must be decided for the next ant colony and particle swarm. Comparing all existing value of the objective function, this latest global best solution can be easily determined. Then the second group of the ants and particles will start their search. The termination condition is still the maximum number of iteration which is set by experience.

In this novel hybrid, ants obtained the characteristic of the particle by transmitting the route information between two different optimization algorithms. The search direction of the ant is not only based on the pheromone trails but also impacted by the particle velocity and particle position. So, the individual ant has the probability to explore other routes even when the pheromone concentration is extremely high. Thus, the novel hybrid method can prevent trapping at a local solution as much as possible and keep a fast convergence speed at the same time.

The flow chart of the hybrid optimization method (MAPO) is illustrated in Figure 6-11.

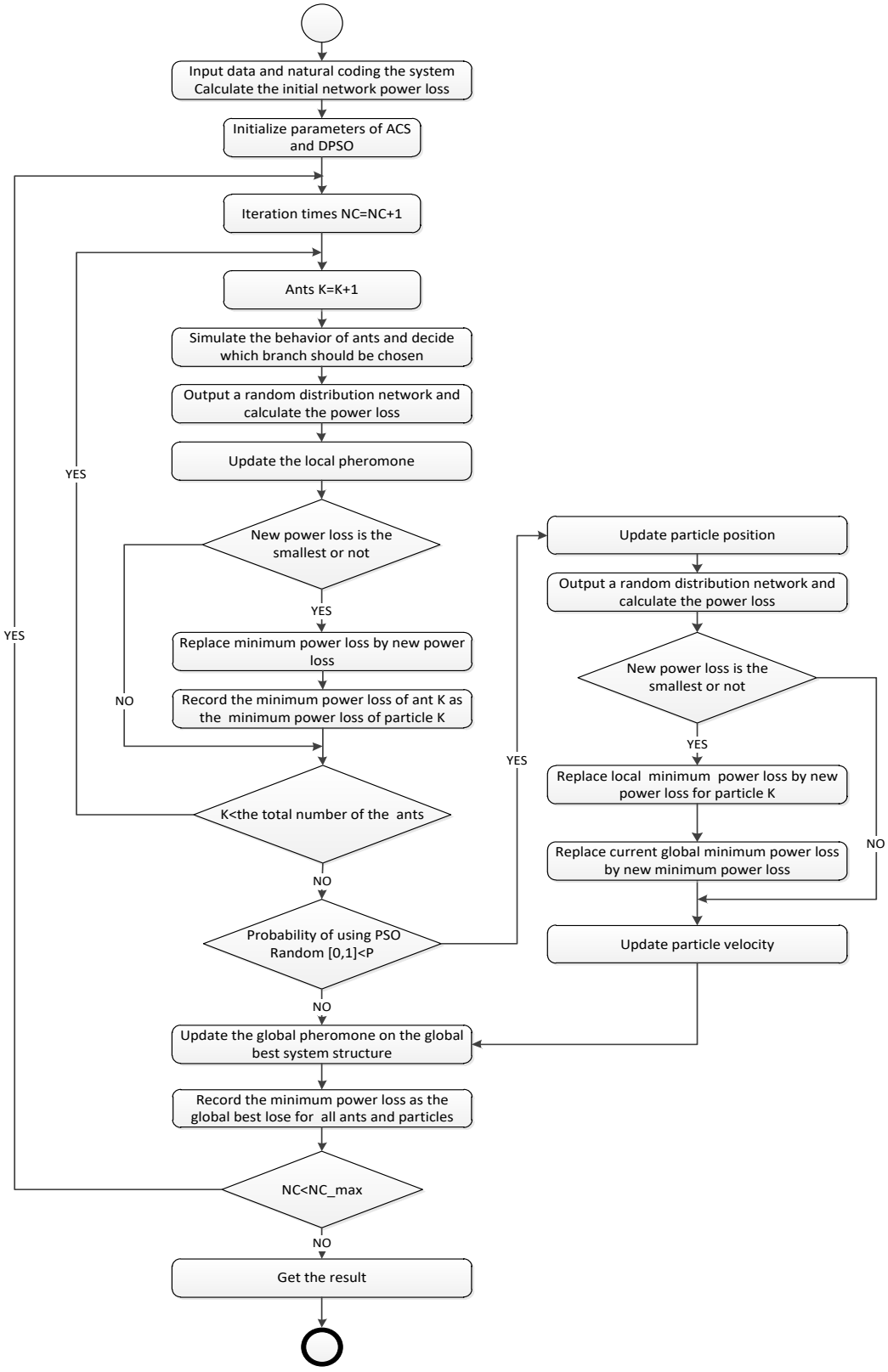

Figure 6-11 Flow chart of MAPO in feeder reconfiguration

6.4.4 Further Possible Improvement of Modular Hybrid Optimization Method

Word ‘M’ in MAPO is ‘modular’. From Figure 6-11, it can be seen that the key procedure of the ant colony system and the discrete particle swarm optimization is not changed. Local and global best information combine these two methods like a motherboard. Further improvements of the ant colony system or the particle swarm optimization can be applied to the corresponding part of the hybrid method which just likes the modular upgrade on a machine.

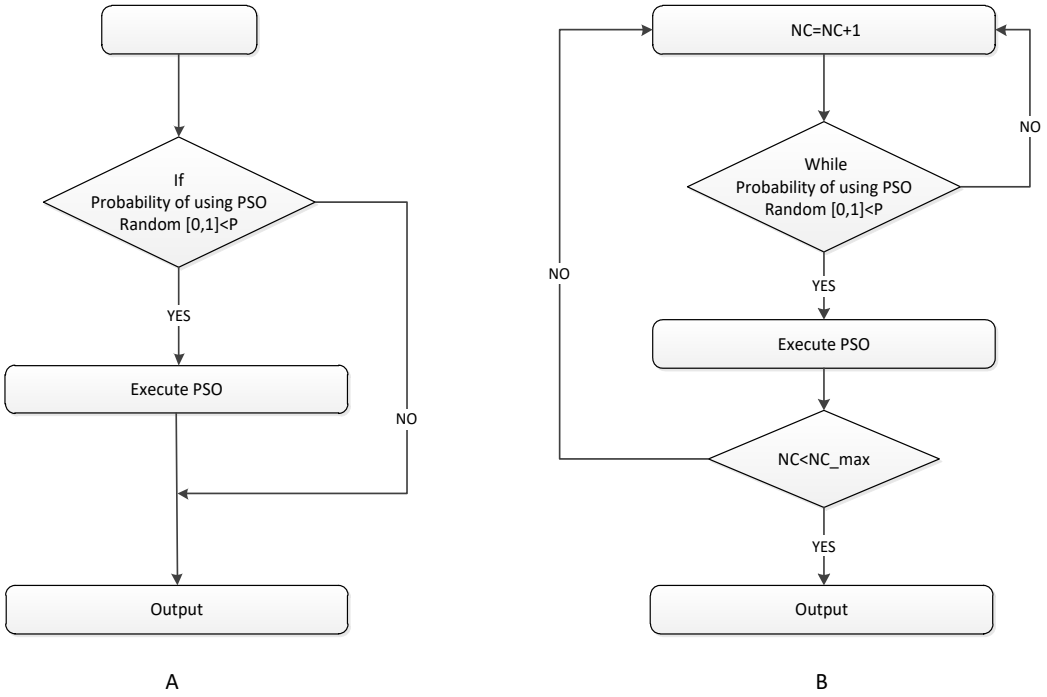

Figure 6-12 Comparison of different loop command of the selection probability

The main body the hybrid method is ant colony system however it can be changed by using different loop command in the programming language. For example, in Figure 6-12 A, the decision which is determined by ‘if’ command can only be executed once. If the value of the random number is small than the probability P_{PSO}. Particle swarm optimization cannot be executed anymore in the current loop.

But, the number of the decision can be set to the necessary value when the ‘while’ command is used. So, if the particle swarm optimization had better search performance than ant colony system after improvement, the particle swarm optimization could become the main body of the hybrid method for improving the search efficiency by simply using the while command.

6.5 Case Study and Discussion of the Modular Hybrid Method

Section 6.4 proposed a novel hybrid optimization method based on the ant colony system and the discrete particle swarm optimization. In this section, the proposed method is applied to IEEE 33-bus, IEEE 69-bus and IEEE 118-bus standard distribution system respectively. Due to the maximum number of iterations is set in advance by experience, three different maximum number of iterations are tested for ensuring that the possible minimum network power loss of each distribution system can be found. Then, these results are compared to those obtained by the ant colony system and tear circuit based discrete particle swarm optimization method to investigate whether the proposed method can find the minimum network power loss faster. The computer which is used for the calculation has an i5 3470 quad-core CPU and an 8G RAM. The operation system is Windows 10.

The setting of the system parameters is shown in Table 6-5.

Table 6-5 Setting of the system parameters

System parameters	α	β	ρ	ξ	Q	$P_{0_{max}}$	$P_{0_{min}}$
Ant colony system	1	1	0.3	0.1	1	0.3	0.1
System parameters	C_{Local}	C_{Global}	ω_{max}	ω_{min}			
Particle swarm	1	5	0.8	0.2			
System parameters	α	β	ρ	ξ	Q	$P_{0_{max}}$	$P_{0_{min}}$
Hybrid Method	1	1	0.3	0.1	1	0.3	0.1
System parameters	C_{Local}	C_{Global}	ω_{max}	ω_{min}	$P_{Selection_{max}}$	$P_{Selection_{min}}$	
Hybrid Method	1	5	0.8	0.2	0.9	0.5	

The meaning of all these system parameters has introduced in the corresponding section of their optimization methods. The maximum number of iterations and the population of ants and particles for three methods are the same for each test.

If it is assumed that the computing time for ant colony system is 1 unit per iteration, the computing time of the discrete particle swarm optimization was also appropriately 1 unit per iteration. The maximum and minimum probability of the proposed method to execute the PSO search is set to 0.9 and 0.5 respectively. Thus, the average computing time of the proposed method can be considered as 1.7 units. The computing time of the optimization method is not the key factor for finding a better solution. This time can be simply influenced by the personal programming skill and the speed of the executing computer. The maximum number of iterations which is set by experience is more important. Thus, optimization methods can be compared when the difference of the computing time is not big and the number of iterations and population size are the same.

In addition, due to the application of the adaptive function in ant colony system and particle swarm optimization is proposed in this chapter, adaptive function only applies to the proposed hybrid method in the following cases.

6.5.1 Case One: IEEE 33-Bus Distribution System

IEEE 33-bus distribution system is shown in Figure 6-5. The system data is provided in Appendix A.1. The population of both ant colony and particle swarm is 20. Three different maximum number of iterations are tested for investigating the final solution of all methods and they are 10, 20 and 40 respectively. The program of all methods is repeating 100 times in these three different maximum iterations. The minimum network power loss distribution diagrams of IEEE 33-bus system in 10, 20 and 40 iterations which calculated by three methods are provided in Figure 6-13, Figure 6-14 and Figure 6-15 respectively. The comparison results are shown in Table 6-6.

Table 6-6 Comparisons of MAPO, ACS and DPSO in IEEE 33-bus distribution system

Method	The number of Iterations	Network Power Loss(kW)			Probability of Finding The Minimum Loss
		Best	Worst	Average	
Ant Colony	10	139.28	150.80	141.50	22%
	20	139.28	147.64	139.60	84%
	40	139.28	142.90	139.29	97%
Discrete Particle Swarm	10	139.28	146.43	144.13	3%
	20	139.28	142.90	141.56	20%
	40	139.28	139.70	139.59	81%
Proposed Method (MAPO)	10	139.28	144.49	139.84	51%
	20	139.28	142.90	139.36	95%
	40	139.28	139.28	139.28	100%
New Tie Switches for the Minimum Network Power Loss		7, 9, 14, 32, 37			

Results obtained by 100 repeat of execution.

The result of the best network power loss is the same obtained by three methods. Then, it can easily determine which method is better from the average value in Table 6-6. Apart from the best value, all value obtained by the discrete particle swarm optimization is the worst in three different kinds of maximum number of iterations. Thus, according to these results, the search performance of the discrete particle swarm optimization is the worst at least in the IEEE 33-bus distribution system. According to the results, the proposed hybrid method has the best performance in this system. Especially, when the maximum number of iterations is 40, all minimum network power losses in 100 program executions are the same by using the proposed method. The 100% probability to find the known latest global best solution means that if the system and the parameters of the optimization method were not changed, the proposed method could always find the latest global best solution with only one program execution. Thus, according to the results in

Table 6-6, 20 iterations are enough for the proposed method and the ant colony system to solve the feeder reconfiguration problem with little program executions. Comparing the proposed method with the ant system colony, more iterations are necessary for the discrete particle swarm optimization. Otherwise, it may difficult to find the same minimum value of the network power loss obtained with another two methods.

The minimum network power loss of 33-bus distribution system in references [17, 18] is 139.55kW which is not the same as the result in Table 6-6. But, the new tie switches for the minimum network power loss in these references are the same with the above results. The tolerance in the value of the minimum network power loss can be generated by using different load flow calculation method. The same network structure is more important to represent the same results of feeder reconfiguration. Thus, the accuracy of these methods in case one can be verified by the same network structure with reference [17, 18]. The network structure with the minimum network power loss is illustrated in Figure 6-13.

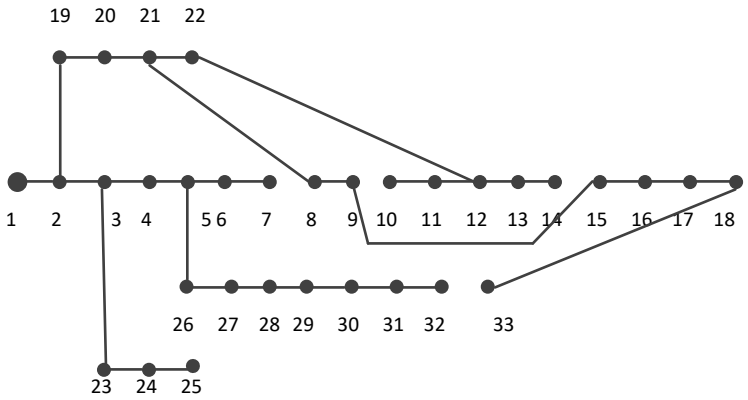

Figure 6-13 IEEE 33-bus network structure with the minimum network power loss

Figure 6-14, Figure 6-15 and Figure 6-16 is the value distribution diagram of the final minimum network power loss in 100 repeat of execution obtained by three optimization methods at 10, 20 and 40 iterations respectively. Blue line is the

results calculated by the proposed hybrid method. The red line represents the results of ant colony system. Results of the tear circuit based particle swarm optimization are shown by the green line. The values of the final minimum network power loss which distributes on these three figures can display the results of Table 6-6 more imagery.

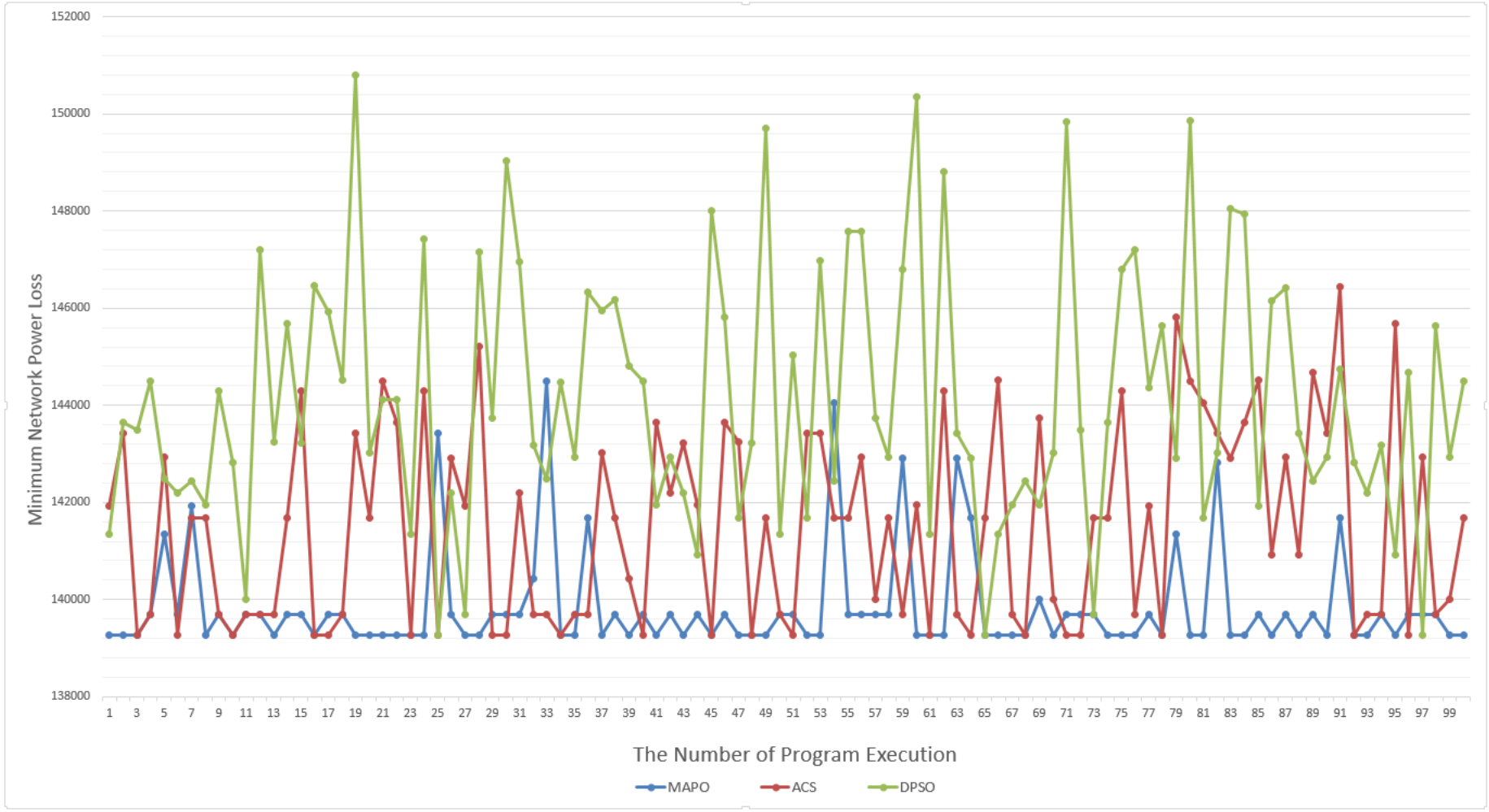

Figure 6-14 Comparisons of the minimum network power loss in 100 program executions with 10 iterations

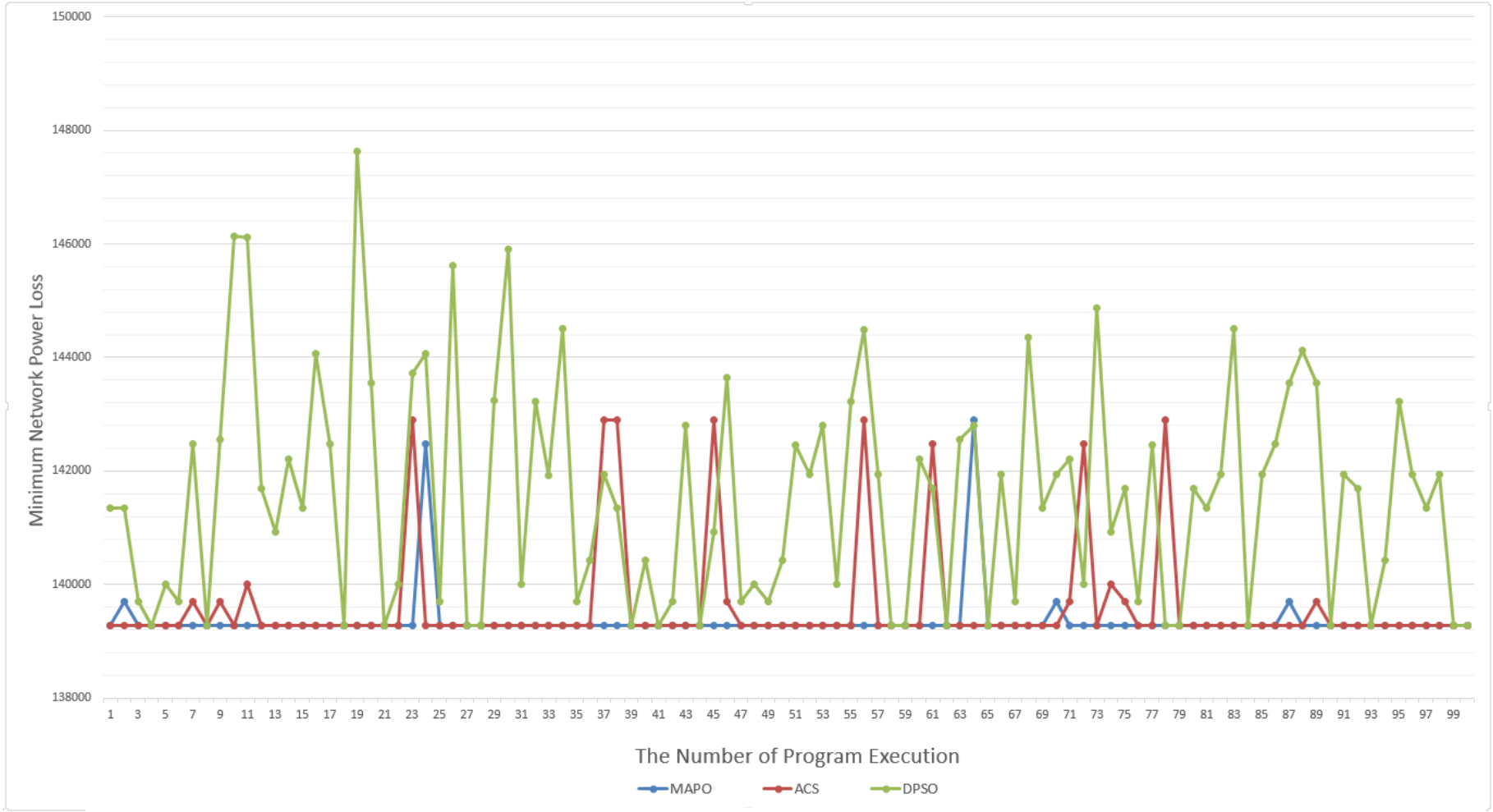

Figure 6-15 Comparisons of the minimum network power loss in 100 program executions with 20 iterations

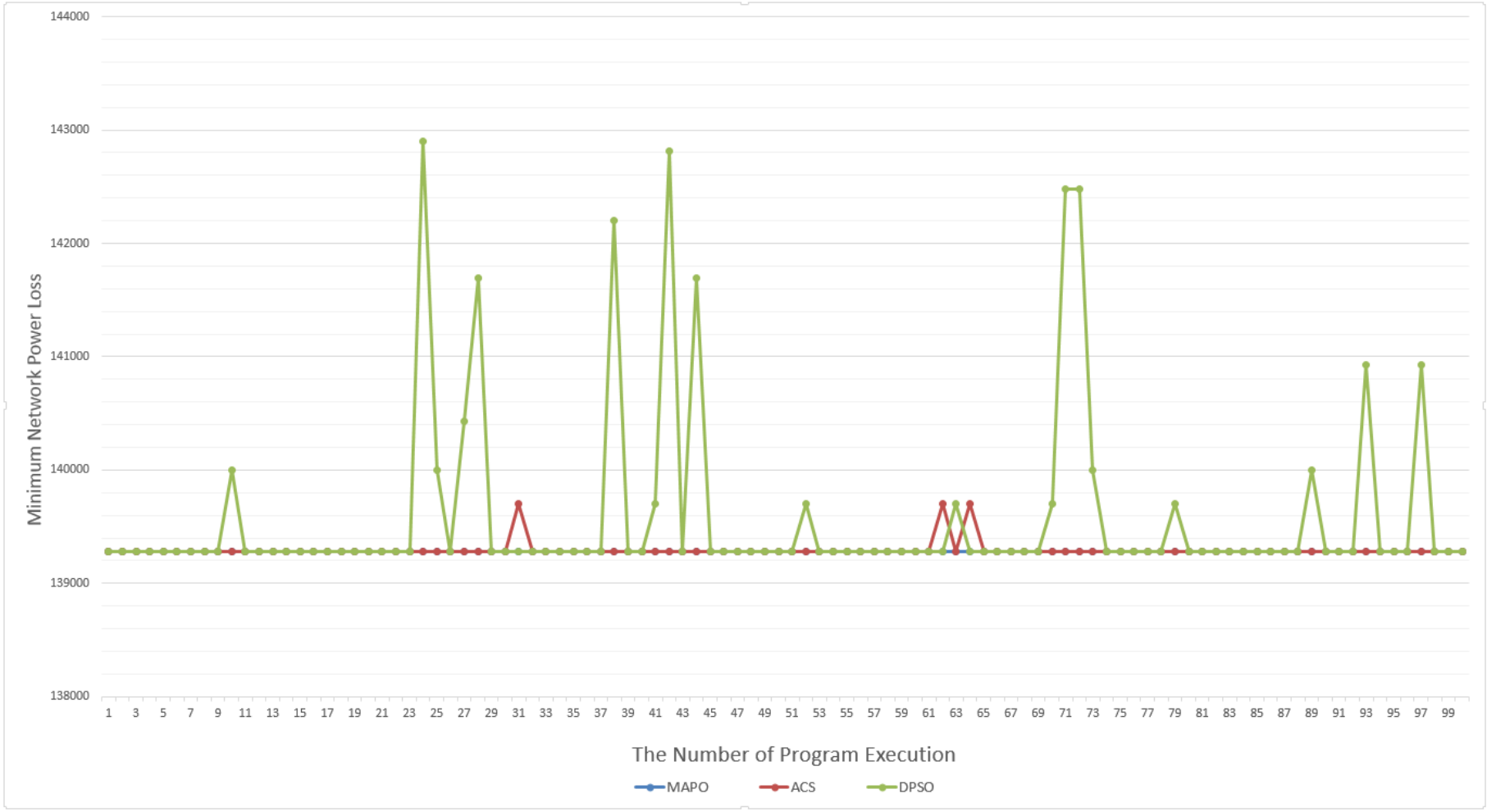

Figure 6-16 Comparisons of the minimum network power loss in 100 program executions with 40 iterations

6.5.2 Case Two: IEEE 69-Bus Distribution System

IEEE 69-bus distribution system is shown in Figure 6-6. The system data is provided in Appendix A.2. The population of both ant and particle is 20. Three different maximum number of iterations are tested for investigating the final solution of all methods and they are 20, 40 and 80 respectively. The program of all methods is repeating 100 times in three different maximum iterations. The minimum network power loss distribution diagrams of IEEE 69-bus system in 20, 40 and 80 iterations which calculated by three methods are provided in Figure 6-18, Figure 6-19 and Figure 6-20 respectively. The comparison results are shown in Table 6-7.

Table 6-7 Comparisons of MAPO, ACS and DPSO in IEEE 69-bus distribution system

Method	The Number of Iterations	Network Power Loss(kW)			Probability of Finding The Minimum Loss
		Best	Worst	Average	
Ant Colony	20	99.36	100.32	100.00	21%
	40	99.36	100.32	99.87	38%
	80	99.36	100.32	99.50	75%
Discrete Particle Swarm	20	99.36	112.14	103.49	4%
	40	99.36	106.39	101.92	10%
	80	99.36	105.20	99.79	59%
Proposed Method (MAPO)	20	99.36	100.41	99.84	35%
	40	99.36	100.32	99.52	79%
	80	99.36	100.32	99.39	93%
New Tie Switches for the Minimum Network Power Loss		14, 46, 50, 69, 70			

Results obtained by 100 repeat of executions.

All results of the minimum network power loss in Table 6-7 are still the same on

the IEEE 69-bus system. So, the average value is still the standard for evaluating the search performance of the optimization method. Similar to the IEEE 33-bus system, the search performance of the discrete particle swarm optimization is still the worst in the IEEE 69-bus distribution system. The proposed hybrid method also has the best performance in this system. But, even if the maximum number of iterations was increased from 40 to 80, it still cannot obtain 100% probability to find the known minimum network power loss. However, the 93% is also a good probability. It means that the complexity of the optimization is not growth linear with the system size. Comparing above with the results with Table 6-6, the probability of finding the minimum network loss by using the discrete particle swarm optimization is 59% which is much better than the results in IEEE 33-bus system. According to the results in Table 6-7, 40 iterations is only enough for the proposed method to solve the feeder reconfiguration problem. Ant system colony and discrete particle swarm optimization both needed more iterations to obtain a better result. Otherwise, it may be difficult to find the same minimum value of the network power loss obtained with the proposed method.

The minimum network power loss of 69-bus distribution system in reference [19] is 99.59kW, and the new tie switches for this power loss in the reference are 14, 45, 52, 69 and 70. But, the results in this chapter show that the minimum network loss is produced by new tie switches 14, 46, 50, 69 and 70. In order to determine which solution is better, the best network structure in reference [19] is tested and its network power loss is 100.32kW by using the same load flow method with the proposed method. Thus, the minimum network power loss found in this section is the latest minimum network power loss of the IEEE 69-bus distribution system. This network structure is shown in Figure 6-17.

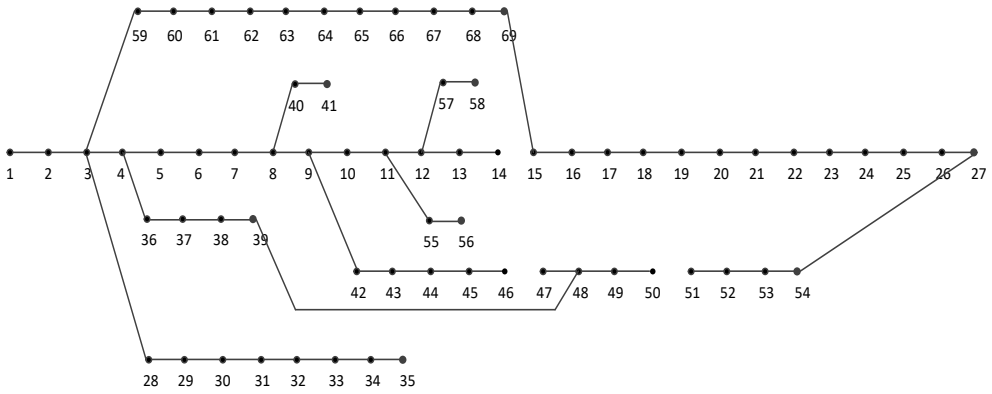

Figure 6-17 IEEE 69-bus network structure with the minimum network power loss

The value distribution diagrams of the final minimum network power loss are illustrated in three figures and they are Figure 6-18, Figure 6-19 and Figure 6-20. These results are also obtained by repeating 100 executions on three optimization methods at 20, 40 and 80 iterations respectively. The color settings are the same with case one. Although discrete particle swarm optimization has a better performance when maximum number of iterations is 80, the gap between it and the other two methods can also be found out easily from these distribution diagrams. The curve of the ant colony system is at the same level of the curve calculated by the proposed method, the difference between these two curves is unclear in Figure 6-18 however it clearly shows that the blue curve has a small average value in Figure 6-19 and Figure 6-20.

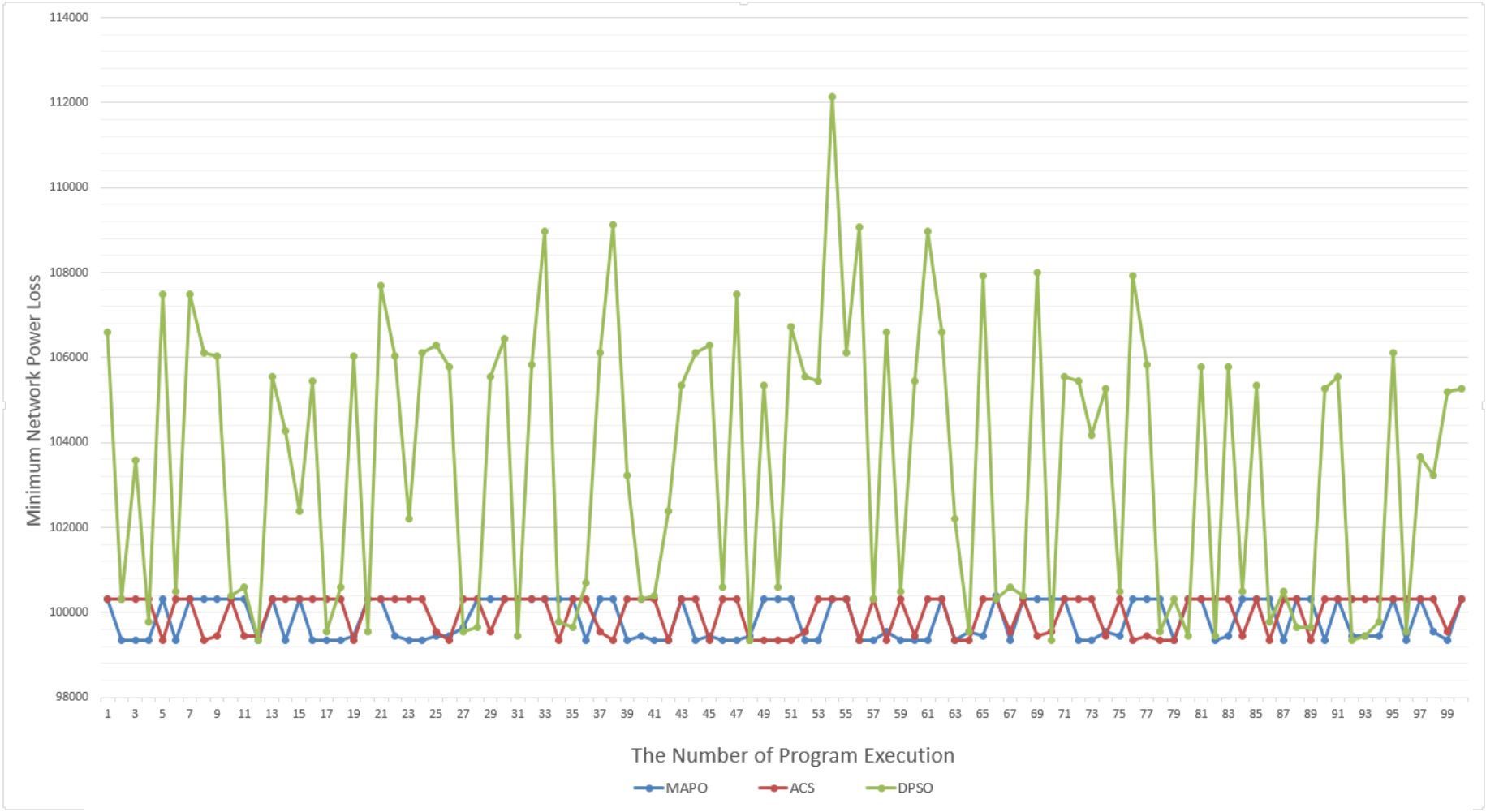

Figure 6-18 Comparisons of the minimum network power loss in 100 program executions with 20 iterations

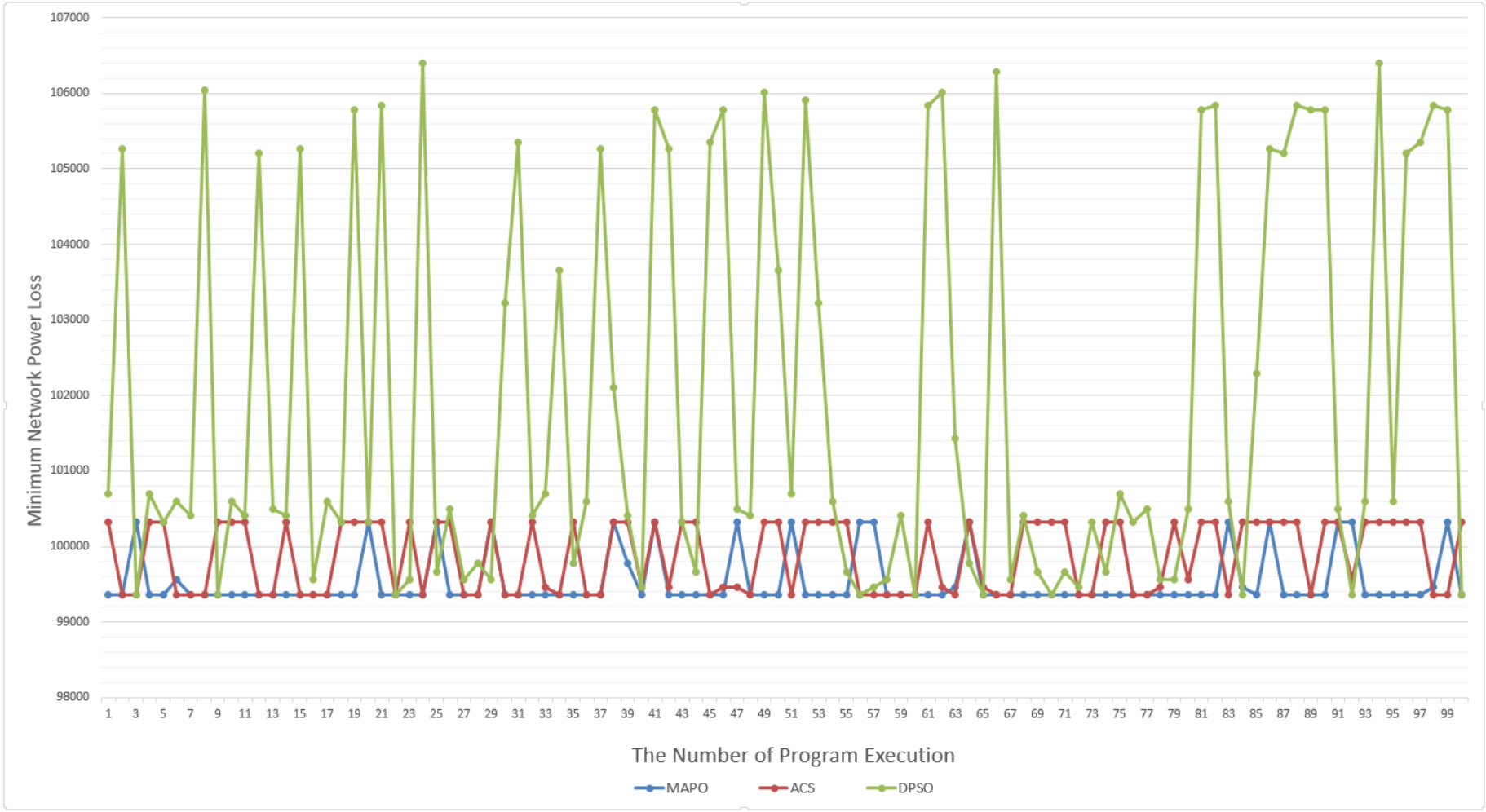

Figure 6-19 Comparisons of the minimum network power loss in 100 program executions with 40 iterations

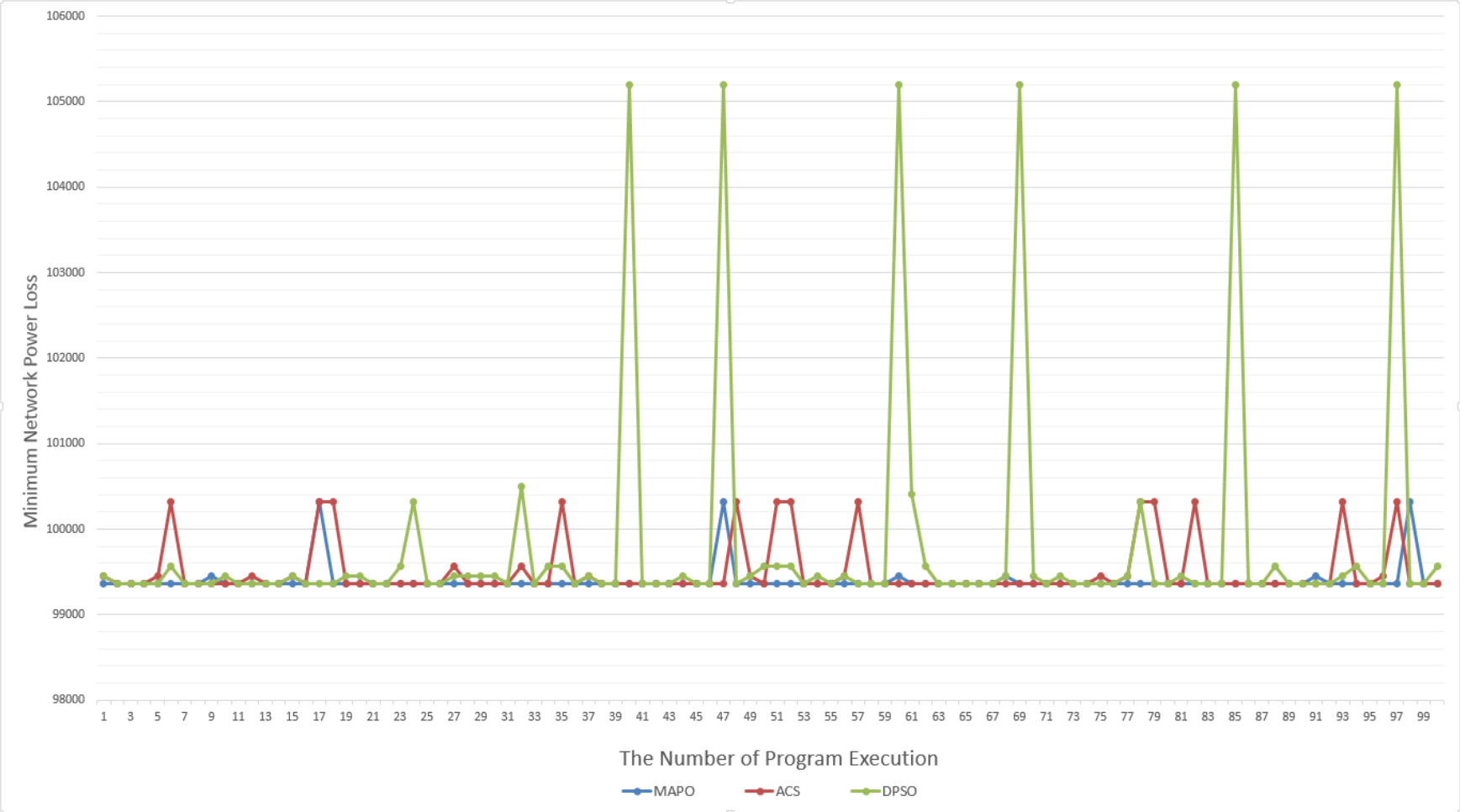

Figure 6-20 Comparisons of the minimum network power loss in 100 program executions with 80 iterations

6.5.3 Case Three: IEEE 118-Bus Distribution System

Tests of distribution network feeder reconfiguration are normally executed in IEEE 33-bus and IEEE 69-bus system which still cannot make sure that one method can work perfectly in all sizes of the distribution systems. Thus, the above three methods are tested in a bigger distribution system. The test system in this case is the 118-bus distribution system. All buses in the distribution system are at the mid-voltage level. Loads and equipment in lower voltage level will be treated as the equivalent load. Thus, a distribution system with 118 buses in one voltage level is big enough. For the convenience of programming, one virtual bus (bus 1) and one virtual branch (branch 1) are connected to the reference bus in this distribution system. The impedance of the branch 1 is zero. So, the virtual system has no impact on this distribution system. Details of the 118-bus system are illustrated in Figure 6-21. The system data is provided in Appendix A.3. In case two, 40 iterations is not enough for the ant colony system and the discrete particle swarm optimization so that three different maximum number of iterations for investigating the final solution are 80, 160 and 300 respectively in this case. The population of both ant and particle is also increased to 35. One hundred program executions are also finished in three different methods. The minimum network power loss distribution diagram of the 118-bus system in 80, 160 and 300 iterations which calculated three methods is provided in Figure 6-23, Figure 6-24 and Figure 6-25 respectively. The comparison results are shown in Table 6-8.

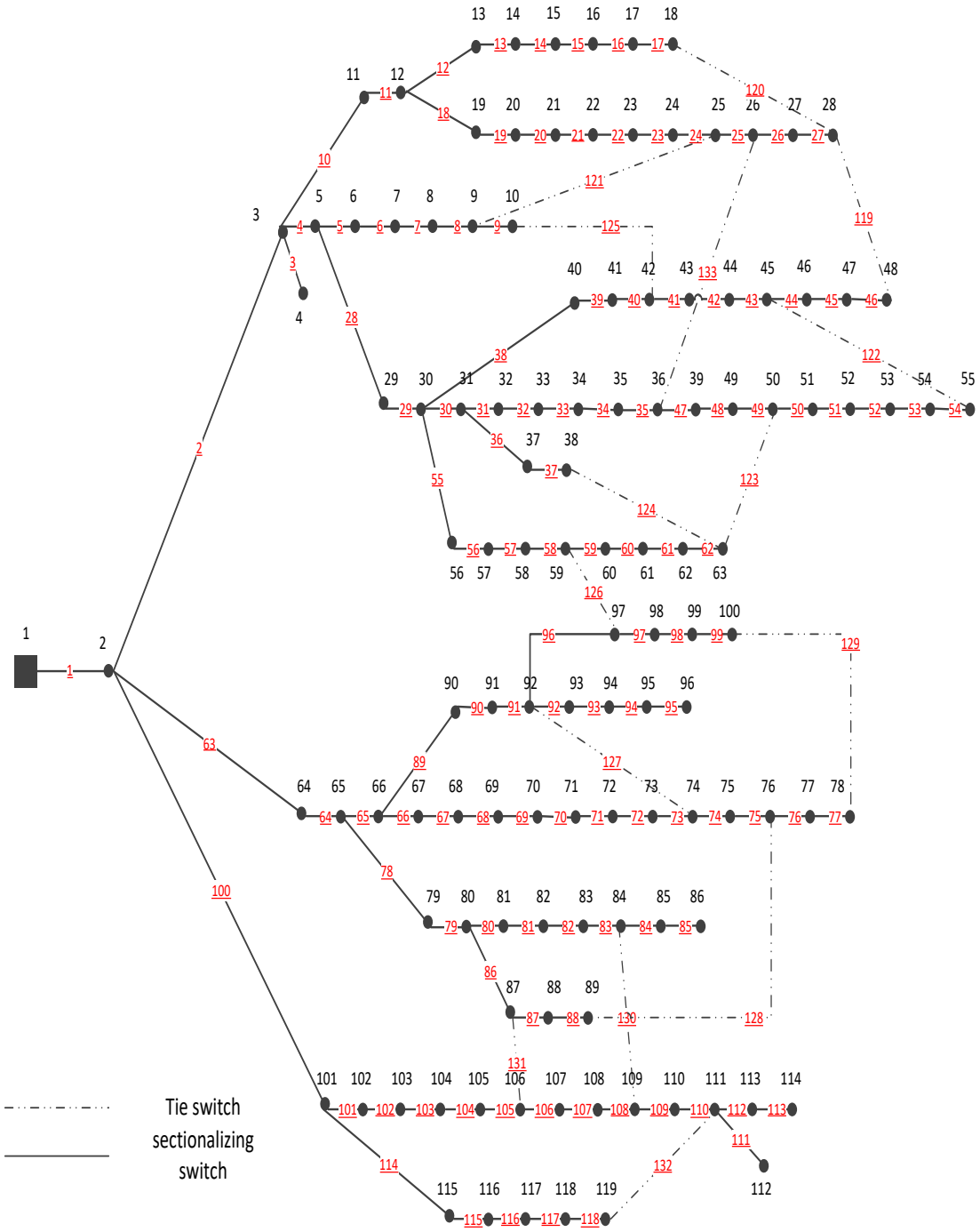

Figure 6-21 IEEE 118-bus distribution system with one virtual bus

Table 6-8 Comparisons of MAPO, ACS and DPSO in 118-bus distribution system

Method	The Number of Iterations	Network Power Loss(kW)			Probability of Finding The Minimum Loss
		Best	Worst	Average	
Ant Colony	80	898.68	1005.84	941.32	0%
	160	870.39	894.83	885.05	0%
	300	869.72	890.26	878.64	10%
Discrete Particle Swarm	80	931.49	1132.89	1002.15	0%
	160	922.37	1061.78	975.22	0%
	300	898.68	1005.84	941.31	0%
Proposed Method (MAPO)	80	870.39	897.68	882.66	0%
	160	869.72	891.72	878.90	5%
	300	869.72	887.93	874.95	24%
New Tie Switches for the Minimum Network Power Loss		24, 27, 35, 40, 43, 52, 59, 72, 75, 96, 98, 110, 123, 130, 131			

Results obtained by 100 repeat of executions.

The biggest change in Table 6-8 when to compare with the results in Table 6-6 and 6-7 is that the six probabilities of finding the minimum network loss are zero. It means that if the maximum number of iteration is 300 and the number of program execution is 10, only ant colony system and the proposed method could find the known minimum loss theoretically. Furthermore, 10% probability cannot guarantee that the known minimum loss will be found in 10 program executions. Thus, only the proposed method can provide a guarantee of finding the known minimum loss in 300 iterations with 10 program executions. The search performance of the discrete particle swarm optimization is awful in this case. It cannot find the same minimum loss with other two methods even the maximum number of iteration is 300. Such a result indicate that when system size becomes large, the complexity of the feeder reconfiguration problem will increase with geometric series. When buses number is larger than 100, the maximum number of

iterations for above three methods should be tested rather than set by personal experience. For this 118-bus system, 300 iterations and 10 program executions are enough for the proposed hybrid method to find the possible best solution for network loss reduction or other objectives.

The minimum network power loss of 118-bus distribution system in references [20, 21] is 865.86kW. The new tie switches for the minimum network power loss in these references are 24, 27, 35, 40, 43, 52, 59, 72, 75, 96, 98, 110, 123, 130 and 131. Similar to the case one, although the value of the minimum network power loss is not the same as the results in Table 6-8, the new tie switches are the same. Thus, it can be decided that above latest global best solution for the feeder reconfiguration in 118-bus distribution system is the same as the global best solution calculated in reference [20, 21]. Figure 6-22 is the network structure after executing the feeder reconfiguration program for network loss reduction in the 118-bus distribution system.

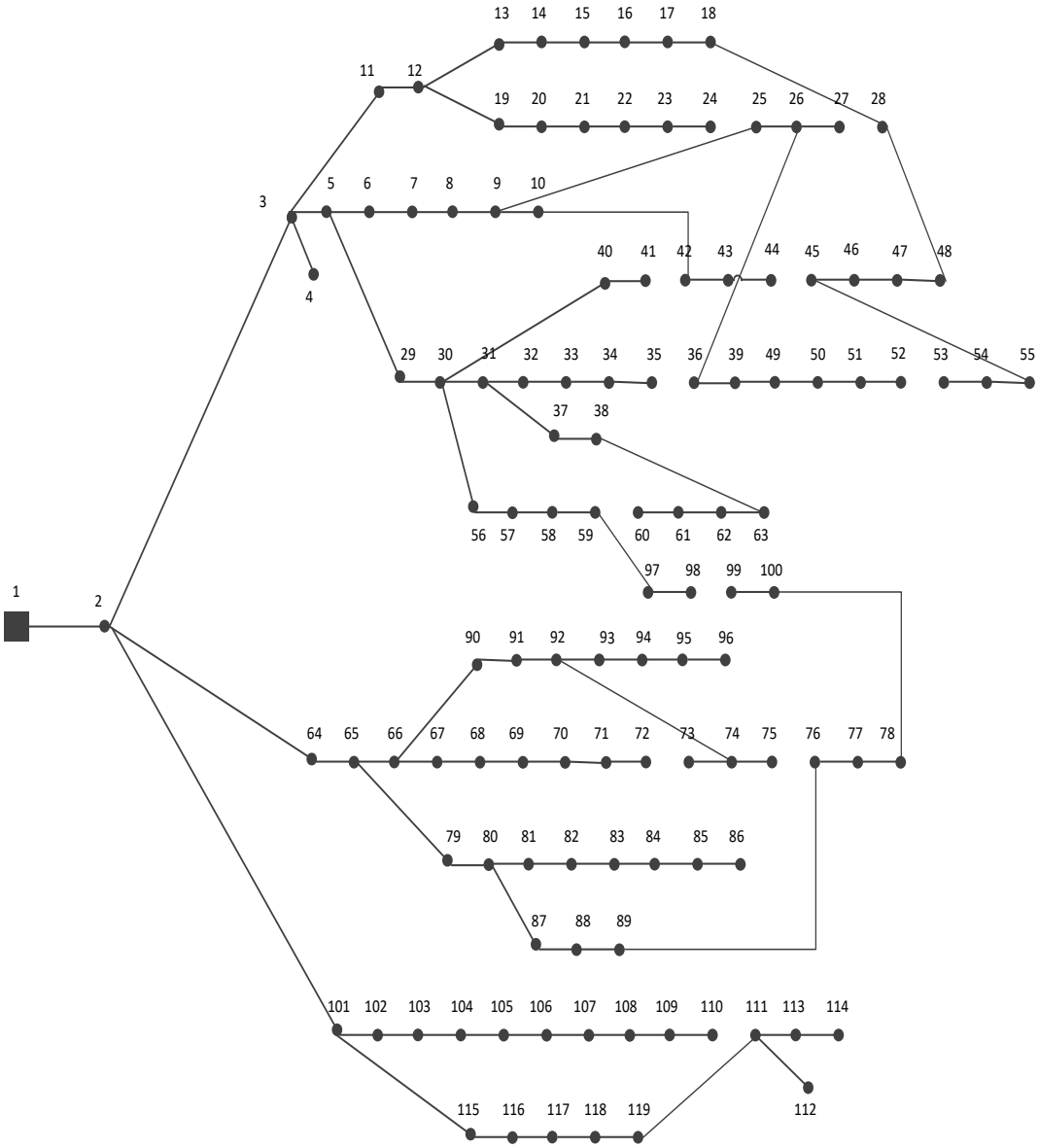

Figure 6-22 IEEE 118-bus network structure with the minimum network power loss

Due to the increment of the system size, the differences of the distribution diagram between above three optimization methods are more and more obvious. In Figure 6-23, three broken lines which composed of the minimum network power loss results by three methods are almost separated. Thus, the proposed method in blue has the best search performance. The searching performance of the particle swarm optimization in green is worst. In Figure 6-24, the broken lines of the ant colony

system and the proposed method stay at the same level. Although they stay at the same level, the location of the blue broken line is obviously lower. Due to the worst search performance, the broken line of the particle swarm optimization has a wide gap with other two broken lines. In Figure 6-25, the blue line and the red line are still at the same level and which one is better is not clear enough. But, if we focus on the number of the dot at the lowest level, which one is better can be identified quickly. The gap between the green broken line with other two lines is wider.

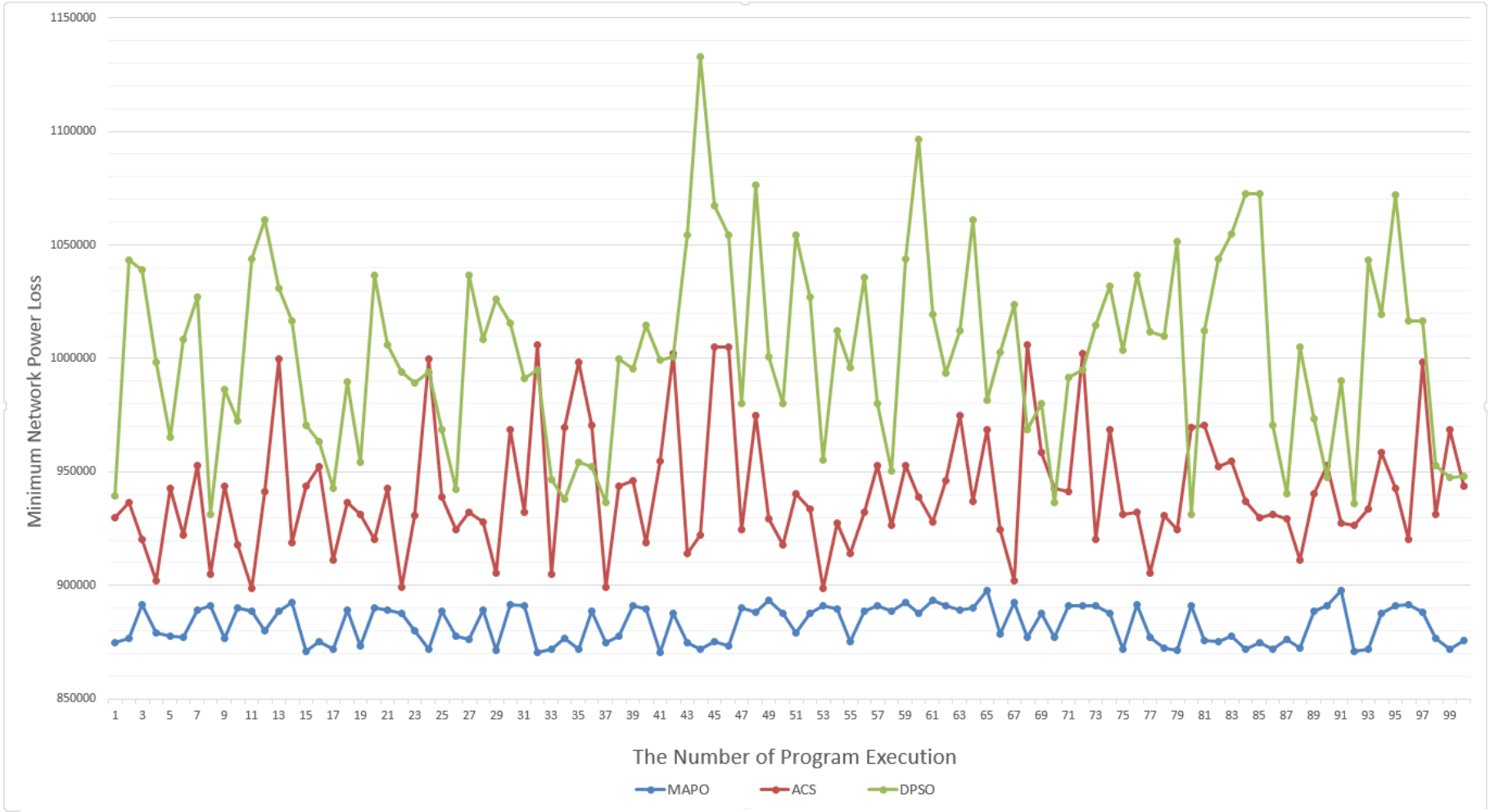

Figure 6-23 Comparisons of the minimum network power loss in 100 program executions with 80 iterations

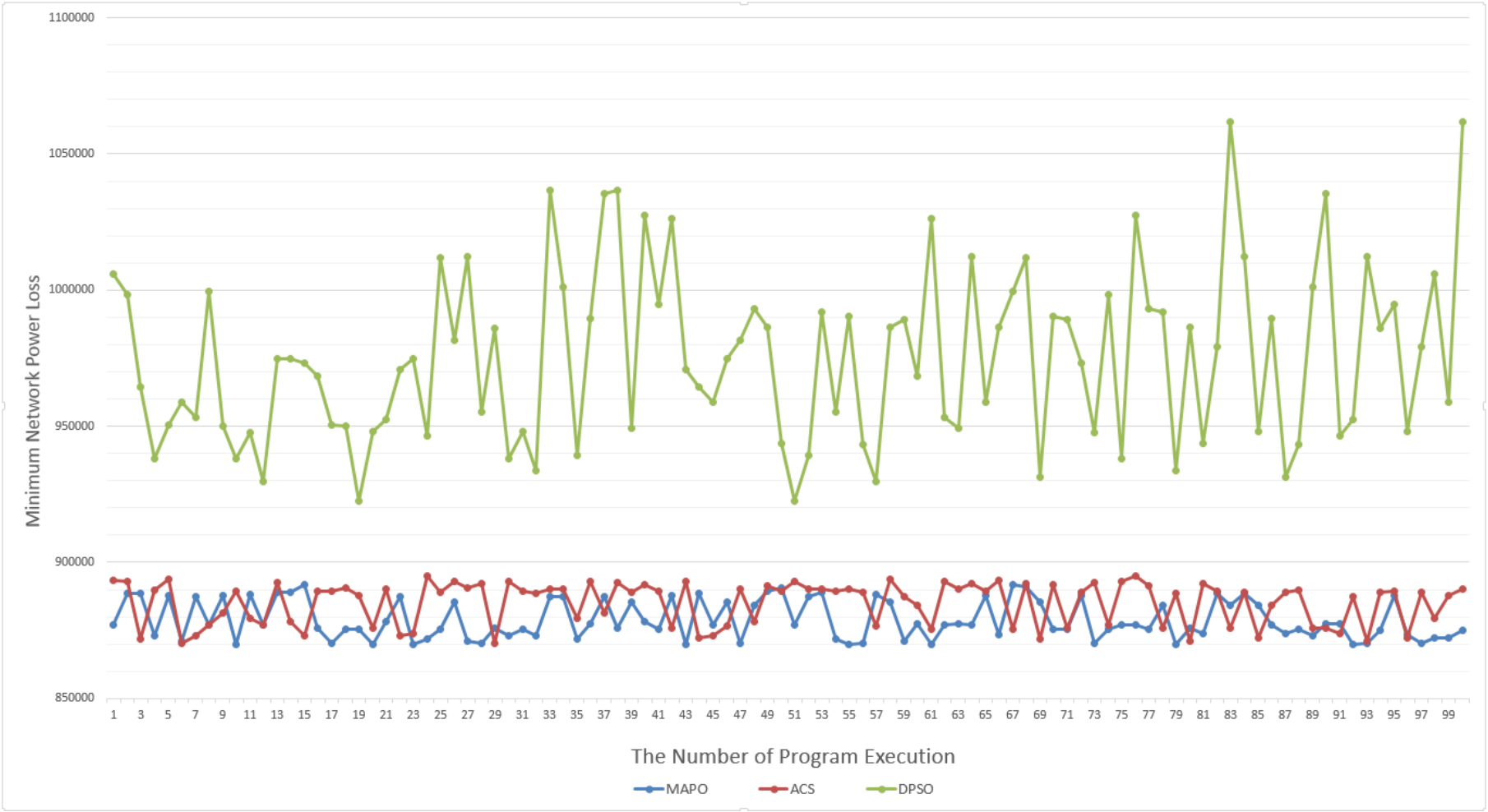

Figure 6-24 Comparisons of the minimum network power loss in 100 program executions with 160 iterations

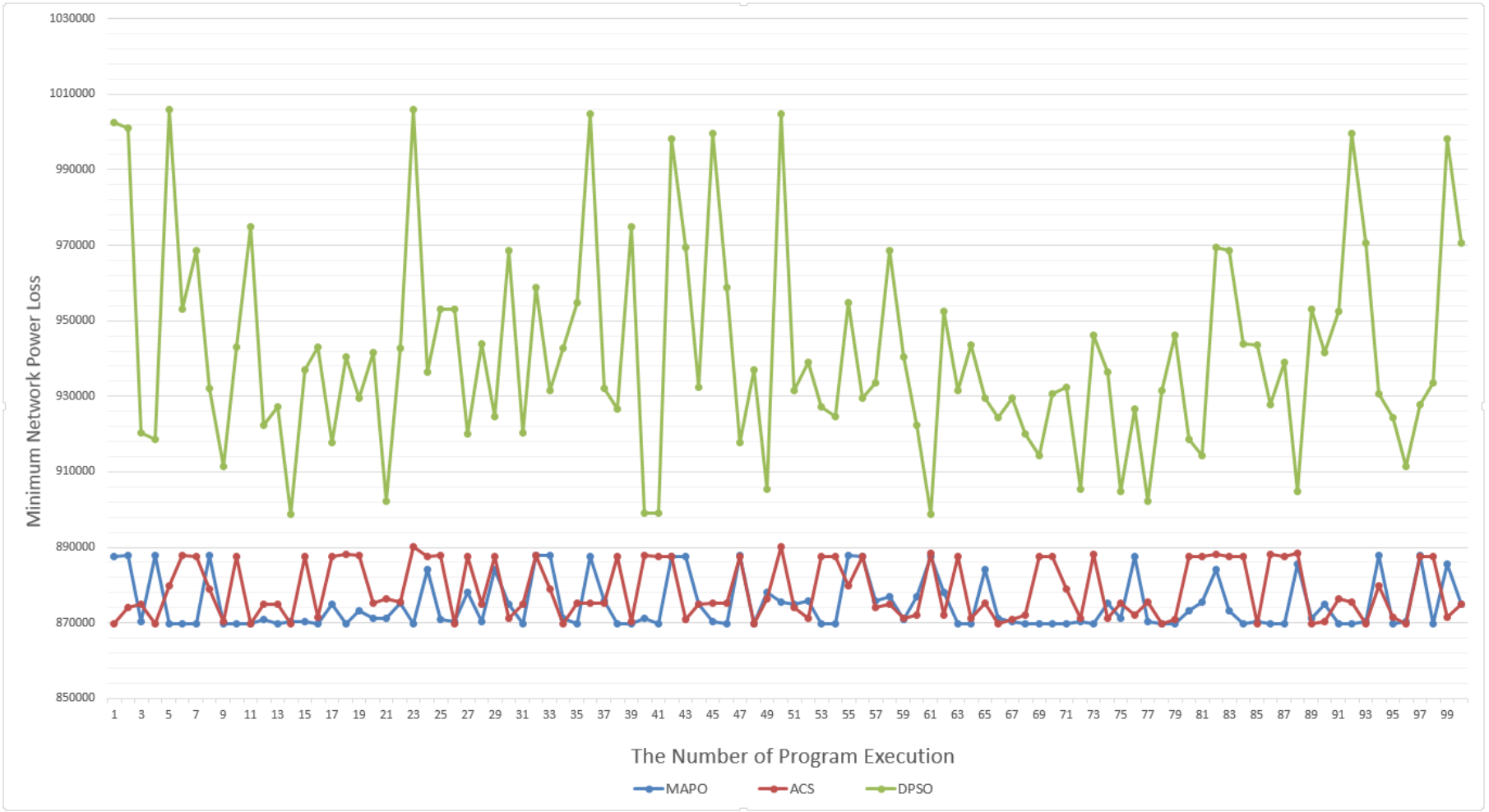

Figure 6-25 Comparisons of the minimum network power loss in 100 program executions with 300 iterations

6.5.4 Result Discussion

According to above three cases, the search performance of the discrete particle swarm optimization is the worst. Due to almost all final solutions of the discrete particle swarm optimization is not the same, good global search ability is proved that it can help a method to prevent being trapped locally. But, a method is still difficult to find the possible global best solution without a strong local search ability in large size and complex optimization problem.

For ant colony system, due to the complexity is not high, strong local search ability helps ants find the known global best solution in a small system (33-bus system) fast. In the medium system (69-bus system), without the good global search ability, the performance of the ant colony system should be worse than the particle swarm optimization. But, the pseudorandom proportional mechanism of the ant colony system has a similar function with the global search ability. The performance of the pseudorandom proportional mechanism is limited by the maximum number of iterations. Small number of iterations cannot provide enough probability to use two different chosen mechanism. Although the maximum number of iterations is not big in the test of case two, the pseudorandom proportional can still provide its contribution to search the latest global best solution. Thus, the results of ant colony system in the medium system is a little better than the discrete particle swarm optimization. In the big system (118-bus system), the maximum number of iteration is set to large. The pseudorandom proportional have enough chance to help ant escape the trap. Thus, ant colony system can find the known global best solution in case three.

For the proposed hybrid method, strong local search ability comes from the ant module and the good global search ability is provided by the particle module. The adaptive function also makes its contribution to search performance. Thus, all results calculated by the proposed hybrid method are the best results in all three

cases.

6.6 Summary

The improvements for search efficiency based on ant colony system and the discrete particle swarm optimization are the theme of this chapter. The original function of the adaptive equation is proposed for the initial particle velocity of the discrete particle swarm optimization. Then, it is discovered that the adaptive equation also has positive impact on the pseudorandom proportional level in the ant colony system and the random level in the discrete particle swarm optimization. This function can also be applied to the selection part of the proposed hybrid method. Thus, this adaptive equation may have a positive impact on everywhere that the place should enlarge the range at the first half stage and rapidly reduce to the minimum range at the second half stage.

The proposed hybrid method applies a novel combination theory to combine the ant colony system and the discrete particle swarm optimization together rather than use them separately in different stages. The selection rules in the proposed hybrid method not only based on the pheromone trails like ants but also consider the velocity and position such as particles. In this hybrid method, the ant colony system and particle swarm optimization can be treated as two black modular boxes. The individuals of the hybrid method can use this two modular boxes anytime to reinforce the search ability. The other improvements for either ant colony system or particle swarm optimization can be applied in the black boxes without changing. The optimization methods in these two black modular boxes are the same with the methods which is introduced in Chapter 5.Thus, further improvements on the ant colony system or the discrete particle swarm optimization can be applied to the hybrid method easily. Furthermore, it can adjust the number of executions of both ant colony or particle swarm module by setting the parameters of the selection

function. The hybrid method obtains the strong local search ability from ants and the perfect global search ability from particles. Comparing with the ant colony system and the discrete particle swarm optimization, the search performance of the hybrid method is significantly better. This conclusion is verified by three case studies in this chapter.

6.7 Reference

[1] Marco Dorigo, Thomas Stu¨tzle, *Ant Colony Optimization*. Cambridge, 2004.

[2] A. Ahuja and A. Pahwa, "Using ant colony optimization for loss minimization in distribution networks," in *Proceedings of the 37th Annual North American Power Symposium, 2005.*, 2005, pp. 470-474.

[3] W. C. Wu and M. S. Tsai, "Application of Enhanced Integer Coded Particle Swarm Optimization for Distribution System Feeder Reconfiguration," *IEEE Transactions on Power Systems,* vol. 26, pp. 1591-1599, 2011.

[4] W. C. Wu, M. S. Tsai, and F. Y. Hsu, "A New Binary Coding Particle Swarm Optimization for Feeder Reconfiguration," in *Intelligent Systems Applications to Power Systems, 2007. ISAP 2007. International Conference on*, 2007, pp. 1-6.

[5] M. S. Tsai and C. C. Chu, "Applications of hybrid EP-ACO for power distribution system loss minimization under load variations," in *Intelligent System Application to Power Systems (ISAP), 2011 16th International Conference on*, 2011, pp. 1-7.

[6] J. Olamei, T. Niknam, A. Arefi, and A. H. Mazinan, "A novel hybrid evolutionary algorithm based on ACO and SA for distribution feeder reconfiguration with regard to DGs," in *GCC Conference and Exhibition (GCC), 2011 IEEE*, 2011, pp. 259-262.

[7] A. Ahuja, S. Das, and A. Pahwa, "An AIS-ACO hybrid approach for multi-objective distribution system reconfiguration," in *Power and Energy Society General Meeting - Conversion and Delivery of Electrical Energy in the 21st Century, 2008 IEEE*, 2008, pp. 1-1.

[8] Y. Yahong, Z. Fuqing, Y. A. O. Yunping, and Z. H. U. Aihong, "A PSO and Simulated Annealing Hybrid Algorithm to Task Allocation Problem for Holonic Manufacturing System," in *2006 6th World Congress on Intelligent Control and Automation*, 2006, pp. 6767-6771.

[9] H. Duan, Q. Luo, Y. Shi, and G. Ma, "Hybrid Particle Swarm Optimization and Genetic Algorithm for Multi-UAV Formation Reconfiguration," *IEEE Computational Intelligence Magazine,* vol. 8, pp. 16-27, 2013.

[10] Sandip K. Lahiri and Nadeem Muhammed Khalfe, "Hybrid Particle Swarm Optimization and Ant Colony Optimization Technique for the Optimal Design of Shell and Tube Heat Exchangers," *http://www.degruyter.com/dg/viewarticle.fullcontentlink:pdfeventlink/$002fj$002fcppm.2015.10.issue-2$002fcppm-2014-0039$002fcppm-2014-0039.pdf?t:ac=j$002fcppm.2015.10.issue-2$002fcppm-2014-0039$002fcppm-2014-0039.xml*, 2015 (May 2016, last access date).

[11] C.-F. Juang, "Combination of Particle Swarm and Ant Colony Optimization Algorithms for Fuzzy Systems Design," *http://www.intechopen.com/books/fuzzy-systems/combination-of-particle-swarm-and-ant-colony-optimization-algorithms-for-fuzzy-systems-design*, May 2016 (last access date).

[12] J. A. Lazzus, "Hybrid Particle Swarm-Ant Colony Algorithm to Describe the Phase Equilibrium of Systems Containing Supercritical Fluids with Ionic Liquids," *Commun. Comput. Phys.,* vol. 14, pp. 107-125, 2013.

[13] H. Q. Biao ZHANG, Shuang-Cheng SUN, Li-Ming RUAN, and He-Ping TAN, "A Novel Hybrid Ant Colony Optimization and Particle Swarm Optimization Algorithm for Inverse Problems of Coupled Radiative And Conductive Heat Transfer," *http://www.doiserbia.nb.rs/img/doi/0354-*

9836/2014%20OnLine-First/0354-98361400023Z.pdf, May 2016 (last access date).

[14] Y. Xiao, X. Song, and Z. Yao, "Improved Ant Colony Optimization with Particle Swarm Optimization Operator Solving Continuous Optimization Problems," in *Computational Intelligence and Software Engineering, 2009. CiSE 2009. International Conference on*, 2009, pp. 1-3.

[15] Anirudh Shekhawat Pratik Poddar Dinesh Boswal, "Ant colony Optimization Algorithms : Introduction and Beyond," http://mat.uab.cat/~alseda/MasterOpt/ACO_Intro.pdf, May 2016 (last access date).

[16] "ISE 410 Heuristics in Optimization Particle Swarm Optimization," http://www.slideshare.net/satish561/swarm-intelligence-pso-and-aco, May 2016 (last access date).

[17] J.A. Martín, A.J. Gil, "A new heuristic approach for distribution systems loss reduction," *Electr. Power Syst. Res.,* vol. 78, pp. 1953–1958, 2008.

[18] B. Enacheanu, B. Raison, R. Caire, O. Devaux, W. Bienia, and N. HadjSaid, "Radial Network Reconfiguration Using Genetic Algorithm Based on the Matroid Theory," *IEEE Transactions on Power Systems,* vol. 23, pp. 186-195, 2008.

[19] J. S. Savier and D. Das, "Impact of Network Reconfiguration on Loss Allocation of Radial Distribution Systems," *IEEE Transactions on Power Delivery,* vol. 22, pp. 2473-2480, 2007.

[20] D. Zhang, Z. Fu, L. Zhang, "An improved TS algorithm for loss-minimum reconfiguration in large-scale distribution systems," *Electr. Power Syst. Res.,* vol. 77, pp. 685–694, 2007.

[21] N. G. Anil Swarnkar, K.R. Niazi "Adapted ant colony optimization for efficient reconfiguration of balanced and unbalanced distribution systems for loss minimization," *Swarm Evol Comput,* vol. 1, pp. 129–137, 2011.

Chapter 7 Impact of Harmonic Sources in Distribution Network Feeder Reconfiguration

7.1 Introduction

New energy refers to the various forms of energy besides traditional energy sources. The term incorporates solar energy, wind energy, biomass, geothermal, hydropower and ocean energy as well as energy derived from renewable biofuels and produced from hydrogen. New energy sources offer significant advantages over traditional energy sources, such as lower levels of pollution and the capacity to help solve the world's most serious environmental issues and resource depletion (particularly in the case of fossil fuels). Of these new forms of generation, wind and photovoltaic energy have shown the most progress in recent years.

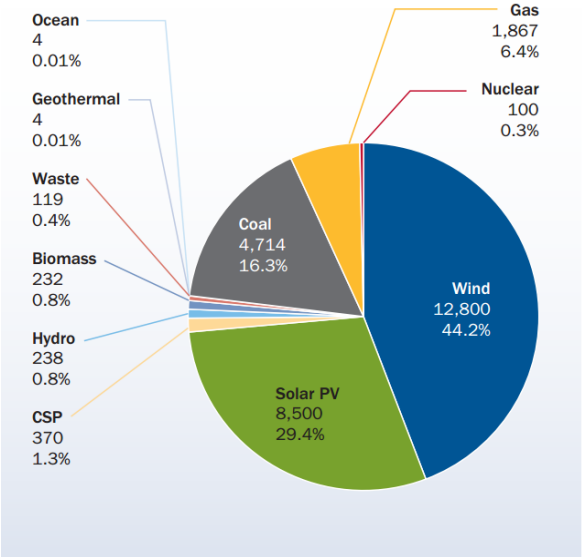

Figure 7-1 2015 share of new power capacity installations. Total 28948.7MW[2]

Figure 7-1 shows the share of new power capacity installations in the EU in 2015.

Wind energy has the highest installation rate (44.2%) with 1.28 GW of new power capacity installations and solar PV came second with 8.5 GW (29.4%). Wind and solar capacitor installations accounted for a total 2.13GW, 73.6% of all new capacity in the EU[2].

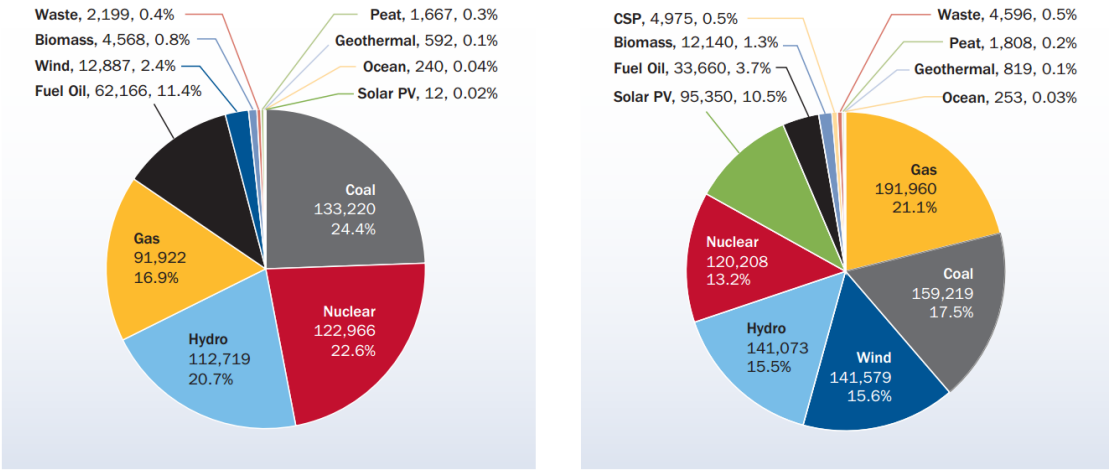

Figure 7-2 EU power mix from 2000 to 2015[2]

Wind power's share of total installed power capacity has increased six-fold since 2000, from 2.4% in 2000 to 15.6% in 2015 as shown in Figure 7-2. Solar power's share of total installed power capacity has also increased from slightly above 0% to 10.5%[2].

About 7% and 3% of EU electricity demand were provided by wind power and solar energy respectively in 2012 [5, 6]. Due to the fact that more than 95% of new renewable energy power capacity installation in 2015 was wind power or solar power[2], it can be said that about 10% of the total EU energy demand is provided by renewable energy. The European Union has set a target of renewable energy meeting 35% of the EU's demand for electricity by 2030[7]. This target is subdivided into 2 steps – the first one being for wind power to provide 15-17% of the EU's electricity demand by 2020, and this proportion to increase to 28.5% by 2030[5]. A similar target has also been set for solar power: 4-8% of the EU's

electricity demand should be met by solar power by 2020, increasing to 10-15% by 2030 [6]. Figure 7-3 shows that renewable energy will supply at least 38.5% of the EU's total electricity demand. This will allow the EU's 2030 electricity targets to be satisfied.

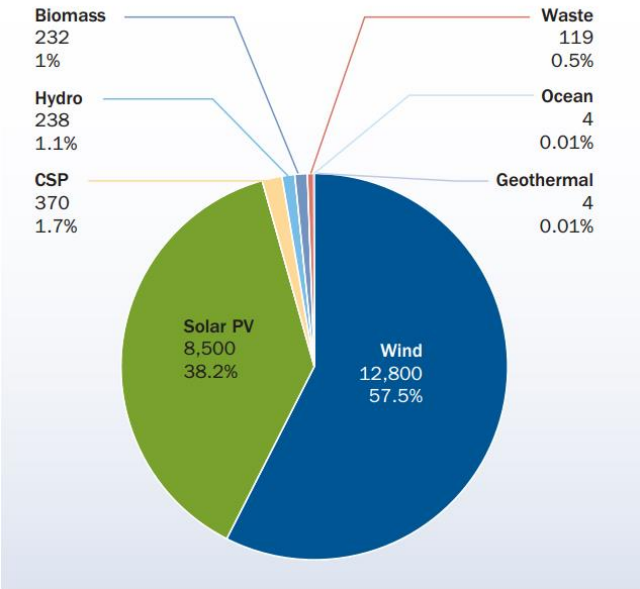

Figure 7-3 2015 share of new renewable power capacity installations. Total 22267.9MW[2]

Renewable power stations are not only applied as main power sources in the transmission network but also considered as distribution generators in the distribution network. Compared with large, centralised grid-connected renewable power stations, small-scale wind or solar power applications offer more advantages. Centralised power plants require large-scale investment, entail high demand for land and are mostly located in areas which are remote from the loads. Electricity power is not normally consumed locally. Transporting this form of energy over long distances entails losses and poses other problems. However, small-scale wind and solar applications require relatively low investment, small construction sites and the electricity generated can be consumed locally. Thus, the application of wind and solar power plants in the distribution network is indispensable.

Although wind and solar energy bring benefits in terms of minimising environmental pollution problems and resource depletion issues, they encounter power quality issues which are caused by harmonic injections. This is because inverter-based renewable generators are main harmonic sources in the power system. The problems caused by system harmonics were introduced in Chapter 3 and Chapter 4 so it is essential to investigate the effects of harmonics on the distribution network and the distribution network feeder reconfiguration.

One of the principal sources of air pollution is vehicle emissions. Furthermore, the price of gasoline is forecast to increase from 4 dollars per gallon in 2012 to 21 dollars per gallon in 2050[8]. Electric vehicles have shown rapid development in recent years, in response to the need to reduce air pollution and uptake has also been encouraged by the financial incentive of avoiding high gasoline prices. However, electric vehicles are also a harmonic source in the power system. A majority of electric vehicles are charged at the low voltage level of the distribution network. Thus, the distribution network and its reconfiguration must take into account the harmonic effects that electric vehicles have on them.

This chapter will apply the improved harmonic backward/forward sweep method to calculate the fundamental and harmonic load flow in the 118-bus system and solve the feeder reconfiguration problem in different scenarios by the proposed hybrid optimization method outlined in Chapter 6. The details of this test system and the spectrums of the used harmonic sources are introduced in Section 7.2. The tests' objectives are also introduced in this section. The impacts of the harmonic sources on feeder reconfiguration are investigated in Section 7.3 when system harmonic capacities are changed and the distributed generators are installed. Section 7.4 features a discussion on the impacts of the changing output of the generators and load demands on feeder reconfiguration. Matlab 2014b is used to program and solve power flow calculations and reconfiguration problems. The

computer used for the calculation has an i5 3470k CPU and 8GB RAM. The operating system is Windows 10.

7.2 Details of The Test System and Harmonic Sources

7.2.1 Test System

Because data from an actual distribution network is not easily available, a 118-bus distribution network which is used as in reference [9] is applied in this chapter. It contains 118 existing buses and one virtual bus (bus 1) which are shown in Figure 7-4. Hence it also contains 118 sectionalizing switches and 15 tie switches. Bus 1 is the slack bus and its rated bus voltage is 11kV. Thus, this is a mid-voltage level distribution system. The total power loads are 22709.7kW and 17041.1kvar. Each load in this network is a mixed load with a step-down transformer. Therefore, this system is big enough to test the distribution network reconfiguration problem. Appendix A.3 contains further details about the data.

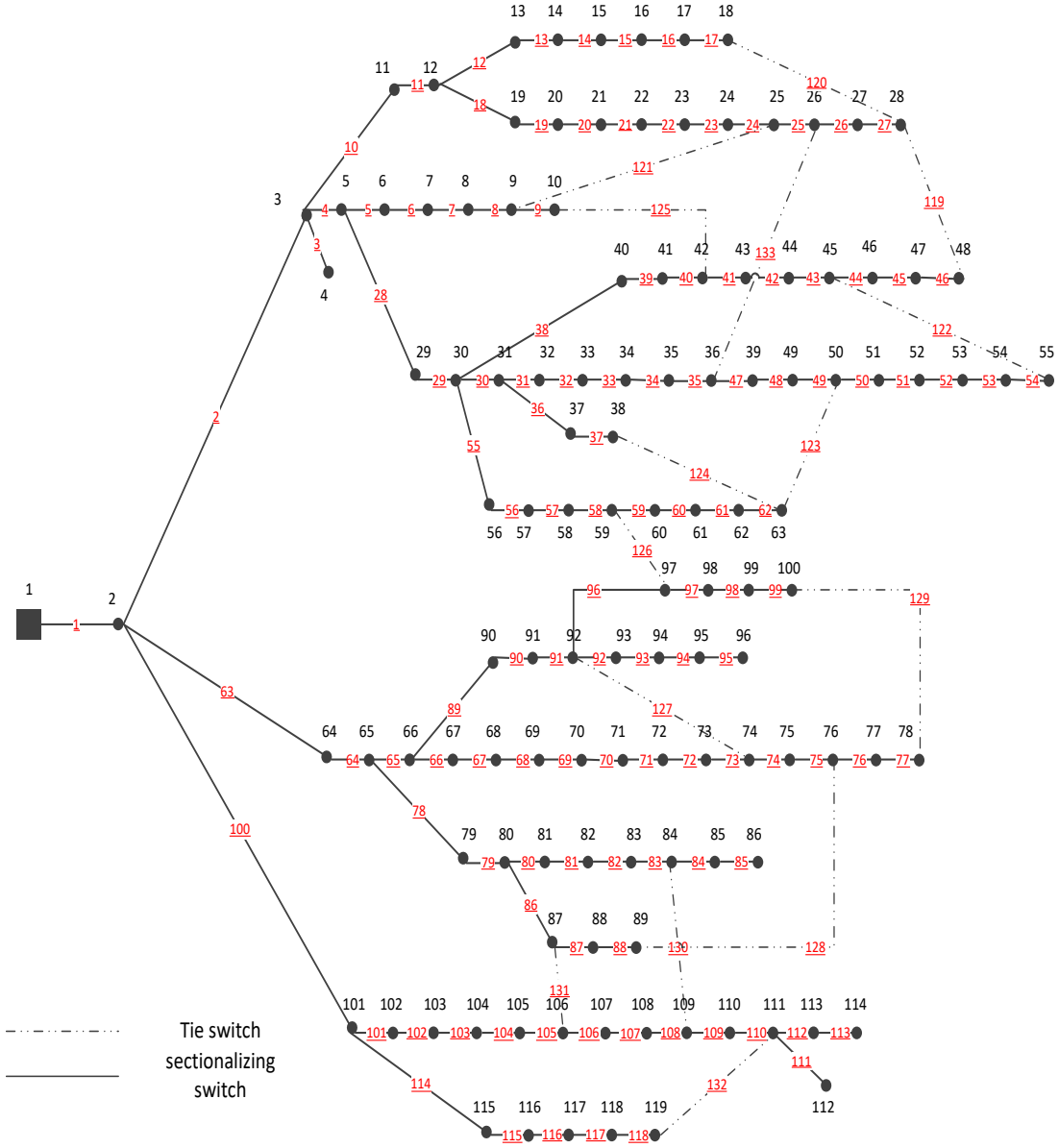

Figure 7-4 Network structure of the 118-bus distribution network[9]

7.2.2 Harmonic Sources and Load Type

Wind turbines and photovoltaic generators are regarded as harmonic sources in this chapter. The injection harmonic current spectrums of these harmonic sources are provided in Table 3-4, 3-5 and 3-6 respectively in Chapter 3. Furthermore, in reference [4], the percentile of the fundamental magnitude values of two samples collected over a week in 2012 were computed and summarised in Table 7-1.

Table 7-1 Harmonic Spectrum of Individual Houses and Service Transformers [4]

Harmonic	House 1	House 2	Transformer Combined
	Magnitude (% Fund)	Magnitude (% Fund)	Magnitude (% Fund)
1	100	100	100
3	8.8	7.9	8.6
5	5.8	4.4	4.7
7	3.5	2.0	2.9
9	2.8	2.8	2.9
11	1.2	0.9	1.1
13	0.9	0.7	0.9

In this table, the magnitudes for various harmonics in each harmonic order which were collected from different houses are almost identical to the data collected from the transformer point. Therefore, these three harmonic spectrums can all be used to represent the harmonic injection current for mixed load in the distribution network.

In order to simulate the distribution network as realistically as possible, the main characteristics of the load type in real systems in reference [3] are shown in Table 7.2.

Table 7-2 Load Type in Real System [3]

Load Type	System 1		System 2	
	MVA	%	MVA	%
Residential	20.96	38.61	47.10	32.0
Commercial	9.53	17.56	67.71	46.0
Industrial	20.54	37.84	26.49	18.0
Public Lighting	3.25	5.99	5.91	4.0

Due to the percentage of commercial loads being too high, the load distribution which is represented by system 1 in Table 7.2 is more common. Thus, the characteristics of the load type in system 1 are chosen as the load distribution in the following test system.

In the following test, the mixed load harmonic spectrum of commercial and residential is expressed by the data of house 1 and the transformer combined respectively in Table 7.1. Public lighting is assumed as a linear load at present. However, modern low power factor lighting such as light-emitting diodes may replace current lighting in the future. Although low power factor lighting offers better performance with less energy consumption, its harmonic emission can be much higher. Its harmonic spectrums are shown in Table 7.3. Due to the high power consumption and the centralised location, the harmonic filter is assumed to be applied to the industrial loads. In such a case, industrial loads might only have a very small effect on harmonics injections. Therefore, the industrial load is treated as the linear load.

Table 7-3 Harmonic Spectrum of Low Power Factor Lighting [4]

Harmonic No.	Low PF Lighting	Harmonic No.	Low PF Lighting
	Magnitude (% Fund)		Magnitude (% Fund)
1	100	9	41
3	75	11	30
5	63	13	18
7	52		

7.2.3 Objectives

The primary objective of the distribution network reconfiguration is to achieve a network loss reduction, as referred to in Section 2.21. Furthermore, some limitation standards for the distribution network also need to be satisfied. In Section 3.2.5, the IEEE harmonic distortion limit standard for the distribution network indicates that the total harmonic voltage distortion cannot exceed 5% and the harmonic voltage at a single harmonic order cannot exceed 3% of the rated voltage. Normally, the lowest voltage magnitude must exceed 0.9 p.u. [3]. Due to distribution lines generally having a maximum branch current capacity, the change of branch current should be noted.

7.3 Distribution Network Feeder Reconfiguration with Variable Harmonic Capacities and Distributed Generators

7.3.1 Scenarios

The nonlinear loads can be expected to increase in future. The U.S. Energy Information Administration's Annual Energy Outlook 2011 forecast electricity consumption trends for different load types for the residential and commercial markets for the years 2010-2035 [1]. Parts of the results of this forecast are shown in Table 7-4. This table indicates that in 2010 the proportion of the system harmonic injection current is about 40% and 44% in commercial and residential loads respectively. For the purposes of this forecast, it is assumed that existing incandescent light bulbs will have been replaced by 200W electronic lighting and twenty percent of households will own an electric vehicle. Thus, the following two conclusions are eliminated: if existing incandescent lightbulbs are not replaced and

the electric vehicle is not adopted, this proportion will increase to 48% and 50% of commercial and residential loads respectively in 2030; if the forecast for electronic lighting and electric vehicles proves to be accurate, this proportion will increase to 60% and 60% of commercial and residential loads respectively in 2030. Reference [1] provides a simplified way of estimating the harmonic injection currents of the utility systems in the year 2030. This simple method is to take the existing harmonic spectrums and multiply them by a factor to incorporate the anticipated growth in power electronic loads. This factor is equal to the proportion of nonlinear loads in 2030 divided by this proportion in 2010. For example, the harmonic injection current spectrum factor in 2030, assuming the spread of electronic lighting and electric vehicles can be calculated as being 60%/40% = 1.5.

Table 7-4 Projection of the Proportion of Power Electronics-Based Loads in Residential and Commercial Categories [1]

Load Categories	2010 Actual	2030 Projection	
		Excluding Electronic Lighting and Drives	Including Electronic Lighting and Drives
Commercial	40%	48%	60%
Residential	44%	50%	60%

According to the projection assumptions made in the reference [1], the load type of the real system in Table 7-3 and the renewable energy power development in section 7.1, the scenarios in this chapter can be modelled and are shown in Tables 7-5 to 7-11.

Table 7-5 Scenario One

Load Type	Power Demands % of Total	Proportion of Power Electronics-Based Loads on One Bus (2010)
Residential	39%	0
Commercial	17%	0
Industrial	38%	0
Public Lighting	6%	0
Generator Type	**Power Capacities % of Total**	**Treat Generators as Harmonic Source (2010)**
Wind Turbine	0	No
Photovoltaic Array	0	No

This scenario assumes that distributed generators cannot be connected to the distribution system. The system harmonic is ignored. The results of this scenario are used for comparison with others for investigating the impact of the system harmonics or the distributed generators.

Table 7-6 Scenario Two

Load Type	Power Demands % of Total	Proportion of Power Electronics-Based Loads on One Bus (2010)
Residential	39%	0
Commercial	17%	0
Industrial	38%	0
Public Lighting	6%	0
Generator Type	**Power Capacities % of Total**	**Treat Generators as Harmonic Source (2010)**
Wind Turbine	7%	No
Photovoltaic Array	3%	No

Table 7-7 Scenario Three

Load Type	Power Demands % of Total	Proportion of Power Electronics-Based Loads on One Bus (2030)
Residential	39%	0
Commercial	17%	0
Industrial	38%	0
Public Lighting	6%	0
Generator Type	Power Capacities % of Total	Treat Generators as Harmonic Source (2030)
Wind Turbine	28.5%	No
Photovoltaic Array	10%	No

In scenario two and three, distributed generators can be connected to the distribution system but system harmonic is ignored. The results of these two scenarios are used for comparison with others for investigating the impact of the distributed generators.

Table 7-8 Scenario Four

Load Type	Power Demands % of Total	Proportion of Power Electronics-Based Loads on One Bus (2010)
Residential	39%	44%
Commercial	17%	40%
Industrial	38%	0
Public Lighting	6%	0
Generator Type	Power Capacities % of Total	Treat Generators as Harmonic Source (2010)
Wind Turbine	0	No
Photovoltaic Array	0	No

In scenario four, the system harmonic is considered, however the distributed

generators are not connected to the network. The results of this scenario are used for comparison with others for investigating the impact of the system harmonics in a different harmonic capacity.

Table 7-9 Scenario Five

Load Type	Power Demands % of Total	Proportion of Power Electronics-Based Loads on One Bus (2010)
Residential	39%	44%
Commercial	17%	40%
Industrial	38%	0
Public Lighting	6%	0
Generator Type	Power Capacities % of Total	Treat Generators as Harmonic Source (2010)
Wind Turbine	7%	Yes
Photovoltaic Array	3%	Yes

Table 7-10 Scenario Six

Load Type	Power Demands % of Total	Proportion of Power Electronics-Based Loads on One Bus (2030) Excluding Electronic Lighting and Drives
Residential	39%	50%
Commercial	17%	48%
Industrial	38%	0
Public Lighting	6%	0
Generator Type	Power Capacities % of Total	Treat Generators as Harmonic Source (2030)
Wind Turbine	28.5%	Yes
Photovoltaic Array	10%	Yes

Table 7-11 Scenario Seven

Load Type	Power Demands % of Total	Proportion of Power Electronics-Based Loads on One Bus (2030) Including Electronic Lighting and Drives
Residential	39%	60%
Commercial	17%	60%
Industrial	38%	0
Public Lighting	6%	100%
Generator Type	Power Capacities % of Total	Treat Generators as Harmonic Source (2030)
Wind Turbine	28.5%	Yes
Photovoltaic Array	10%	Yes

In scenario five, six and seven, distributed generators connect to the distribution system and the system harmonic is considered.

The load entered in reference [3] only indicates the proportion. Thus, according to these proportions, the load distribution in the 118-bus distribution system is assumed and illustrated in Figure 7.5 and Table 7-12. The assumed locations of the wind and solar power plants are also shown in Table 7-12.

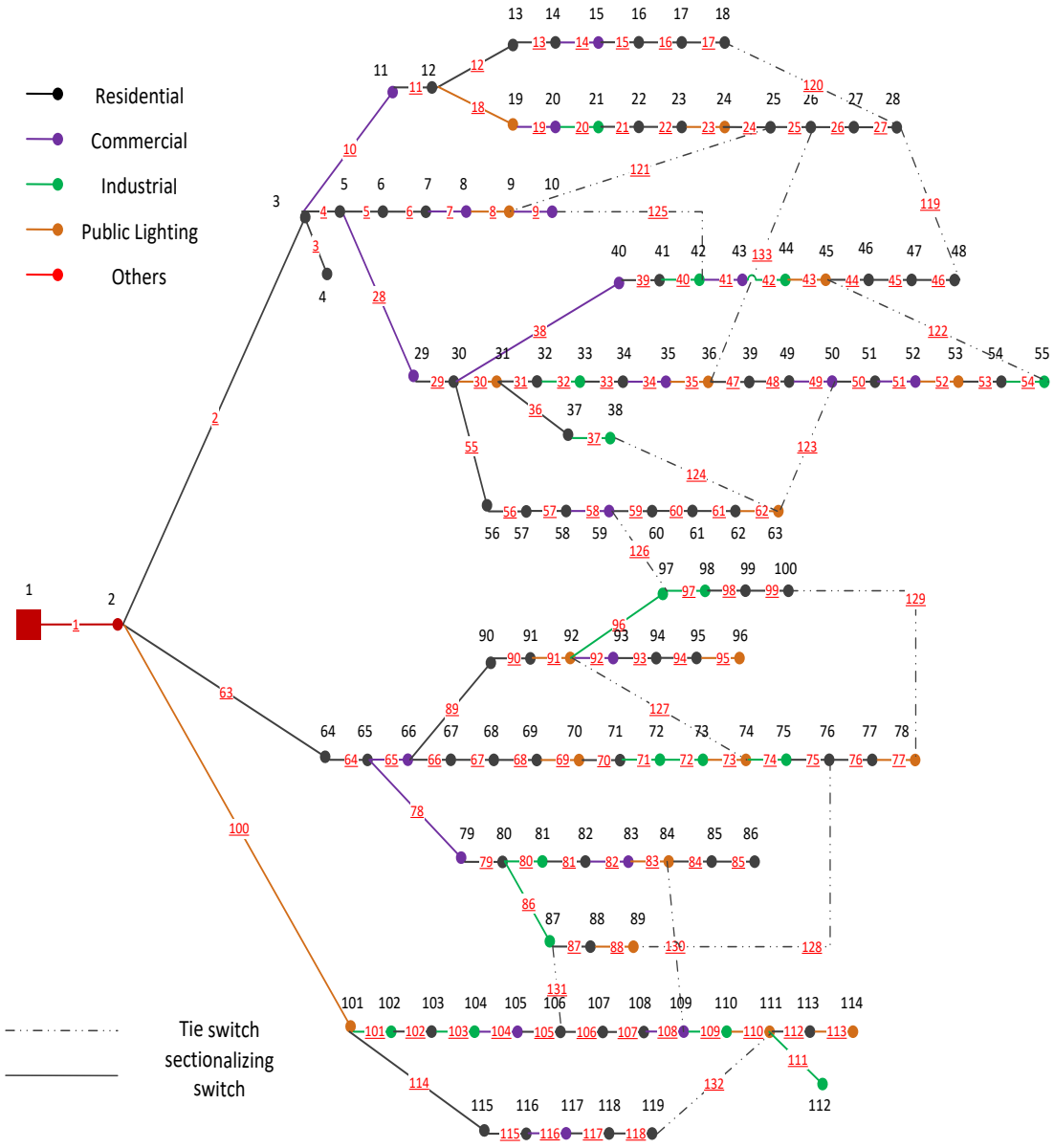

Figure 7-5 Loads distribution in the 118-bus system

Table 7-12 Loads Distribution in the 118-Bus Distribution System

Load Type	Power Demands (kW)	Bus Number of the Location
Whole System	22709.72(100%)	1-119
Residential	8857.274(39%)	3-7,12-14,16,17,19,22,23, 25-28,30,32,34,37,41,46-49, 51,54,56-58,60-62,64, 65,67-69,71,76,77,80,82,85, 86,90,91,94,95,99,100,103, 106-108,113,115,116,118,119
Commercial	3862.95(17%)	8,10,11,15,20,29,35,40,43,50, 52,59,66,79,83,93,105,109,117
Industrial	8622.06(38%)	21,33,38,42,44,55,72,73,75, 81,87,97,98,102,104,110,112
Public Lighting	1367.436(6%)	9,18,24,31,36,45,53,63,70,74, 78,84,89,92,96,101,111,114
Generator Type	Power Capacities (kW)	Bus Number of the Location
Wind Turbine	1589.68(7%)	49 (800kW),73 (789.68kW)
	6472.27(28.5%)	49(3000kW),73(2000kW), 26(1472.27kW)
Photovoltaic Array	681.29(3%)	109(681.29kW)
	2271.00(10%)	109(2271kW)

All above scenarios also comply with the following assumptions:

a) All loads are assumed fully loaded.

b) The power capacities of the wind and solar generators are defined as power generation capacities. The locations of these generators are fixed.

c) These is no limitation on the maximum capacity of the distribution lines.

d) One 72 SWT-2.3-93 and one 54 PMSGs wind turbine connect to bus 49 and bus 73 respectively when the capacity of the wind generators is 7% of the total load demand. When the capacity of the wind generators is 28.5% of the total

load demand, two 72 SWT-2.3-93 wind turbines connect to bus 49 and bus 26 respectively. And one 54 PMSGs wind turbine connects to bus 73.

7.3.2 Results of Scenarios

a) Scenario one

Harmonic and distributed generators will not be taken into consideration in scenario one. The results of this scenario are used as a basis to make a comparison with the results of other scenarios. The sample network loss in the 118-bus system is 1298.1 kW, which is 5.72% of the total active power demand. This percentage is a little higher than the average percentage of the distribution network loss in UK (5.5%)[10]. After feeder reconfiguration, the new tie switches for the minimum network power loss are 24, 27, 35, 40, 43, 52, 59, 72, 75, 96, 98, 110, 123, 130 and 131. The minimum network loss is 869.72kW which is 3.83% of the total active power demand. The network loss decreased 33%. Two bus voltage magnitude curves are shown in Figure 7-6.

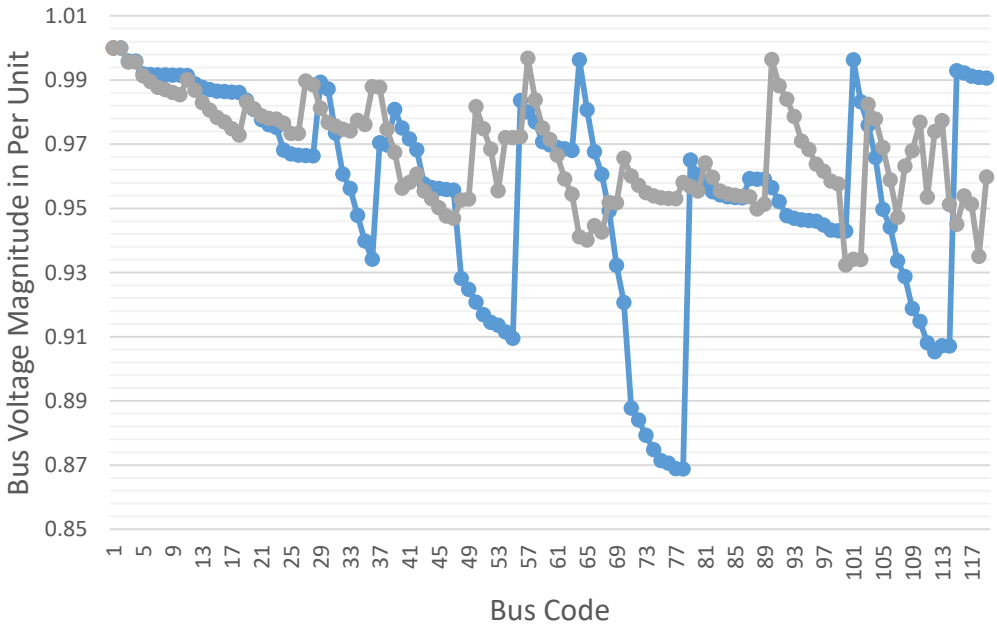

Figure 7-6 Bus voltage magnitudes comparison in per unit for scenario one

In Figure 7-6, the blue curve is the bus voltages distribution in the sample network and the grey one is the bus voltages distribution after feeder reconfiguration. The lowest voltage magnitude in the blue curve is 0.8688 per unit on bus 78. Due to the voltage magnitude limitation in the distribution network being 0.9 per unit, the bus voltage from bus 71 to bus 78 cannot satisfy the voltage limitation. Thus, these bus voltages should be faults in the sample network. The lowest voltage magnitude in the grey curve is 0.9323 per unit on bus 100. The average voltage magnitude is increased from 0.9559 per unit to 0.9673 per unit. It can therefore be seen that the feeder reconfiguration has improved the voltage drop and the bus voltage faults in the sample network are removed after feeder reconfiguration in this case. Two curves which represent the branch currents magnitude before and after feeder reconfiguration are shown in Figure 7-7.

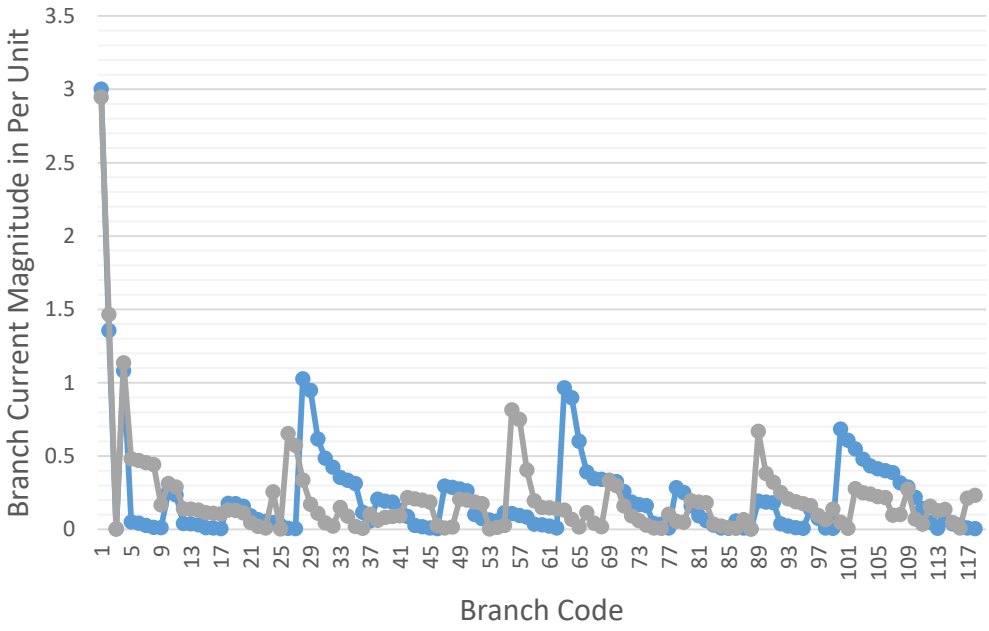

Figure 7-7 Branch current comparison in per unit for scenario one

In Figure 7-7, the blue curve is the branch currents magnitude distribution in the

sample network and the grey one is the branch currents magnitude distribution after feeder reconfiguration. Figure 7-7 demonstrates that branch currents can experience large changes after reconfiguration. Thus, if the maximum capacity of these branches cannot satisfy this change, additional power cables are needed or the solution for feeder reconfiguration must be changed.

b) Scenario two

In this scenario, distributed generators are connected to the network. According to the reference [5, 6], about 7% and 3% of EU electricity demand were provided by wind power and solar energy respectively in 2012. Thus, the capacity of the wind and solar distributed generators are 7% and 3% respectively in this scenario. In light of these results, this scenario could be taken as representative of the impact of renewable generators in the EU in 2012 across a distribution network.

When the capacity of the wind and solar generators are 7% and 3% of total load demand, the sample network loss is 1185kW which is 5.22% of the total active power demand. After reconfiguring the network, the new tie switches are 24, 40, 43, 53, 59, 72, 75, 86, 96, 98, 108, 110, 120, 123 and 133. The minimum network loss is 718.17kW which is 3.16% of the total active power demand. The network loss decreased 39.4%. The two bus voltage magnitude curves are shown in Figure 7-8.

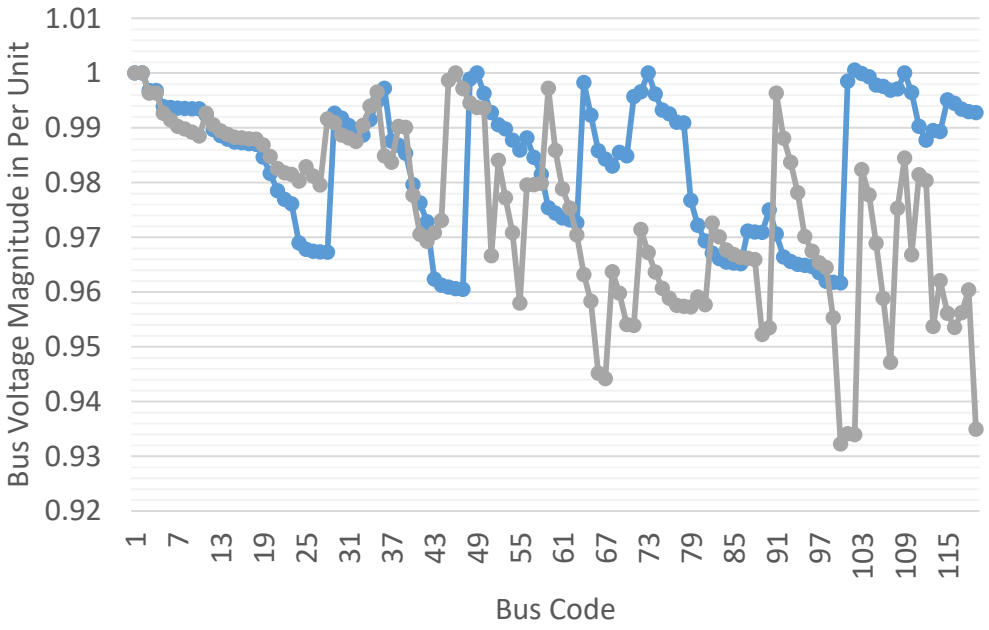

Figure 7-8 Bus voltage magnitude comparison in per unit for scenario two

In Figure 7-8, the blue and the grey curves are the bus voltages distribution in the sample network and the reconfigured network respectively. The lowest voltage magnitude in the blue curve is 0.9605 per unit on bus 47. The lowest voltage magnitude in the grey curve is 0.9022 per unit on bus 100. In this scenario, the voltage drop is worse after the feeder reconfiguration. However, the lowest bus voltage is still larger than 0.9 per unit. Therefore, despite the bus voltage performing worse following the network reconfiguration, the suggested solution in this scenario is still acceptable. The average bus voltage magnitude decreases from 0.9837 per unit to 0.9749 per unit. The feeder reconfiguration therefore has a negative impact on the voltage drop in this case. Two curves which represent the branch currents magnitude before and after the feeder reconfiguration for scenario two are shown in Figure 7-9.

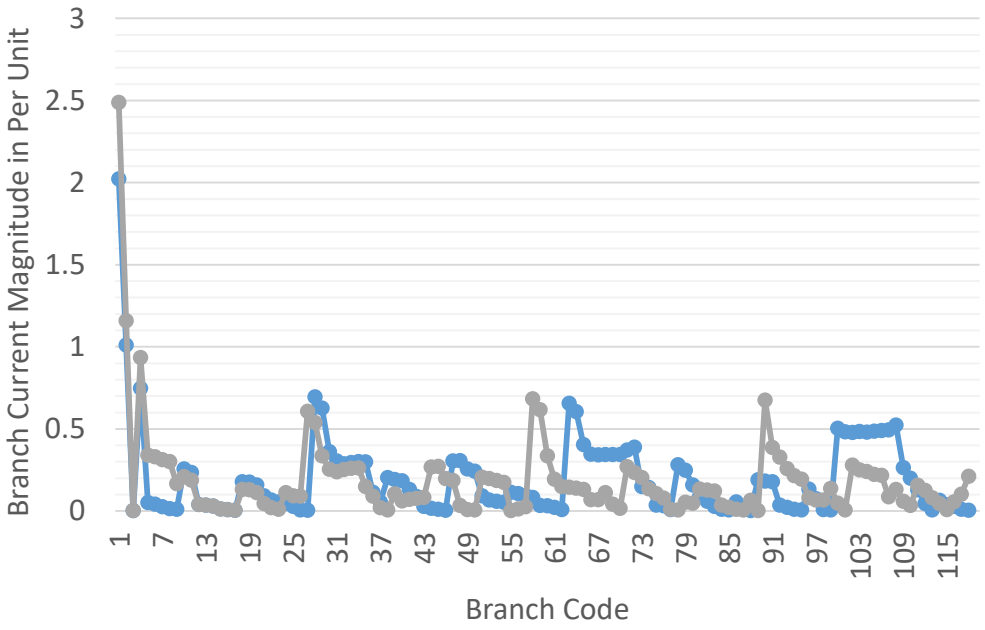

Figure 7-9 Branch current comparison in per unit for scenario two

In Figure 7-9, the blue curve is the branch currents magnitude distribution in the sample network and the grey one is the branch currents magnitude distribution after network reconfiguration. Figure 7-9 demonstrates that branch currents experience a reduction on most parts of the branches. If 1.0 per unit is the maximum capacity of the normal distribution line, only two distribution lines on branches 1 and 2 need additional power cables.

c) Scenario three

According to the reference [5, 6], the EU specifies that 28.5% and 10% of its electricity demand must be provided by wind power and solar power respectively by 2030. Therefore, scenario three assumes a capacity of 28.5% and 10% for wind and solar distributed generators respectively.

When the capacity of the wind and solar generators are 28.5% and 10% of the total load demand, the sample network loss is 484.42kW, which is 2.13% of the total

active power demand. After finishing the feeder reconfiguration, the new tie switches are 23, 33, 40, 47, 75, 86, 96, 107, 120, 121, 122, 124, 127, 129 and 130. The minimum network loss is 352.6kW which is 1.55% of the total active power demand. The network loss decreased 27.2%. Two curves of buses voltage magnitudes are shown in Figure 7-10.

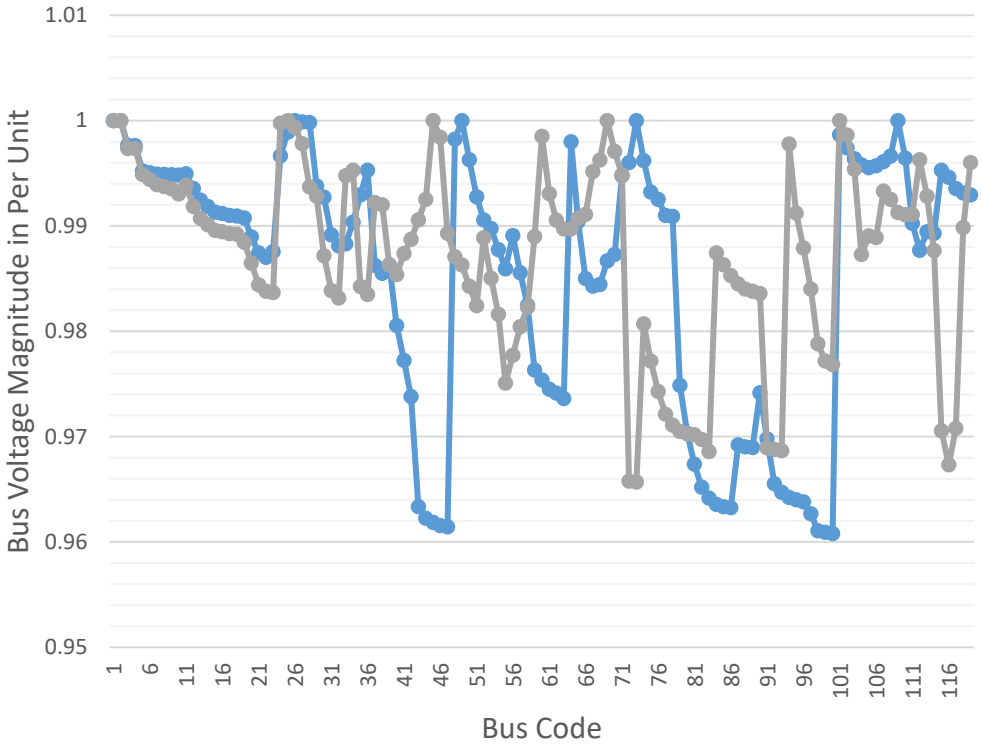

Figure 7-10 Bus voltage magnitude comparison in per unit for scenario two

In Figure 7-10, the blue and grey curves are the bus voltages distribution in the sample network and reconfigured network respectively. The lowest voltage magnitude in the blue curve is 0.9608 per unit on bus 100. The lowest voltage magnitude in the grey curve is 0.9656 per unit on bus 73. The values of the average bus voltage magnitude and the lowest voltage magnitude on the sample system and reconfigured system are almost the same. In this case, the feeder reconfiguration does not have much influence on the bus voltage drop.

Two curves which represent the branch currents magnitude before and after feeder reconfiguration for scenario three are shown in Figure 7-11.

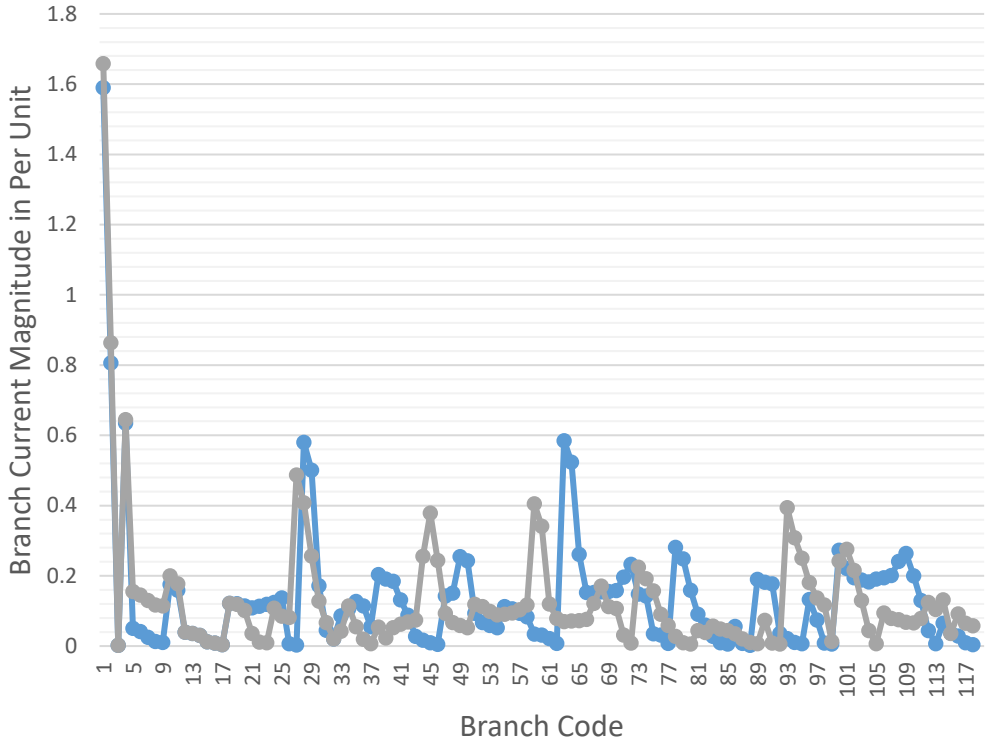

Figure 7-11 Branch current comparison in per unit for scenario two

In Figure 7-1, the blue curve is the branch currents magnitude distribution in the sample network and the grey one is the branch currents magnitude distribution after feeder reconfiguration. Conclusions regarding branch currents in such a case are similar to those reached for scenario two.

d) Scenario four

Harmonic analysis is considered in this scenario. It is assumed that distributed generators are not connected to the network. In Table 7-4, the proportion of power electronics-based loads on residential and commercial loads was about 44% and 40% respectively in 2010. Thus, the performance of a distribution network without

distributed generators in 2010 can be represented by this case.

After considering the system harmonic, the sample network loss for this scenario is 1309.90kW which is 5.77% of the total active power demand. After finishing the feeder reconfiguration, the new tie switches are 24, 27, 35, 40, 43, 52, 59, 72, 75, 96, 98, 110, 123, 130 and 131. The minimum network loss is 877.36kW which is 3.86% of the total active power demand. The network loss decreased 33.02%. Two bus voltage magnitude curves are shown in Figure 7-12.

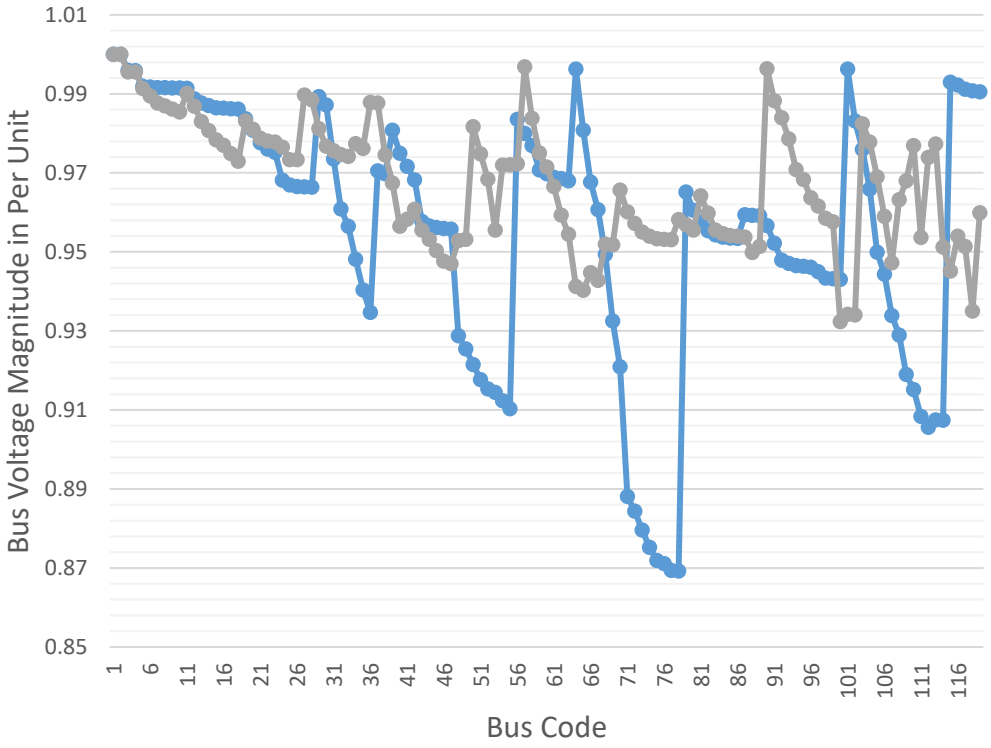

Figure 7-12 Bus voltage magnitude comparison in per unit for scenario four

In Figure 7-12, the blue and grey curves are the bus voltages distributions in the sample network and reconfigured network respectively. The lowest voltage magnitude in the blue curve is 0.8693 per unit on bus 78. The bus voltage faults on bus 71 to bus 78 are still in the sample network. It demonstrates that the impact of system harmonics on bus voltage is slight. The lowest voltage magnitude in the

grey curve is 0.9324 per unit on bus 100. The average voltage magnitude increases from 0.9561 per unit to 0.9674 per unit. Two curves which represent the branch currents magnitude before and after the feeder reconfiguration in scenario four are shown in Figure 7-13.

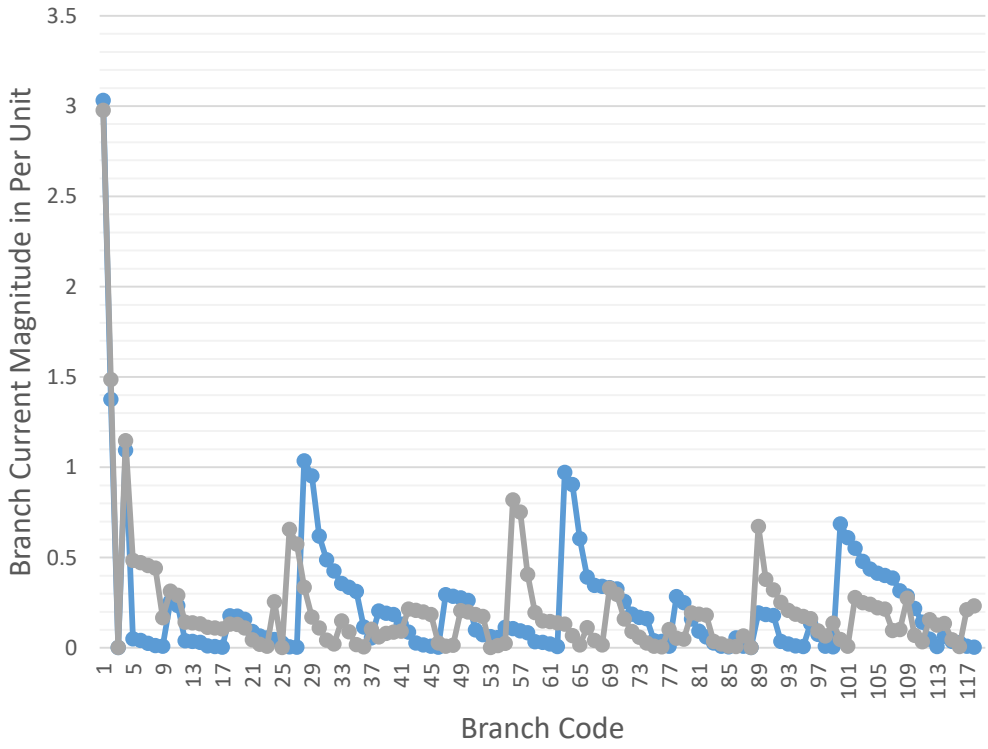

Figure 7-13 Branch current comparison in per unit for scenario four

Due to the difference between this scenario and scenario one being that the harmonic impact on residential and commercial loads is considered, the results of bus voltages and branch currents are similar to those derived in scenario one.

Figure 7-14 shows the value of the total harmonic voltage distortion on each bus. The blue bars and orange bars represent the sample and reconfigured networks in scenario four respectively. The largest value of the total harmonic voltage distortion is 4.37% on bus 55 in the sample system and 2.02% on bus 68 in the reconfigured system respectively. The largest percentage value of the harmonic

voltage on single harmonic order is 2.71% on bus 55 at the 5th harmonic order in the sample system and 1.30% on bus 68 at the 5th harmonic order in the reconfigured system respectively. The largest percentage value of the total harmonic voltage distortion and the harmonic voltage on the single harmonic order in both systems satisfy the IEEE-519 harmonic voltage limits for public power systems. It can be seen that the total harmonic voltage distortion experiences a significant reduction after feeder reconfiguration in this test.

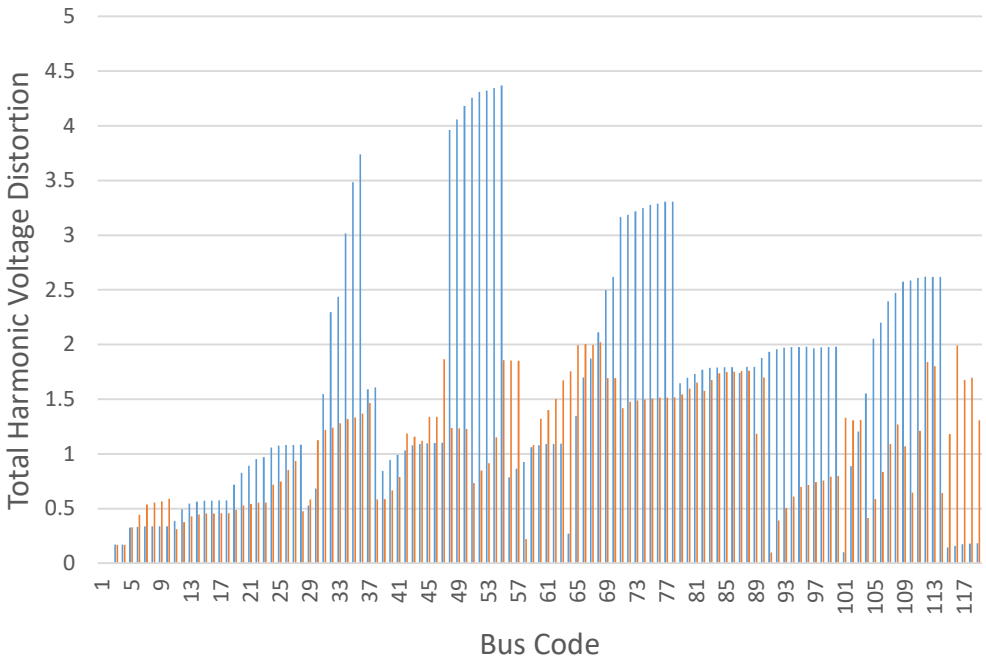

Figure 7-14 Total harmonic voltage distortion for scenario four

e) Scenario five

This scenario is the harmonic analysis based on the data provided for renewable generators in 2012 and the data provided for proportion of power electronics-based loads in 2010. The details of this data are provided in Table 7-9. The sample network loss for this scenario is 1195.20kW which is 5.26% of the total active power demand. After finishing the feeder reconfiguration, the new tie switches are

23, 40, 43, 53, 59, 72, 75, 86, 96, 98, 108, 110, 120, 123 and 133. The minimum network loss is 723.1kW which is 3.18% of the total active power demand. The network loss decreased 39.5%. Two bus voltage magnitude curves are shown in Figure 7-15.

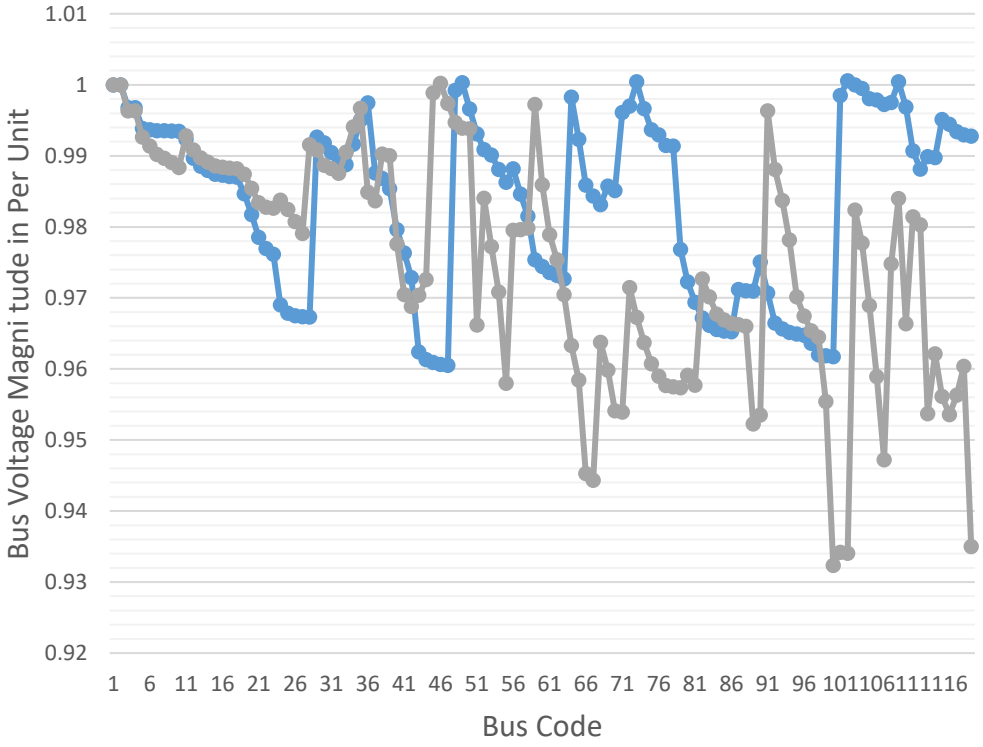

Figure 7-15 Bus voltage magnitude comparison in per unit for scenario five

In Figure 7-15, the curves convey the same meaning as set out in the previous scenarios for bus voltage magnitude comparison. The lowest voltage magnitude in the blue curve is 0.9605 per unit on bus 47. The lowest voltage magnitude in the grey curve is 0.9323 per unit on bus 100. The average voltage magnitude increases from 0.9838 per unit to 0.9750 per unit. Although the difference between this scenario and scenario two being that the harmonic impact is considered, the performance of the buses' voltage drop on the reconfigured system is better than its performance in scenario two. The branch currents in these two scenarios are

similar. The curves which represent the branch currents magnitude before and after feeder reconfiguration for scenario five are shown in Figure 7-16.

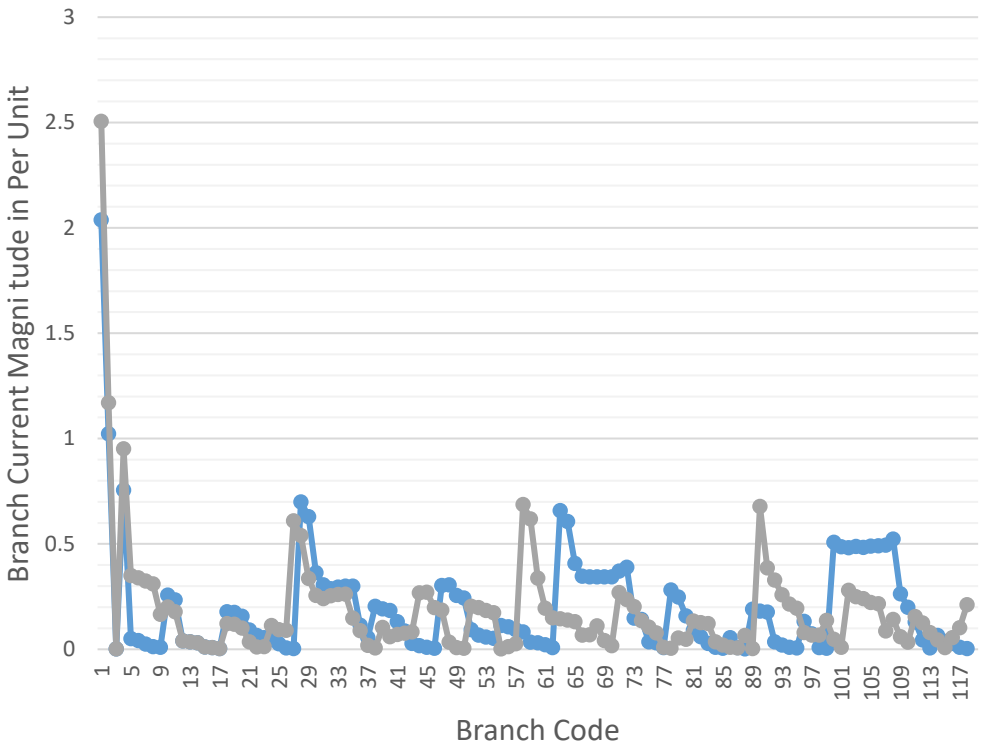

Figure 7-16 Branch current comparison in per unit for scenario four

Figure 7-17 is the value of the total harmonic voltage distortion on each bus. The blue bar and orange bar represent the sample system and the reconfigured system in scenario five respectively. The largest value of the total harmonic voltage distortion is 3.02% on bus 79 in the sample system and 2.00% on bus 51 in the reconfigured system respectively. The largest percentage value of the harmonic voltage on single harmonic order is 2.01% on bus 109 at the 5^{th} harmonic order in the sample system and 1.32% on bus 46 at the 5^{th} harmonic order in the reconfigured system respectively. The largest percentage value of the total harmonic voltage distortion and the harmonic voltage on the single harmonic order

in both systems satisfy the IEEE-519 harmonic voltage limits in this test. Moreover, the total harmonic voltage distortion is reduced following the feeder reconfiguration in this test.

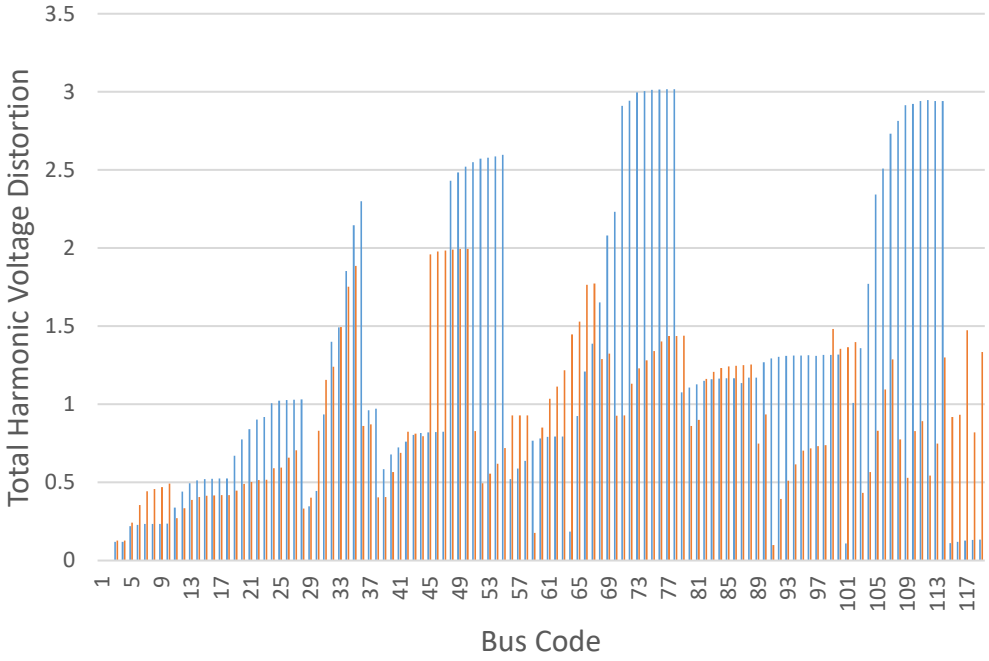

Figure 7-17 Total harmonic voltage distortion for scenario five

f) Scenario six

This scenario is the feeder reconfiguration taking into consideration the harmonic based on forecast data for proportion of power electronics-based loads in 2030. The details of this data are provided in Table 7-10. Due to electronic lighting and electric vehicle chargers being excluded in this case, the proportion of power electronics-based loads on residential and commercial loads is 50% and 48% respectively. The sample network loss for this scenario is 488.58kW, which is 2.15% of the total active power demand. After finishing the feeder reconfiguration, the new tie switches are 33, 40, 43, 54, 75, 86, 96, 107, 120, 121, 124, 127, 129, 130 and 133. The minimum network loss experienced by this network is 352.46kW,

which is 1.55% of the total active power demand. The network loss decreased 27.9%. Two bus voltage magnitude curves are shown in Figure 7-18.

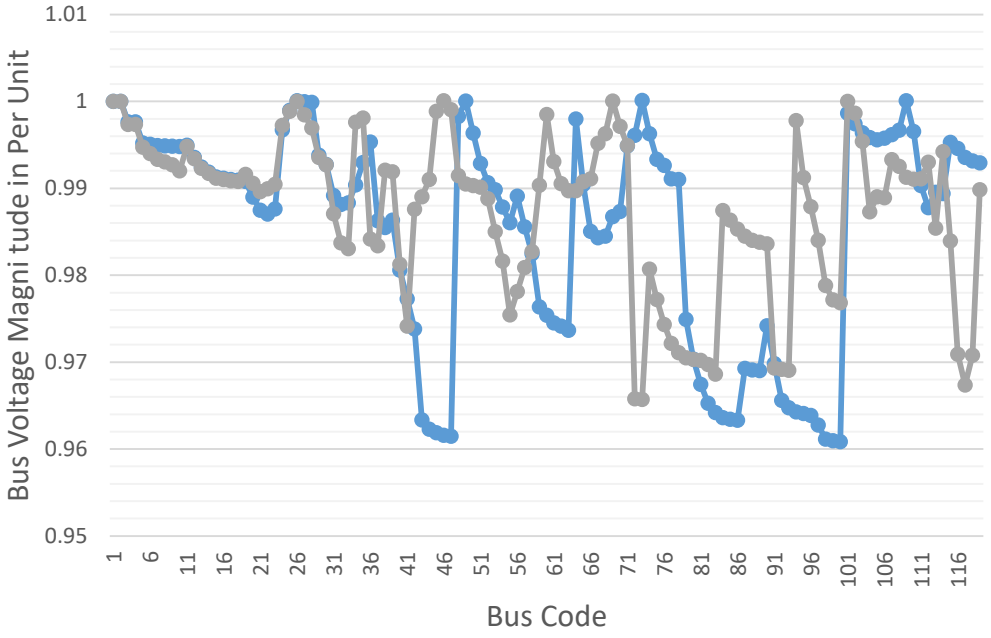

Figure 7-18 Bus voltage magnitude comparison in per unit for scenario six

In Figure 7-18, the curves convey the same meaning as set out in the previous scenarios for bus voltage magnitude comparison. The lowest voltage magnitude in the blue curve is 0.9609 per unit on bus 100. The lowest voltage magnitude in the grey curve is 0.9657 per unit on bus 73. The average voltage magnitude increases from 0.9854 per unit to 0.9876 per unit. In comparison with the bus voltage magnitudes distribution curves in figure 7-10, although the system harmonics are considered in this scenario, the bus voltage magnitudes curves and the branch currents magnitude distribution in scenario three and this scenario are similar.

Two curves to represent the branch currents magnitude before and after feeder reconfiguration for scenario six are shown in Figure 7-19.

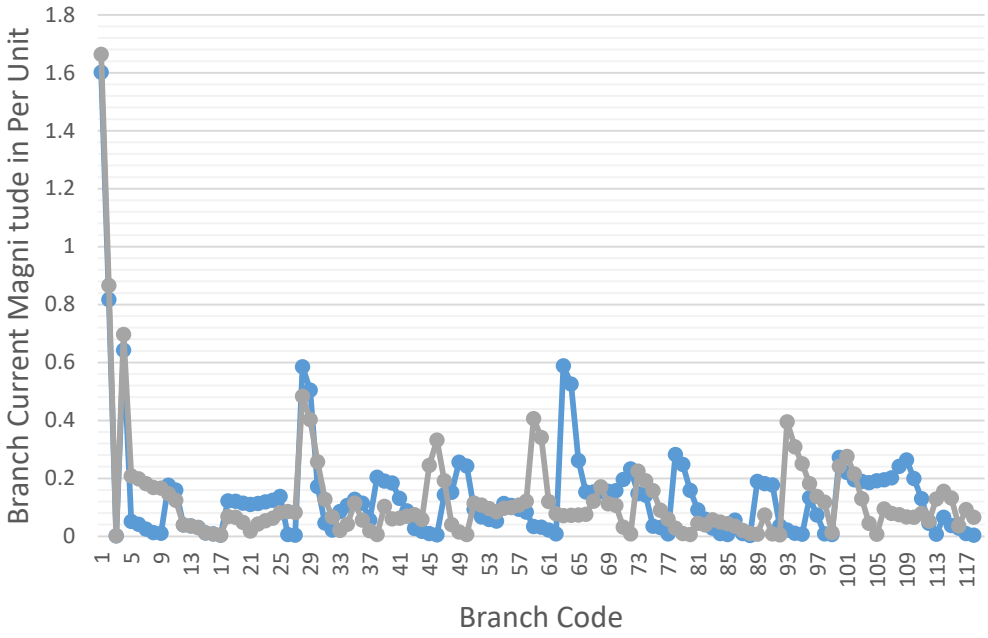

Figure 7-19 Branch current comparison in per unit for scenario four

Figure 7-20 is the value of the total harmonic voltage distortion on each bus. The blue bar and orange bar represent the sample system and the reconfigured system in scenario six respectively. The largest value of the total harmonic voltage distortion is 1.51% on bus 79 in the sample system and 1.18% on bus 47 in the reconfigured system respectively. The largest percentage value of the harmonic voltage on single harmonic order is 1.05% on bus 55 at the 5^{th} harmonic order in the sample system and 0.82% on bus 46 at the 5^{th} harmonic order in the reconfigured system respectively. The largest percentage value of the total harmonic voltage distortion and the harmonic voltage on the single harmonic order in both systems satisfy the IEEE-519 harmonic voltage limits. Although the performance of the total harmonic voltage distortion is improved, this test shows that no significant improvement is achieved as a consequence the feeder reconfiguration.

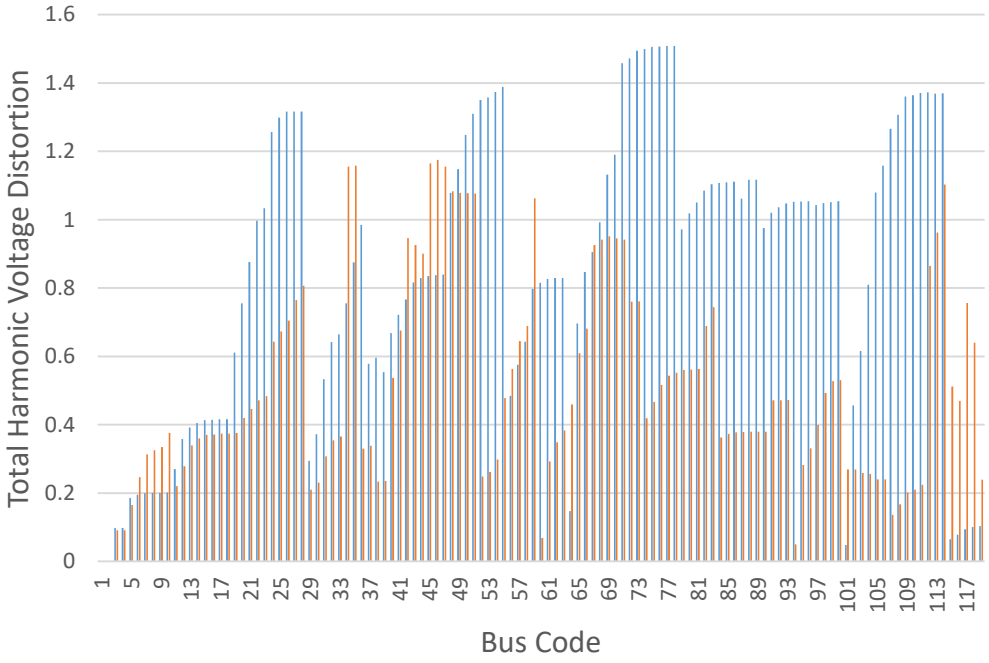

Figure 7-20 Total harmonic voltage distortion for scenario six

g) Scenario seven

As with scenario six, this case is also the feeder reconfiguration taking into consideration the harmonics based on forecast data for proportion of power electronics-based loads in 2030. The details of this data are provided in Table 7-11. The difference between this scenario and scenario six is that electronic lighting and electric vehicle chargers are included in this scenario. Moreover, it is assumed that public lighting will use low power factor lighting. Both residential and commercial loads are subject to a 60% increase in proportion of power electronics-based loads due to the inclusion of electronic lighting and electric vehicle chargers. Therefore, the sample network loss for this scenario is 675.25kW which is 2.24% of the total active power demand. After finishing the feeder reconfiguration, the new tie switches are 17, 23, 33, 39, 42, 58, 75, 98, 107, 110, 122, 124, 126, 127 and 131. The minimum network loss is 509.15kW which is 1.55% of the total active power

demand. The network loss decreased 24.6%. Two bus voltage magnitude curves are shown in Figure 7-21.

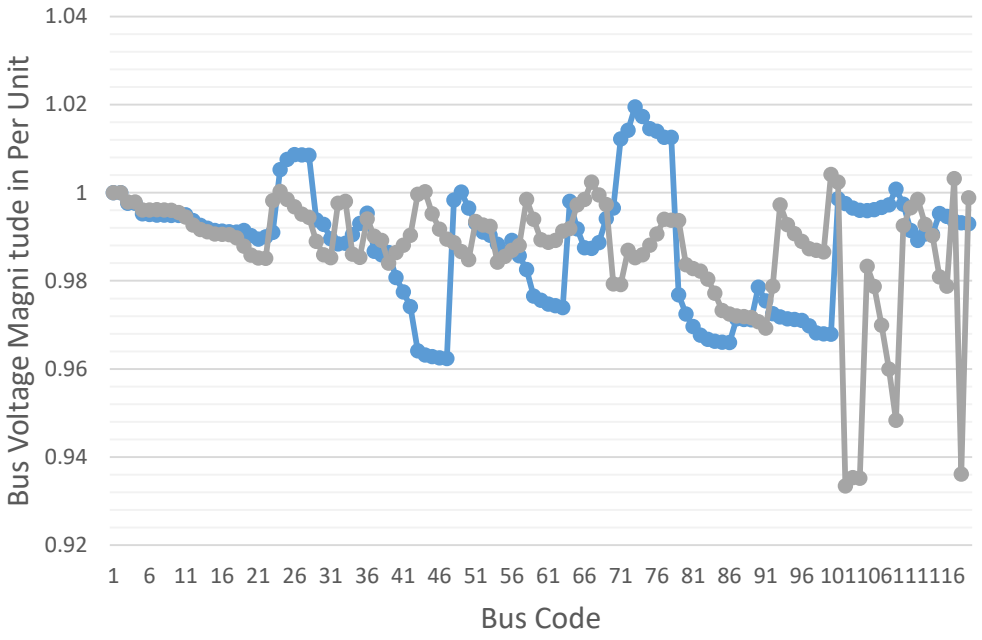

Figure 7-21 Bus voltage magnitude comparison in per unit for scenario six

In Figure 7-21, the curves convey the same meaning as set out in the previous scenarios for bus voltage magnitude. The lowest voltage magnitude in the blue curve is 0.9624 per unit on bus 47. The lowest voltage magnitude in the grey curve is 0.9335 per unit on bus 102. The average voltage magnitude increases from 0.9885 per unit to 0.9873 per unit. When Table 7-1 is compared with Table 7-3, each harmonic value associated with low power factor electric lighting displays a much greater percentage value than the value associated with normal residential and commercial loads. Thus, the bus voltage distribution curves in this case differ from the curves in Figure 7-18.

Two curves to express the branch currents magnitude before and after feeder reconfiguration for scenario seven are shown in Figure 7-22.

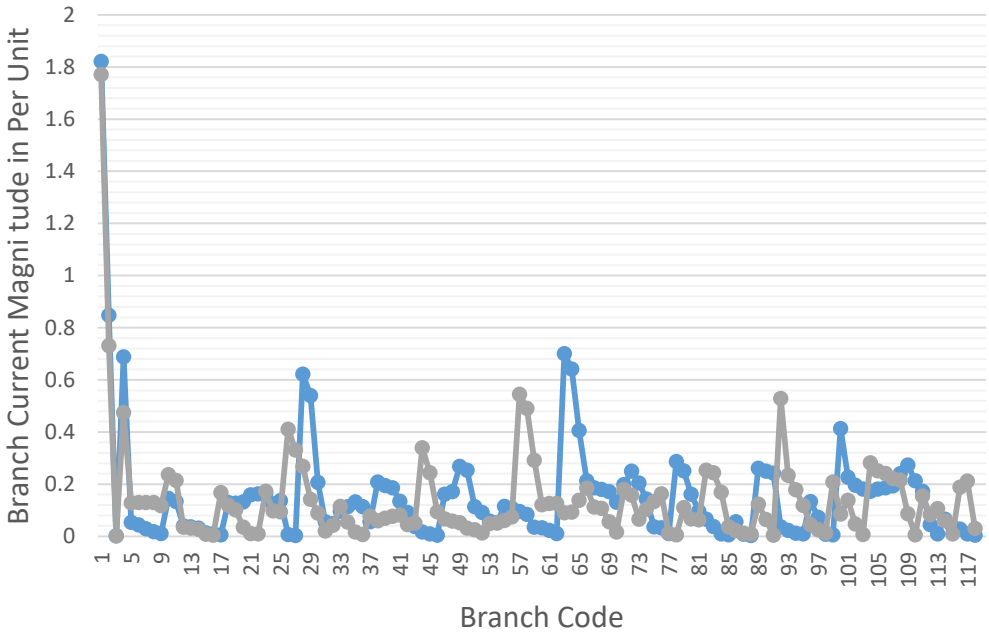

Figure 7-22 Branch current comparison in per unit for scenario four

Figure 7-23 is the value of the total harmonic voltage distortion on each bus. The blue bars and orange bars represent the sample system and the reconfigured system in scenario four respectively. The largest value of the total harmonic voltage distortion is 21.02% on bus 79 in the sample system and 9.75% on bus 93 in the reconfigured system respectively. The largest percentage value of the harmonic voltage on single harmonic order is 12.19% on bus 78 at the 7^{th} harmonic order in the sample system and 5.46% on bus 92 at the 7^{th} harmonic order in the reconfigured system respectively. Even though the largest percentage value of the total harmonic voltage distortion and the harmonic voltage on the single harmonic order in both systems show significant improvements following the feeder reconfiguration, results still cannot satisfy the IEEE-519 harmonic voltage limits. Figure 7-23 provides evidence of an improvement of such significance. Hence, the positive impact of the feeder reconfiguration for loss reduction on the total harmonic voltage distortion can be proved by above three scenarios.

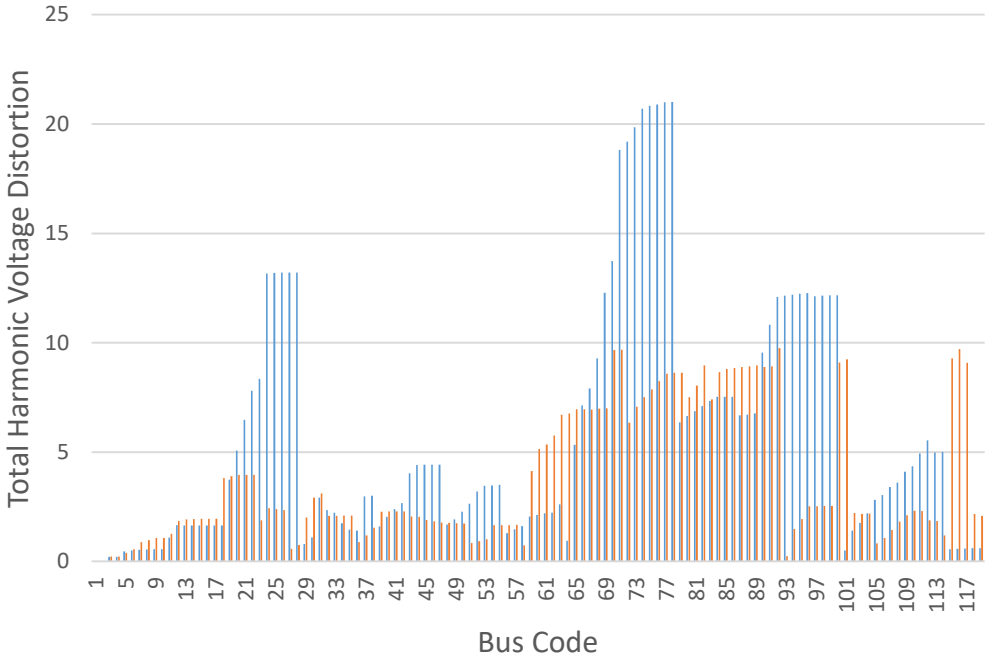

Figure 7-23 Total harmonic voltage distortion for scenario seven

7.3.3 Results Summary and Discussions

The results of the bus voltage, branch current, minimum network loss and total harmonic voltage distortion for seven scenarios are shown in above section. These scenarios include the fundamental and harmonic analysis for the same distribution network with or without renewable generators. By comparing the results between these scenarios, the impact of renewable generators and system harmonics can be investigated.

a) Minimum network loss

In order to facilitate comparisons, results from scenarios concerning the minimum network loss are expressed in Table 7-13.

Table 7-13 Comparisons of Minimum Network Loss

Scenario	Network Loss(kW)			New Tie Switches
	Original System	Reconfigured System	% Loss Reduction	
1	1298.1	869.72	33.0%	24, 27, 35, 40, 43, 52, 59, 72, 75, 96, 98, 110, 123, 130, 131
2	1185	718.17	39.4%	24, 40, 43, 53, 59, 72, 75, 86, 96, 98, 108, 110, 120, 123, 133
3	484.42	352.6	27.2%	23, 33, 40, 47, 75, 86, 96, 107, 120, 121, 122, 124, 127, 129, 130
4	1309.90	877.36	33.0%	24, 27, 35, 40, 43, 52, 59, 72, 75, 96, 98, 110, 123, 130,131
5	1195.20	723.1	39.5%	23, 40, 43, 53, 59, 72, 75, 86, 96, 98, 108, 110, 120, 123, 133
6	488.58	352.46	27.9%	33, 40, 43, 54, 75, 86, 96, 107, 120, 121, 124, 127, 129, 130, 133
7	675.25	509.15	24.6%	17, 23, 33, 39, 42, 58, 75, 98, 107, 110, 122, 124, 126, 127, 131

In this table, scenarios 1, 2 and 3 are the results of the feeder reconfiguration with variable renewable generator capacity. All of these scenarios ignore the system harmonic. Thus, the impact of the distributed renewable generators on the feeder reconfiguration problem can be determined. In scenario 2, the capacity of the distributed generators is the 10% of the total load demand which represents an EU distribution network in 2012. With 10% of the load demand supplied by the distributed generators locally, the network loss in the sample network is reduced by 8.7%, and the network loss in the reconfigured network is reduced by 44.7%. In scenario 3, the capacity of the renewable generators is the 38.5% of the total

load demand which represents an EU distribution network in 2030. The network loss of the sample network and the reconfigured network is reduced by 62.7% and 72.8% respectively after the distributed generators are connected to the network. Thus, it can be seen that the network loss is reduced by installing distributed generators in the distribution network. Furthermore, the increase in the installed distributed generator capacity does not lead to a linear network loss reduction. A suitable distributed generator capacity can maximise the reduction of the network loss at a reasonable cost. Also, the new tie switches for the reconfigured network are totally different in these three scenarios. If the reconfigured network for scenario 2 is used in scenario 3, the network loss will be 589.85kW. This network loss is even larger than the network loss in the sample system (484.42kW). It indicates that the network structure must be reconfigured to minimise the network loss when the capacity of the distributed generators is changed. Therefore, the network should be analysed and reconfigured again whenever the distributed generator capacity is changed, with the goal of minimising the network loss.

According to the forecast data in the references [5, 6], the impact of the system harmonic is taken into account in scenario 4 to scenario 7. The impacts of the system harmonics in the scenario 1 test system are investigated in scenario 4. When the results of these two scenarios are compared, it can be seen that the sample network in scenario 4 experiences slightly larger network losses than is seen in scenario 1. This suggests that the system harmonic will increase the network loss. The new tie switches in scenario 1 and scenario 4 are identical. The results demonstrate that when proportion of power electronics-based loads in residential and commercial loads are subjected to 44% and 40% respectively, this has no influence on the feeder reconfiguration solution in this test system. However, the sample network loss is increased when taking into consideration system harmonics.

Similarly to scenario 4, scenario 5 also investigates the impact of the system

harmonics in the same test system. When the results of scenarios 2 and 5 are compared, the network loss reduction percentages differ slightly. Furthermore, the new tie switches between the two scenarios are also different. If the new tie switches in scenario two are applied in scenario 5, the network loss will be 723.30kW, which is slightly greater than the calculated minimum network loss (723.1kW) in scenario 5. This suggests that the solution for the network loss reduction may be changed when the influence of the system harmonics is taken into consideration. In these two scenarios, when the impact of distributed generators is compared, the impact of the system harmonic is slight.

Scenarios 6 and 7 investigate the impact of the system harmonic based on the test system in scenario 3, which represents the system harmonic penetration of an EU distribution network in 2030. Due to the harmonic injection currents of low power factor lighting and electric vehicle chargers, which are significantly higher than residential and commercial loads, two different scenarios are tested. In scenario 6, the proportion of power electronics-based loads on residential and commercial loads is 50% and 48% respectively, and public lighting loads are linear. In scenario 7, the proportion of power electronics-based loads on both residential and commercial loads increases to 60%. In particular, low power factor bulbs are installed in all public lighting so that the proportion of power electronics-based loads on public lighting is 100%. Scenarios 3 and 6 exhibit similar results. Although the new tie switches are different, the minimum network loss gap between these two scenarios is minimal. On the other hand, large differences between the results of scenarios 3 and 7 can be seen. Due to more harmonic currents being injected into the distribution system, the network loss caused by the harmonics is increased. The sample network loss is increased from 484.42kW to 675.25kW. If the new tie switches in scenario 3 are applied in scenario 7, the network loss is 577.07kW. However, the minimum network loss in scenario 7 is 509.15kW. It can be seen that a further 12% network loss (67.92kW) can be

reduced by considering the system harmonic in scenario 7.

When Table 7-1 is compared with Table 7-3, it can be seen that the percentage value on each harmonic order of low power factor electric lighting is much higher than the value of residential and commercial loads. For example, the percentage of the 5^{th} harmonic order is 4.7%, 5.8% and 63% on residential, commercial and low power factor lighting respectively. Compared with low power factor electric lighting, the harmonic impact of residential and commercial loads is very small. Hence, the impact of the system harmonics in scenario 6 is much lower than its impact in scenario 7. In addition, the even and triple harmonics are ignored in these tests. Thus, if the even and triple harmonics are taken into consideration in these tests, the impact of the system harmonics will be greater. In cases where loads have a large harmonic injection, the feeder reconfiguration for loss reduction will be greatly influenced by the system harmonics. With power electronic devices expected to be used extensively in the future, the distribution network feeder reconfiguration problem must incorporate the impact of system harmonics.

b) Voltage magnitudes

When the system harmonic components are not large, the difference in bus voltage magnitudes is difficult to identify. The harmonic components of low power factor lighting are very large. Thus, the waveform of the root mean square (RMS) value of voltage magnitudes from the sample system in scenarios 3, 6 and 7 are illustrated in Figure 7-24. Due to the harmonic penetration of low power factor lighting and electric vehicle chargers being excluded in scenario 6, the voltage magnitude curves in blue and orange from scenario 3 and 6 almost coincide with each other. However, the parts of the waveform (grey) in scenario 7 are noticeably different. Figure 7-24 and Table 7-12 demonstrate that the differences between these waveforms can be explained by the buses which are present in public lighting loads. So, when the system harmonic components are large, the influence of the harmonic

voltage components cannot be ignored.

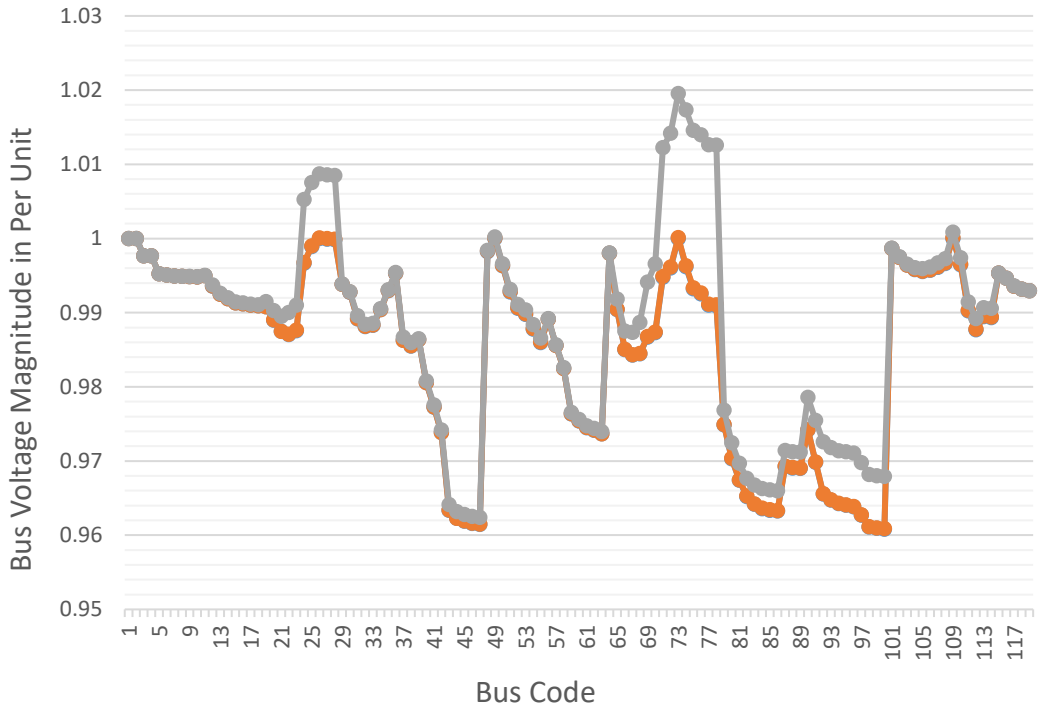

Figure 7-24 The impact of system harmonics on bus voltage magnitudes from scenarios 3, 6 and 7

Compared with the system harmonics, the impacts of the distributed generators on bus voltage magnitudes are great. The distributed generators are assumed to be located at the buses which are subject to heavy demand in the test distribution network. In this context, the only way to significantly improve the voltage drop is to install the distributed generators. The bus voltage magnitude distributions from scenarios 1, 2 and 3 are shown in Figure 7-25. The blue, orange and grey curves represent the bus voltage magnitude distribution in the sample test system of scenarios 1, 2 and 3 respectively. It can be seen that the buses with low voltage magnitude in scenario 1 are supported by the distributed generators and their value almost increase to the rated value. Although the capacity of the renewable

generators in scenario 3 is greater than their capacity in scenario 2, the increased capacity does not have a big impact on the improvement of the bus voltage drop. Thus, an appropriate location for the distributed generators can improve the voltage drop greatly in the distribution network.

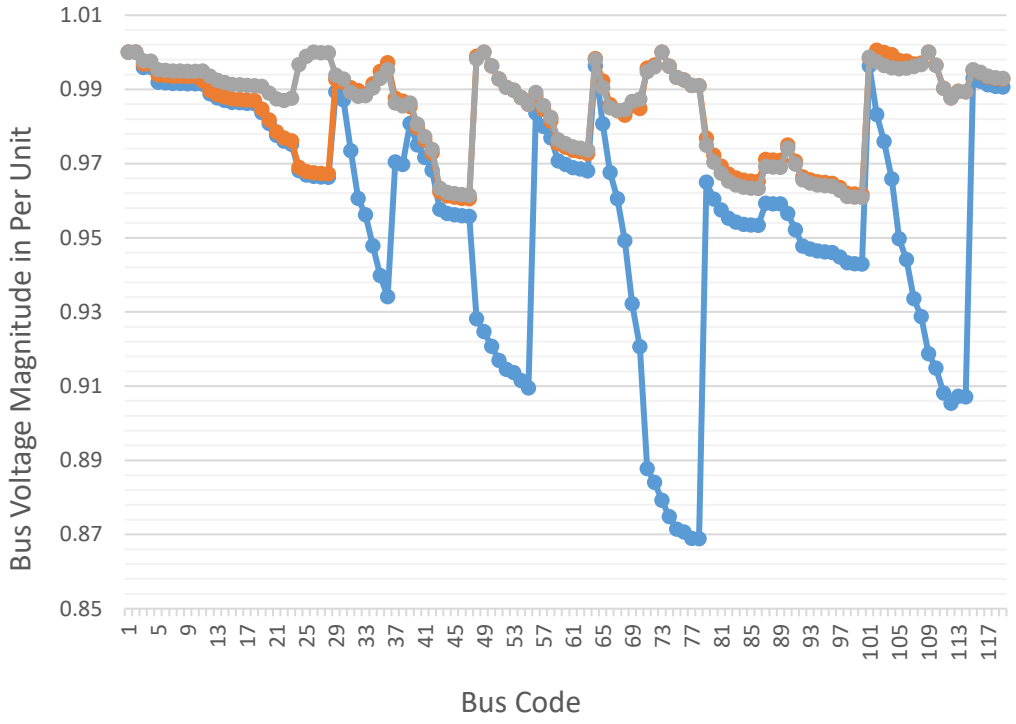

Figure 7-25 The impact of distributed generator on bus voltage magnitudes

The limitation of the lowest voltage magnitudes in distribution is 0.9 [3]. From the results of all scenarios, all lowest bus voltage magnitudes are greater than 0.9 except scenario 1. Feeder reconfiguration for network loss reduction significantly improved the voltage drop in the test system without distributed generators. However the voltage drop may be worse in those systems which contain distributed generators. Thus, the conclusion that feeder reconfiguration for loss reduction must also improve the voltage performance is not established when distributed

generators are already connected to the network.

c) Total harmonic voltage distortion

The results of scenarios 4 to 7 demonstrate that the total harmonic voltage distortion value is improved in the reconfigured system. When scenario 4 is compared with the other scenarios which include harmonic, the distributed generators changes have no significant effect on the positive influence that the feeder reconfiguration for loss reduction exerts on the decreased value of the total harmonic voltage distortion. It is therefore reasonable to conclude that the feeder reconfiguration for loss reduction also improves the performance of the system total harmonic voltage distortion.

Due to the small harmonic components of residential and commercial loads, the total harmonic voltage distortion value in scenarios 4, 5 and 6 satisfy the IEEE-519 harmonic voltage limits for public power systems. However, Figure 7-23 demonstrates that the value of total harmonic voltage distortion on parts of the buses in neither the sample system nor the reconfigured system can satisfy the limitation when low power factor lighting and electric vehicle chargers are included in scenario 7. The maximum value of the harmonic voltage at the single harmonic order in both systems also fails to satisfy the limitation.

In order to investigate the impact of the feeder reconfiguration for loss reduction on total harmonic voltage distortion, the summary of bus numbers of total harmonic voltage distortion is shown is Table 7-14.

Table 7-14 The Summary of Numbers of Total Harmonic Voltage Distortion in Scenario Seven

Categories	Number of Buses	
	Original System	Reconfigured System
0 – 5%	72	81
5 – 10%	22	38
> 10%	25	0

In Table 7-14, the number of buses which satisfy the IEEE harmonic distortion limit standard is increased from 72 to 81. Following feeder reconfiguration, those buses whose value of total harmonic voltage distortion exceeds 10% disappear. Although 38 buses still exceed the limitation in the reconfigured system, the positive impact of the feeder reconfiguration on controlling the value of the total harmonic voltage distortion can be proved. It is worth noting that the objective of the feeder reconfiguration is loss reduction rather than harmonic distortion reduction. Results might improve if the objectives are changed to the reduction in value of total harmonic voltage distortion. The maximum value of the harmonic voltage at single harmonic order is also reduced from 0.122 per unit to 0.055 per unit in the reconfigured system.

d) Branch current magnitudes

Due to the network structure being changed following the feeder reconfiguration, the currents on each branch may also be significantly changed. It can be seen from the results of the seven scenarios that it is hard to determine the changed rate on a single branch. However, apart from a few branches, the maximum change in the value of the branch currents is lower than 1 per unit of the base current. Thus, to avoid the branch currents exceeding their limiting values, a standard maximum current value for most parts of the branches can be determined in advance.

7.4 Distribution Network Feeder Reconfiguration Considering Seasonal and Daily Generation and Load Tracking

In the previous section, eight scenarios have been analysed to investigate the impact of the renewable generator and system harmonic in the distribution network. In these scenarios, all loads are assumed fully loaded and all renewable generators are assumed to be working at their maximum level of output power all the time. However, the peak load of all load types and the output power of the renewable generators vary widely a lot over the course of a day. Moreover, the output power of the photovoltaic generator exhibits significant changes according to the season. The impact of the loads diversity and renewable generators in the distribution network feeder reconfiguration over the course of a day is demonstrated in this section.

With the development of power electronic technology and proposals for a smart grid, all manual switches will be substituted with automatic switches in upcoming years. Thus, the short-term switch operation in the distribution network can be achieved. The feeder reconfiguration will then be able to provide effective system backup and contingency for situations such as the main transformers overloading [11].

The replacement of all manual switches may require many years' work. The test system for scenario 7 in section 7.3 is a distribution system with the same penetration of renewable generators and system harmonic as laid out in the targets for2030. So, this system is designed to investigate the daily influence of variable loads and renewable generators in this section. The details of the test system for this section are shown in Table 7-11.

7.4.1 Scenarios

a) Peak load curves

As mentioned above, the peak load of different kinds of loads varies over 24 hours. Figure 7-26 to Figure 7-29 are the peak load curves of residential, commercial, industrial and public lighting respectively [3].

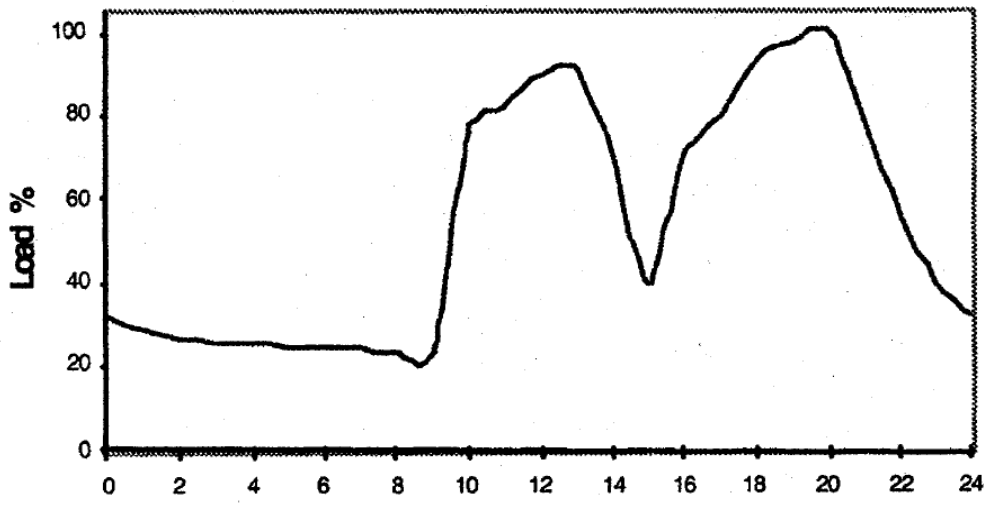

Figure 7-26 Peak load curve of residential loads [3]

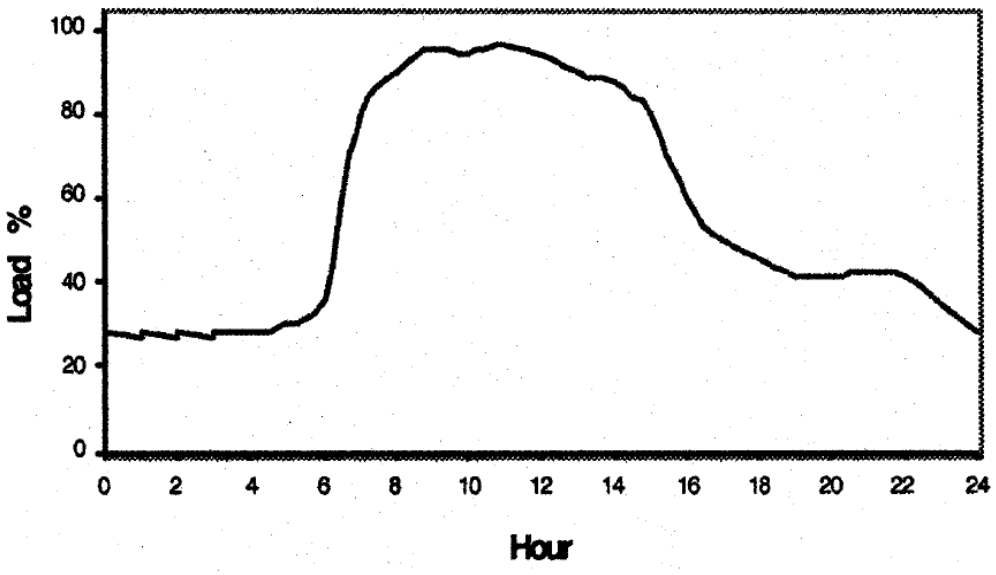

Figure 7-27 Peak load curve of commercial loads [3]

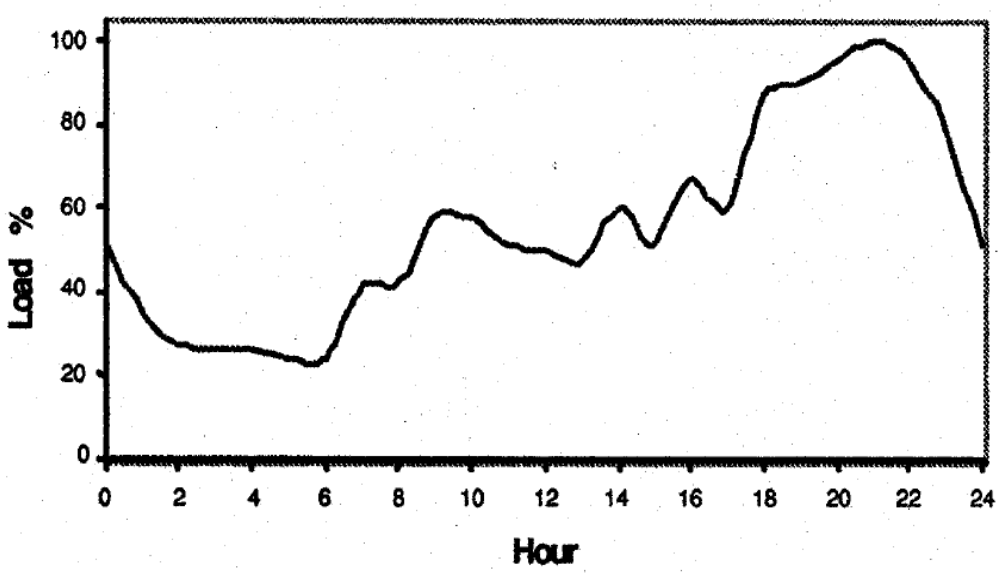

Figure 7-28 Peak load curve of industrial loads [3]

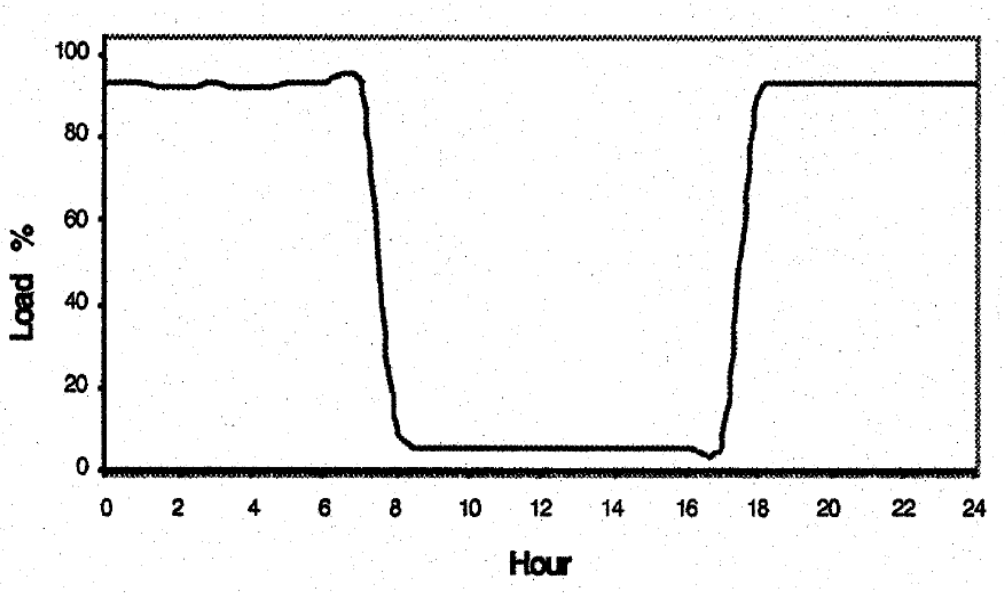

Figure 7-29 Peak load curve of public lighting[3]

A time-interval based strategy is adopted to deconstruct these daily load forecasts. Taking the useful life of the switches into consideration, the network cannot be

reconfigured constantly. A day can be divided into three sections in accordance with these four curves' characteristic and people's lifestyles. To ensure that voltage and current constraints are satisfied during the time intervals, the equivalent load is the maximum value of the corresponding segment[11]. Then, three individual reconfiguration problems with constant loads can be used to investigate the daily impact of the variable loads.

b) Output curves of the renewable generators

The daily generation model of wind generators which is provided in the reference [12] is used in this section. Its output curve is shown in Figure 7-30. The details of the data are shown in Table B-1 in Appendix B. In order to investigate the impacts of the wind generator in feeder reconfiguration problem, the wind generator's output power curve in this section is assumed as same with the curve in Figure 7-30 and its output curve is assumed as the same in every day of the year.

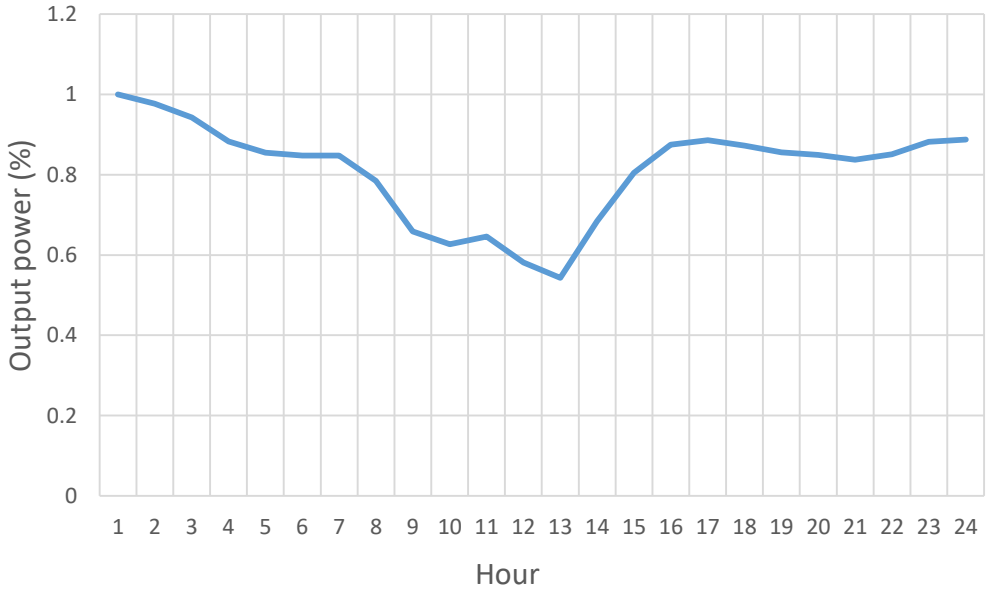

Figure 7-30 Daily output power curve of wind generators [12]

The number of sunlight hours obviously varies from summer to winter. Hence, the solar generators' output power curve is divided into two parts and shown in Figure

7-31. In this figure, the blue curve and the orange curve express the output power of solar generators in summer and winter respectively. This data is shown in greater detail in Table B1 in Appendix B [12]. In order to investigate the impacts of the solar generator in feeder reconfiguration problem, the solar generator's output power curve in this section is assumed as same with the curve in Figure 7-31 its output power curve is assumed as the same in every day in one of two seasons.

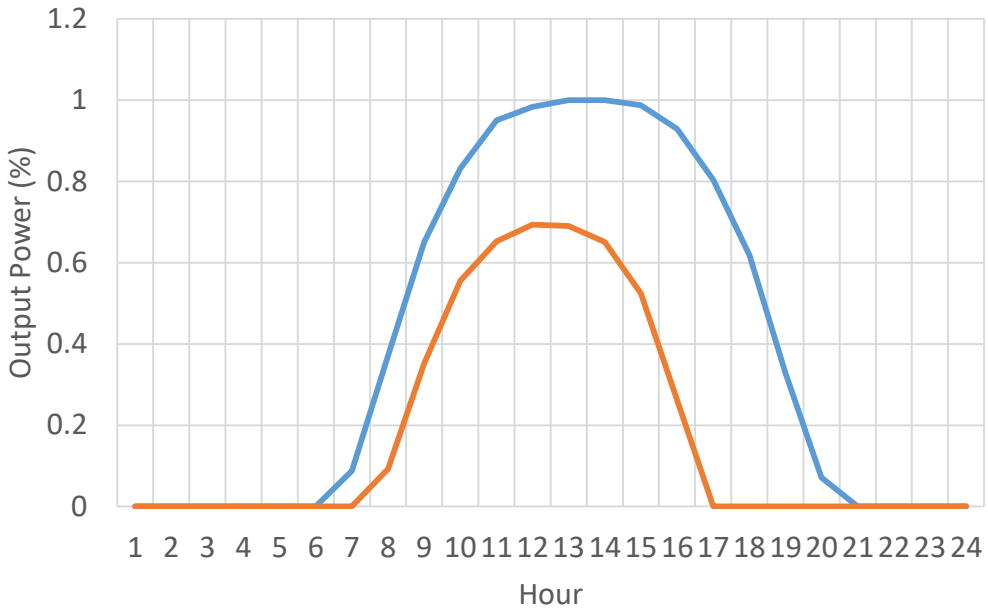

Figure 7-31 Daily output power curve of solar generators in summer and winter[12]

As is the case with the loads, the output curves are also divided into three segments. The time-interval for these three segments is the same as the time-interval for the loads. The output power in each segment is the average value of the output power in this time-interval. Then, the distribution network feeder reconfiguration with seasonal and daily generation and load tracking can be transformed into six individual feeder reconfiguration problems.

c) Scenarios

According to the characteristics of the curves in Figure 7-26 to Figure 7-31, the

simplified and normalised real-time load profiles of each load type and real-time output power of each generator are presented in Table 7-15 and Table 7-16 respectively. Using the information presented in this table, feeder reconfiguration for loss reduction should not be seen as a uniform operation, but should instead be carried out in three segments, with the two seasons considered separately. As the solar generator output power does not vary in the 22:00 - 05:59 time segment across the two seasons, the only time-interval to be tested is the one from 22:00 to 5:59.

Table 7-15 Proportion of the Real-Time Load When Comparing with Peak Load over 24 Hours on Different Load Type

Load Type	6:00-16:59	17:00 -21:59	22:00-5:59
Residential	90%	100%	60%
Commercial	100%	50%	33%
Industrial	60%	100%	90%
Public Lighting	10%	93%	93%

Table 7-16 Proportion of the Real-Time Output When Comparing with Rated Generator Output over 24 Hours on Different Generator Type

Generator Type	6:00-16:59	17:00 -21:59	22:00-5:59
Wind	72%	85%	91%
Solar (summer)	70%	25%	0
Solar (winter)	40%	0	0

It is assumed that the injection harmonic spectrums of the loads and generators are constant no matter how their capacity changes.

7.4.2 Results and Discussions

Normally, feeder reconfiguration does not take system harmonics, loads tracking and the fluctuations in the output of the renewable generators into consideration.

However, their impacts cannot be ignored. In order to investigate these impacts on the feeder reconfiguration problem, the sample network in scenario 3 of Section 7.3.2 is used as the test system in this section. The reconfigured network which is determined in the scenario 3 of Section 7.3.2 is also used as a comparison sample. Low power factor bulbs are installed in all public lighting. Due to this reconfigured network being determined without considering system harmonics, variable load demands and output of distributed generators, its network losses will have tolerance when these factors are considered in three daily segments. Therefore, for each time interval, it is necessary to re-calculate the real network loss in the test system before comparisons are made.

a) Network loss reduction

In this section, the network losses of the reconfigured system which were determined in scenario 3 of Section 7.3.2 are re-calculated in the three-segment by taking impacts of the system harmonics and the fluctuations in the loads demands and output of the renewable generators into consideration. The new minimum network losses which consider these factors in advance are also calculated. Comparisons of all minimum network losses and their average losses are shown in Table 7-17.

Table 7-17 Comparisons of Feeder Reconfiguration for Network Loss Reduction in Different Time-Interval

Summer	6:00-16:59	17:00 - 21:59	22:00-5:59
Original	307.69kW	984.90kW	792.50kW
Include Harmonics	244.10kW	589.09kW	338.74kW
Exclude Harmonics	296.75kW	1199.14kW	1083.08kW
Winter	6:00-16:59	17:00-21:59	22:00-5:59
Original	405.33kW	1173.10kW	792.50kW
Include Harmonics	285.59kW	645.62kW	338.74kW
Exclude Harmonics	483.51kW	1588.95kW	1083.08kW

Summer	Average	% Loss Reduction
Original	610.38kW	-
Include Harmonics	347.52kW	43.06%
Exclude Harmonics	746.86kW	-22.36%
Winter	Average	% Loss Reduction
Original	816.81kW	-
Include Harmonics	378.31kW	56.10%
Exclude Harmonics	913.67kW	-6.02%

In the table and following results, ‘original’ is the original network in scenario 3 of Section 7.3.2 and will not be changed in any segment; ‘Include Harmonics’ means the reconfigured network is calculated by feeder reconfiguration taking the system harmonics, the fluctuations in the loads’ demands and output of the renewable generators into consideration. Additionally, the different segments will be used as a framework to re-determining the network structure. ‘Exclude Harmonics’ means that the reconfigured network is constant in all segments. Moreover, system harmonics, the fluctuations in the loads’ demands and output of the renewable generators are not considered when determining the new tie switches in this network.

Due to the results of ‘exclude harmonics’ being determined without considering the system harmonics, the fluctuations in the loads’ demands and output of the

renewable generators, the network losses in almost all segments are greater than the network loss in the original network. So, the average network loss over 24 hours is greater than that found in the original network. It can be concluded that if the impact of the fluctuations in the loads' demands and output of the renewable generators are not considered, the results of the feeder reconfiguration may be worse than the results of the original network in the realistic distribution network. Therefore, it is impossible to attain the stated objective of reducing the network loss.

In Table 7-17, all network loss results are determined taking the impact of the system harmonics, the fluctuations in the loads demands and output of the renewable generators into are much lower than the results of the original network. The average reduction of the three segments for summer and winter is 43.06% and 56.10% respectively.

The results shown in Table 7-17 demonstrate that fluctuations in the loads' demands and the renewable generators' output both have an important impact which cannot be ignored.

b) Bus voltage magnitudes

The comparisons of bus voltage magnitudes on the title of the network 'original', 'include harmonics' and 'exclude harmonics' are shown in Figure 7-32 to Figure 7-36.

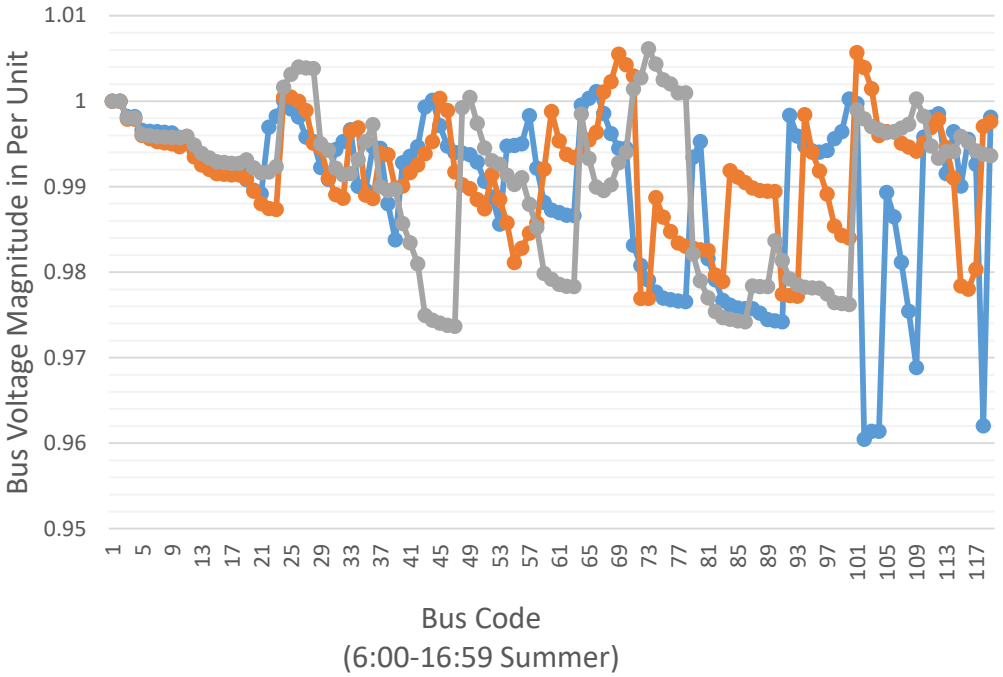

Figure 7-32 Comparison of bus voltage magnitudes from 6:00 to16:59 in summer

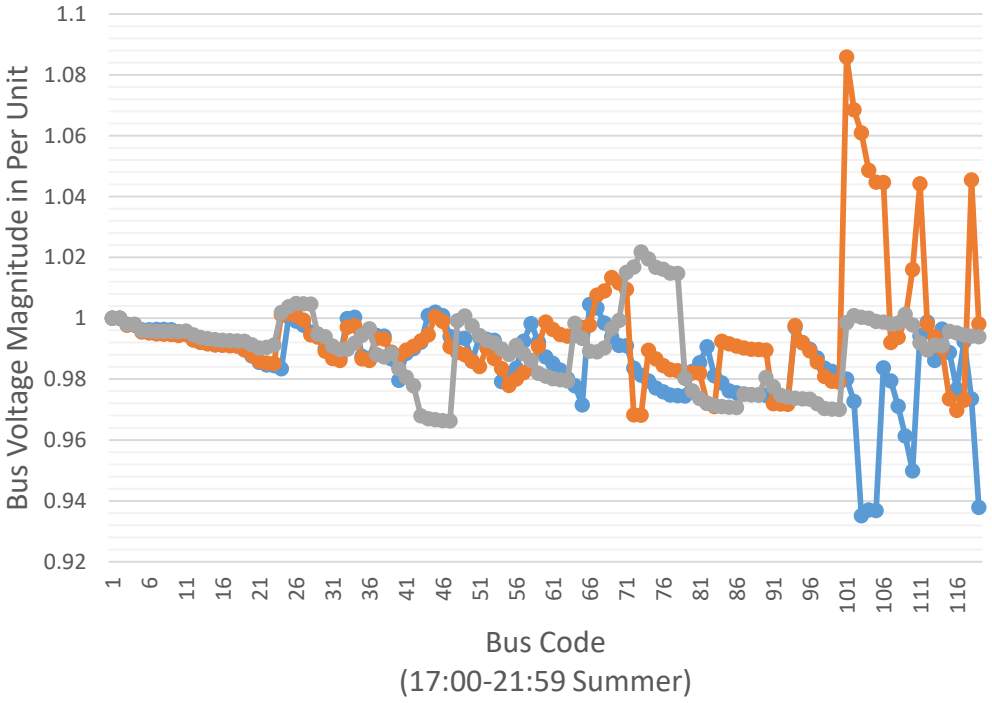

Figure 7-33 Comparison of bus voltage magnitudes from 17:00 to 21:59 in summer

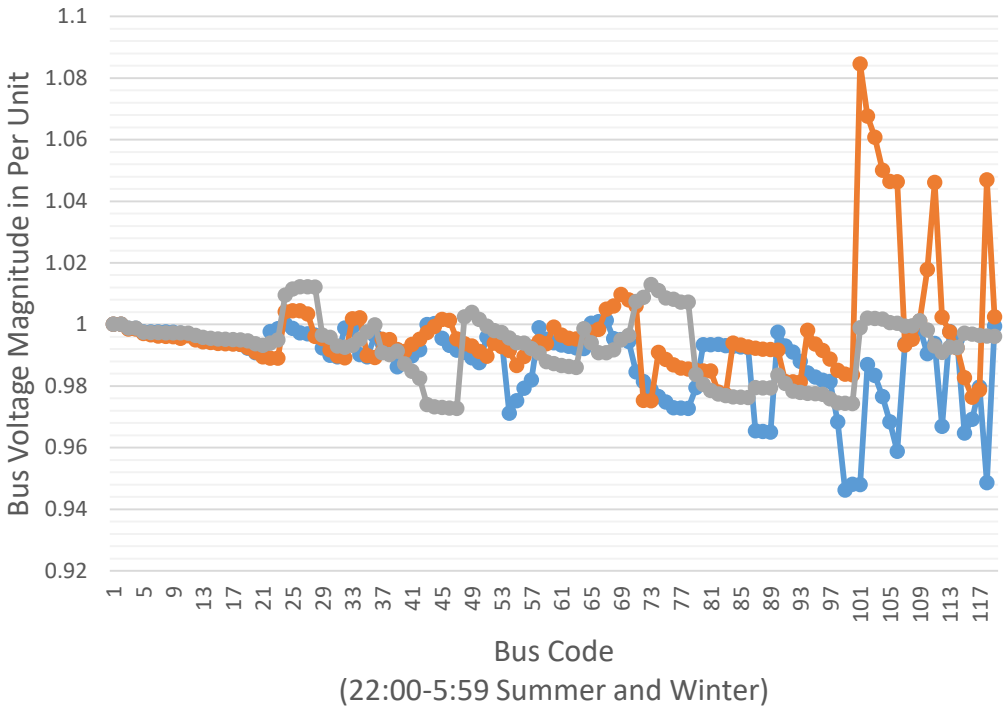

Figure 7-34 Comparison of bus voltage magnitudes from 22:00 to 5:59 in summer and winter

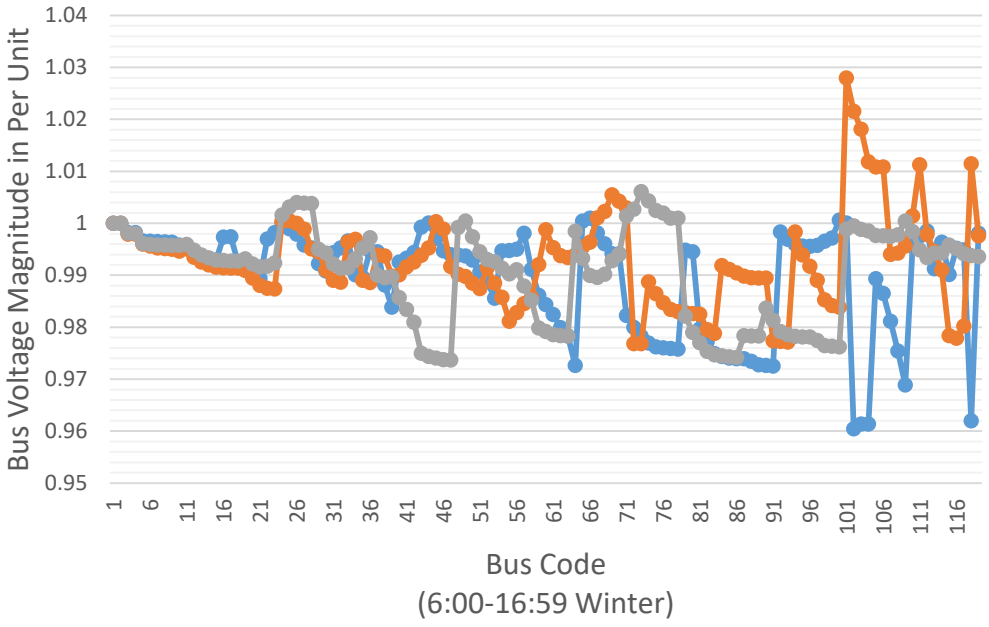

Figure 7-35 Comparison of bus voltage magnitudes from 6:00 to16:59 in winter

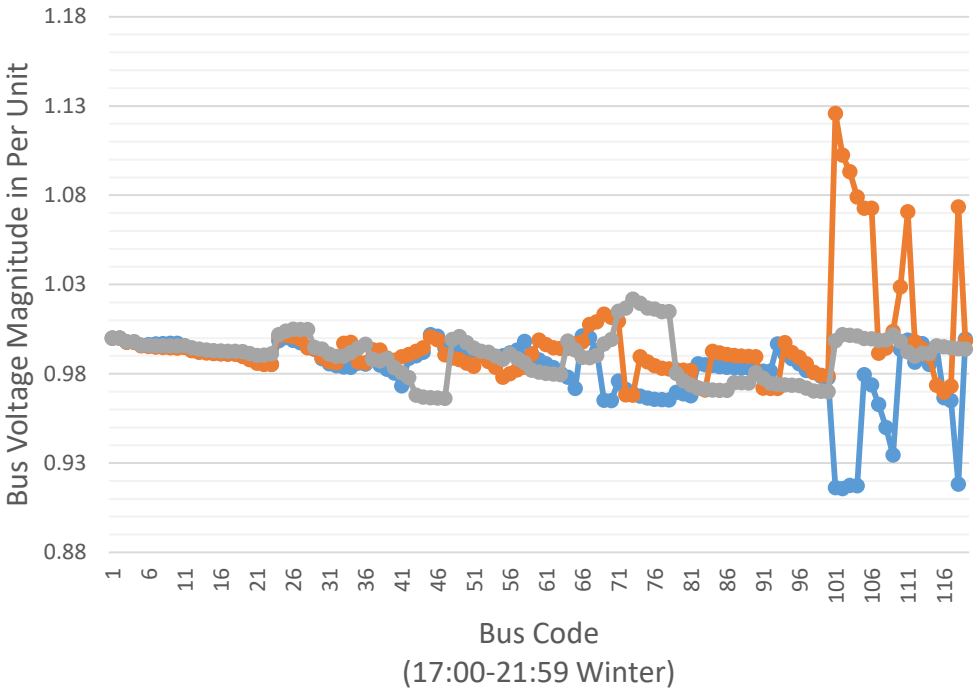

Figure 7-36 Comparison of bus voltage magnitudes from 17:00 to 21:59 in winter

In Figure 7-32 to Figure 7-36, the blue, orange and grey curves represent the bus voltage magnitudes in per unit of the 'including harmonics' network, the 'excluding harmonics' network and the 'original' network respectively. For the system harmonics, due to the bus voltage magnitudes possibly being greater than the reference voltage, the limitation of the voltage deviation on buses replaces the limitation of the voltage drop. According to the 0.9 per unit limitation of the voltage drop, the limitation of the voltage deviation is assumed to be 10%. The original system exhibits the lowest voltage deviation, as can be seen in the five figures above. The reason for this situation may be that all renewable generators are located at the heavy load in the test system and these distributed generator locations are the best positions for improving the voltage drop. Although the voltage deviation of the blue curve is worse than the grey one, it is better than the orange one except in the 6:00 to 16:59 segment in summer. Furthermore, the lowest voltage magnitude is 0.916 per unit in the blue curve in Figure 7-36, which satisfies

the voltage deviation limitation. If 10% is the limitation of the voltage deviation in the distribution network, the largest bus voltage magnitude is 1.126 per unit in the orange curve, this does not satisfy the limitation. Hence, in this test, although it cannot improve the voltage deviation after taking into consideration the fluctuations in the loads demands and output of the renewable generators, the performance of voltage deviation in the ‘include harmonics’ network is better than the performance in the ‘exclude harmonics’ network.

The bus voltage magnitudes results show that although the performance of the bus voltage magnitudes is worse following feeder reconfiguration, it still satisfied the voltage deviation limitation in the distribution network. Moreover, these results are subject to change according to the location of the distributed generators. This result is acceptable, as the objective of the feeder reconfiguration is not to improve the network’s voltage magnitude deviation.

c) Total harmonic voltage distortion

The comparison of total harmonic voltage distortions on the ‘original’ network, the ‘include harmonics’ network and the ‘exclude harmonics’ network are shown in Figure 7-37 to Figure 7-41.

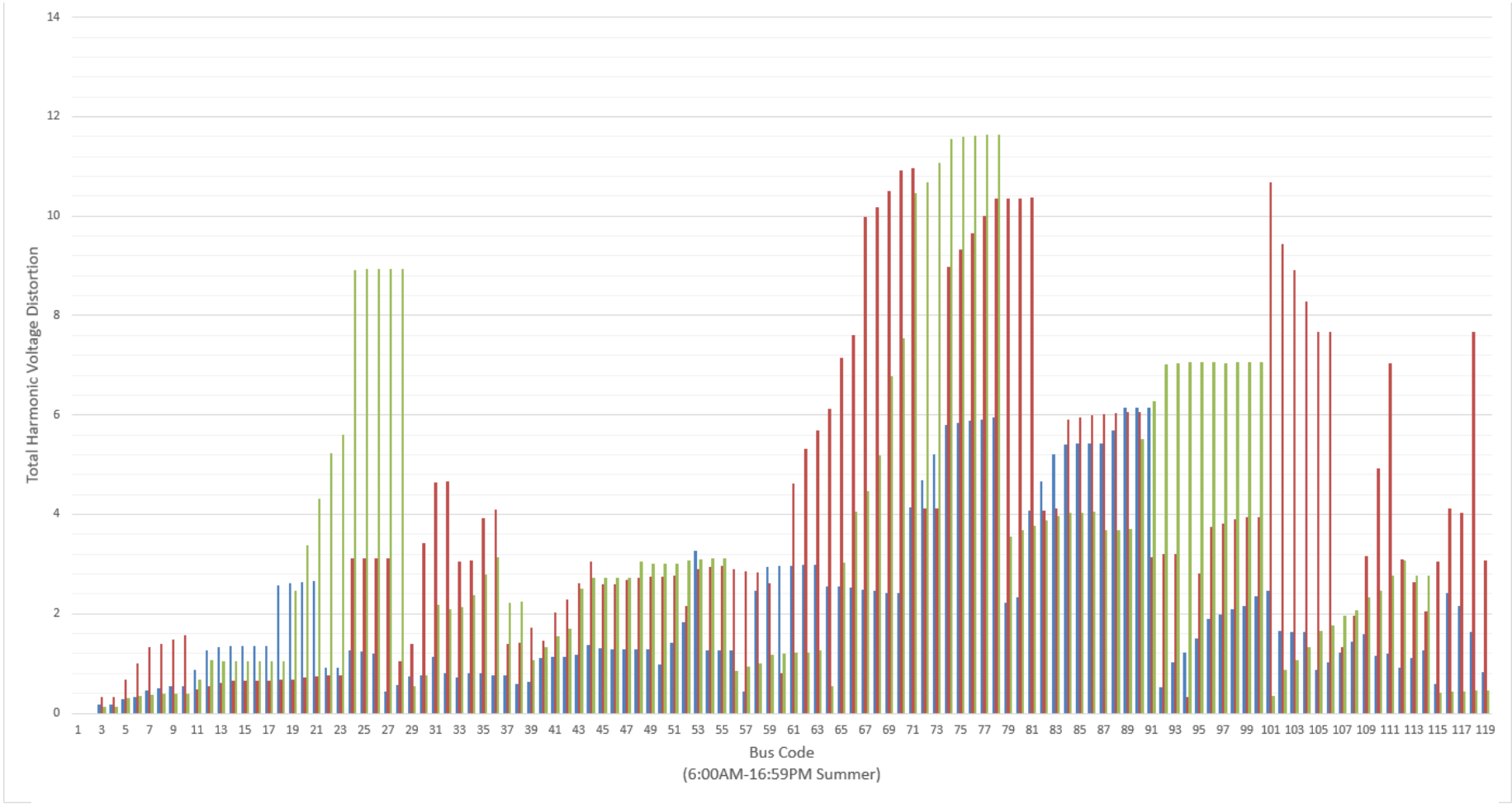

Figure 7-37 Comparison of total harmonic voltage distortion from 6:00 to16:59 in summer

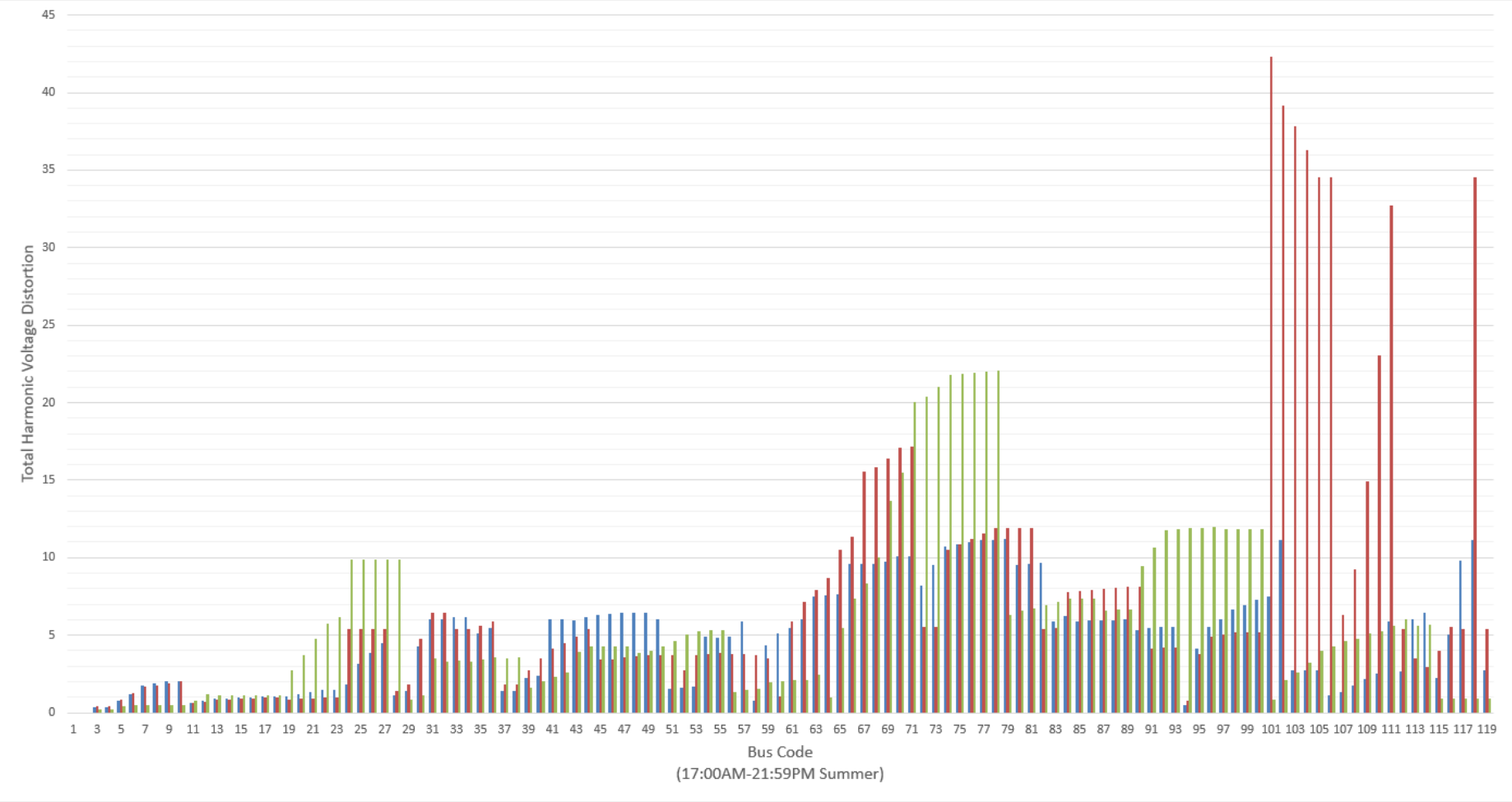

Figure 7-38 Comparison of total harmonic voltage distortion from 17:00 to 21:59 in summer

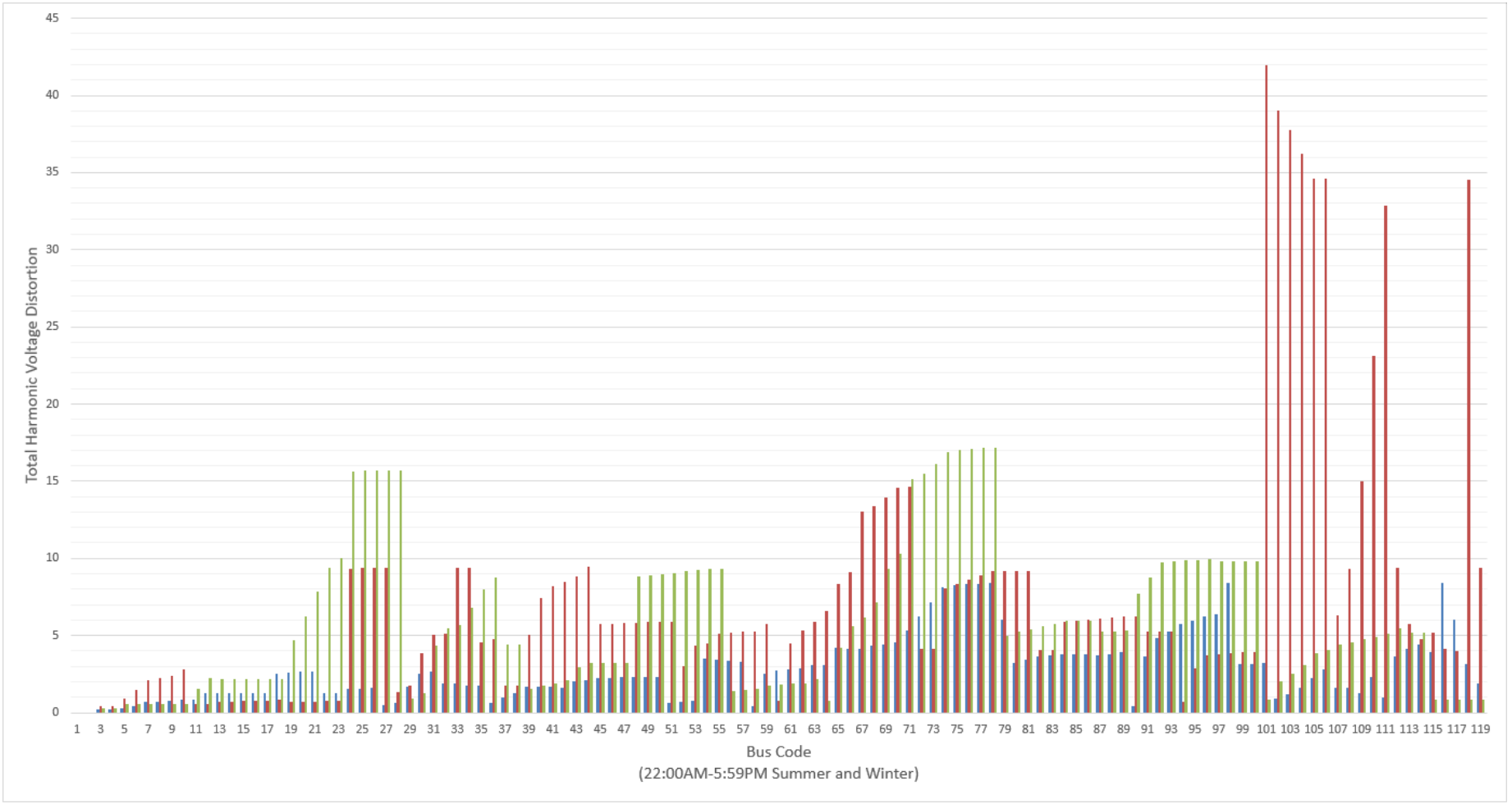

Figure 7-39 Comparison of total harmonic voltage distortion from 22:00 to 5:59 in summer and winter

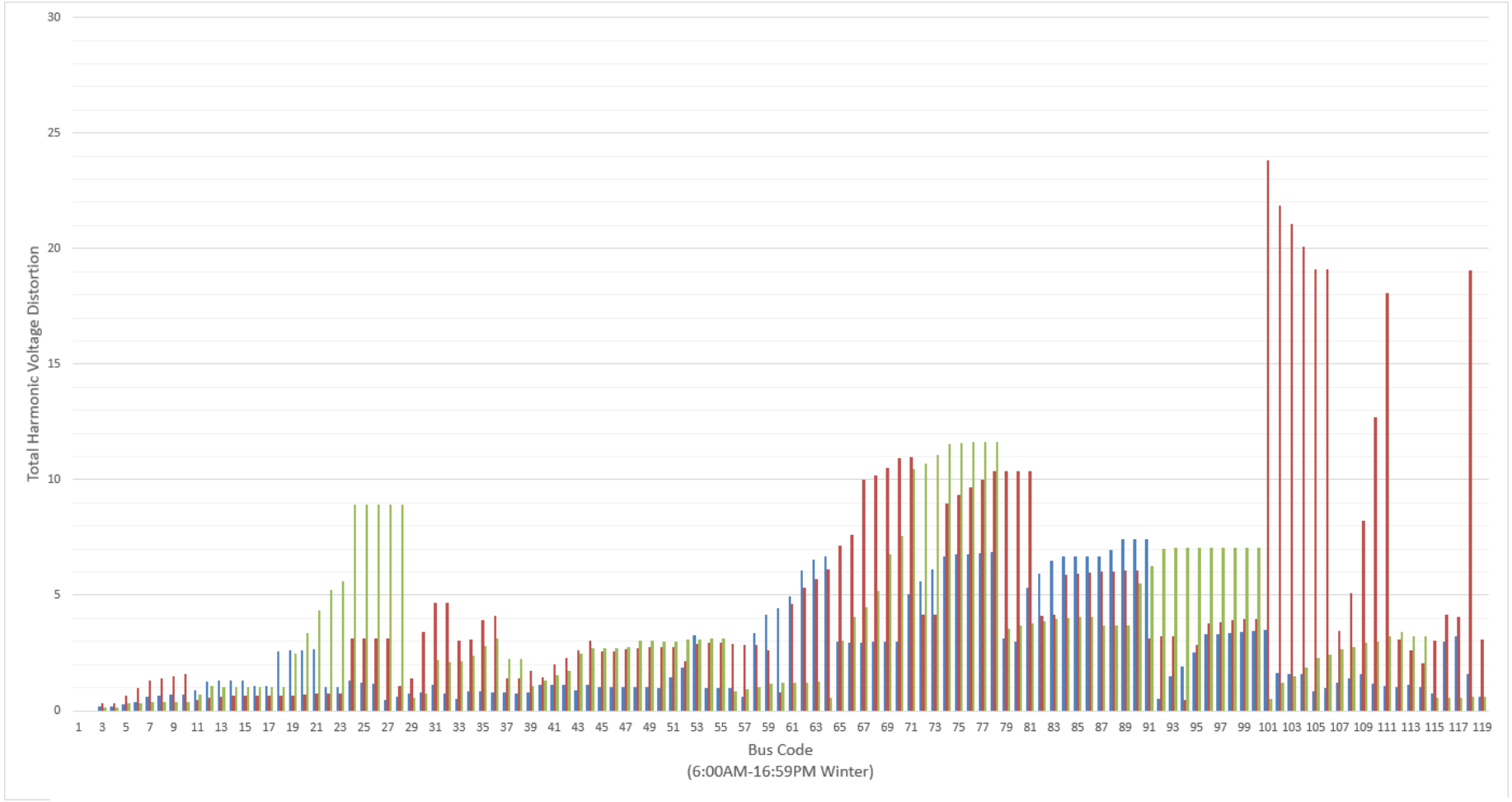

Figure 7-40 Comparison of total harmonic voltage distortion from 6:00 to16:59 in winter

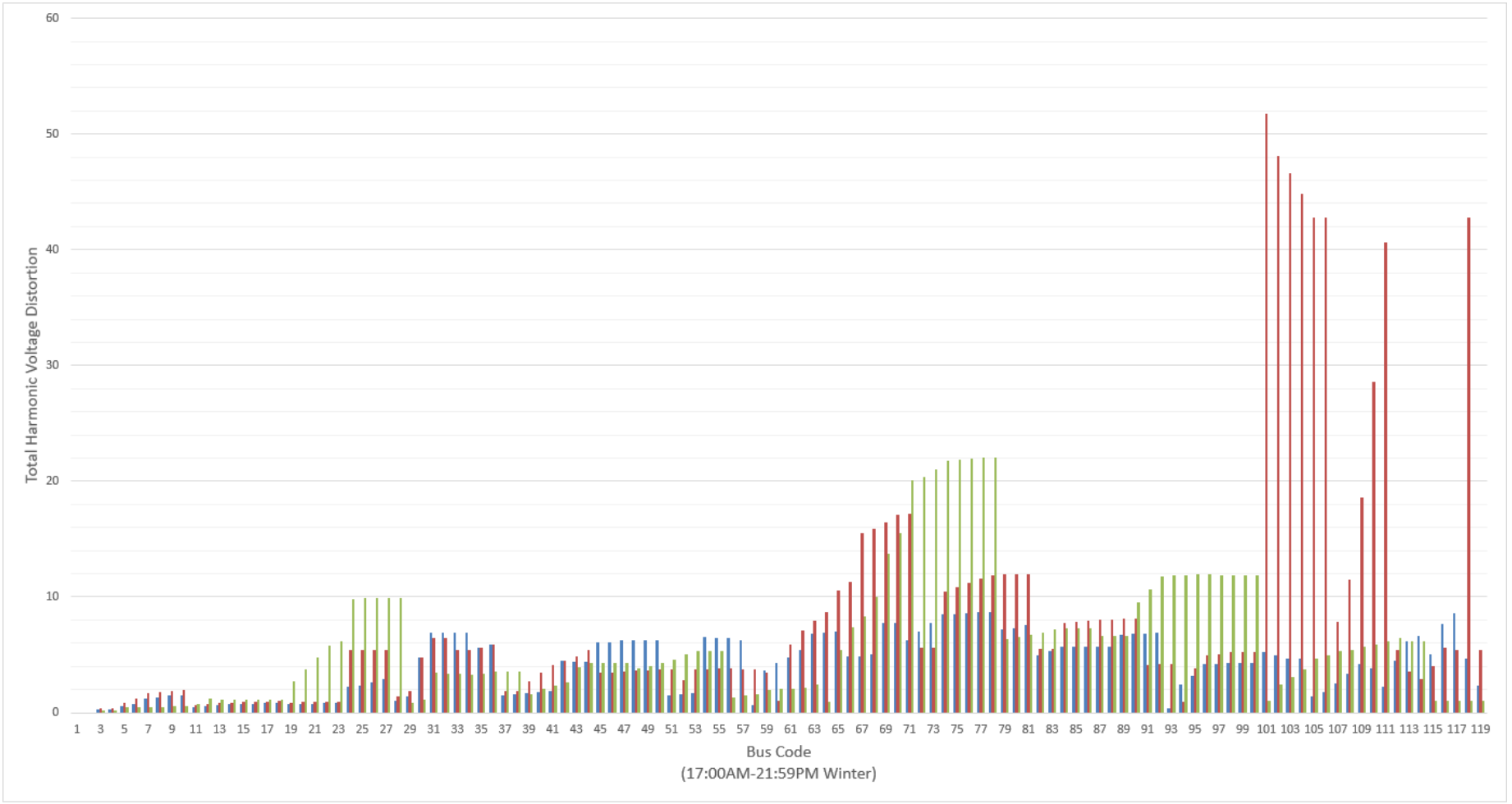

Figure 7-41 Comparison of total harmonic voltage distortion from 17:00 to 21:59 in winter

In Figure 7-37 to Figure 7-41, the blue, red and green bars express the total harmonic voltage distortion on each bus of the ‘including harmonics’ network, the ‘excluding harmonics’ network and the ‘original’ network respectively. The blue bar on each bus is obviously lower than the others in all five figures. The value of the highest blue bar is approximately 50% of the value of the green bar. This proves that the feeder reconfiguration for loss reduction considering harmonics can also reduce the value of the total harmonic distortion.

In all five figures, parts of the red bar are much higher than others. In some segments, its total harmonic voltage distortion value is greater than 50% while all green bars are lower than 20% and all blue bars are lower than 10%. This indicates that the impacts of fluctuations in the loads demands and output of the renewable generators are also important for reducing the total harmonic voltage distortion.

7.4.3 Results Summary

The results and discussions in section 7.4.2 prove that the fluctuations in the loads demands and output of the renewable generators can significantly affect the feeder reconfiguration solution. When the objective is a network loss reduction, the average network loss of the reconfigured system, which is determined considering the fluctuations in the loads demands and output of the renewable generators, is much lower than the original network loss. On the other hand, the average network loss of the reconfigured system which does not take these factors into consideration is greater than the network loss produced by the original network. Thus, it is important to consider the fluctuations in the loads demands and output of the renewable generators when undertaking the feeder reconfiguration.

Section 7.3 proves that feeder reconfiguration for loss reduction has a positive impact on the total harmonic voltage distortion. However, the loads demands and the output of the generators are constant. In a realistic distribution network, such a

conclusion may change when the impacts of the fluctuations in the loads demands and output of the renewable generators are ignored. In order to retain the feeder reconfiguration's positive impact on the total harmonic voltage distortion, the impacts of the fluctuations in loads demands and output of the renewable generators must be considered.

In comparison with the network loss reduction and total harmonic voltage distortion, the impacts of the fluctuations in the loads demands and output of the renewable generators are uncertain on the bus voltage magnitudes. Different conclusion will be drawn as a consequence of the differing location of the distributed generators. According to the test results, it is better to consider the fluctuations in the loads demands and output of the renewable generators rather than ignore them.

7.5 Summary

In the results of the scenarios in Section 7.3, the impact of the system harmonics on feeder reconfiguration are affected by the harmonic capacity and quantity. When the harmonic capacity and quantity is small, the results of the feeder reconfiguration may not be affected by harmonics. In other words, the difference in results may not be large enough to have anything other than a slight impact on how the program is engineered. In scenario 7 in Section 7.3, a further 12% network loss is reduced after taking the system harmonics into consideration. Thus, if the harmonic capacity and quantity in a system are large, the impact of system harmonics on feeder reconfiguration cannot be ignored.

Renewable generators not only inject harmonics but also improve distribution networks' voltage drop. According to the test results, where generators are located is a more important factor than their capacity. With regards to harmonics, their impact on voltage drop is lower than the impact of the renewable generators'

location.

The results in section 7.4 show that the impact of the fluctuations in the loads demands and output of the renewable generators cannot be ignored. In other words, the network loss and total harmonic voltage distortion of the reconfigured system are greater than the sample network loss. In section 7.4, 24 hours are divided into three segments. Although the values of the load demands and generator power output vary slightly in each segment, it is reasonable to suggest that more segments over a 24-hour period will contribute to a lower average network loss for the same network. However, the useful life of the switches is limited. Hence, a reasonable time interval for 24 hours or 365 days will bring more profits through network loss reduction.

The system harmonics and renewable generators data in this chapter is cited from the forecasts available on the official EU website. So, the test systems can be treated as a realistic model of the EU distribution network. According to the forecast and the test results in this chapter, to reduce the network loss in the future distribution system, the impact of the system harmonics and the fluctuations in the loads demands and output of the renewable generators must be taken into consideration. In other words, feeder reconfiguration will result in a distribution system that incurs greater real network loss than that experienced by the original system.

7.6 Reference

[1] U. S. E. I. A. (EIA), "Annual Energy Outlook 2011 With Projections to 2035," *http://electricdrive.org/ht/a/GetDocumentAction/id/27843*, last data of access 01.06.2016.

[2] I. Pineda, "Wind in power , 2015 European statistics," *http://www.ewea.org/fileadmin/files/library/publications/statistics/EWEA-Annual-Statistics-2015.pdf*, last date of access 15.05.2016.

[3] E. Lopez, H. Opazo, L. Garcia, and P. Bastard, "Online reconfiguration considering variability demand: applications to real networks," *IEEE Transactions on Power Systems,* vol. 19, pp. 549-553, 2004.

[4] H. Sharma, M. Rylander, and D. Dorr, "Grid Impacts Due to Increased Penetration of Newer Harmonic Sources," *IEEE Transactions on Industry Applications,* vol. 52, pp. 99-104, 2016.

[5] E. W. E. Association, "2030: the next steps for EU climate and energy policy," *http://www.ewea.org/fileadmin/files/library/publications/reports/2030.pdf*, last date of access 28.05.2016.

[6] S. O. Gaëtan masson, Becquerel Institute, "Global Market Outlook For Solar Power / 2015 - 2019," *http://helapco.gr/pdf/Global_Market_Outlook_2015_-2019_lr_v23.pdf*, last date of access 30.05.2016.

[7] S. POTHECARY, "SolarPower Europe calls for 35% by 2030 renewable target," *http://www.pv-magazine.com/news/details/beitrag/solarpower-europe-calls-for-35-by-2030-renewable-target_100023590/#axzz4AFXkVS6j*, last date of

access 28.5.2016.

[8] T. Olson, "Preliminary Electric Vehicle Demand Forecast," *http://www.energy.ca.gov/2013_energypolicy/documents/2013-10-01_workshop/presentations/06_Tim_Olson_Preliminary_Electric_Vehicle_Demand_Forecast.pdf*, the date of access 28.05.2016.

[9] Z. F. D. Zhang, L. Zhang, "An improved TS algorithm for loss-minimum reconfiguration in large-scale distribution systems," *Electr. Power Syst. Res.,* vol. 77, pp. 685–694, 2007.

[10] Ofgem, "Electricity Distribution Loss Percentages by Distribution Network Operator (DNO) Area," *[Online].Available: https://www.ofgem.gov.uk/ofgem-publications/43516/distribution-units-and-loss-percentages-summary.pdf*, last data of access 10.11.2015.

[11] S. Jazebi, M. M. Hadji, and R. A. Naghizadeh, "Distribution Network Reconfiguration in the Presence of Harmonic Loads: Optimization Techniques and Analysis," *IEEE Transactions on Smart Grid,* vol. 5, pp. 1929-1937, 2014.

[12] J. Lv, "A New Method for Harmonic Penetration Study in Power Networks with Renewable Generation," *PhD thesis at the University of Strathclyde,* 2014.

Chapter 8 Conclusions and Future Work

8.1 Conclusions

To reduce carbon dioxide emissions, renewable energy generators and modern electric devices are widely used in the distribution network. These pieces of equipment are harmonic sources. The harmonic sources will increase the branch currents so that transmission losses on distribution lines will increase. For this reason, the impact of harmonics on the feeder reconfiguration problem cannot be ignored. The widely used backward/forward sweep load flow method is a fundamental distribution network load flow method. So, it is impossible to directly analyse such a network with the backward/forward sweep load flow method which is normally used. Hence, a suitable load flow method for feeder reconfiguration in distribution network considering distributed generators and system harmonics is proposed in this thesis. Furthermore, as one of the most important methods for reducing network losses in the distribution network, feeder reconfiguration has been researched for many years. With increasing distribution network sizes, the accuracy of the currently used optimization methods (ant colony system and discrete particle swarm optimization) for feeder reconfiguration is reduced. Thus, a novel hybrid optimization method with higher searching accuracy is proposed for a large distribution system in this thesis. And, better solutions of the hybrid method than the solution obtained by ant colony system or particle swarm optimization is proved in the results of Chapter 6.

A real-world network with the 24-hour variations in load demands and renewable generator output do over the course of a year is used. A distribution network with unchanged load demands and output of the renewable generators cannot produce practical results. Thus, the impacts of the load and the generator output diversity and alterations over 24 hours in a year on optimal configuration is investigated in

this thesis. The test results show that these impacts have a big influence on distribution network feeder reconfiguration and cannot be ignored.

The key findings of this thesis have been presented by following three steps: (a) An improved harmonic backward/forward sweep method is proposed in this thesis for analysing the distribution network with distributed generators under harmonic conditions. (b) A hybrid optimization method is developed based on the ant colony system and discrete particle swarm optimization for increasing the accuracy of the optimization method in feeder reconfiguration problem. (c) The impacts of variable load demands and output of the renewable generators on the distribution network feeder reconfiguration have been investigated. The results obtained from these three steps are summarised in the following three sub-sections.

8.1.1 Improved Harmonic Backward/Forward Sweep algorithm

Because of the fast calculation speed, the backward/forward sweep algorithm is a widely used load flow analysis method in distribution networks. A layered method is combined with the backward/forward sweep algorithm so that the sequence of bus voltages and branch currents can be calculated based on the system levels instead of the codes of the buses. In the course of this study, it was found that the system structure is changed whenever the optimization method reveals a different feasible solution. By combining the layered method with the backward/forward sweep algorithm, the recoding process of the bus codes when the system structure is changed is avoided. Hence, this layered backward/forward sweep method is particularly suitable for the feeder reconfiguration problem and it is determined as the load flow analysis method for feeder reconfiguration in the distribution network. Before this method can be applied, two issues are resolved, which are explained below.

a) In a modern distribution network, renewable generators will connect to the

network as the distributed generators to supply the electric energy locally. However, the layered backward/forward sweep method cannot address the PV type distributed generators directly. Hence, the PV type distributed generators are transformed to the PQ type according to the relationship between the voltage increment vector and compensation reactive power in this thesis. The results in Chapter 4 show that the layered backward/forward sweep method can analyse the distribution network with PV type generators accurately after transforming the PV type generators to PQ type generators.

b) The fast harmonic analysis method in distribution networks which is based on backward/forward sweep algorithm is verified in a special distribution network by the author, in which all connected loads are nonlinear. The application of the harmonic backward/forward sweep method used in a distribution network which includes linear and nonlinear loads and distributed generators is not verified. Chapter 4 carries details of a case study in which the accuracy of this method is verified. It is found that the normal harmonic backward/forward sweep method will ignore the harmonic currents in parts of tributary branches when these tributaries do not contain a harmonic source. So, there is a large tolerance on the value of calculated harmonic branch currents, harmonic bus voltages and total harmonic voltage distortions. In this thesis, the ignored tributary harmonic branch currents are calculated according to Kirchhoff's Current Law and an additional branch current forward sweep based on the distribution network levels. For this improvement, the improved harmonic backward/forward sweep method can be used to accurately analyse a distribution network with random harmonic sources.

8.1.2 Hybrid Optimization Method.

In recent years, both the ant colony system and particle swarm optimization have

gained in popularity as optimization methods. Ant colony system offers a good local search ability which means that ants can quickly search for better solutions based on an existing solution. The advantage of particle swarm optimization is that it offers high-performance global search ability. This means that particles can quickly find feasible solutions in all possible search areas. The advantages offered by each of these methods could be integrated into a single system. Therefore, a hybrid optimization method based on the ant colony system and discrete particle swarm optimization is proposed to solve the optimal configuration problem in this thesis. In the proposed hybrid method, the strong local search ability comes from the ant module and the good global search ability is provided by the particle module. Moreover, an adaptive function is proposed for enhancing the global search ability at the first half stage of the search process.

The proposed hybrid method was tested on 33-bus, 69-bus and 118-bus distribution networks in three different maximum number iterations respectively to investigate the minimum network loss. Furthermore, the results were compared to those results which were obtained by the ant colony system and discrete particle swarm optimization. According to the optimal network loss comparisons in these nine case studies, the proposed hybrid method not only always offered a greater probability of finding the minimum network loss in any of the case studies but also build networks with smaller network losses than the other two methods in large size distribution network. In another word, in large size distribution system, the proposed hybrid method must have a better searching performance than the individual ant colony system and discrete particle swarm optimization. Therefore, the proposed hybrid method can accomplish the distribution network feeder reconfiguration with more accurate results.

8.1.3 Effects of Variable Load Demands and Renewable Generators Output

In this thesis, the impact of system harmonics and distributed generators on the distribution network feeder reconfiguration is investigated by applying the proposed hybrid method to the 118-bus distribution system. Four different bus types (residential, commercial, industrial and public lighting) are included in the case study. Their forecast harmonic emissions spectra data for the years 2010 and 2030 are quoted using the U.S. Energy Information Administration's Annual Energy Outlook 2011. The case study also relies on official EU renewable generation data for the years 2012 and 2030. Seven scenarios are tested for simulating the traditional passive distribution network, the modern distribution network and the future distribution network in the EU.

The impacts of system harmonics and distributed generators can be divided into four categories: network loss reduction, voltage drop, branch current changing rate and total harmonic voltage distortion. The results are compared in Chapter 7, and from these, it can be seen that the four categories are impacted in the following ways:

a) Network loss reduction

   Based on the feeder reconfiguration, the network loss can be further reduced by connecting suitable capacity of the distributed generators into the network. When harmonic injection currents from the harmonic sources are large, the network loss will be further reduced by considering system harmonics. If the harmonic injection currents from the harmonic sources are small, the impact of system harmonics is slight.

b) Voltage drop

Distributed generators can improve the voltage drop significantly, especially when the distributed generators are located on heavy loads. However, its impact on system harmonics can be ignored.

c) Branch current changing rate

As a consequence of the change in system structure, the maximum current on each branch cannot be determined before the solution is calculated. However, according to the test results, almost all branch currents are smaller than the base current.

d) Total harmonic voltage distortion

The renewable generators are harmonic sources, so the value of the total harmonic voltage distortion on each bus will increase after the renewable generators are connected to the network. Although the objective of the feeder reconfiguration in this thesis is network loss reduction, the maximum value of the total harmonic voltage distortion is reduced by about 50% in major scenarios. Thus, it can be said that feeder reconfiguration for network loss reduction can also improve the performance of the total harmonic voltage distortion on buses.

The impact of variable peak demands on each type of load and the variable output of the renewable generators over 24 hours on the feeder reconfiguration problem considering harmonics is investigated by the proposed hybrid method in a 118-bus distribution system in this thesis.

In the modelled scenarios, each 24-hour period is divided into three segments following the load demand curves and wind and solar generator outputs. In addition, the difference between the output of the solar generators in summer and winter is also considered. According to the test results in Chapter 7, if the load demands and output of the renewable generators are assumed to be unchanged in

the test system, after feeder reconfiguration, the average network loss over 24 hours in this system will be larger than the network loss in the sample network when variable load demands and output of the renewable generators are considered. Furthermore, some buses also experience greater total harmonic voltage distortion and voltage drops. If the difference in load demands and output of the distributed generators are considered in advance, the average network loss will be an approximate 50% reduction and the total harmonic voltage distortion on some buses will also be smaller. Thus, the variable load demands and output of the renewable generators must be considered when solving the feeder reconfiguration problem in a practical distribution network.

8.2 Suggestions and Future Work

This thesis contributes to developing an accurate optimization method for feeder reconfiguration on distribution networks considering system harmonics. The impact of system harmonics, variable load demands and output of renewable generators over 24 hours on the feeder reconfiguration problem are also investigated. The objective of the feeder reconfiguration is network loss reduction and the system is assumed to be a three-phase balanced system. However, there are still several areas showing potential for expansion and improvements. The following areas would therefore be fruitful subjects for future research.

a) The network loss reduction is the only objective in this thesis, however, in Chapter 2, there are many other purposes for feeder reconfiguration which can be investigated. Furthermore, economic factors should be considered for these purposes. For example, feeder reconfiguration is a method to reduce

costs during power transmission. If the cost of equipment incurred by the feeder reconfiguration is higher than the value of the reduced network loss, the feeder reconfiguration will be meaningless. Thus, the impact of economic factors will be evaluated and analysed in the future.

b) The settings of the system elements will have a large influence on the ant colony system and particle swarm optimization solution. All these system elements are determined by experience. Thus, a standard or a procedural method to determine the best values for these system elements can be considered in future study.

c) The location and the capacity of the renewable generators are randomly set by the author in this thesis. The network loss and the voltage drop may be improved by a reasonable location and capacity of these generators. Thus, an optimization method for determining the location and the capacity of the increased number of renewable generators may be considered in future study.

d) The proposed harmonic backward/forward sweep method in this thesis is designed in the balanced three-phased power system. However, normally, the distribution system is an unbalanced three-phase power system. The feasibility of this proposed method should be investigated in an unbalanced three-phased system. Hence, the three-phase unbalanced power system should be considered in the future.

e) Automatic switches might replace all manual switches in the power system in the future. Then, the status of the switches may change in hours over 24 hours for the purpose of feeder reconfiguration. According to the results in Chapter 7, the more time-intervals are set over 24 hours, the more network losses will be reduced. However, the computing time for the optimal solution in the large size distribution network may need hours, and it is difficult to reduce the computing time from hours to minutes in the large size distribution

system. From the results in Chapter 6, it can be seen that the network loss will be significantly reduced within a very short time at the beginning of the feeder reconfiguration process. Hence, it is worth researching how to balance the computing time and the time-interval so that the average reduced network loss over 24 hours can be smaller.

Appendix A Distribution System Date

A.1 IEEE 33-bus system

Table A-1 Data of IEEE 33-Bus distribution System

Sending Node	Receiving node	Branch Number	Branch Impedance(Ω)	Node Apparent Power(MVA)
1	2	1	0.0922+j*0.0047	0.100+j*0.060
2	3	2	0.4930+j*0.2511	0.090+j*0.040
3	4	3	0.3660+j*0.1864	0.120+j*0.080
4	5	4	0.3811+j*0.1941	0.060+j*0.030
5	6	5	0.8190+j*0.7070	0.060+j*0.020
6	7	6	0.1872+j*0.6188	0.200+j*0.100
7	8	7	0.7114+j*0.2351	0.200+j*0.100
8	9	8	1.0300+j*0.7400	0.060+j*0.020
9	10	9	1.0440+j*0.7400	0.060+j*0.020
10	11	10	0.1966+j*0.0650	0.045+j*0.030
11	12	11	0.3744+j*0.1238	0.060+j*0.035
12	13	12	1.4680+j*1.1550	0.060+j*0.035
13	14	13	0.5416+j*0.7129	0.120+j*0.080
14	15	14	0.5910+j*0.5260	0.060+j*0.010
15	16	15	0.7463+j*0.5450	0.060+j*0.020
16	17	16	1.2890+j*1.7210	0.060+j*0.020
17	18	17	0.3720+j*0.5740	0.090+j*0.040
2	19	18	0.1640+j*0.1565	0.090+j*0.040
19	20	19	1.5042+j*1.3554	0.090+j*0.040
20	21	20	0.4095+j*0.4784	0.090+j*0.040
21	22	21	0.7089+j*0.9373	0.090+j*0.040
3	23	22	0.4512+j*0.3083	0.090+j*0.050
23	24	23	0.8980+j*0.7091	0.420+j*0.200
24	25	24	0.8960+j*0.7011	0.420+j*0.200
6	26	25	0.2030+j*0.1034	0.060+j*0.025
26	27	26	0.2842+j*0.1447	0.060+j*0.025
27	28	27	1.0590+j*0.9337	0.060+j*0.020
28	29	28	0.8042+j*0.7006	0.120+j*0.070
29	30	29	0.5075+j*0.2585	0.200+j*0.600
30	31	30	0.9744+j*0.9630	0.150+j*0.070

31	32	31	0.3105+j*0.3619	0.210+j*0.100
32	33	32	0.3410+j*0.5362	0.060+j*0.040
8	21	33	2.0000+j*2.0000	Tie switch
9	15	34	2.0000+j*2.0000	Tie switch
12	22	35	2.0000+j*2.0000	Tie switch
18	33	36	0.5000+j*0.5000	Tie switch
25	29	37	0.5000+j*0.5000	Tie switch

System reference voltage of the IEEE 33-bus is 12.66kV

A.2 IEEE 69-bus system

Table A-2 Data of IEEE 69-Bus distribution System

Sending Node	Receiving node	Branch Number	Branch Impedance(Ω)	Node Apparent Power(MVA)
1	2	1	0.0005+j*0.0012	0
2	3	2	0.0005+j*0.0012	0
3	4	3	0.0015+j*0.0036	0
4	5	4	0.0251+j*0.0294	0
5	6	5	0.3660+j*0.1864	0.0026+j*0.0022
6	7	6	0.3810+j*0.1941	0.0404+j*0.030
7	8	7	0.0922+j*0.0470	0.075+j*0.054
8	9	8	0.0493+j*0.0251	0.030+j*0.022
9	10	9	0.8190+j*0.2707	0.028+j*0.019
10	11	10	0.1872+j*0.0619	0.145+j*0.104
11	12	11	0.7114+j*0.2351	0.145+j*0.104
12	13	12	1.0300+j*0.3400	0.008+j*0.005
13	14	13	1.0440+j*0.3450	0.008+j*0.0055
14	15	14	1.0580+j*0.3496	0
15	16	15	0.1966+j*0.0650	0.0455+j*0.030
16	17	16	0.3744+j*0.1238	0.060+j*0.035
17	18	17	0.0047+j*0.0016	0.060+j*0.035
18	19	18	0.3276+j*0.1083	0
19	20	19	0.2106+j*0.069	0.001+j*0.0006
20	21	20	0.3416+j*0.1129	0.114+j*0.081
21	22	21	0.0140+j*0.0046	0.005+j*0.035

22	23	22	0.1591+j*0.0526	0
23	24	23	0.3463+j*0.1145	0.028+j*0.020
24	25	24	0.7488+j*0.2475	0
25	26	25	0.3089+j*0.1021	0.014+j*0.010
26	27	26	0.1732+j*0.0572	0.014+j*0.010
3	28	27	0.0044+j*0.0108	0.026+j*0.0186
28	29	28	0.0640+j*0.1565	0.026+j*0.0186
29	30	29	0.3978+j*0.1315	0
30	31	30	0.0702+j*0.0232	0
31	32	31	0.3510+j*0.1160	0
32	33	32	0.8390+j*0.2816	0.014+j*0.010
33	34	33	1.7080+j*0.5646	0.0195+j*0.014
34	35	34	1.4740+j*0.4873	0.006+j*0.004
4	36	35	0.0034+j*0.0084	0
36	37	36	0.0851+j*0.2083	0.079+j*0.0564
37	38	37	0.2898+j*0.7091	0. 3847+j*0.2745
38	39	38	0.0822+j*0.2011	0.3847+j*0.2745
8	40	39	0.0928+j*0.0473	0.0405+j*0.0283
40	41	40	0.3319+j*0.1114	0.0036+j*0.0027
9	42	41	0.1740+j*0.0886	0.00435+j*0.0035
42	43	42	0.2030+j*0.1034	0.0264+j*0.019
43	44	43	0.2842+j*0.1447	0.024+j*0.0172
44	45	44	0.2813+j*0.1433	0
45	46	45	1.5900+j*0.5337	0
46	47	46	0.7837+j*0.2630	0
47	48	47	0.3042+j*0.1006	0.100+j*0.072
48	49	48	0.3861+j*0.1172	0
49	50	49	0.5075+j*0.2585	1.244+j*0.888
50	51	50	0.0974+j*0.0496	0.032+j*0.023
51	52	51	0.1450+j*0.0738	0
52	53	52	0.7105+j*0.3619	0.227+j*0.162
53	54	53	1.0410+j*0.5302	0.059+j*0.042
11	55	54	0.2012+j*0.0611	0.018+j*0.013
55	56	55	0.0047+j*0.0014	0.018+j*0.013
12	57	56	0.7394+j*0.2444	0.028+j*0.020
57	58	57	0.0047+j*0.0016	0.028+j*0.020
3	59	58	0.0044+j*0.0108	0.026+j*0.01855
59	60	59	0.0640+j*0.1565	0.026+j*0.01855
60	61	60	0.1053+j*0.1230	0

61	62	61	0.0304+j*0.0355	0.024+j*0.017
62	63	62	0.0018+j*0.0021	0.024+j*0.017
63	64	63	0.7283+j*0.8509	0.0012+j*0.001
64	65	64	0.3100+j*0.3623	0
65	66	65	0.0410+j*0.0478	0.006+j*0.0043
66	67	66	0.0092+j*0.0116	0
67	68	67	0.1089+j*0.1373	0.03922+j*0.0263
68	69	68	0.0009+j*0.0012	0.03922+j*0.0263
11	66	69	0.5000+j*0.5000	Tie switch
13	20	70	0.5000+j*0.5000	Tie switch
15	69	71	1.0000+j*0.5000	Tie switch
27	54	72	1.0000+j*0.5000	Tie switch
39	48	73	2.0000+j*1.0000	Tie switch

System reference voltage of the IEEE 69-bus is 12.66kV

A.3 IEEE 118-bus system

Table A-3 Data of IEEE 118-Bus Distribution System

Sending Node	Receiving node	Branch Number	Branch Impedance(Ω)	Node Apparent Power(kVA)
1	2	1	0.0000 + 0.0000i	0
2	3	2	0.0360 + 0.0130i	133.84 + 101.14i
3	4	3	0.0330 + 0.0119i	16.214+ 11.292i
3	5	4	0.0450 + 0.0162i	34.315+ 21.845i
5	6	5	0.0150 + 0.0540i	73.016 + 63.602i
6	7	6	0.0150 + 0.0540i	144.2 + 68.604i
7	8	7	0.0150 + 0.0125i	104.47 + 61.725i
8	9	8	0.0180 + 0.0140i	28.547 + 11.503i
9	10	9	0.0210 + 0.0630i	87.56 + 51.073i
3	11	10	0.1660 + 0.1344i	198.2 + 106.77i
11	12	11	0.1120 + 0.0789i	146.8 + 75.995i
12	13	12	0.1870 + 0.3130i	26.04 + 18.687i
13	14	13	0.1420 + 0.1512i	52.1 + 23.22i
14	15	14	0.1800 + 0.1180i	141.9+ 117.5i
15	16	15	0.1500 + 0.0450i	21.87 + 28.79i

16	17	16	0.1600 + 0.1800i	33.37 + 26.45i
17	18	17	0.1570 + 0.1710i	32.43 + 25.23i
12	19	18	0.2180 + 0.2850i	20.234 + 11.9060i
19	20	19	0.1180 + 0.1850i	156.94 + 78.5230i
20	21	20	0.1600 + 0.1960i	546.29 + 351.4i
21	22	21	0.1200 + 0.1890i	180.31 + 164.2i
22	23	22	0.1200 + 0.0789i	93.167 + 54.594i
23	24	23	1.4100 + 0.7230i	85.18 + 39.65i
24	25	24	0.2930 + 0.1348i	168.1 + 95.178i
25	26	25	0.1330 + 0.1040i	125.11 + 150.22i
26	27	26	0.1780 + 0.1340i	16.03 + 24.62i
27	28	27	0.1780 + 0.1340i	26.03 + 24.62i
5	29	28	0.0150 + 0.0296i	594.56 + 522.62i
29	30	29	0.0120 + 0.0276i	120.62 + 59.117i
30	31	30	0.1200 + 0.2766i	102.38 + 99.554i
31	32	31	0.2100 + 0.2430i	513.4 + 318.5i
32	33	32	0.1200 + 0.0540i	475.25 + 456.14i
33	34	33	0.1780 + 0.2340i	151.43 + 136.79i
34	35	34	0.1780 + 0.2340i	205.38 + 83.302i
35	36	35	0.1540 + 0.1620i	131.6 + 93.082i
31	37	36	0.1870 + 0.2610i	448.4 + 369.79i
37	38	37	0.1330 + 0.0990i	440.52 + 321.64i
30	40	38	0.3300 + 0.1940i	112.54 + 55.134i
40	41	39	0.3100 + 0.1940i	53.963 + 38.998i
41	42	40	0.1300 + 0.1940i	393.05 + 342.6i
42	43	41	0.2800 + 0.1500i	326.74 + 278.56i
43	44	42	1.1800 + 0.8500i	536.26 + 240.24i
44	45	43	0.4200 + 0.2436i	76.247 + 66.562i
45	46	44	0.2700 + 0.0972i	53.52 + 39.76i
46	47	45	0.3390 + 0.1221i	40.328 + 31.964i
47	48	46	0.2700 + 0.1779i	39.653 + 20.758i
36	39	47	0.2100 + 0.1383i	66.195 + 42.361i
39	49	48	0.1200 + 0.0789i	73.904 + 51.653i
49	50	49	0.1500 + 0.0987i	114.77 + 57.965i
50	51	50	0.1500 + 0.0987i	918.37 + 1205.1i
51	52	51	0.2400 + 0.1581i	210.3 + 146.66i
52	53	52	0.1200 + 0.0789i	66.68 + 56.608i
53	54	53	0.4050 + 0.1458i	42.207 + 40.184i
54	55	54	0.4050 + 0.1458i	433.74 + 283.41i
30	56	55	0.3910 + 0.1410i	62.1 + 26.86i

56	57	56	0.4060 + 0.1461i	92.46 + 88.38i
57	58	57	0.4060 + 0.1461i	85.188 + 55.436i
58	59	58	0.7060 + 0.5461i	345.3 + 332.4i
59	60	59	0.3380 + 0.1218i	22.5 + 16.83i
60	61	60	0.3380 + 0.1218i	80.551 + 49.156i
61	62	61	0.2070 + 0.0747i	95.86 + 90.758i
62	63	62	0.2470 + 0.8922i	62.92 + 47.7i
2	64	63	0.0280 + 0.0418i	478.8 + 463.74i
64	65	64	0.1170 + 0.2016i	120.94 + 52.006i
65	66	65	0.2550 + 0.0918i	139.11 + 100.34i
66	67	66	0.2100 + 0.0759i	391.78 + 193.5i
67	68	67	0.3830 + 0.1380i	27.741 + 26.713i
68	69	68	0.5040 + 0.3303i	52.814 + 25.257i
69	70	69	0.4060 + 0.1461i	66.89 + 38.713i
70	71	70	0.9620 + 0.7610i	467.5 + 395.14i
71	72	71	0.1650 + 0.0600i	594.85 + 239.74i
72	73	72	0.3030 + 0.1092i	132.5 + 84.363i
73	74	73	0.3030 + 0.1092i	52.699 + 22.482i
74	75	74	0.2060 + 0.1440i	869.79 + 614.775i
75	76	75	0.2330 + 0.0840i	31.349 + 29.817i
76	77	76	0.5910 + 0.1773i	192.390 + 122.43i
77	78	77	0.1260 + 0.0453i	65.75 + 45.37i
65	79	78	0.5590 + 0.3687i	238.15 + 223.22i
79	80	79	0.1860 + 0.1227i	294.55 + 162.47i
80	81	80	0.1860 + 0.1227i	485.57 + 437.92i
81	82	81	0.2600 + 0.1390i	243.53 + 183.03i
82	83	82	0.1540 + 0.1480i	243.53 + 183.03i
83	84	83	0.2300 + 0.1280i	134.25 + 119.29i
84	85	84	0.2520 + 0.1060i	22.71 + 27.96i
85	86	85	0.1800 + 0.1480i	49.513 + 26.515i
80	87	86	0.1600 + 0.1820i	383.78 + 257.16i
87	88	87	0.2000 + 0.2300i	49.64 + 20.6i
88	89	88	0.1600 + 0.3930i	22.473 + 11.806i
66	90	89	0.6690 + 0.2412i	62.93 + 42.96i
90	91	90	0.2660 + 0.1227i	30.67 + 34.93i
91	92	91	0.2660 + 0.1227i	62.53 + 66.79i
92	93	92	0.2660 + 0.1227i	114.57 + 81.748i
93	94	93	0.2660 + 0.1227i	81.292 + 66.526i
94	95	94	0.2330 + 0.1150i	31.733 + 15.96i
95	96	95	0.4960 + 0.1380i	33.32 + 60.48i

92	97	96	0.1960 + 0.1800i	531.28 + 224.85i
97	98	97	0.1960 + 0.1800i	507.03 + 367.42i
98	99	98	0.1866 + 0.1220i	26.39 + 11.7i
99	100	99	0.0746 + 0.3180i	45.99 + 30.392i
2	101	100	0.0625 + 0.0265i	100.66 + 47.572i
101	102	101	0.1501 + 0.2340i	456.48 + 350.3i
102	103	102	0.1347 + 0.0888i	522.56 + 449.29i
103	104	103	0.2307 + 0.1203i	408.43 + 168.46i
104	105	104	0.4470 + 0.1608i	141.48 + 134.25i
105	106	105	0.1632 + 0.0588i	104.43 + 66.024i
106	107	106	0.3300 + 0.0990i	96.793 + 83.647i
107	108	107	0.1560 + 0.0561i	493.92 + 419.34i
108	109	108	0.3819 + 0.1374i	225.38 + 135.88i
109	110	109	0.1626 + 0.0585i	509.21 + 387.21i
110	111	110	0.3819 + 0.1374i	188.5 + 173.46i
111	112	111	0.2445 + 0.0879i	918.03 + 898.55i
111	113	112	0.2088 + 0.0753i	305.08 + 215.37i
113	114	113	0.2301 + 0.0828i	54.38 + 40.97i
101	115	114	0.6102 + 0.2196i	211.14 + 192.9i
115	116	115	0.1866 + 0.1270i	67.009 + 53.336i
116	117	116	0.3732 + 0.2460i	162.07 + 90.321i
117	118	117	0.4050 + 0.3670i	48.785 + 29.156i
118	119	118	0.4890 + 0.4380i	33.9 + 18.98i
48	28	119	0.5258 + 0.2925i	Tie switch
18	28	120	0.5258 + 0.2916i	Tie switch
9	25	121	0.4272 + 0.1539i	Tie switch
55	45	122	0.4800 + 0.1728i	Tie switch
63	50	123	0.3600 + 0.1296i	Tie switch
38	63	124	0.5700 + 0.5720i	Tie switch
10	42	125	0.5300 + 0.3348i	Tie switch
59	97	126	0.3957 + 0.1425i	Tie switch
74	92	127	0.6800 + 0.6480i	Tie switch
89	76	128	0.4062 + 0.1464i	Tie switch
100	78	129	0.4626 + 0.1674i	Tie switch
109	84	130	0.6510 + 0.2340i	Tie switch
106	87	131	0.8125 + 0.2925i	Tie switch
111	119	132	0.7089 + 0.2553i	Tie switch
26	36	133	0.5000 + 0.5000i	Tie switch

System reference voltage of the IEEE 118-bus is 11kV

A.4 12-bus system

Table A-4 12-bus system parameters

start	end	branch	Impedance(p.u.)	power(p.u.)
5	2	7	0.0048+0.0186i	0
2	11	6	0.0245+0.0213i	0
2	1	3	0.0056+0.0186i	0.0348+0.0116i
2	7	5	0.0390+0.0219i	0.0348+0.0116i
11	10	9	0.0245+0.0213i	0.024+0.008i
1	4	11	0.0126+0.0124i	0.042+0.014i
1	3	1	0.0056+0.0186i	0
1	12	8	0.0245+0.0213i	0
3	6	2	0.0245+0.0213i	0.03+0.01i
3	9	10	0.0390+0.0219i	0.045+0.015i
12	8	4	0.0245+0.0213i	0.042+0.014i

System reference voltage of the 12-bus is 12.66kV

Appendix B Output Power Data of Wind and Solar Generators

Table B-1 Hourly Breakdown of Renewable Resources (MW)

Hour	Wind	Solar (Summer)	Solar (Winter)
1	4284	0	0
2	4185	0	0
3	4036	0	0
4	3780	0	0
5	3660	0	0
6	3632	0	0
7	3630	350	0
8	3361	1478	367
9	2820	2591	1402
10	2684	3312	2213
11	2766	3785	2597
12	2490	3916	2761
13	2328	3981	2748
14	2930	3981	2592
15	3447	3933	2086
16	3746	3699	1044
17	3796	3200	0
18	3736	2463	0
19	3666	1311	0
20	3636	283	0
21	3586	0	0
22	3646	0	0
23	3777	0	0
24	3801	0	0